Using Aircraft Observations and Modelling to Improve Understanding of Mineral Dust Transport and Deposition Processes

Natalie Ratcliffe

Department of Meteorology

University of Reading

A thesis presented for the degree of

Doctor of Philosophy

August 2024

Declaration

I confirm that this is my own work and the use of all material from other sources has been properly and fully acknowledged.

Natalie G. Ratcliffe

Acknowledgements

First and foremost, I would like to say a huge thank you to my supervisors in Reading, Claire Ryder and Nicolas Bellouin. You have provided excellent advice, scientific discussion and huge amounts of support throughout my PhD. Also thank you to my supervisors at the Met Office, Steph Woodward, Ben Johnson and Anthony Jones. You have been so supportive and have provided a wealth of knowledge on the MetUM and all things dust modelling.

A quick thank you to Franco Marenco, who without his help and expertise, I wouldn't have been able to go to Cape Verde in my second year as part of the DAZSAL campaign, and measure dust firsthand.

I wouldn't have enjoyed my PhD experience without the friends I made along the way. To everyone in my year, but also to my friends in the years above and below me, thank you for making doing a PhD significantly more bearable. Charlie and Alanna, it's been a comfort knowing that I could turn up at your house any day and be welcomed with some biscuits and a blanket. Blair, Ellen and Thea, you were wonderful housemates in a maybe slightly less than wonderful house!

To my partner, Rob, you have been such a huge support over the last two and half years, from helping me out the door at 2am when I was so nervous to fly to Cape Verde, to waking me up with breakfast when I refused to hear the alarm. I'm so thankful for having you around.

A huge thank you to my family who have constantly supported me and always nod along whenever I start rambling about dust. Finally, thank you to all the animals who were ferociously petted whenever I needed animal therapy: Poppy, Freyja, Crumb, Baxter, and Rico.

Abstract

With more than 400-3000 Mt of mineral dust lofted into the atmosphere annually, dust affects the Earth's radiation budget, hydrological and carbon cycles, human health, energy production, aviation and more. Recent observations revealed that coarse (5-10 µm) and super-coarse (10-62.5 µm) dust particles are more abundant after long-range transport than expected. Having different impacts on the Earth system than fine particles, it is vital that we understand how these particles travel so far to fully comprehend the impacts of dust globally. In this thesis, I analyse the dust size distribution evolution from the Sahara to the western Caribbean in aircraft observations and compare to a climate model, then use the model to understand the sensitivity of coarse particle lifetime to transport and deposition processes. I show that the model deposits coarse particles too quickly, resulting in an underestimation of dust mass of increasing orders of magnitude with westwards transport. Processes in the model which may increase coarse transport are tested. Coarse dust is shown to be most sensitive to sedimentation, with reductions in sedimentation beyond 80% increasing the volume size distribution by up to 7 orders of magnitude, bringing the model into agreement with observations. Convective and turbulent mixing, impaction scavenging, and shortwave absorption are found to have minimal impact on long-range transport of coarse particles. Raising the dust in the model to 5km at the Sahara with the hope to increase long-range transport is shown to increase particle lifetime, though the coarsest dust is still deposited within 24 hours. Findings in this thesis suggest the presence and importance of processes not in the model which could counteract sedimentation, such as asphericity and electric charging, and suggest that explicit convection representation could improve model transport. This work demonstrates the need for thorough research of these undetermined processes to accurately model size distribution evolution.

List of Figures

List of Tables

Notation

Notation	Description
γ	Value for calculating interparticle forces
λ	Mean free path of gas molecules in air
Λ	Scavenging coefficient
μ_{air}	Dynamic viscosity of air
ρ_0	Rainfall intensity
ρ_a	Air density
ρ_p	Particle density
σ_g	Standard deviation
σ_{ext}	Aerosol extinction coefficient
σ_{sca}	Scattering coefficient
τ	Aerosol optical depth (AOD)
υ_{air}	Kinematic viscosity of air
ψ_h	Stability function
ω_0	Single scattering albedo (SSA)
ω_1	Grid box mean soil moisture
ω	Volumetric soil moisture
ω'	Minimum soil moisture for erosion threshold
A	Droplet diameter
B	Bare soil fraction
C	Constant of proportionality
$C_{(d)}$ or $C_{(i)}$	Mass or number concentration of particles with diameter d or in size bin i
Cc	Cunningham correction factor
C_{ext}	Single-particle extinction cross section
D	Tunable multiplier of horizontal dust flux
D_g	Brownian diffusivity
D_p or d	Particle diameter
D_{rep}	Representative diameter of a size bin

Notation	Description
E	Collision efficiency of a given particle size
F	Vertical dust flux
F_c	Clay fraction of soil
g	Acceleration due to gravity
G	Horizontal dust flux
i	Dust size bin
k	von Karman constant
k_1	Tunable multiplier of friction velocity
k_2	Tunable multiplier of top level soil moisture
M_i	Ratio of dust mass in size bin i to total mass
N	Number concentration
N_{tot}	Total number concentration
Q_{ext}	Extinction
r	Particle radius
R	Precipitation rate
R_A	Aerodynamic resistance
R_B	Surface layer resistance
Re_{*t}	Reynolds number at the erosion threshold
Sc	Schmidt number
St	Stokes number
t	Time
U^*	Wind friction velocity
U^*_M	U^* calculated by the model
U^*_t	Threshold friction velocity
U^*_{td}	Dry threshold friction velocity
V_D	Deposition velocity
V_S	Stokes deposition velocity
z	Reference height for wind velocity
z_0	Aerodynamics roughness length

Acronyms

Acronym	Meaning
ADRIMED	Aerosol Direct Radiative Impact on the regional climate in the MEDiterranean region
AEJ	African easterly jet
AER-D	AERosol Properties – Dust
AEW	African easterly wave
AOD	Aerosol optical depth
BL	Boundary Layer
CALIOP	Cloud-Aerosol Lidar with Orthogonal Polarization
CALIPSO	Cloud-Aerosol Lidar and Infrared Pathfinder Satellite Observations
CAS-DPOL	Cloud and Aerosol Spectrometer with Depolarization Detection
CCN	Cloud condensation nuclei
CDNC	Cloud droplet number concentration
CDP	Cloud droplet probe
ChArMEx	Chemistry-Aerosol Mediterranean Experiment
CLASSIC	Coupled Large-scale Aerosol Simulator for Studies in Climate
CIP15	Cloud Imaging Probe
CMIP	Coupled Model Intercomparison Project
DAZSAL	Diurnal vAriation of the vertically resolved siZe distribution in the Saharan Air Layer
DLR	Falcon Deutsches Zentrum fur Luft- und Raumfahrt
DRE	Direct radiative effect
FAAM	Facility for Airborne Atmospheric Measurements
FRAGMENT	FRontiers in dust minerAloGical coMposition and its Effects upoN climaTe
GCM	Global climate model
GERBILS	Geostationary Earth Radiation Budget Intercomparison of Longwave and Shortwave Radiation
GLOMAP	Global Model of Aerosol Processes
HadGEM3	Hadley Centre Global Environment Model 3

Acronym	Meaning
INP	Ice nucleating particle
ITCZ	Inter-tropical convergence zone
JJA	June, July, August
JULES	Joint UK Land Environment Simulator
LES	Large-eddy simulation
LLJ	Low level jet
MBL	Marine boundary layer
MCA	Mass centroid altitude
MEDUSA	Model of Ecosystem Dynamics, nutrient Utilisation, Sequestration and Acidification
MetUM	Met Office Unified Model
MODIS	Moderate Resolution Imaging Spectroradiometer
MSC	Mesoscale convective system
NPP	National Polar orbiting Partnership
NWP	Numerical weather prediction
OAP	Optical array probe
OPC	Optical particle counter
PCASP	Passive Capacity Aerosol Spectrometer Probe
PSAP	Particle Soot Absorption Photometer
RE	Radiative effects
SABL	Saharan atmospheric boundary layer
SAL	Saharan air layer
SALTRACE	Saharan Aerosol Long-range Transport and Aerosol–Cloud-Interaction Experiment
SAMUM	SAharan Mineral Dust Experiment
SHL	Saharan heat low
SkyOPC	Grimm Sky OPC
SSA	Single scattering albedo
SST	Sea surface temperature
TCM	Total column mass
TOA	Top of the atmosphere
UHSAS-A	Ultra High Sensitivity Aerosol Spectrometer
UKCA	United Kingdom Aerosols and Chemistry
VIIRS	Visible Infrared Imaging Radiometer Suite
VSD	Volume size distribution
WAM	West African monsoon
WRF	Weather Research and Forecasting model

Contents

Chapter 1

Introduction

1.1 Background

1.1.1 Dust in the Earth System

Mineral dust plays a vital role in the Earth system as it is transported from sources across the globe. The main sources are based in the low latitudes, in the so-called 'dust belt', with the Sahara Desert being the largest source. Every year, 400-3000 Mt of mineral dust is lofted globally (Huneeus et al. 2011; Shao et al. 2011) and transported great distances before being deposited thousands of kilometers from its source, impacting the Earth's radiative budget, hydrological and carbon cycles, human health, energy production, and aviation.

Lofted dust can interact with the Earth's radiation budget in two ways; directly and indirectly (Figure 1.1). Shortwave (SW) and longwave (LW) radiation is scattered and absorbed by dust particles in the direct radiative effect (DRE)(Kok et al. 2018; Tegen and Lacis 1996)(Figure 1.1a). At the top of the atmosphere (TOA), there is a net cooling effect from dust, estimated to be -0.23 ± 0.35 W m^{-2} (Kok et al. 2023; Li et al. 2021), whereby a large degree of uncertainty extends the estimate into the positive. This is mostly a consequence of the strong SW cooling effect caused by the scattering of SW radiation (-0.4 ± 0.3 W m^{-2}), though the absorption and scattering of LW radiation results in a warming DRE at the TOA ($+0.25 \pm 0.15$ W m^{-2}). The magnitude of the TOA forcing perturbation is partially dependent on the surface albedo below the lofted dust. Over a dark, low albedo surface, such as an ocean, the SW scattering enhances the cooling effect. Whereas over a bright surface, such as snow/ice or cloud, where much of the SW radiation is usually reflected back, warming from the SW absorption effect will be enhanced (Claquin et al. 1998).

In terms of the indirect radiative effect, dust can alter cloud properties, such as

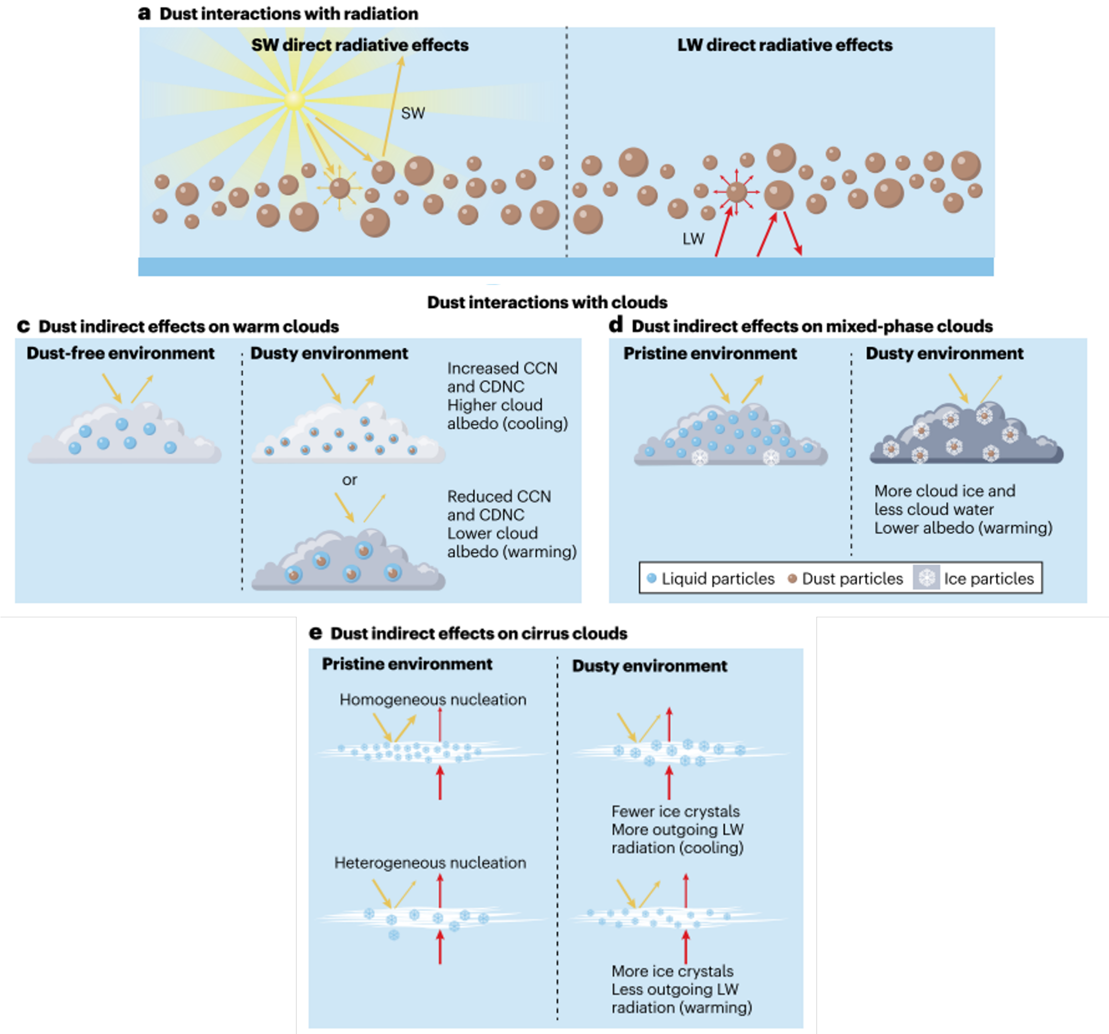

Figure 1.1: Schematic showing the direct (a) and indirect effect of dust in warm (c), mixed-phase (d) and ice (e) clouds. Figure edited from Kok et al. (2023).

droplet number and size (Lohmann and Feichter 2005; Price et al. 2018), and the precipitation efficiency (Rosenfeld et al. 2008), thus altering the radiative balance (Figure 1.1cde). However, aerosol-cloud-radiation interactions, including those of dust in clouds, are still one of the greatest sources of uncertainty in climate modelling (Arias et al. 2021). Dust can act as cloud condensation nuclei (CCN) and ice nucleating particles (INP) in clouds. Introducing dust as CCN into a warm cloud environment increases the number of surfaces for water vapour to condense onto, thus increasing the cloud droplet number concentration (CDNC)(Figure 1.1c). This microphysical change increases the reflectivity of the cloud, as well as making it less likely to produce precipitation-sized droplets, reducing the precipitation efficiency of the cloud (Lohmann and Feichter 2005). However, in a cooler, mixed-phase cloud, the dust can act as INP and form ice crystals in the cloud (Figure 1.1d) in temperatures as low as −38°C (Pruppacher and Klett 2010). As the ice crystals form, the lower saturation vapour pressure of ice (compared to liquid water), means that the ice crystals grow quickly and drain the surrounding air of super-cooled water and vapour (Hoose and Möhler 2012). The increasing ratio of ice crystals to liquid water droplets reduces the brightness of the cloud (Vergara-Temprado et al. 2018). The resultant ice crystals end up quickly growing to precipitation-size, increasing precipitation efficiency and decreasing the lifetime of the cloud (Lohmann and Feichter 2005).

The Earth's surface albedo is also susceptible to change as a consequence of dust deposition. The albedo of snow and ice covered surfaces can be reduced significantly with the deposition of dust; this can result in increased surface radiation absorption and thus the heating and melting of snow and ice, reducing the overall snow cover, resulting in further surface heating (e.g. Di Mauro et al. (2015) and Dumont et al. (2020)). Xie et al. (2018) explained that decreased snow cover could lead to further dust emissions.

Dust contains important nutrients, such as iron, nitrogen and phosphorus (Baker et al. 2006; Dansie et al. 2017; Prospero et al. 2020), and thus, dust deposition can result in significant biological and ecological impacts. Approximately 95% of global atmospheric iron (Mahowald et al. 2009) and 82% of atmospheric phosphorus (Mahowald et al. 2008) come from lofted mineral dust. Half a billion tonnes of minerals are deposited to the world's oceans every year by dust (Mahowald et al. 2005). Deposition of dust to ocean surfaces can lead to an increase in primary productivity by phytoplankton, driven by increased nutrient availability (Dansie et al. 2022; Mahowald et al. 2018). This increase in activity can lead to the formation of algal blooms, which can provide a source of food for other marine life. However, these blooms can also be harmful as they can deplete dissolved oxygen in the water and contain toxic species which introduce toxins to marine life and/or humans through the food chain (Hallegraeff et al. 2003). Dust containing phosphorous is transported from the Sahara and deposited into the Amazon rain forest providing between 8-48 Tg of dust every year (Prospero et al. 2020; Yu et al. 2015). Phosphorous is a crucial nutrient required for encouraging tree growth. Saharan dust deposition aids the Amazon in avoiding phosphorus depletion; Yu et al. (2015) suggest that as much Phosphorus is deposited to the Amazon every year by Saharan dust as is removed by hydrological loss.

Despite providing a fertilising effect to plants, dust deposition to their leaves can decrease plant photosynthesis and overall plant growth (Javanmard et al. 2020; Zia-Khan et al. 2015). This decrease in plant growth impacts yields from agriculture; for example, cotton leaves showed 28% reduction in yield when exposed to dust at 10-day intervals (Zia-Khan et al. 2015). Agriculture is also impacted by contamination of soil and water sources, reduced health of livestock, damaged crops from sand-blasting and the burial of seedlings (Stefanski and Sivakumar 2009). Anthropogenic endeavours in solar energy production can also be negatively impacted. The deposition of dust on photovoltaic panels reduces the panel efficiency (Sayyah et al. 2014; Sulaiman et al. 2014), increases cleaning costs, and damages the panels with sand-blasting.

Atmospheric dust also poses a significant threat to the aviation industry, both by reducing visibility significantly at the surface, raising the risk of collision and delaying departure (Middleton 2017), by degrading and sand-blasting the engines (Ryder et al. 2024), and by exacerbating icing in the engines (Nickovic et al. 2021). The vertical distribution of the dust is important once the aircraft are in-flight. Nickovic et al. (2021) discussed the potential threat posed by dust acting as INP and found that predicted ice particle number sharply increased in the presence of dust and could have contributed to the icing of aircraft engines in two previous aircraft accidents. The dust in these cases had been taken to the upper troposphere by convective circulation. Ryder et al. (2024) found that the vertical dust distribution during takeoff and landing was important for the amount of degradation the engines would experience. Thus, it is very important to have an understanding of the vertical distribution of dust in the atmosphere.

1.1.2 Dust Physics

Composition, morphology and size distribution

Mineral dust is dominantly composed of silicates and carbonates (Scheuvens and Kandler 2014), though the relative contribution of minerals in a sample can vary drastically depending on the source location. Dust is therefore assumed to have a density of 2.6 g cm^{-3}.

The global dust TOA DRE sits within the range of -0.23 to $+0.35$ W m^{-2}, where some research suggests that up to 97% of the uncertainty is a consequence of uncertainty in source soil (Li et al. 2021). The dust DRE is partially dependent on the particles' mineralogical composition, specifically the iron-oxide content for the SW DRE (Sokolik and Toon 1999). The abundance of iron oxides in the soil varies across the Sahara between different local source regions, hence understanding the specific source of airborne dust can aid the DRE quantification.

Mineral dust particles tend to be non-spherical; Otto et al. (2011) suggest that a prolate spheroid is the most common particle shape, with Huang et al. (2020) suggesting the length could be up to 5 times the particle height. The total sphericity of dust particles within a plume has been observed to change over the course of long-range transport, with Asian dust tending to become more spherical, while African dust became less spherical (Huang et al. 2020). This could in part be due to chemical reactions altering the shape of the dust particles, or due to preferential settling of the spherical particles.

The size distribution is an important factor which plays a significant role in the impact of many of the processes which were discussed in Section 1.1.1. A mineral dust size distribution typically ranges from less than 100 nm to more than 100 µm in diameter (Scheuvens and Kandler 2014). The lognormal number size distribution comes from Seinfeld and Pandis (2016) and is calculated

$$\frac{dN}{dr} = \frac{N_{tot}}{(2\pi)^{1/2} r \ln\sigma_g} exp(-\frac{(\ln r - \ln r_g)^2}{2(\ln\sigma_g)^2}) \tag{1.1}$$

where N is the number concentration (in cm^{-3}), r is the particle radius, N_{tot} is the total number concentration, σ_g is the standard deviation and r_g is the median particle radius. The size distribution can also be portrayed as a volume, surface area and mass distribution.

Optical properties

As mentioned previously, dust can interact with SW and LW radiation by scattering or absorbing and then re-emitting it as thermal energy. The non-dimensional particle extinction (Q_{ext}) is the sum of scattering and absorption at a particular wavelength and relates to the efficiency with which a particle extinguishes radiation in relation to its size (Seinfeld 1986).

$$Q_{ext} = \frac{C_{ext}}{\pi r^2} \tag{1.2}$$

where C_{ext} is the single-particle extinction cross section in m^2 and r is the particle radius in µm. The aerosol extinction coefficient (σ_{ext}; m^{-1}) is defined as,

$$\sigma_{ext} = NC_{ext} \tag{1.3}$$

where N is the number of particles per cubic metre of air. When vertically integrated over height dz, σ_{ext} provides the aerosol optical depth (AOD or τ), which is dimensionless.

$$\tau = \int \sigma_{ext} dz \tag{1.4}$$

AOD represents the total radiation extinguished by the dust in a vertical column of the atmosphere at a particular wavelength, often given at 550 nm. Additionally, σ_{ext} can be used to calculate the single-scattering albedo (SSA or ω_0); the dimensionless ratio of scattering to extinction.

$$\omega_0 = \frac{\sigma_{sca}}{\sigma_{ext}} \tag{1.5}$$

where σ_{sca} is the scattering coefficient (cm^{-1}). SSA is a useful metric as it reveals the fraction of radiation scattered by the particles. An SSA value of 0 means that all extinction is due to absorption. Dust tends to have a relatively low SSA compared to other aerosols as it is more absorbing than, for example, sulfate aerosol (Highwood and Ryder 2014). By understanding the extinction and scattering of aerosols, we can understand how much of a warming/cooling effect they will have on the atmosphere around them, which can result in circulation changes (Miller and Tegen 1998).

Emission

At the surface, dust emissions are produced by wind blowing across a suitable surface; the production of atmospheric dust is dependent on certain characteristics. Factors such as soil moisture, surface roughness, soil aggregation, surface crusting and the presence of non-erodible substances can decrease the dust production efficiency (Schepanski et al. 2017).

The wind friction velocity, U^* (in m s^{-1}), has to reach a certain threshold friction velocity, U_t^* (in m s^{-1}), before the interparticle forces which hold the particles together, the particles mass, and cohesion forces induced by soil moisture can be overcome (Marticorena and Bergametti 1995). Soil moisture and soil roughness can alter U_t^*; both greater soil moisture and rougher surfaces result in greater U_t^*. Once this threshold velocity has been reached, individual particles are released from the surface and their motion is dependent on their size, shape and density. U_t^* is a size-dependent property which can be calculated in many different ways. One way uses the following equation by Shao and Lu (2000) which includes the electrostatic forces involved in the interparticle cohesion forces.

$$U_t^*(D_p) = [A_N(\frac{\rho_p g D_p}{\rho_a} + \frac{\gamma}{\rho_a D_p})]^{0.5} \tag{1.6}$$

where D_p is the particle diameter (in µm), ρ_p is the particle density (assumed to be 2.6 g cm^{-3}), ρ_a is the air density in kg m^{-3} and g is acceleration due to gravity in m s^{-2}. $A_N = \sqrt{f(Re_{*t})} \approx 0.0123$, $f(Re_{*t})$ is the function (f) of the Reynolds number (Re_{*t}) at the erosion threshold, where f is inversely proportional to an empirical coefficient associated with aerodynamic drag. The term $\frac{\gamma}{\rho_a D_p}$ accounts for the interparticle forces, where γ is adjusted based on observations recorded in wind-tunnel experiments (Greeley and Iversen 1985). Up to ~60 µm diameter, U_t^* decreases with increasing diameter, however, beyond ~100 µm, U_t^* begins to increase again. Marticorena (2014) presents some different calculations of U_t^* and shows that some uncertainty remains as to where the minimum in U_t^* occurs but all agree that the most easily erodible soils contain particles in the 60-100 µm range. The existence of the minima between 60-100 µm suggests that emitting dust is a size-segregating process and that the emitted size distribution may be different to the soil size distribution.

The vertically integrated emitted horizontal flux of dust (G; in kg m^{-2} s^{-1}) can be calculated

$$G = C\frac{\rho_a}{g}U_t^{*3}(1 - \frac{U_t^*}{U^*})(1 + \frac{U_t^{*2}}{U^{*2}}) \tag{1.7}$$

where C is a constant of proportionality (White 1979). The above equation is an example of one way to calculate the emitted dust flux. This is one of the more commonly used equations as Marticorena (2014) explains; both equations by Bagnold (1941) and White (1979) have been found to most closely agree with experimental data.

Particles with diameter greater than 1000 µm roll along the ground with a creeping motion. Smaller particles (70-1000 µm) are raised and quickly deposited downwind in a ballistic, saltating motion. The force of this impact is strong enough to break apart the binding forces allowing for the ejection of smaller particles which become entrained in the wind, and other particles which are sent into a saltating motion (Marticorena 2014). If the terminal fall velocity of a lofted particle is lower than the vertical wind velocity, the particles will be lofted and can be transported away. The impact from saltation can also lead to the disaggregation of aggregated particles (Shao 2001). Saltation is the most important mechanism for lofting particles in the fine size range as they have a much higher U_t^*. Aerodynamic entrainment can occur, though it is expected to only occur in conditions with very high U^*, where the particles are lifted without the need for bombardment by saltating particles.

Deposition

I will now focus on the physics of dust deposition. Aerosols are subject to dry and wet deposition; whereby the efficiency of the removal is impacted by the particle size.

Dry deposition

Dry deposition is a fairly size-dependent process with fine and coarse particles being affected by different processes. Fine particles smaller than 0.1 µm diameter are subject to deposition via Brownian motion, which increases the deposition velocity (V_D) with decreasing particle size below 0.1 µm. The coarsest particles are subject to gravitational settling which increases V_D with increasing particles size; this is the most limiting factor for coarse particle transport. The optimal particle size with the lowest V_D occurs between 0.1-2 µm (Bergametti and Foret 2014), where the deposition occurs due to turbulent processes, such as impaction and interception. The lifetime of dust decreases exponentially with increasing diameter beyond this optimal size according to these assumptions (Kok et al. 2017). V_D is represented using an inverse resistance analogue method (Seinfeld 1986), given in m s^{-1} by

$$V_D = (R_A + R_B + R_A R_B V_S)^{-1} + V_S \tag{1.8}$$

where R_A is the aerodynamic resistance (in s m^{-1}), R_B is the resistance of the quasi-laminar surface layer (in s m^{-1}) and V_S is the Stokes deposition velocity. R_A is a function of the wind speed, atmospheric stability and surface roughness. In neutral atmospheric conditions, R_A can be calculated

$$R_A = \frac{1}{kU^*}[\ln(\frac{z}{z_0}) - \psi_h] \tag{1.9}$$

where k is the von Karman constant, z is the reference height for wind velocity, z_0 is the aerodynamics roughness length of the surface and ψ_h is the stability function.

R_B, also known as the surface layer resistance, is the resistance experienced by the particles in the laminar sublayer adjacent to the surface and so R_B is based on molecular scale transport. Incorporating particle motion by both Brownian diffusion and inertial effects, R_B is calculated

$$R_B = \frac{1}{U^*(Sc^{-2/3} + 10^{-3/St})} \tag{1.10}$$

where Sc is the Schmidt number and St is the Stokes number. Sc is the ratio between viscous and diffusion forces associated with Brownian diffusion, calculated

$$Sc = \upsilon_{air} D_g^{-1} \tag{1.11}$$

where υ_{air} is the kinematic viscosity of air and D_g is Brownian diffusivity.

As briefly mentioned, Equation 1.10 includes inertial effects in the form of St, which is calculated

$$St = \frac{U^{*2} V_S}{g \upsilon_{air}} \tag{1.12}$$

The calculation of V_S includes the Cunningham correction factor (C_c) which accounts for slip flow and can impact the deposition rate of fine particles below 1 µm diameter by up to 10%. V_S is calculated,

$$V_S = \frac{D_p^2 \rho_p g C_c}{18 \mu_{air}} \tag{1.13}$$

where μ_{air} is the dynamic viscosity of air. C_c is expressed as (Seinfeld 1986)

$$C_c = 1 + \frac{2\lambda}{D_p}(1.257 + 0.4e^{\frac{-1.1D_p}{2\lambda}}) \tag{1.14}$$

where λ is the mean free path of gas molecules in air (6.6×10^{-6} cm).

Wet deposition

In wet deposition, there are multiple pathways in which dust particles can be removed from the atmosphere. In-cloud scavenging consists of the particles either colliding with existing droplets or ice crystals, or by activating as CCN or INP. Alternatively, the particles can be scavenged below-cloud by impaction with falling rain droplets; this is a more efficient process for the removal of coarse particles, whereas in-cloud scavenging is more efficient for sub-micron particles (Bergametti and Foret 2014).

In-cloud scavenging can be dependent on the mineralogy of the particle; for example, particles containing potassium feldspar are more efficiently activated as INP than some other minerals (Atkinson et al. 2013). Dust particles are typically fairly hydrophobic (Fan et al. 2004), however chemical processing of the particles can result in a changing composition of the particle. Compounds such as sulfates can aggregate onto the particle surface, potentially increasing the CCN efficiency (Fan et al. 2004). There remains a fair level of uncertainty in the efficiency of in-cloud scavenging due to the lack of understanding of the processes involved.

The rate of below-cloud scavenging is dependent on the rain intensity (ρ_0), collision efficiency (E) and raindrop size distribution (Laakso et al. 2003). The rate of change of mass or number concentration of dust (C) in each time step (t) is calculated

$$\frac{dC_d}{dt} = -\Lambda_d C_d \tag{1.15}$$

where d is the particle diameter and Λ is the scavenging coefficient, calculated,

$$\Lambda_{(d)} = \frac{3}{2}\frac{E_{(d)(A)}\rho_0}{A} \tag{1.16}$$

where A is the droplet diameter. E is the ratio between the number of droplet-particle collisions and the number of particles in the column taken by a falling droplet. There is a minimum in E at particles with diameter ~0.5 µm (Greenfield 1957). Smaller than this, E increases due to Brownian motion, whereas above 0.5 µm, E increases again but due first to interception and then at larger size ranges, due to inertial impaction.

1.1.3 Dust Transport

Global dust

Approximately, 95% of emitted mineral dust comes from low latitude sources, while 5% comes from high-latitude sources (Bullard et al. 2016). The 'dust belt' describes a band of low latitude deserts that circumnavigate the globe's continents; the Sahara is the largest source of mineral dust within this belt and on Earth. Specifically, the Bodélé depression in Chad and a region of Mali, Mauritania and Algeria are the two largest emitters of dust (Scheuvens and Kandler 2014).

North African dust

Dust emissions are driven by local surface wind speed, which is in turn driven by large-scale circulation. Dust uplift at the Sahara is predominantly driven by three meteorological features: the Harmattan winds, the Saharan heat low (SHL) and the West African monsoon (WAM) (Schepanski et al. 2017). The combination of these three as well as the position of the intertropical convergence zone (ITCZ) make the boreal summer months the most productive for dust emissions (Marsham et al.

2008). Hence, we will focus on the summer (June, July, August; JJA) climatology here. This aligns with the timing of observations which will be analysed in this thesis (introduced in Chapter 3).

Throughout the year, the ITCZ moves between its most southerly point at ∼5°N in January and reaches its most northerly point of 15-20°N in July (Tsamalis et al. 2013). The proximity of the ITCZ to the Sahara encourages dust uplift. The continental-scale pressure gradient between the ITCZ and the subtropical subsidence zone further north drive northeasterly surface winds over North Africa, called the Harmattan winds (Schepanski et al. 2017). Harmattan winds are an important factor in the development of nocturnal low level jets (LLJs). The WAM transports cool, moist air north from the Gulf of Guinea. This intrusion of air can lead to the generation of nocturnal LLJs. LLJs are the dominant and frequent drivers of dust uplift over the Sahara (Marsham et al. 2013). Additionally, the moist air allows for the formation of mesoscale convective systems (MCSs), particularly along the African Easterly Jet (AEJ). These both have the potential to create uplift of dust from the Sahara.

The SHL forms from intense radiative heating of the Sahara, creating a thermal low-pressure area. The SHL is typically over northwest Africa during the summer, however, the location, depth and extent of the SHL affects large-scale circulation over North Africa (Lavaysse et al. 2009). The depth of the low can influence the strength of the Harmattan winds, the monsoon flow and, if strong enough, the position of the AEJ, impacting the formation of African easterly waves (AEWs) (Diedhiou et al. 1998; Thorncroft and Blackburn 1999).

From the surface to up to 6 km altitude, the Saharan atmospheric boundary layer (SABL) sits over the Sahara (Cuesta et al. 2009). Figure 1.2 shows the diurnal cycle of the SABL. Dust is transported in the SABL by dry convection. As this dusty layer moves towards the ocean, it raises up and is eroded from the base by the moist marine boundary layer (MBL) to create the Saharan air layer (SAL; Braun (2010), Carlson (2016), and Marsham et al. (2013)). The SAL typically has near constant potential temperature and water vapour mixing ratio values, with one inversion at the base, separating it from the MBL, and another at the top, separating it from the free atmosphere (Carlson 2016; Dunion and Velden 2004). In summer, the SAL is transported west towards the Americas via the AEJ, where it begins to lower through the atmosphere (Carlson 2016).

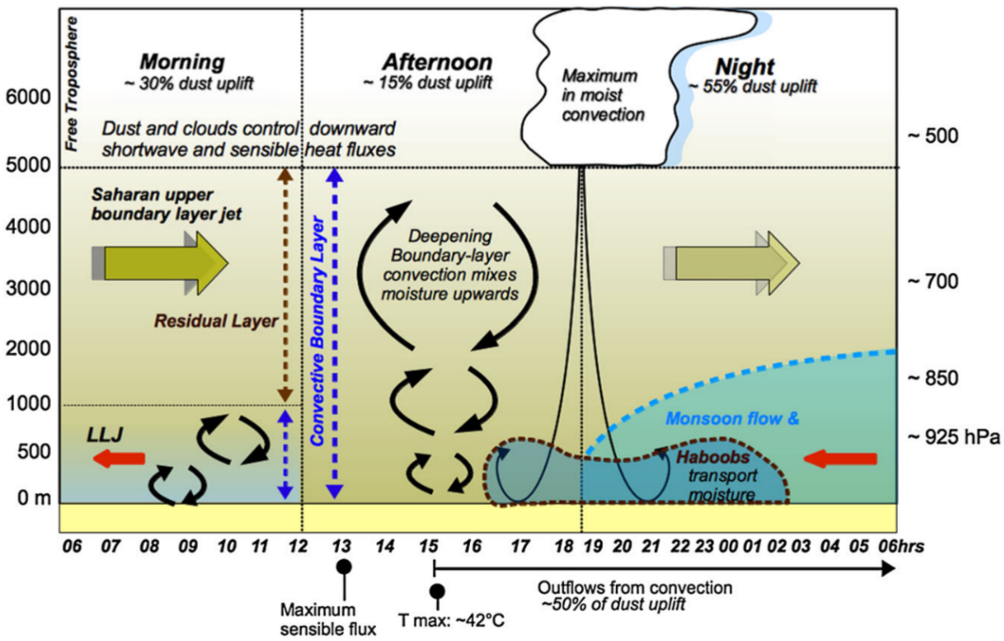

Figure 1.2: Diurnal cycle and structure of the SABL. Figure taken from Marsham et al. (2013).

1.1.4 Observations of Dust

As the need to analyse airborne dust grows, a variety of methods are required. In the last couple of decades, observations made by satellites, ground-based networks and in-situ aircraft have been vital for improving our understanding of the processes involved in dust emissions, transport and deposition. By combining these methods, we are able to analyse dust on local, regional and global scales. Observations tend to fall into two categories as described by Mona et al. (2023): coordinated measurements at network-level which tend to work on a long timescale (e.g. satellites and ground-based networks), and shorter term intensive measurements as part of experimental campaigns (e.g. in-situ aircraft campaigns). A combination of these are required to fully understand processes from very small scales (e.g. the emitted size distribution of dust) to much larger scales (e.g. transport of dust across the Atlantic ocean). Thus, both are vital for the advancement of our understanding of the Earth system.

Long-term

In order to gather the largest scale of observations, satellite retrievals cover great swathes of the Earth every day providing various products. This means that satellite retrievals are useful for analysing large-scale meteorological phenomena and are key for assessing global models and informing reanalysis datasets.

Visible images from satellites are useful for identifying sources and dust plumes. Two examples of visible satellite products are from the Moderate Resolution Imaging Spectroradiometer (MODIS) imagery instrument onboard the Terra and Aqua (current planned satellite lifetime of 26 and 24 years, respectively) satellites (Levy et al. 2013), and the Visible Infrared Imaging Radiometer Suite (VIIRS) onboard the Suomi National Polar orbiting Partnership (Suomi NPP) satellite launched in 2011 and still producing data to present (Hillger et al. 2013). MODIS also measures the AOD which is retrieved on a spatial scale of 0.5° and a temporal scale of once a day. The Cloud-Aerosol Lidar with Orthogonal Polarization (CALIOP) instrument onboard the Cloud-Aerosol Lidar and Infrared Pathfinder Satellite Observations (CALIPSO) satellite (Winker et al. 2009) measured 3D distributions of backscatter, extinction and depolarization ratio of aerosols, including dust for 17 years (2006-2023). Yu et al. (2015) used data from CALIOP to estimate the mass of dust deposited to the Amazon every year.

Satellite retrievals allow for analysis of large-scale processes and phenomena over long periods of time. However, there are many sources of uncertainty with using satellite retrievals. For example as Yu et al. (2015) states, satellite lidar observations can be subject to many uncertainties, including vertical profile shape of dust, dust mass extinction efficiency, the dust size distribution and the presence of clouds blocking the 'view' of the lidar down to the surface.

Ground-based networks allow for observations of dust over long timescales at a cheaper cost than satellites. These sites can often be set up to record smaller scale phenomena, but due to their limited spatial coverage from only observing single points in space, they are not reliable for recording large-scale phenomena in the same way as satellite retrievals. One of the longest running ground-based observations is at Barbados, which has collected data nearly continuously since 1965, recording the easterly transport of Saharan dust (Prospero and Lamb 2003).

Short-term

Shorter-term campaigns can also be run with instrumentation at the surface to produce a dataset from intensive observation periods. These detailed small-scale observations can help us to understand smaller scale processes, such as emission and deposition of dust particles. These campaigns can be relatively expensive due to the instrumentation used and the small spatial scale of the results achieved.

An exmaple is the recent FRontiers in dust minerAloGical coMposition and its Effects upoN climaTe (FRAGMENT) project; González-Flórez et al. (2023) discussed the results from the this campaign in Morocco. For the month of September in 2019, detailed observations at the surface were taken including meteorological (precipitation, wind speed and direction, temperature, and upwelling and downwelling radiative fluxes), size-resolved dust concentration, and saltation flux measurements. These detailed measurements allow us to gain a deeper understanding of the processes involved in particle emissions.

The only way to be certain of the characteristics of particles being transported is to measure them during transport, i.e. using aircraft campaigns. These kinds of campaigns provide information on the particle characteristics (shape, size, concentration etc.), and cover a greater spatial scale than the ground-based campaigns (though this does also raise the campaign cost). An example of these campaigns is the Fennec campaign, occurring in June 2011 used an aircraft to collect measurements of dust in vertical profiles of the atmosphere at the Sahara (Ryder et al. 2013b).

1.1.5 Coarse Dust

The size of a dust particle can have a significant impact on the consequent effects of that dust particle. In this section, we will focus on the importance of coarse ($2.5 < d < 10$ µm), super-coarse ($10 < d < 62.5$ µm) and giant ($d > 62.5$ µm) dust particles (size ranges defined in Adebiyi et al. (2023)).

Importance of particle size

Coarse and super-coarse dust can have differing magnitude impacts compared to fine particles ($d < 2.5$ µm), which typically dominate in terms of the number of particles. Figure 1.3 visualises the ways in which these coarser particles can interact with the Earth system from emission to deposition. These differences are driven by variations in particle characteristics such as mass, composition and morphology. With increasing mass, it becomes increasingly difficult to raise particles from the surface during emission (Section 1.1.2), as well as having a shorter atmospheric lifetime due to having a greater dry deposition velocity than smaller, and therefore lighter, particles. Additionally, in terms of the particle characteristics, coarser particles are more likely to have a complex shape (Scheuvens and Kandler 2014), be charged positively rather than negatively (Nicoll et al. 2020) and be composed of fewer clays.

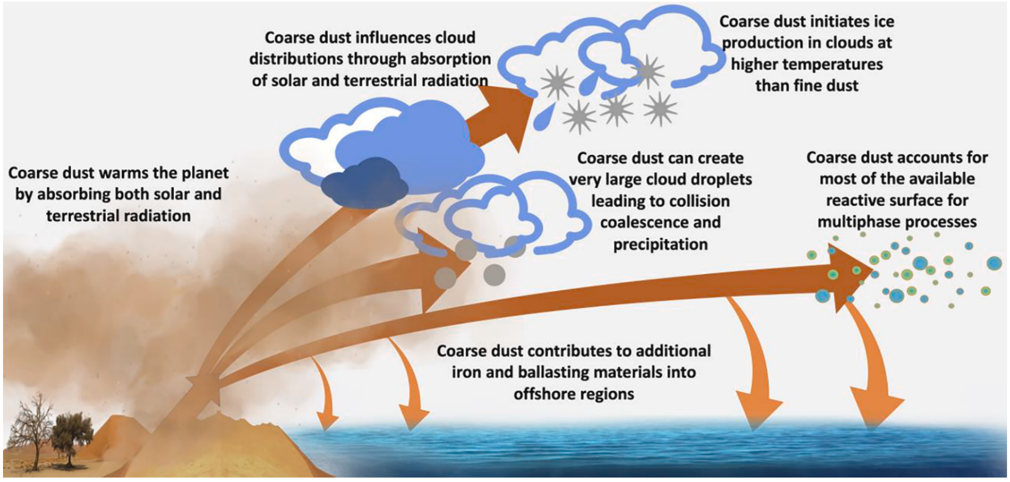

Figure 1.3: Schematic taken from Adebiyi et al. (2023) to illustrate the impacts of coarse dust on the Earth system.

As discussed previously, dust has varying impacts on the Earth's radiative budget. In terms of the SW direct effect of dust on the Earth's radiative budget, the balance between the amount of SW radiation that is scattered or absorbed depends on the particle size. As particle size increases, absorption increases. Coarse and super-coarse particles account for ~75% of SW extinction due to absorption (Adebiyi et al. 2023). Coarser dust has a lower single-scattering albedo (SSA; ratio of scattered radiation to the total extinguished radiation) than fine dust (Kok et al. 2023). As diameter increases, the SSA decreases: submicron dust has an SSA of close to 1, 2 µm dust has an SSA of between 0.9-0.97 and 10 µm dust has an SSA of between 0.75-0.85 (Adebiyi et al. 2023; Tegen and Lacis 1996). Thus, the presence of coarser dust means that the TOA SW effect is less cooling as shown in Figure 1.4b (Adebiyi and Kok 2020). In terms of the LW direct effect, coarse dust accounts for the majority of LW extinction due to its size, with the peak in extinction occurring at ~5 µm. Super-coarse dust has the next largest contribution and fine particles have the least impact.

Both the decreased SW cooling and increased LW warming effects mean that coarser dust has a net warming effect at the TOA (Figure 1.4a). The SW cooling effect of fine dust is great enough that the total DRE of all dust at the TOA is still net cooling (approximately -0.15 ± 0.35 W m^{-2} (Kok et al. 2023)), though much uncertainty remains in this value, partly due to poor understanding of the quantity and atmospheric lifetime of coarse dust.

Induced heating and cooling throughout the atmosphere caused by the coarser dust can encourage the formation of clouds, thus altering the radiative budget (Do-

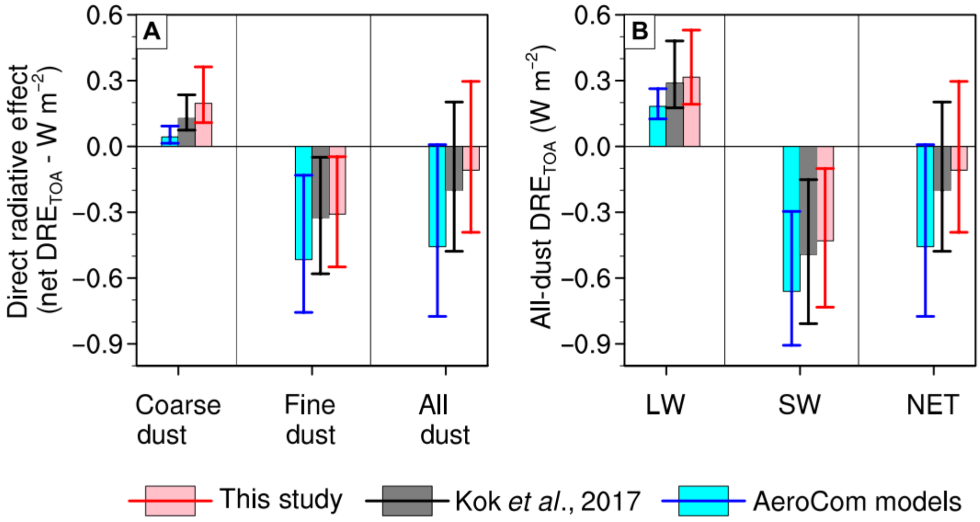

Figure 1.4: Net DRE at TOA in W m^{-2} split by coarse (5-20 µm) and fine (0.1-5 µm) dust fractions (a). DRE at TOA of all dust sizes split by the LW and SW effect, with the net effect shown on the right (b). 'This study' refers to the work in Adebiyi and Kok (2020). The error bars refer to the 95% confidence interval. Plot taken from Adebiyi and Kok (2020).

herty and Evan 2014; Wong et al. 2009). An increase in the ratio of coarse-to-fine dust would inhibit cloud formation due to increased absorption creating atmospheric stability, inhibiting the formation of condensation (e.g. Samset et al. 2016). Although Samset et al. (2016) simulate the heating mechanism by increasing black carbon concentrations, the hypothesis stands regardless of the initial forcing mechanism.

Alternatively, if the dust is in a cloud, it can act as CCN and INPs. In ice clouds, coarser particles are also more likely to activate ice nucleation; at warmer temperatures coarse particles dominate the total fraction of INP (Adebiyi et al. 2023).

Upon deposition, dust particles can provide helpful nutrients to land surfaces and oceans. While coarser particles have a greater potential for nutrient supply due to their greater mass, this also means that they have a reduced time in ocean surface water (Barkley et al. 2021). With iron being one of the most important nutrients in marine ecosystems to come from dust (Boyd and Ellwood 2010; Jickells et al. 2005), if the particles do not contain forms of iron that are readily soluble, then the coarser particles will sink before having released any nutrients.

The above impacts all concern the Earth system, however, coarse particles can also impact the way the dust interacts with the human body (Kotsyfakis et al. 2019). Super-coarse particles ($10 < d < 62.5$ µm) are too large to be transported into the respiratory system, so they mostly impact the skin and eyes, whereas coarse particles (2.5 < d < 10 µm) are respirable and fine (d < 2.5 µm) particles are small enough to enter the bloodstream.

Observations of coarse dust

Until fairly recently, super-coarse and giant particles were assumed to be short-lived in the atmosphere due to their larger mass and consequently greater Stokes' settling velocity, and thus frequently not measured in observational campaigns, and due to difficulties in measuring larger particle sizes due to instrument inlets or pipework in the instrumentation (Rosenberg et al. 2014). However, once campaigns began to measure into this larger size range, it became apparent that these particles were more frequently present and are transported further from the source than expected (e.g. Ryder et al. (2019) and Weinzierl et al. (2017)). Here we will briefly discuss the findings of campaigns such as Fennec, AER-D, SALTRACE, SAMUM, GERBILS and ChArMEx/ADRIMED. Volume size distributions (VSD) from these campaigns are shown in Figure 1.5. The VSD reveals how the volume of the dust population is spread across the measured size range. The calculation needed for the population size distribution was shown in Section 1.1.2.

The Fennec (Ryder et al. 2013b) and Saharan Mineral Dust Experiment (SAMUM; Weinzierl et al. 2009) campaigns both collected data close to the Sahara Desert dust source. The Fennec campaign occurred in June 2011 and was the first to measure particles up to 300 µm diameter in a remote region of the Sahara Desert. Ryder et al. (2019) estimate that 93% of dust mass over the Sahara is made up of particles larger than 5 µm, and 40% is made up of particles > 20 µm. Also close to the Sahara, SAMUM-1 occurred in May-June 2006 in southern Morocco measuring particles up to 100 µm diameter (Weinzierl et al. 2009). Larger particles were also measured during this campaign which led to Ryder et al. (2013b) suggesting that coarser particles were at least more prevalent close to the source than previously anticipated.

The Fennec campaign also collected data at the Canary Islands as part of the same flights which travelled to the Sahara in June 2011 (Ryder et al. 2013a). The location of these measurements mark the next stage in the transport and life cycle of dust as the MBL begins to form below the SAL. Ryder et al. (2013a) observed a 60-90% loss of particles greater than 30 µm more than 12 hours after uplift. The AERosol Properties – Dust (AER-D) campaign, occurring in August 2015, also

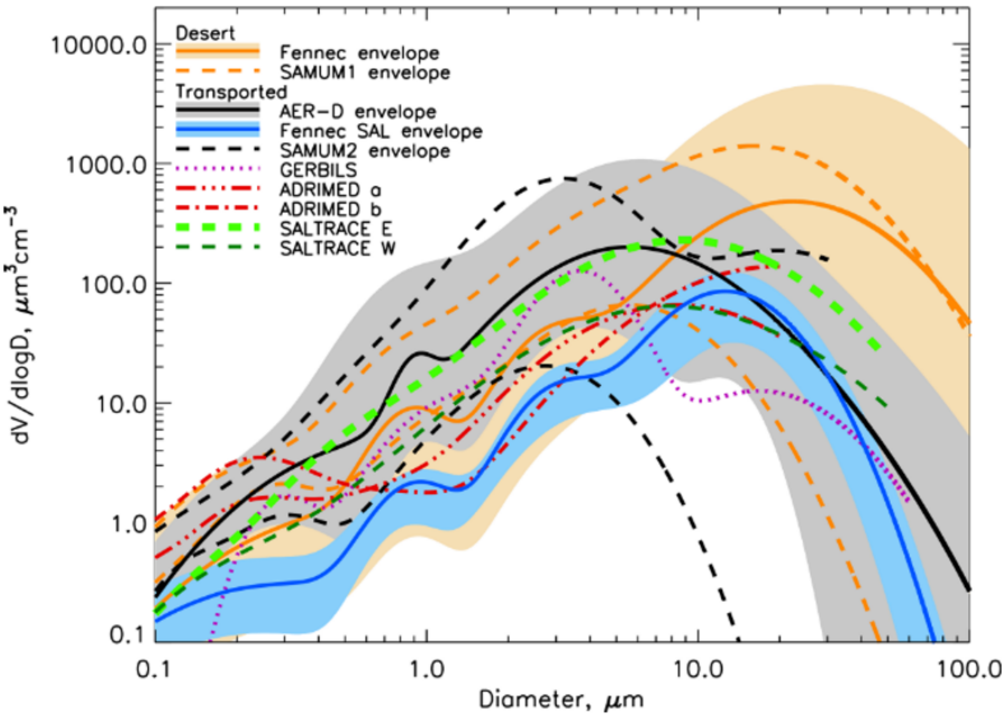

Figure 1.5: Volume size distributions from recent aircraft campaigns measuring Saharan dust at various points throughout long-range transport. Orange measurements were made close to source. ADRIMED a and b represent data taken above and below 3 km, respectively. SALTRACE E and W represent data taken in the East and West Atlantic, respectively. Plot taken from: Ryder et al. (2019).

measured dust up to 100 µm diameter in the SAL and MBL at Cape Verde and the Canary Islands (Ryder et al. 2018). The ChArMEx/ADRIMED (Chemistry-Aerosol Mediterranean Experiment/Aerosol Direct Radiative Impact on the regional climate in the MEDiterranean region) campaign occurred in June-July 2013 and was focused in the Mediterranean (Mallet et al. 2016). This campaign measured up to 32 µm diameter. The SALTRACE (Saharan Aerosol Long-Range Transport and Aerosol–Cloud-Interaction Experiment) aircraft campaign measured dust both at Cape Verde and in the West Atlantic at the Caribbean in June-July 2013 (Weinzierl et al. 2017). Based on Stokes' settling velocity, we would expect to see very few particles > 7 µm diameter reaching the Caribbean, however, the SALTRACE campaign measured a large quantity (Figure 1.5). In all campaigns mentioned and those shown in Figure 1.5, except for GERBILS (Geostationary Earth Radiation Budget Intercomparison of Longwave and Shortwave Radiation)(Haywood et al. 2011) and SAMUM-2 (Ansmann et al. 2017), coarse and super-coarse dust was found in greater quantities than is expected based on the particles large mass (Denjean et al. 2016; Ryder et al. 2013a; Ryder et al. 2018).

GERBILS likely measured aged dust events which showed a depleted volume of coarse particles (Ryder et al. 2019) relative to the other campaigns mentioned here (Figure 1.5). The second observational period of the SAMUM campaign, SAMUM-2, occurred in January-February 2008 at Cape Verde (Weinzierl et al. 2011). As this campaign occurred at a different time of year to the others, it is likely that different meteorological conditions contributed to the smaller volume of coarse particles measured (Ryder et al. 2019; Tsamalis et al. 2013)

This abundance of coarse particles has also been observed in deposition measurements across the Atlantic (van der Does et al. 2018; van der Does et al. 2016). Dust was collected in five submarine deposition buoys spread across the tropical North Atlantic, giant dust particles were found 3500 km west of the African coast, significantly further than allowed by our understanding of the forces acting upon these particles. It should be noted, however, that as these measurements are taken from 1.1-3.6 km below the sea surface, we should not assume that the particles collected in the sediment traps were deposited directly above the traps (i.e. had been transported through the atmosphere to the distance of the trap), as they could have been transported horizontally through the water.

All these campaigns focus on westwards transport of Saharan dust along the trans-Atlantic summertime dust pathway. However, giant dust particles have also been recorded transported elsewhere from the Sahara, including to the Arctic. Varga et al. (2021) found >100 µm dust particles from the Sahara in Iceland during multiple spring-time dust events. Thus, this shows that it is not just conditions occurring during summer which results in the long-range transport of coarse, super-coarse or giant dust particles and that there must be processes which act at different times of the year in different transport pathways which encourage this long-range transport.

Through these observations, we see that coarse, super-coarse and giant mineral dust particles appear more frequently and in greater concentrations than previously thought possible due to their great mass.

1.1.6 Modelling Dust

For a long time, models have been used as a tool to improve our understanding of large-scale processes related to the emission, transport and deposition of dust across the globe.

The emissions are dependent on factors such as the surface winds, land surface properties and vegetation, though it depends on the model as to how these are represented. Dust concentrations in models can be represented by size bins, modal distributions or bulk concentrations. Zhao et al. (2022) shows the various dust size representations by models in the Coupled Model Intercomparison Project 6 (CMIP6) suite, as well as the emissions schemes used.

Challenges

Despite models being an effective tool to better understand dust, there are often many flaws in the ways the dust is modelled, some stemming from our own lack of understanding (as is evidenced by recent research into the coarser size distribution). In part due to a lot of assumptions that have to be made about the dust-related processes in order to reduce computational cost. An assumption that nearly all global climate models (GCMs) make is that the dust particles are perfectly spherical, whereas dust in the real world tends to be fairly aspherical; Huang et al. (2020) found particle length was often 5 times the particle height.

Models often succeed at representing the dust AOD in terms of magnitude and location in comparison to observations. In recent years, this improved modelling of AOD is due to increasing use of data assimilation of AOD satellite retrievals (e.g. Benedetti et al. (2009) and Di Tomaso et al. (2017)). However, these model AODs are often produced by increasing the number of fine dust particles (which AOD calculations are most sensitive to) present in the atmosphere, leading to a fine bias in the dust size distribution (O'Sullivan et al. 2020). Previous research (e.g. Räisänen et al. 2013) has shown that randomly oriented aspherical particles in models have only minor impacts on the SW TOA DRE. Thus, choosing to model spherical particles reduces computational cost, and the biases created can be easily reduced with tuning. However, this tuning leaves gaps in GCMs in relation to how asphericity impacts, for example, gravitational settling, chemical interactions and ice nucleation, which may have further impacts which have not been extensively studied. It should also be noted that the assumption that any aspherical particles are randomly oriented ignores the potential for uniformly oriented particles (caused by electrical charging; Ulanowski et al. 2007).

Additional to this, the fine bias is further exacerbated by the under-representation of coarser particles in models and an over-representation of fine particles (Evan et al. 2014; Kok 2011; Kok et al. 2017). Coarser particles tend to be excluded from GCMs (Zhao et al. 2022) in part to reduce computational cost, but also due to historical assumptions that coarser particles were not abundant or transported over long distances. In the CMIP6 suite, the maximum particle diameter ranges from

0.01 to 63.2 µm. Due to these underestimations of coarser particles, models tend to underestimate dust mass; Ryder et al. (2019) suggested dust mass at the Sahara was underestimated by 5 times in models when compared to observations and Checa-Garcia et al. (2021) discussed issues relating to the misrepresented deposition of dust mass due to incorrect transported size distribution. Ansmann et al. (2017) observed this fine bias increasing with magnitude with distance from the dust source. This is likely associated with another issue which models seem to face; fast removal of coarse particles during transport. Not only do models not appear to emit enough of the coarsest particles, but many studies have observed these coarser particles depleting in quantity at a faster rate in models than in observations (Ansmann et al. 2017; Ratcliffe et al. 2024; Ryder et al. 2019).

Not only do we not fully understand the size distributions of emitted and transported particles, but recently, Emerson et al. (2020) and Mailler et al. (2023) suggested that widely-used dry deposition parameterisations (e.g. by Zhang et al. (2001)) may be incorrect. Mailler et al. (2023) suggest that with the inclusion of the Clift and Gauvin (1971) drag correction coefficient, the settling velocity of 100 µm particles could be reduced by ∼25%.

The issue of vertical transport of dust in models appears in two different manners. Firstly, O'Sullivan et al. (2020) found that a MetUM NWP model often placed dust too low in the model atmosphere; this could be an issue with the meteorology in the model. Alternatively, Ginoux (2003) suggests that numerical diffusion between the vertical layers may result in fast settling of dust particles in the atmosphere.

Due to uncertainty in the mineralogical composition, size and shape of the dust particles, a large amount of uncertainty remains in models over the radiative impacts of dust. Recent research suggests that dust in models may be too weakly absorbing (Adebiyi and Kok 2020; Balkanski et al. 2021; Di Biagio et al. 2020).

1.1.7 Mechanisms to Extend Coarse Dust Lifetime

Coarse particles have been found a greater distances from their source than expected. Recent research has explored the potential mechanisms which could increase the lifetime of coarser particles in the atmosphere, thereby increasing the distance transported. Here, I will discuss the mechanisms which are related to individual particle characteristics, before looking at mechanisms which are more related to meteorology.

As has been mentioned in previous sections, dust particles are fairly aspherical, but tend to be modelled as spherical. However, if asphericity is considered, then the forces on the particle in the atmosphere are different, with higher drag counteracting gravity. Some studies have looked at the impact of including asphericity in their models; Colarco et al. (2014) and Yang et al. (2013) showed that aspherical particles were likely to have a higher mean altitude than spherical particles. Huang et al. (2020) showed that asphericity increased particle lifetime by ∼20% and Saxby et al. (2018) found that asphericity increased transport distance of 100 µm volcanic ash particles by 44%. Asphericity was also found to increase in-plume heating by up to 20% (Otto et al. 2011), which could increase mixing within the plume, raising coarse dust higher, thus transporting it further.

Dust plumes often tend to carry some level of electric charge (e.g. Harrison et al. (2018); Méndez Harper et al. (2022)) and this charging is another suggested mechanism to increase coarse particle lifetime. The process of particles continuously hitting into each other, both at emission and during transport, to create an electric charge is known as triboelectrification (van der Does et al. 2018). This charging of the particles has been shown in real-world (Renard et al. 2018) and laboratory (Toth III et al. 2020) settings to keep coarser particles suspended higher and for longer in the atmosphere during transport. Nicoll et al. (2020) clarifies that the charging of a particle can be dependent on both its size and mineralogy, with larger particles charging positively and quartz particles more likely experiencing charging. Méndez Harper et al. (2022) estimate that 10 µm particles experience the greatest change in atmospheric lifetime due to charging.

It is worth noting at this stage that particle charging will likely orient an aspherical particle in the direction whereby its longest axis is placed vertically (Ulanowski et al. 2007), thereby nullifying the effect of the asphericity on settling velocity. Mallios et al. (2020) assessed the importance of aspherical particle orientation and found that horizontally oriented particles had a longer atmospheric lifetime than vertically oriented particles. Thus, it is unlikely that these mechanisms can work in unison to further increase the lifetime of the particles. For example, the coarsest particles found at buoys placed in the Atlantic were fairly spherical and predominantly made up of quartz (van der Does et al. 2018), suggesting that charging could have been the dominant mechanism of the two discussed so far.

Next, I will think about meteorological-scale processes which impact the dust from emission to deposition. Shortly after emission, dust plumes that encounter raised topography may experience additional lifting of particles. Heisel et al. (2021)

and Rosenberg et al. (2014) found that topography enhanced the upward transport of super-coarse dust particles into the BL, where they are able to interact with larger scale motions in the free atmosphere, increasing the possibility of longer range transport.

Turbulence in the atmosphere acts in both an upwards and downwards motion on dust particles (Garcia-Carreras et al. 2015). Denjean et al. (2016) found in data from the ChArMEx/ADRIMED campaign that turbulent updraft and downdraft motions could have been enhancing coarse particle lifetime. They observed updrafts an order of magnitude greater than the settling velocity of particles ∼8 µm in diameter. Cornwell et al. (2021) found emitting modelled particles into a more turbulent atmosphere increased the mass of coarse particles at height.

Larger scale vertical mixing has also been proposed as a mechanism which could increase the atmospheric life of dust (Gasteiger et al. 2017; Takemi 2005; van der Does et al. 2018; Xu et al. 2018). Gasteiger et al. (2017) suggest that repeated diurnal convective mixing in the SAL could increase the lifetime of coarse dust. Moist convective cells can mix dust up beyond the top of the SAL. Though they are more susceptible to wet deposition in these systems, satellite observations have shown that the particles can escape at high altitudes, creating a pathway for long-range transport. However, van der Does et al. (2018) suggest that this mechanism of lifting the particles above the SAL repeatedly would deplete the concentration of coarse particles transported long distances by too much to correspond to concentration observations based on research by Sauter and L'Ecuyer (2017).

It is proposed that self-lofting of dust as a result of in-plume heating can lift dust to higher altitudes, potentially increasing the lifetime (Colarco et al. 2014). New evidence to suggest that dust could be more absorbing than previously thought (based on coarser size distributions and varying particle mineralogy) suggests that dust plumes could be experiencing more internal heating than previously thought (Di Biagio et al. 2020). Plus, increased radiative heating in the lower SAL from lower water vapour content can increase atmospheric heating by 17% (Ryder 2021). This heating in the atmosphere has the potential to modify the atmospheric stability, potentially encouraging and/or sustaining turbulence (van der Does et al. 2018).

Despite the existence of potential mechanisms to increase coarse particle lifetime, many of them are not strong enough individually to enable the long-range transport of coarser particles seen in observations. Thus, we may expect a combination of these mechanisms, or additional mechanisms not yet considered to be the cause.

Improving model representation compared to observations

Some studies have changed certain model parameters as a proxy to represent the previously mentioned poorly understood mechanisms for increasing coarse particle lifetime. These changes have resulted in an improvement in the model's performance in comparison with observations. Huang et al. (2020) suggest reducing the dust settling velocities by 13%. By decreasing settling velocities of dust by 40-80%, Drakaki et al. (2022) improved the model representation of dust size distributions over the Sahara and Eastern Atlantic. This change in deposition velocity is not realistic or related to a specific mechanism, but rather suggests that the dry deposition velocity is being counteracted by a mechanism or group of mechanisms by up to 80% of the downwards force. Similarly, Meng et al. (2022) reduced the particle density from 2500 kg m^{-3} to 125-250 kg m^{-3} and the settling velocity by 13% (in accordance with Huang et al. (2020)) to achieve an improved modelled dust mass concentration near the Sahara. Despite this order of magnitude change, the dust volume in outflow regions was still underestimated in the model compared to observations. Alternatively, Maring et al. (2003) found that by adding an upward velocity of 0.33 cm s^{-1} to dust Stokes' settling velocities in a model, they were able to bring a model into line with observations.

The following research has looked into the effect of better representing turbulent mixing in a model on the long-range transport of dust. Cornwell et al. (2021) found that by emitting particles later in the day in a model, they were able to increase the rate at which the particles reached cloud level. A midday release of 10 µm particles led to a 700% increase of these particles remaining above 1500 m by the end of the simulation. Approximately 50% of dust uplift at the Sahara occurs at night (Marsham et al. 2013). If a model was found to be emitting a large proportion of dust at night, this could inhibit its vertical transport and therefore its atmospheric lifetime. With high temporal resolution observations, the diurnal cycle of emissions compared to a model could be analysed as the models could be releasing particles at the wrong time of day, hindering particle altitude and thus, atmospheric lifetime. Finally, in a promising study, Rodakoviski et al. (2023) show that coarse particle lifetime can be increased by up to a factor of 2 when modelling eddy motion in a large-eddy simulation (LES) model, resulting in improved modelled long-range transport of super-coarse dust.

Attempts to replicate observed long-range coarse particle transport in models generally find that particle characteristics or settling velocities have to be reduced by unrealistic amounts to produce results vaguely resembling observations. Experiments such as that by Rodakoviski et al. (2023) which are conducted in high resolution, expensive simulations are more realistic, potentially suggesting that the coarse resolution and parameterisations included in GCMs may not be capable of representing long-range coarse dust transport due to complicated sub-grid scale processes.

1.2 Objectives of This Work

The overarching aim of this thesis is to improve our understanding of long-range transport of coarse mineral dust particles and to better understand why models are unable to achieve such transport. To achieve this, I will focus on three separate research questions which I will tackle in three chapters of work. The research questions are as follows:

1. How does dust size distribution evolve over long-range transport in both observations and a climate model?

2. How sensitive are coarse dust particles to different transport and deposition processes in the model?

3. Does plume altitude at the Sahara impact coarse particle transport?

1.3 Thesis Outline

Chapter 2 is a methodology containing a description of the Met Office Unified Model configuration (HadGEM3-GA7.1) which is used throughout this thesis. The dust scheme used in the model will also be discussed thoroughly. Chapter 3 contains an evaluation of the representation of dust size distribution evolution over long-range transport in the HadGEM3-GA7.1 model against aircraft observations. Chapter 3 also contains a detailed methodology of the observational datasets used within this thesis. Chapter 4 contains the relevant methodology and results from a series of sensitivity studies on the model. Chapter 5 contains the relevant methodology, results and discussion of a set of model experiments testing the sensitivity of coarse particle transport to release altitude at the Sahara. Finally, Chapter 6 presents an overview of the conclusions from the previous three Chapters, an in-depth discussion of the results and suggestions for future research.

Chapter 2

Dust in the Met Office Unified Model

In this Chapter, the climate model used in this thesis will be introduced, the simplifications of theory implemented in the model will be explored, and finally, the complexities of comparing between observations and models will be discussed.

A Hadley Centre Global Environment Model 3 (HadGEM3-GA7.1) (Mulcahy et al. 2020; Walters et al. 2019) configuration of the Met Office Unified Model (MetUM) run at version 10.7 is used here. Throughout this thesis, varying setups of the same model are used for different purposes. Here, the setup and parts of the model that are relevant to this thesis and remain consistent throughout will be discussed. Chapters 4 and 5 will contain a short methodology of changes to the model specific to the work of that chapter. Chapter 3 Section 3.2.2. contains some overlap with this Chapter as it is a journal article and thus contains largely similar information although more detail has been included here for the purpose of this thesis.

2.1 MetUM Introduction

HadGEM3-GA7.1 is an atmosphere-only global climate model (GCM) which contributed to the Coupled Model Intercomparison Project phase 6 (CMIP6). As an atmosphere-only configuration, the atmosphere is not coupled with the ocean; instead prescribed sea surface temperatures (SSTs) and sea ice concentrations are used (Eyring et al. 2016). The model uses a horizontal grid resolution of 1.875° longitude x 1.25° latitude (sometimes referred to as N96). This is the coarsest resolution available in the HadGEM3 setup corresponding to a grid box width of ~210 km at the equator. In the vertical, the model has 85 model levels which increase in depth with height so that 29 of which are concentrated below 6 km altitude. At this resolution, the model has a 20-minute time step. Some of the key parameterisations used in the atmosphere-only HadGEM3-GA7.1 configuration are shown in Table 2.1.

	Documentation
Dynamics	Wood et al. (2014)
Clouds	Morcrette (2012), Van Weverberg et al. (2016), and Wilson et al. (2008)
Precipitation	Wilson and Ballard (1999)
Convection	Gregory and Rowntree (1990) and Lock et al. (2000)
Radiation	Edwards and Slingo (1996) and Manners et al. (2015)

Table 2.1: Main parameterisation schemes used in the HadGEM3-GA7.1 setup (Walters et al. 2019).

Dust is modelled in HadGEM3-GA7.1 using the Coupled Large-scale Aerosol Simulator for Studies in Climate (CLASSIC) scheme, as described in Woodward (2001) and Woodward et al. (2022). The dust is mixed externally with other aerosols, which are simulated in the United Kingdom Aerosols and Chemistry (UKCA) Global Model of Aerosol Processes (GLOMAP-mode) scheme (Bellouin et al. 2013). The dust interacts with radiation (Section 2.5) and ocean biogeochemistry via the Model of Ecosystem Dynamics, nutrient Utilisation, Sequestration and Acidification (MEDUSA) scheme. In this atmosphere-only configuration, MEDUSA is not used and so will not be discussed further. The dust cannot act as cloud condensation and ice nuclei or chemically interact with the model.

Dust is simulated in terms of its mass mixing ratio (kg of dust per kg of air), this has been converted here to a mass concentration of dust using the air density calculated from the model's temperature and pressure at each model level.

2.2 Dust Emission

At each model time step, dust emissions are calculated interactively using the friction velocity, soil moisture, and soil particle size distribution with the models land surface and vegetation modelling. The emissions are calculated by using the horizontal flux of dust (G) in nine size bins between 0.0632-2000 µm diameter. G is then used to calculate the vertical flux of dust (F) transported into the atmosphere in six size bins up to 63.2 µm diameter. A fraction of these particles are deposited to the ground within the same time step as that in which they are lofted. The representative diameter (D_{rep}) of each size bin is used in calculating the emitted size distribution and the particle settling velocity. All nine size bins are shown in Table 2.2 with their diameter size ranges, D_{rep}, dry threshold friction velocity (U^*_{td}) and wet deposition scavenging coefficient for the relevant size bins.

Table 2.2: Size range, representative diameter (D_{rep}), dry threshold friction velocity (U^*_{td}) and wet scavenging coefficient (Λ) of the modelled mineral dust size bins in the CLASSIC aerosol scheme described in Woodward (2001). D_{rep} is shown for the 6 transported size bins. Within each size bin, $dV/dlog(r)$ is assumed constant, where V is particle volume and r is particle radius.

Bin number	Bin diameter range (µm)	Representative diameter (D_{rep}; µm)	Dry threshold friction velocity (U^*_{td}; m s^{-1})	Scavenging coefficient (Λ)
1	$0.0632 \leq$ d < 0.2	0.112	0.85	2×10^{-5}
2	$0.2 \leq$ d < 0.632	0.356	0.72	2×10^{-5}
3	$0.632 \leq$ d < 2	1.12	0.59	3×10^{-5}
4	$2 \leq$ d < 6.32	3.56	0.46	6×10^{-5}
5	$6.32 \leq$ d < 20	11.2	0.33	4×10^{-4}
6	$20 \leq$ d < 63.2	35.6	0.16	4×10^{-4}
7	$63.2 \leq$ d < 200		0.14	
8	$200 \leq$ d < 632		0.18	
9	$632 \leq$ d < 2000		0.28	

G and H are calculated using the method described in Marticorena and Bergametti (1995)(in kg m^{-2} s^{-1}). Threshold friction velocity (U^*_t; in m s^{-1}) from Bagnold (1941) with a correction for soil moisture based on the soil clay fraction (F_c) and the method in Fecan et al. (1998) are used. G is calculated in each size bin, i, as in Woodward et al. (2022)

$$G_{(i)} = \rho_a B U^{*3}(1 + \frac{U^*_{t(i)}}{U^*})(1 - (\frac{U^*_{t(i)}}{U^*})^2)\frac{M_{(i)}CD}{g} \tag{2.1}$$

where ρ_a is the air density (in kg m^{-3}), B is the bare soil fraction in the grid box depending on the land surface, U^* is the surface layer friction velocity (in m s^{-1}), $M_{(i)}$ is the ratio of dust mass in the size division i to the total mass based on soil clay, silt and sand fractions, C is a constant of proportionality (set to 2.61 based on wind-tunnel experiments by White (1979)) and g is the acceleration due to gravity (in m s^{-2}). D is a dimensionless tunable parameter; i.e. a coefficient that can be varied to improve model representation. M is calculated from the soil clay, silt and sand fractions. The ratio of U^* to U^*_t and M therefore act together to calculate the emitted size distribution, with U^*_t being dependent on particle size using D_{rep} values from Table 2.2.

$$U^*_t = I\log_{10}(D_{rep}) + J\omega + L \tag{2.2}$$

where ω is the volumetric soil moisture and I, J and L are determined constants.

The emissions are tuned using three dimensionless parameters: D, k_1 and k_2. These represent a global multiplier to the horizontal dust flux, a friction velocity multiplier and a top level soil moisture multiplier, respectively. Tuning is carried out to improve agreement between the model with observations of AOD, near-surface dust concentrations and dust deposition rates (Woodward et al. 2022). In the CMIP6 configuration of HadGEM3-GA7.1, the three parameters are set as D=2.25, k_1=1.45 and k_2=0.5.

As the model calculates variables for whole grid boxes and full time steps, as opposed to instantaneous point sources which were used to derive Equation 2.1, U^* is adjusted to correct for the spatial and temporal averaging. The model value (U^*_M) and k_1 are used to calculate U^*

$$U^* = k_1 U^*_M \tag{2.3}$$

In dry conditions, a dry threshold friction velocity (U^*_{td}) applies, the values of which were obtained by Bagnold (1941) (values in Table 2.2). When the soil is moist, U^*_t is related to U^*_{td} by

$$\begin{gathered}
\frac{U^*_t}{U^*_{td}} = 1 \text{ for } \omega < \omega' \\
\frac{U^*_t}{U^*_{td}} = (1 + 1.21(\omega - \omega')^{0.68})^{0.5} \text{ for } \omega > \omega' \\
\omega' = 0.14F_C^2 + 17.0F_C
\end{gathered} \tag{2.4}$$

where ω' is the minimum soil moisture for which the erosion threshold increases. The final tunable parameter, k_2 is used in the calculation of ω.

$$\omega = k_2 \omega_1 \tag{2.5}$$

where ω_1 is the grid box mean soil moisture in the top soil level (in kg m^{-2}). The above works in arid and semi-arid regions. Additional derivation is required for moister soil, though as I focus on the Sahara in this thesis, I will not discuss this further.

According to Marticorena and Bergametti (1995) and based on the measurements from Gillette (1979), the size distribution in G follows on from the equivalent size bins of F. F is given in each of the first six size bins by

$$F_{(i)} = 10^{(13.4F_c - 6.0)} G_{(i)} \frac{\Sigma_{i=1,9}(G_{(i)})}{\Sigma_{i=1,6}(G_{(i)})} \tag{2.6}$$

2.3 Mixing of Dust in the Atmosphere

Convective mixing in the model occurs in the presence of a positive buoyant surface flux (Lock et al. 2000). Parameterised convective mixing is responsible for both upwards and downwards movements of dust through the model atmosphere and is based on the mass flux scheme of Gregory and Rowntree (1990), with additions of downdrafts (Gregory and Allen 1991) and convective momentum transport. This is a larger scale process than the turbulent mixing.

Turbulent mixing in the model's atmosphere plays a role in the dry deposition of dust near the surface. Turbulent mixing is parameterised as a first-order closure scheme in HadGEM3-GA7.1 (Lock et al. 2000), with additions from Brown et al. (2008) and Lock (2001). As Walters et al. (2019) explains, turbulent mixing can be triggered in two regions in an unstable model profile: the surface (caused by surface heating and wind shear) and cloud-tops (caused by radiative and evaporative cooling). The resultant turbulent mixing acts as a function of height within the boundary layer. Mixing at the top of the boundary layer is via an entrainment parameterisation, meaning that turbulent mixing is seen throughout the depth of the boundary layer and extending just above. Turbulent mixing is a smaller scale process than the convective mixing.

2.4 Dust Deposition

Dust can be deposited by either dry or wet deposition in the model. Both are given as a mass flux in kilograms per metre squared per second (kg m^{-2} s^{-1}). Wet deposition is calculated first in a model time step, followed by dry deposition. The order of this is constrained by a dependence on the ordering of different routines throughout the UM.

2.4.1 Dry deposition

Dust can be deposited to the model surface by either gravitational settling or turbulent mixing. Dry deposition occurs from the two lowest model levels to the surface (0-36 m and 36-76 m) in one time step (20 minutes). The total dry deposition velocity (V_D) is represented using an inverse resistance analogue method (Seinfeld 1986), given by Equation 1.8 in Section 1, repeated here

$$V_D = (R_A + R_B + R_A R_B V_S)^{-1} + V_S$$

In this equation, V_S is responsible for the gravitational settling, while resistances R_A and R_B are used in representing the turbulent mixing of dust. Thus, both deposition by gravitational settling and turbulent mixing are calculated at the same time in the model. V_S is used to calculate the downward flux of dust, as was shown in Section 1.1.2 Equation 1.13 and is taken from Pruppacher and Klett (2010)

$$V_{S(i)} = \frac{{D_{rep(i)}}^2 g \rho_p C_c}{18.0 \mu_{air}}$$

where D_{rep} is the representative diameter (size bin values in Table 2.2; in µm), ρ_p is the particle density (in g m^{-3}), C_c is the Cunningham correction factor (calculated using Equation 1.14), and μ_{air} is the dynamic viscosity of air (in Pa s^{-1}).

2.4.2 Wet deposition

Wet deposition of dust is given by the impaction scavenging of dust below-cloud and up to the cloud-top. Wet deposition is decomposed into two diagnostics: wet deposition by convective precipitation and by large-scale precipitation. In the model, due to the ordering of routines, the removal of dust due to large-scale precipitation occurs first, followed by the convective precipitation removal. In this thesis, these two methods of wet deposition will be collated and treated as one. Removal by both convective and large-scale precipitation are calculated in the same way. The rate of impaction scavenging is controlled by a dimensionless scavenging coefficient (Λ), the precipitation rate (R), and dust concentration (C) using the equation,

$$\frac{\delta C_{(i)}}{\delta t} = -\Lambda_{(i)} R C_i \tag{2.7}$$

The values of Λ for each size bin, i, are shown in Table 2.2 and generally increase with particle diameter. These values are based on experimental measurements by Volken and Schumann (1993) and have more recently been corroborated by Laakso et al. (2003). More information on the impaction scavenging scheme is given in Jones et al. (2022).

2.5 Radiative Effect of Dust

Dust interacts directly with radiation in the shortwave and longwave spectral regions of the model. This means the dust can alter aspects of the model such as wind and temperature profiles, and dust emissions by heating and cooling of the atmosphere. Each dust division is treated independently by the radiation scheme, with the model having prescribed values for the absorption, scattering and asymmetry parameter of each size bin in six and nine different spectral bands for the shortwave and longwave, respectively. The radiative properties are calculated from Mie theory and assume that the particles are spherical. The refractive indices of dust are provided in Table 2 in Woodward (2001).

The interaction of dust with radiation can be turned off in the model which allows two simulations with different dust distributions to follow the same evolution in meteorology, as interactions with radiation are the only way for dust to interact with the model here. Doing so removes changes in meteorology due to internal variability, allowing for a clearer comparison between simulations. This has been done for most simulations in Chapter 4 and all simulations in Chapter 5. Clarity will be provided in each chapters methodology as to whether radiative effects have been removed or not.

2.6 Comparing Between Models and Observations

In order to assess the skill of the model, we need to understand the physical, dynamical and possibly chemical mechanisms that influence dust in the real world using in-situ observations. As explained in Chapter 1 Section 1.1.4, aircraft observations are a vital resource which can be incredibly useful for assessing model representation. In this thesis, I analyse observations taken during three aircraft campaigns sampling the summer Saharan trans-Atlantic dust plume at various locations during long-range transport of dust. The Fennec, AER-D and SALTRACE campaigns provide in-situ observations at the Sahara, Canary Islands, Cape Verde and the Caribbean. I refer to the results from these campaigns throughout the thesis, however, the results are dominantly discussed in Chapter 3 which also contains methodology associated with the observations.

Comparisons between observations and models are fairly difficult for many reasons, including differences in both temporal and spatial scales. For example, at points in this thesis I compare the monthly mean output of a climate model to aircraft observations which cover as little as 45 hours over a 10 day period. I have carried out work to assess how representative of normal conditions the campaigns are, and if not, whether any bias in data collection is large enough to skew my results. I discuss this more in Chapter 3. I have additionally ensured that when using the model to use a long average to cover a sufficiently large degree of variability. In Chapter 3 Section 3.3, I found that five model June months contained enough variability in the AOD to produce a mean representative of 'normal' model conditions. In Chapter 4 Section 4.1, it was deemed that a longer average of 20 model June months was required to fully assess the impact of the experiments carried out.

Chapter 3

Evaluation of the Met Office Unified Model Against Aircraft Observations

Preface

This chapter has been published at the Copernicus journal, Atmospheric Chemistry and Physics (Ratcliffe et al. 2024). The introduction and methodology in this paper may contain material repeated from Chapters 1 and 2.

Author contributions: 90% of the work in this paper is contributed to by Natalie Ratcliffe (NGR). NGR carried out the analysis and wrote the paper. NGR, CLR and NB designed the research. All authors discussed the methodology and results. BW, LMW, JG and MD provided the SALTRACE data. All authors read and commented on the paper.

Abstract

Coarse mineral dust particles have been observed much further from the Sahara than expected based on theory. They have impacts different to finer particles on Earth's radiative budget, as well as carbon and hydrological cycles, though they tend to be under-represented in climate models. We use measurements of the full dust size distribution from aircraft campaigns over the Sahara, Canaries, Cabo Verde and Caribbean. We assess the observed and modelled dust size distribution over long-range transport at high vertical resolution using the Met Office Unified Model, which represents dust up to 63.2 µm diameter, greater than most climate models. We show that the model generally replicates the vertical distribution of the total dust mass but transports larger dust particles too low in the atmosphere. Importantly, coarse particles in the model are deposited too quickly, resulting in an underestimation of dust mass that is exacerbated with westwards transport; the

20–63 µm dust mass contribution between 2 and 3.7 km altitude is underestimated by factors of up to 11 in the Sahara, 140 in the Canaries and 240 in Cabo Verde. In the Caribbean, there is negligible modelled contribution of d > 20 µm particles to total mass, compared to 10% in the observations. This work adds to the growing body of research that demonstrates the need for a process-based evaluation of climate model dust simulations to identify where improvements could be implemented.

3.1 Introduction

Every year, 400–2200 Mt of mineral dust is lifted from Earth's surface and becomes suspended in the atmosphere (Huneeus et al. 2011). This lofted dust can alter the global radiation budget by directly reflecting and absorbing radiation (Kok et al. 2018) and altering cloud properties (Lohmann and Feichter 2005; Price et al. 2018) and precipitation patterns (Rosenfeld et al. 2008) by activating ice and liquid droplet nucleation. Shao et al. (2011) estimate that 75% of the uplifted dust is deposited on land, providing important nutrients to locations such as the Amazon rainforest (Prospero et al. 2020) as well as altering the surface albedo upon deposition, for example on snow and ice (Dumont et al. 2020; Painter et al. 2007). The remaining dust supplies valuable nutrients to nutrient-poor oceans, potentially resulting in the formation of phytoplankton blooms (Dansie et al. 2022; Jickells et al. 2005). Lofted dust also negatively impacts aviation (Nickovic et al. 2021), energy production (Piedra et al. 2018) and human health (Kotsyfakis et al. 2019). Many of these processes are sensitive to particle size.

Coarse (2.5 < d < 10 µm), super-coarse (10 < d < 62.5 µm) and giant (d > 62.5 µm) dust particles (size ranges as reviewed and defined in Adebiyi et al. (2023)) have vastly different impacts on the Earth system than fine (d < 2.5 µm) particles. The lifetime of dust in the atmosphere decreases exponentially with increasing particle diameter (Kok et al. 2017). Sedimentation varies strongly with particle size and dominantly affects super-coarse and giant particles (Foret et al. 2006). The larger particles are also more susceptible to wet deposition processes as they are efficient in-cloud nucleators of ice (Adebiyi et al. 2023; Hoose and Möhler 2012; Pruppacher and Klett 2010; Sassen et al. 2003) and, after undergoing in-cloud chemical processing, liquid water (Karydis et al. 2011; Nenes et al. 2014). Coarser particles are also more likely to be removed by below-cloud scavenging (Jones et al. 2022). Coarser particles decrease the amount of outgoing longwave radiation at the top of the atmosphere (TOA) and increase shortwave absorption in the atmosphere, both of which cause a net warming effect at the TOA (Kok et al. 2018). Larger particles also contain a greater mass of the nutrients which provide vital sustenance for the biosphere (Baker et al. 2006; Barkley et al. 2021; Dansie et al. 2017). Simulating the lifetime and transport range of differently sized dust particles in models is therefore key to capturing their various effects and impacts.

Recent field campaigns have revealed that coarse, super-coarse and giant particles are transported further across the Atlantic from the Sahara than expected, given their estimated deposition velocity and amount of time in transit (Denjean et al. 2016; Ryder et al. 2019; Ryder et al. 2018; van der Does et al. 2016; Weinzierl et al. 2017). The processes responsible for this unexpected long-range transport are unclear. Additionally, many global climate models (GCMs) do not represent super-coarse or giant particles and fail to represent the mass concentration of coarse particles at any stage of transport (Adebiyi and Kok 2020; Ansmann et al. 2017; Huang et al. 2021; O'Sullivan et al. 2020). Ryder et al. (2019) estimate that by not representing these particles, dust mass over the Sahara in GCMs is underestimated by up to a factor of 5. The lack of representation of coarser dust particles in GCMs means that they may simulate a direct radiative effect (DRE) forcing that is too small in the longwave (positive DRE) and too negative in the shortwave (negative DRE) (Adebiyi and Kok 2020; Kok et al. 2017) and therefore are too negative in total forcing (shortwave plus longwave). By representing particles up to 20 µm, Adebiyi and Kok (2020) estimate that the dust DRE at the TOA in AeroCom models (currently in the range of -0.78 to -0.03 W m^{-2}) would be shifted to approximately -0.4 to $+0.3$ W m^{-2}, meaning that dust could have a net warming or cooling impact on climate.

By comparing observations to model simulations, previous studies have been able to evaluate the representation of dust size distribution at various points throughout the dust life cycle. Ansmann et al. (2017) found that several dust numerical weather prediction (NWP) forecasts were accurate up to 2000 km west of the coast of Africa, but, beyond this, rapid dust removal reduced the quality of the forecast in terms of the total dust mass concentration and 500–550 nm extinction coefficient. Dust-related processes in models are often tuned so that the modelled aerosol optical depth (AOD) matches observed AODs retrieved by satellite instruments. O'Sullivan et al. (2020) show that observations from a campaign obtaining in situ and remote sensing measurements over the eastern Atlantic agreed with an NWP forecast and a reanalysis output in terms of the AOD but struggled to show the correct vertical and horizontal distribution of coarser particles. By tuning models to AOD, a fine bias is often created in the dust size distribution to compensate for the under-represented (or absent) coarser particles.

Some studies have shown that altering certain fixed parameters in the model, such as settling velocity or particle density, can improve model agreement with observations. Drakaki et al. (2022) found that decreasing the settling velocities of dust in the model by 40%–80% produced good agreement of the size distribution with in situ aircraft observations over the Sahara and the eastern Atlantic. By reducing the settling velocity (by 13% in line with suggestions by Huang et al. (2020) and lowering the dust particle density from 2500 to between 125 and 250 kg m^{-3}, Meng et al. (2022) were able to improve model agreement with observations in terms of the super-coarse-particle volume near the Sahara, though the dust volume was still underestimated in dust outflow regions. These significant, order-of-magnitude changes to particle density and settling velocity are not representative of realistic uncertainties in these variables or processes and instead act as a proxy for representing poorly understood processes which can potentially impact particle lifetime, such as electric charging (Méndez Harper et al. 2022; Renard et al. 2018; Toth III et al. 2020; van der Does et al. 2018), asphericity (Colarco et al. 2014; Huang et al. 2020; Huang et al. 2021; Mallios et al. 2020; Saxby et al. 2018; Yang et al. 2013), turbulence (Denjean et al. 2016; Rodakoviski et al. 2023), topography (Heisel et al. 2021; Rosenberg et al. 2014) and vertical mixing (Cornwell et al. 2021; Gasteiger et al. 2017). Nowottnick et al. (2010) found that an improvement of wet scavenging processes in a model improved coarse particles' lifetime.

The Fennec (Ryder et al. 2013a, 2015; Ryder et al. 2013b), AERosol properties – Dust (AER-D) (Ryder et al. 2018), and Saharan Aerosol Long-range Transport and Aerosol-Cloud-Interaction Experiment (SALTRACE) (Weinzierl et al. 2017) airborne campaigns measured vertically resolved size distributions at four locations between the Sahara and Caribbean and thus represent observations at different stages in the long-range trans-Atlantic transport of Saharan dust. These campaigns measured the full size range of lofted mineral dust particles using open-path wing probes, unlike many previous campaigns which assumed the transport of coarser particles to be minimal. They therefore did not substantially measure into the coarse, super-coarse or giant size range, or measurements of coarser particles were restricted by sampling constraints due to instrument inlets and pipework (Rosenberg et al. 2014; Ryder et al. 2019). This study is the first time that these three campaigns will have been analysed together, in particular taking the vertical distribution of dust size into account. In order to better understand the ability of models to simulate dust transport and deposition, these campaigns will be analysed and compared to a Met Office Unified Model (MetUM) climate simulation (HadGEM3-GA7.1) (Walters et al. 2019). HadGEM3-GA7.1 includes a representation of coarse dust particles up to 63.2 µm in diameter, a notably larger upper size limit than other models which tend to cut off the represented dust size distribution at ∼20 µm (Huneeus et al. 2011; Mahowald et al. 2014; Zhao et al. 2022). The HadGEM3-GA7.1 dust simulation has not yet been extensively compared with in situ airborne observations. The campaigns and model have not had their vertically resolved dust size distribution evolution assessed in such detail before and over such a large spatial extent, representing the vertically resolved size distribution evolution over long-range transport. (O'Sullivan et al. 2020) suggest that the earlier MetUM NWP GA6.1 configuration (notably different with dust represented by two size bins) often places dust too low in the atmosphere, over the eastern Atlantic, which we investigate in this study.

This study aims to gain a more in-depth insight into the systematic biases between modelled and observed size distributions and how those biases evolve during transport. Such assessments of model performance are crucial in guiding improvements to the model representation of mineral dust transport and deposition.

In Sect. 3.2, we introduce the aircraft campaigns, the model setup used in this study and our methodology for the analysis. In Sect. 3.3, we investigate the relationship between the coarser-dust size distribution and the AOD in the aircraft observations. In Sect. 3.4, we present and discuss our results, analysing the vertical dust structure, size distribution and concentration evolution across the Atlantic in the model and observations. In Sect. 3.5 we summarise and present conclusions.

3.2 Methods

3.2.1 Aircraft Observations

The vertically resolved in situ aircraft observations used in this study were taken during scientific flights in the Sahara, the Canary Islands, Cabo Verde and the Caribbean during the Fennec, AER-D and SALTRACE campaigns. Figure 3.1 shows the location of the observations (flight tracks) used in this study. All aircraft observations are presented at ambient conditions. The Fennec and AER-D campaigns made use of the Facility for Airborne Atmospheric Measurements (FAAM) BAe-146 aircraft and instruments (Ryder et al. 2013a; Ryder et al. 2018; Ryder et al. 2013b), while the SALTRACE campaign used the Deutsches Zentrum für Luft- und Raumfahrt (DLR) Falcon aircraft and instruments (Weinzierl et al. 2017). The following two sections describe these two different aircraft and instrumentation setups.

Henceforth all aerosol sizes will be given in diameters.

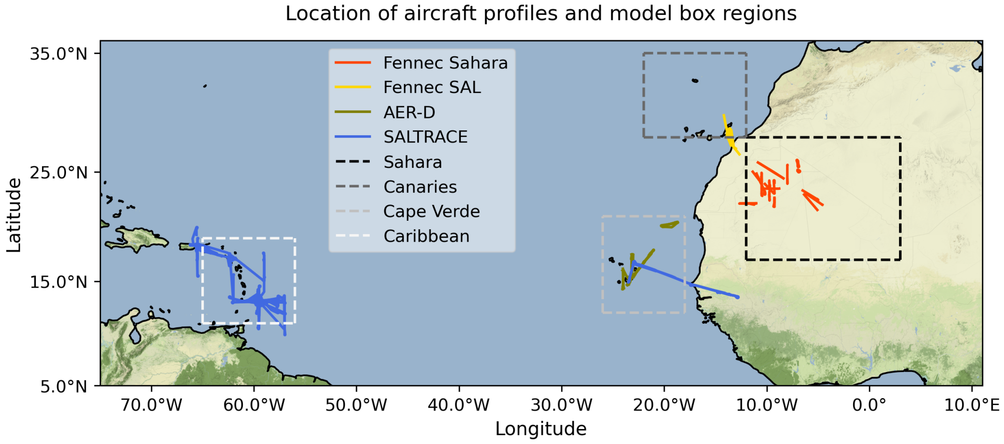

Figure 3.1: Location of the vertical profiles measured during the Fennec and AER-D campaigns, as well as the flight paths followed during the SALTRACE campaign (solid lines), and box regions used for analysis of the model data (dashed lines).

FAAM BAe-146 Aircraft Setup

The Fennec campaign took place in June 2011, flying over a remote region of the Sahara (Mauritania and Mali), as well as over the Canary Islands (Fig. 3.1; Fennec Sahara and Fennec SAL, respectively). This campaign therefore provides data at two separate locations: firstly over the desert close to dust sources (Fennec Sahara) (Ryder et al. 2013b) and secondly as the Saharan air layer (SAL) forms over the marine boundary layer (MBL) between the western coast of Africa and the Canary Islands (Fennec SAL) (Ryder et al. 2013a). In total, 41 vertical profiles were conducted during the Fennec campaign: 20 over the Canaries and 21 over the Sahara (Table 3.1). These profiles are conducted as the aircraft ascends/descends between the minimum safe altitude (around 160 m above ground level depending on visibility) and up to 8 km. The profiles in the Canaries were measured as the aircraft travelled to and from Fuerteventura Airport (28.4° N 13.8° W) and the Sahara, so two profiles were usually measured per flight. The lowest portion of the profile was over the ocean, while the highest altitude of the profile lies just over the continent.

The AER-D campaign took place in August 2015, conducting 26 vertical profiles in the Cabo Verde region. The flights from which these profiles are taken are described in Table 3.2.

Flight number	Date	Time of flights (UTC)	Number of profiles
b600	17 June 2011	10:00-12:30	1C 1Ma 1Mu
b601	17 June 2011	15:00-19:30	2C 1Ma 1Mu
b602	18 June 2011	08:30-12:30	2C 1Ma 1Mu
b604	20 June 2011	13:00-17:30	2C 2Mu
b605	21 June 2011	10:00-12:00	1C 2Mu
b606	21 June 2011	14:00-19:00	2C 1Mu
b609	24 June 2011	11:30-16:30	2C 1Mu
b610	25 June 2011	07:30-12:00	2C 2Mu
b611	25 June 2011	14:30-19:00	2C 2Mu
b612	26 June 2011	07:30-12:00	2C 2Mu
b613	26 June 2011	14:00-18:00	2C 3Mu

Table 3.1: Details of the Fennec flights used in this study including date and time of flights. Time is given to nearest 30 minutes. The number of profiles are described by the number taken from the Canaries (C) and the number at North Mali (Ma) and North Mauritania (Mu). Data taken from: Ryder et al. (2013a) and Ryder et al. (2013b).

Flight number	Date	Time of in-situ sampling (UTC)	Number of profiles
b920	7 Aug 2015	15:00-17:00	7
b924	12 Aug 2015	15:30-16:30	1
b928	16 Aug 2015	15:30-16:30	6
b932	20 Aug 2015	11:00-12:00	6
b934	25 Aug 2015	15:00-17:45	6

Table 3.2: Details of the AER-D flights and the times of in-situ sampling used in this study.

Instrument	Abbreviation	Size range (µm)	Fennec	AER-D	SALTRACE
Passive cavity aerosol spectrometer probe 100-X	PCASP	0.13-3.83	Y	Y	N
Cloud Droplet Probe	CDP	2.86-20	Y	Y	N
Cloud Imaging Probe	CIP15	15-63.2	Y	N	N
Two-dimensional stereo probe	2DS	20-63.2	N	Y	N
TSI Integrating Nephelometer 3563*	Nephelometer*	< 3	Y	Y	N
Radiance Research Particle Soot Absorption Photometer*	PSAP*	< 3	Y	Y	N
Ultra High Sensitivity Aerosol Spectrometer	UHSAS-A	0.08-3	N	N	Y
Grimm Sky OPC	SkyOPC	0.3-3	N	N	Y
Cloud and Aerosol Spectrometer with Depolarization Detection	CAS-DPOL	0.5-50	N	N	Y

Table 3.3: Size distribution instruments and scattering and absorption instruments used during the Fennec and/or AER-D campaign, where Y/N indicates instrument operation/not-operational. Sizes are given as geometric diameter. Size ranges correspond to data selected for model intercomparisons (as opposed to the full range measured by the instruments). * Indicates an instrument is located in-cabin, behind an inlet. Additional details are provided in the supplementary material in Table 3.8. Data taken from: Ryder et al. (2015), Ryder et al. (2018), and Ryder et al. (2013b), Walser (2017) and Weinzierl et al. (2017).

Table 3.3 shows the instruments operated in each campaign and the size range applied from each instrument, adjusted from geometric to optical diameter (see Ryder et al. (2013a) and Ryder et al. (2018) for details). Both the Fennec and AER-D campaigns measured particles up to 300 µm diameter. In order to tailor our analysis to the model, only observations corresponding to the model size bins (up to 63.2 µm diameter) are used in this study.

uring Fennec, wing-mounted (i.e. with no fuselage inlet) optical particle counter (OPC) probes were operated to measure the accumulation mode and coarse- to super-coarse-mode size distributions (Passive Cavity Aerosol Spectrometer Probe, PCASP; Cloud Droplet Probe, CDP), while measurements from a wing-mounted optical array probe (OAP), the Cloud Imaging Probe (CIP15), are used for the super-coarse and giant modes. The OPCs use light-scattering measurement techniques, and therefore the size bins applied are adjusted for a dust refractive index of 1.53–0.001i, based on scattering and absorption measurements (Ryder et al. 2013a). Errors due to uncertainties and oscillations in the Mie scattering curve for the OPCs, in addition to systematic error for the PCASP and random (counting) errors for all probes, were propagated through to size distribution uncertainties. Full details of Fennec instrument processing are given in (Ryder et al. 2013a; Ryder et al. 2013b).

During AER-D, the same wing-mounted OPCs were operated (PCASP and CDP), while measurements from the OAP Two-Dimensional Stereo Probe (2DS) are used for the super-coarse to giant mode. As with Fennec, the size bins applied to the OPC data are adjusted for a dust refractive index of 1.53–0.001i based on scattering and absorption measurements (Ryder et al. 2018). Sizing for the 2DS is performed using the mean of the x and y dimensions of each particle image, in order to be consistent with Fennec data processing, and is also curtailed at 300 µm for this reason, though few particles approaching this size were detected during AER-D. We propagate errors in the size and number distribution due to uncertainties and oscillations in the Mie scattering curve for the OPCs, in addition to random errors (from counting and discretisation errors) and systematic errors (from the sample area) for all instruments. Full details of AER-D instrument processing are given in (Ryder et al. 2018).

During both Fennec and AER-D, the aircraft measured the scattering coefficient with a TSI Integrating Nephelometer 3563 and absorption coefficient with a Radiance Research Particle Soot Absorption Photometer (PSAP) (Ryder et al. 2015). These instruments are located in the cabin, behind Rosemount inlets, with an estimated 50% efficiency for diameters below 3 µm, resulting from inlet losses and pipework transmission losses (Ryder et al. 2018; Ryder et al. 2013b). The sum of scattering and absorption provides extinction; this has been integrated vertically to provide AOD at 550 nm, representing AOD for d $<$ 3 µm. AOD at the time of observation could therefore be marginally larger than the AODs presented here.

Due to dust-induced visibility reductions impacting the minimum safe altitude for flying, the minimum height of observational data in the Sahara varies by flight, from around 100–500 m above ground. Therefore, we impose a minimum altitude threshold of 500 m here for the Fennec Sahara profile analysis to avoid sampling bias across different flight, weather and dust conditions. Data collected in the MBL may contain contaminated dust and non-dust aerosols, such as sea salt and anthropogenic pollution. Compositional analysis carried out by Ryder et al. (2018) of the aerosols measured during the AER-D campaign showed that particles of d $>$ 0.5 µm were dominated by aluminosilicates and quartz, while, for those between 0.1 and 0.5 µm, the dominant particles were sulfates and salts. As we are most interested in the coarser dust particles in this study, these finely sized contaminants should not impact our analysis. Therefore, profiles over the Canary Islands and during AER-D are analysed at their minimum sampling altitude ($\sim$16 m or during landing at Fuerteventura Airport). Finally, filtering of the data removed noise based on a signal-to-noise ratio as a function of diameter.

Falcon DLR Aircraft Setup

The SALTRACE campaign took place in June and July 2013, conducting flights in the eastern Atlantic in the Cabo Verde region (SALTRACE-E) and in the western Atlantic around the Caribbean (SALTRACE-W) (Fig. 3.1 and Table 3.4).

Flight number	Date	Location	Time of measurements (UTC)	Number of segments / full profiles
130611b	11 Jun 2013	La Palma (ES) to Sal (CV)	12:51-16:25	17 / 2
130612a	12 Jun 2013	Sal to Dakar (SN)	08:52-12:08	19 / 2
130612b	12 Jun 2013	Dakar to Sal	13:12-16:10	13 / 2
130614a	14 Jun 2013	Sal to Dakar	09:06-12:37	29 / 2
130614b	14 Jun 2013	Dakar to Sal	13:47-15:54	27 / 2
130617a	17 Jun 2013	Sal to Praia (CV)	11:06-12:27	17 / 2
130620a	20 Jun 2013	Barbados	12:01-15:55	32 / 2
130621a	21 Jun 2013	Barbados	18:32-22:01	36 / 2
130622a	22 Jun 2013	Barbados	18:05-21:55	33 / 2
130626a	26 Jun 2013	Barbados	23:25-03:15	10 / 2
130630a	30 Jun 2013	Barbados to Antigua	13:03-16:28	10 / 2
130701a	1 Jul 2013	San Juan (PR) to Antigua	14:22-18:12	16 / 4
130701b	1 Jul 2013	Antigua to Barbados	19:48-23:30	12 / 4
130705a	5 Jul 2013	Barbados	12:10-16:01	0 / 2
130708a	8 Jul 2013	Barbados	18:55-22:46	0 / 4
130710a	10 Jul 2013	Barbados	15:07-19:18	25 / 4
130711a	11 Jul 2013	Barbados	12:37-15:03	10 / 2
130711b	11 Jul 2013	Barbados to San Juan	18:04-21:05	24 / 2

Table 3.4: Details of the SALTRACE flights, including location, and the time (UTC) of flights. Where ES is Spain, CV is Cape Verde, SN is Senegal and PR is Puerto Rico. The number of horizontal segments and vertical profiles measured during each flight are shown; each horizontal segment is measured over 150 seconds. Data taken from: Weinzierl et al. (2017) supplementary material.

During SALTRACE, the DLR Falcon took measurements using a combination of OPCs: GRIMM Sky OPC (SkyOPC), Ultra-High Sensitivity Aerosol Spectrometer (UHSAS-A), and the Cloud and Aerosol Spectrometer with Depolarization Detection (CAS-DPOL). Some details of these instruments are shown in Table 3. Full details can be found in Walser (2017) and the supplement of Weinzierl et al. (2017).

We use data from both vertical profiles and horizontal segments in our analysis of the SALTRACE data. SALTRACE data from horizontal flight legs are broken down into 330 flight segments, each lasting for 150 s. These have been inverted and represented using lognormal modes in order to consistently propagate measurement uncertainties (e.g. optical particle counter response and properties, correction for refractive index) (Walser 2017). These horizontal segments provide size distributions at a high resolution in diameter space. Additionally, in order to provide a vertically continuous description of dust mass and size variation with altitude, we use SALTRACE profile observations. The profile data have not undergone such extensive processing as the horizontal segments, and instead adjustments to the instrument bin sizes were applied to account for refractive index. Comparisons between the detailed size distributions from horizontal segments and those from profiles show good agreement (not shown). This allowed 44 size-resolved vertical profiles from SALTRACE to be analysed.

In order to calculate AOD, retrieved mass concentration profiles calculated from size distributions were combined with a mass extinction efficiency determined from an optical model (Gasteiger and Wiegner 2018). This produced profiles of the extinction coefficient which were vertically integrated to provide AOD at 500 nm. See Wieland et al. (2024) for details. The SALTRACE AODs therefore represent the full size range in contrast to those which use the FAAM data.

Atmospheric concentrations of coarse and super-coarse particles during the airborne measurements of the presented mean vertical mass concentration profiles were often near to or below the detection limit of the CAS-DPOL. Hence, the mean mass concentrations should be considered a lower threshold.

Processing of Aircraft Data

For all campaigns, profile data were aggregated across instrument size bins to match the broader six size bins of the model (Table 3.5), assuming homogeneous distributions across instrument size bins. For example, for Fennec Sahara, model size bin 1 is compared against corresponding data at sizes measured by the PCASP ($0.0632 \leq d < 0.2$ µm), while model size bin 6 ($20 \leq d < 63.2$ µm) is compared against data from the CIP15. Where model and instrument size bins did not match up perfectly, the number concentration was proportioned across instrumental size bins. For example, for SALTRACE, model size bin 4 ($2 \leq d < 6.32$ µm) is compared against concentrations measured by the CAS-DPOL over instrumental size bins 11 to 15 as well as half of the number concentration from bin 10 (see the Supplement for full details; Table 3.8). This provides measured number concentrations corresponding to each model size bin as a function of time for the aircraft data. Assuming the density of dust to be 2.65 g cm^{-3} (Hess et al. 1998) and that the particles are spherical, we calculate mass concentrations for each of these size bins using standard volumetric and mass equations, based on the instrumental mid-bin diameter. These size- and time-resolved mass concentrations can then be manipulated as follows to provide mass concentration profiles and size distributions.

Table 3.5: Size range and representative diameter (D_{rep}) of the modelled transported mineral dust size bins in the CLASSIC aerosol scheme described in Woodward (2001). D_{rep} is used in calculating the emitted size distribution and the particle settling velocity. Within each size bin, $dV/dlog(r)$ is assumed constant, where V is particle volume and r is particle radius.

Bin number	Bin diameter range (µm)	Representative diameter (µm)
1	$0.0632 \leq d < 0.2$	0.112
2	$0.2 \leq d < 0.632$	0.356
3	$0.632 \leq d < 2$	1.12
4	$2 \leq d < 6.32$	3.56
5	$6.32 \leq d < 20$	11.2
6	$20 \leq d < 63.2$	35.6

Profiles are measured as either one single "deep" profile or several smaller profile segments combined together. Quasi-vertical profile data are averaged over 50 m intervals for high-resolution analysis and model evaluation, for both FAAM and DLR measurements. For size distribution analysis, FAAM (i.e. Fennec, AER-D) aircraft profiles were averaged over 500 m altitude intervals. DLR (i.e. SALTRACE) size distributions were taken from horizontal flight segments, and measurements performed within 500 m altitude bands were averaged. The data are regionally averaged for each campaign. In some portions of our analysis, we do not analyse data below 1 km or above 6 km in order to avoid the observed data becoming skewed by non-dust particles in the MBL or at the top of/above the SAL.

A caveat of our analysis is that this removes any measured particles outside the model limits ($0.063 < d < 63.2$ µm). Particles larger than 63.2 µm accounted for

10%–40% of the total dust mass measured in the Sahara below 5 km, but in the Canaries and Cabo Verde, these particles accounted for less than 10% of the dust mass and only occurred below 2 km (not shown). Hence, these giant particles were not included in this study as we focus our comparison on the size range transported in the model's atmosphere. Particularly over the Sahara, giant dust particles are likely to be omitted by model simulations, and the extent of this should be addressed in the future but is not in the scope of this study.

3.2.2 Model Setup

The GA7.1 atmosphere-only version of the Hadley Centre Global Environment Model 3 (HadGEM3-GA7.1) (Walters et al. 2019) configuration of the MetUM is used to model, among other variables, global mineral dust concentrations and aerosol optical depths. This setup is identical to those used in the HadGEM3 CMIP6 (Coupled Model Intercomparison Project Phase 6) AMIP (Atmospheric Model Intercomparison Project) simulations and configured to use observed sea surface temperatures (SSTs) and CMIP6 historical inventories (Eyring et al. 2016). The model has a horizontal grid resolution of $1.875° \times 1.25°$ (N96) and 85 height levels, 50 of which are concentrated below 18 km. The finest vertical resolution is the lowest layer, with a depth (dZ) of 36 m. dZ increases with altitude so that at $\sim$500 m altitude, dZ is 120 m; at $\sim$2 km altitude, dZ is 226 m; and at $\sim$5 km altitude, dZ is 373 m. The relatively high vertical resolution suggests that sensitivity to vertical numerical diffusion is unlikely to be important, though this may have a small effect (Zhuang et al. 2018). Mineral dust is represented by the Coupled Large-scale Aerosol Simulator for Studies in Climate (CLASSIC) scheme, described in Woodward (2001) and Woodward et al. (2022). The CLASSIC dust emission scheme calculates horizontal flux in nine size bins of between 0.0632 and 2000 µm diameter and uses this to derive vertical flux in six size bins up to 63.2 µm. Dust emissions are calculated interactively at each time step from modelled fields of friction velocity, soil moisture and the soil particle size distribution together with the model's land surface and vegetation data. A fraction of the coarsest particles are re-deposited to the surface within the same time step as they are emitted, and these never enter the model atmosphere. The remaining particles are lofted into the atmosphere and are transported as independent tracers corresponding to the six size bins shown in Table 3.5. The dust scheme is called at every model time step, using the driving fields calculated directly from HadGEM3-GA7.1 and the Joint UK Land Environment Simulator (JULES) (Woodward et al. 2022). The dust is mixed externally with other aerosols, which are simulated by the United Kingdom Chemistry and Aerosols

(UKCA) GLobal Model of Aerosol Processes (GLOMAP-mode) scheme (Bellouin et al. 2013). The dust cannot act as cloud condensation nuclei or ice-nucleating particles or chemically interact with the model. The dust interacts with the rest of the model through radiative interactions with the atmosphere. The dust particles are also assumed to be spherical.

The dust emission scheme is described in detail in Woodward et al. (2022). The method of calculating horizontal (G) and vertical flux (F) is derived from the work of Marticorena and Bergametti (1995), using dry threshold friction velocities (U_t^*) from Bagnold (1941) with a correction for soil moisture, based on the method of Fecan et al. (1998), and the clay fraction (F_c). Measurements from Gillette (1979) are used to relate G and F by assuming a clay content of less than 20%. G is calculated in each of the nine size bins i, representing the horizontal flux:

$$G_{(i)} = \rho_a B U^{*3}(1 + \frac{U^*_{t(i)}}{U^*})(1 - (\frac{U^*_{t(i)}}{U^*})^2)\frac{M_{(i)}CD}{g} \tag{3.1}$$

where ρ_a is the air density, B is the bare soil fraction in the grid box, U^* is the surface layer friction velocity, M_i is the ratio of dust mass in the size division i to the total mass, C is a constant of proportionality, D is a dimensionless tunable parameter and g is the acceleration due to gravity. The ratio of U^* to U_t^* and M combine to calculate the emitted size distribution, with U_t^* being dependent on particle size using D_{rep} values from Table 3.5. M is calculated from the soil clay, silt and sand fractions. The total vertical flux (F) is represented with six size bins. The mass in each is related to the total horizontal flux across all nine size bins (Woodward et al. 2022) according to

$$F_{(i)} = 10^{(13.4F_c - 6.0)} G_{(i)} \frac{\Sigma_{i=1,9}(G_i)}{\Sigma_{i=1,6}(G_{(i)})} \tag{3.2}$$

The particles are then transported as six independent tracers and are subject to deposition by below-cloud scavenging, gravitational settling and turbulent mixing in the boundary layer (BL). The impact of gravitational settling on the distribution of dust mass is calculated by computing the flux of dust out of a given layer and down to up to two model levels below (determined partly by the vertical spacing of the model levels), in proportion to the Stokes velocity and the length of the time step. The sensitivity of model results to the precise numerics has not been tested. Dry deposition in the BL is calculated using a resistance analogue method where the particle deposition velocity is treated as an inverse resistance based on gravitational settling and turbulent mixing (Seinfeld 1986).

The model dust emissions are tuned to improve agreement between the simulation and observations of AOD, near-surface concentrations and deposition rates. To do this, three dimensionless parameters are altered: a global emission multiplier, a friction velocity multiplier and a soil moisture multiplier. The purpose of tuning is to correct for the effects of processes not included in the model, such as the gustiness of wind at the source and the relationship of soil moisture in the model's top level and at the soil surface (Woodward et al. 2022). The dust was not specifically tuned for this study, and an improved dust simulation would almost certainly be achievable if tuning were undertaken. However, we chose to use this configuration of settings as it is the same as those used in the HadGEM3 CMIP6 AMIP simulations (Eyring et al. 2016) and has been widely used.

The model is free-running but uses observed SSTs to simulate 5 June months, 2010–2014, outputting vertically resolved daily mean dust mass mixing ratios for each size bin. The averaged 5 June months provide a "June climatology" which is used to compare with our campaign averages. As the model is free-running, it does not represent specific meteorology and dust events, and therefore we cannot compare the specific dates on which the measurements were taken. We found minimal variability in Moderate Resolution Imaging Spectroradiometer (MODIS) Terra AOD in the two adjacent 5-year periods (2005–2009 and 2015–2019), suggesting that this 5-year period captures relatively average conditions and is of a sufficient length for this study. The data are averaged over boxes representative of the campaign locations (Fig. 3.1). Careful consideration was taken to make sure that the boxes were suitably located so as to represent the locations measured during the observations. The Sahara, Canaries and Cabo Verde boxes do not overlap with the African coast as this was found to alter the distribution and magnitude of the vertical dust profile.

The daily mean dust mixing ratio, temperature and pressure at model levels are used to calculate the air density and the mass, number, volume and surface area concentration per size bin. The calculations of the size distributions and normalisations were carried out in the same way as with the aircraft data. The model data are not averaged in the vertical.

3.3 Confirming Representativity of the Aircraft Observations

As shown in Tables 3.1, 3.2 and 3.4, the aircraft campaigns cover limited periods of time, often only taking measurements for 2 to 3 weeks. The data collected during these campaigns can be biased towards certain types of events; for example, an effort may be made to schedule and direct flights through forecasted high-concentration dust events. Assuming that there may have been a scheduling bias towards high-concentration dust events during the campaigns, it is important to understand to what extent the dust size distribution, especially at the coarser size range, is dependent on the AOD, which we are using to represent the magnitude of the dust event. In this section, we show that any bias in data collection is unlikely to impact the findings from this study.

3.3.1 Spatial AOD Comparisons

In order to ascertain whether the dust conditions measured during the campaigns are representative of average conditions, combined MODIS Dark Target and Deep Blue AOD retrievals for land and ocean (Hsu et al. 2013; Levy et al. 2013) from the Terra satellite are used. A monthly mean AOD at 550 nm during the campaigns (June 2011 for Fennec, June 2013 for SALTRACE and August 2015 for AER-D) at the campaign locations (i.e. regional boxes shown in Fig. 3.1) was compared to a 5-year (2010–2014) and 20-year (2000–2019) average of AOD in June (or August for AER-D). During the Fennec campaign in June 2011, the variability in the AOD in the Sahara was comparable to the longer-term June averages, whereas in the Canaries, the AOD during the Fennec campaign in June 2011 was greater (AOD between 0.4 and 0.6) than the 5- and 20-year averages (0.2–0.4), seemingly due to a slightly more northwestwards transport of dust during June 2011. In Cabo Verde during the AER-D campaign, the mean August AOD was comparable to the longer-term August averages. However, in June 2013, during the SALTRACE campaign, the AOD in Cabo Verde and the Caribbean was greater (0.5–1.0 and 0.3–0.6, respectively) than the longer averaging periods (0.5–0.6 and 0.3–0.4, respectively). This suggests that the campaigns observed conditions similar to (Fennec Sahara and AER-D) or dustier than average (Fennec SAL, SALTRACE-E and SALTRACE-W). Next, we analyse whether greater AOD impacts the shape of the measured coarse size distribution.

3.3.2 Relationship Between AOD and Size Distribution

As AOD is the vertical integral of extinction caused by aerosols, which partially depends on the number concentration, as well as size-varying optical properties, we expect a greater concentration of dust to coincide with a higher AOD value. We aim to test this hypothesis with our observational data, and, additionally, we want to understand the dependence of coarse-particle size distribution on AOD: do high-AOD events contain a different proportion of particles from the coarser size bins 5 and 6 (6.32–63.2 µm) than low-AOD events?

Here, we show the impact of AOD on the size distribution by splitting campaign flights into low-, medium- and high-magnitude AOD events based on in situ AOD measurements taken during the Fennec (Ryder et al. 2015) AER-D and SALTRACE campaigns. The minimum, maximum and mean AOD from the AER-D campaign profiles was 0.06, 0.92 and 0.42, respectively. The AOD thresholds used to split up each campaign is given in the Table 3.6 caption; these thresholds were chosen as they approximately split the number of profiles from each campaign into thirds and are different for each campaign. We use Student's t test to test the statistical significance of our proposed hypotheses. The smaller the returned p value, the greater the statistical significance of the observed difference. We propose that the null hypothesis states that there is no difference between the total dust mass concentration profile in low- (L), medium- (M) and high-AOD (H) events. We found a statistically significant difference (at the 95% confidence interval) between the total dust mass concentration and the AOD measured in the Sahara, the Canaries and Cabo Verde during L, M and H events (Table 6 indicated by small p values) in most cases; hence, we reject our null hypothesis. Thus, low-AOD events measured during the two campaigns, for example, had a significantly different concentration profile for medium- or high-AOD events.

Next, we look at the relationship between the AOD and the relative mass contribution of coarse particles to the total mass concentration at each location. It is difficult to determine the relationship between AOD and the size distribution in observations because these measurements often characterise a different subset of the full dust size range, but even qualitative insights are worthwhile. Figure 3.2 shows AOD as a function of the mass contribution of size bin 6 for the Fennec, AER-D and SALTRACE campaigns (see the Supplement for the equivalent figure of size bin 5). AOD is calculated differently between the Fennec and AER-D and SALTRACE campaigns due to different instrumentation, but no campaign individually shows a strong correlation between the coarse mass contribution and AOD. Combining campaign data, there is a suggestion of a correlation between the AOD and coarse mass contribution, whereby coarse contribution may increase with AOD, which is to be expected in some cases as a result of different transport distances for each campaign region. So, a model bias in AOD is unlikely to be a dominant cause for simulating too few or too many coarse particles. The next section investigates the difference in the size distribution further to identify additional causes.

Table 3.6: P-values resulting from a Student's t-test to test the null hypothesis: there is no difference between the total mass concentration profile in low (L), medium (M) and high (H) AOD events. Bold values are significant to a 95% confidence interval. This is tested for the Fennec (Sahara and Canaries) and the AER-D (Cape Verde) campaign data. Each set of aircraft profiles from each location was split into thirds based on AOD at 550 nm measurements from the aircraft. The thresholds separating the low to medium, and medium to high AOD categories at the Sahara, Canaries, and Cape Verde are: 0.75 and 1.5, 0.5 and 0.75, and 0.4 and 0.6, respectively.

Total concentration µg m^{-3}		
Sahara	M	H
L	**0.014**	**4.473**e^{-18}
M	-	**1.100**e^{-8}
Canaries	M	H
L	**2.460**e^{-7}	**6.837**e^{-10}
M	-	0.463
Cape Verde	M	H
L	**3.167**e^{-8}	**1.028**e^{-14}
M	-	**1.110**e^{-4}

3.4 Results

In this section, the observations at the four observed locations (Sahara, Canaries, Cabo Verde and Caribbean) will be compared to the model simulation. Initially, this comparison will investigate the specifics of the vertical structure of the dust layer before focusing on the evolution of the observed and modelled size distributions over long-range transport.

3.4.1 Vertical Structure

In terms of the absolute values, we have analysed the mean total mass concentration profile from each location for between 0.063 and 63.2 µm diameter to match the modelled size range and between 1 and 6 km altitude to avoid contamination from the MBL or above the SAL. The mean mass concentration from observations between 1 and 6 km from each set of profiles has been calculated: 341 µg m^{-3} in the Sahara, 162 µg m^{-3} in the Canaries, 161 and 1680 µg m^{-3} in Cabo Verde (AER-D and SALTRACE-E, respectively), and 340 µg m^{-3} in the Caribbean. Despite the expectation that the highest mean concentration would be measured in the Sahara, the SALTRACE-E mean is almost 5 times larger, while the SALTRACE-W mean

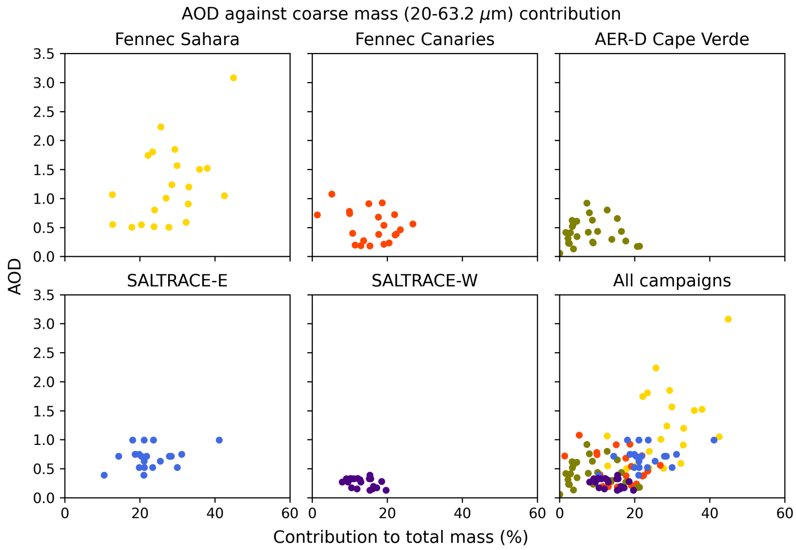

Figure 3.2: AOD against coarse mass (20-63.2 μm; size bin 6) contribution to total mass in each campaign. For Fennec and AER-D, AODs represent particles with diameters below 3 μm and mass contribution was averaged over profiles between 1-5 km at the Sahara, 0-5.5 km at the Canaries and 0-5 km at Cape Verde. For SALTRACE, AOD represents the full size range and mass contribution is taken from horizontal segments.

is nearly as large as that measured in the Sahara. This suggests that the events measured during the SALTRACE campaign were significantly larger than those measured during Fennec and AER-D. Despite these campaigns covering a range of magnitudes, the model tends to underestimate the mean total dust mass by a factor of between 4 and 44 (not shown), with the largest underestimations occurring with the comparison to the SALTRACE-E data. It is likely that this underestimation is partly due to a bias in the model size distribution towards smaller particles which constitute less mass. This underestimation is also likely a consequence of the tuning which has been applied to the model emissions as well as the different temporal scales which we are comparing. Due to the large magnitude of difference between the model and campaigns, the vertical mass profiles have been normalised. In order to compare the vertical distribution of dust, the profiles have been normalised by the mean dust mass concentration between 1 and 6 km altitude.

Figure 3.3 shows the normalised observed and modelled vertical profiles of the total dust mass concentration at each location from each campaign. Firstly, in terms of the observations, in the Sahara (Fig. 3.3a), dust mass is highest near to the surface, likely due to the high quantity of coarse and super-coarse particles which are lofted and settle relatively close to the source. The mass concentration gradually decreases to nearly zero at 5.5 km, marking the top of the Saharan atmospheric boundary layer (SABL) – a well-mixed, dry layer over the Sahara extending from the surface, often up to ∼6 km over the Sahara (Cuesta et al. 2009). In the Canaries (Fig. 3.3b), the observations start to show the formation of the SAL – the dry, dusty air layer formed when the SABL rises isentropically over the Atlantic Ocean's MBL (Carlson, 2016), residing between ∼1 and 6 km – with higher concentrations of dust between 2.5 and 3.5 km altitude, though the profile has relatively high concentrations up to 5.5 km where it is capped at the top of the SAL. With more time and distance from the Sahara, profiles in Cabo Verde (Fig. 3.3c) represent a more mature version of the SAL; the AER-D profile has a more well-defined base and cap to the SAL with a more concentrated centre between 2 and 4 km. Though not as dramatic as the AER-D profile, the SALTRACE-E profile still peaks between 2 and 4.5 km and tails off both at the top and bottom ends of the profile. Finally, in the Caribbean (Fig. 3.3d), the dust plume has lowered, bringing the dust mass closer to the surface and lowering the SAL cap to below 5 km.

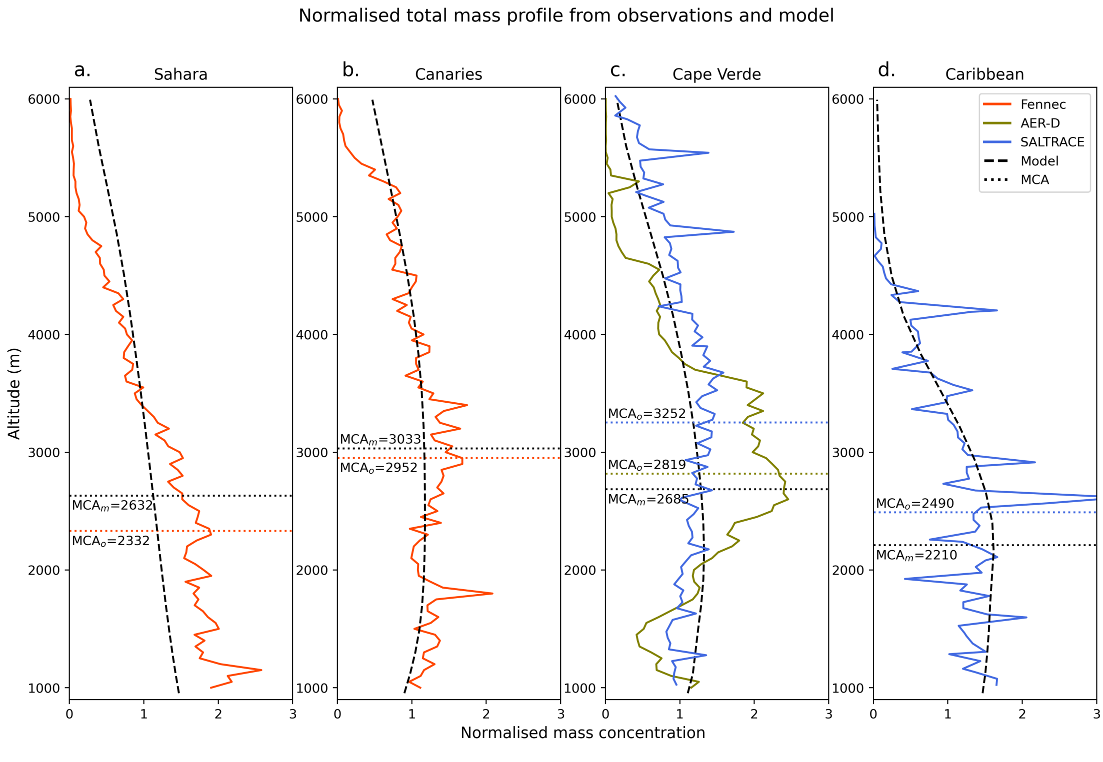

Figure 3.3: Normalised observed (coloured solid line) and modelled (black dashed line) total dust mass concentration profile and dust mass centroid altitude (MCA; dotted horizontal lines in metres) between 1 and 6 km. MCA$_o$ and MCA$_m$ respectively represent the observed and modelled MCA values. Plots show all four observed locations: Sahara (a), Canaries (b), Cabo Verde (c; AER-D and SALTRACE-E) and Caribbean (d; SALTRACE-W) from the Fennec (orange), AER-D (green) and SALTRACE (blue) campaigns. Data has been normalised by the mean profile concentration between 1 and 6 km altitude.

Generally, the shape of the modelled vertical profile resembles the observed profile. However, the model has struggled to represent the rate of change in concentration with height, failing to capture the relative magnitude of the maximum and minimum values measured during Fennec and AER-D (Fig. 3.3 a, b and c). In the Sahara, the model represents a more well-mixed profile whereby the concentration decreases more gradually with altitude than in the observations. The model does not have the same sharp cap at the top of the SABL that we see in the observations. Although the model does not represent the greater mid-SAL concentrations measured in AER-D well in Cabo Verde, its vertical distribution lies fairly close to that from SALTRACE-E (Fig. 3.3c).

The model appears to represent the top of the SAL most effectively in the Caribbean as the only location where the modelled concentration drops close to zero at the observed SAL top. The model failing to capture this sharp decrease could be in part due to our temporal averaging of the model data, suggesting that the top of the modelled SAL could vary significantly and can occur above 6 km altitude, except for in the Caribbean. The smooth profiles could also be a consequence of limited spatial resolution and numerical diffusion in the model.

The model represents the shape of the observed profiles very well despite the campaigns measuring fairly different total mass concentrations. However, although the AER-D campaign measured mean mass concentrations in Cabo Verde similar to those in the Canaries during Fennec, the AER-D profile is the least well-fitted to the model profiles, as well as appearing fairly different in structure to the SALTRACE-E profile. This difference could be caused by variation in the location of dust emission, which may alter the dust size distribution and distance transported before measurement. The difference could also be a consequence of the different time of year in which the AER-D campaign took place; Fennec and SALTRACE both occurred in June, whereas AER-D happened during August. The time of year impacts the location of the Inter-Tropical Convergence Zone (ITCZ) and the strength of the Saharan heat low (SHL), which work together as the main cause of intense dust uplift in the early summer (Marsham et al. 2008). The difference in meteorology could be why we see a different profile structure measured during the AER-D campaign.

The dust mass centroid altitude (MCA) between 1 and 6 km – the altitude at which 50% of the mass is below and 50% is above (Lu et al. 2023) – is shown in Fig. 3. We have not included particles in the lowest 1 km of the atmosphere in our calculations of the MCA due to potential interference from non-dust particles measured in the observations which may lower the MCA. Hence, this value is not a total column mass but is representative of the dust mass between 1 and 6 km at each location. At every location, the modelled MCA is at an altitude similar to the observed MCA, suggesting that the model distributes the total dust mass well in the SAL when compared to observations, in terms of the vertical distribution.

Moving away from the Sahara where the observed MCA is 2332 m, the MCA rises as the dust mass travels to the Canaries and Cabo Verde in the observations. The formation of the MBL aids in the removal of dust mass from the base of the SAL, causing the MCA to rise: 2952 m in the Canaries and 2819 and 3252 m in Cabo Verde. Though, as the plume sinks over the western Atlantic, the MCA reduces to 2490 m in the Caribbean. This raising and lowering of the MCA across the Atlantic is exactly what we would expect to see in our observations (e.g. Carlson (2016)). The model succeeds in representing vertical change in the MCA across the Atlantic. We have shown that the model represents the total dust mass vertical distribution fairly well. O'Sullivan et al. (2020) previously found that an NWP GA6.1 configuration of the MetUM placed dust 0.5–2.5 km too low in the atmosphere when compared with observations. Our analysis of these profiles suggests that this MetUM climate configuration may transport the dust at altitudes and distributions similar to the observations, at least in terms of the total mass across the whole size distribution.

In order to analyse the size distribution that makes up the vertical structure at these locations, we have broken the profiles (shown in their normalised form in Fig. 3.3) down into the six size bins used by the CLASSIC scheme in HadGEM3-GA7.1. We analyse the percentage contribution of mass to the total mass as a function of size. Figure 3.4 shows the contribution by size bin and the mean total mass concentration from each campaign for both the model and observations. Table 3.7 contains the mean percentage mass contribution to the total mass between 2 and 3.7 km altitude from the three coarsest size bins (2–6.32, 6.32–20 and 20–63.2 µm; green, blue and purple in Fig. 3.4) at each location from the observations and model.

In the Sahara, up to 90% of the observed dust mass up to 5 km comes from particles 6.32–63.2 µm in diameter (size bins 5 and 6; blue and purple in Fig. 3.4a). As the dust moves westwards over the Atlantic, the contribution of these coarsest particles decreases as they are deposited from the dust plume. Between 2 and 3.7 km, the 6.32–63.2 µm contribution decreases from ~87% in the Sahara to ~82% in the Canaries, ~45%–79% in Cabo Verde and ~60% in the Caribbean (Table 3.7). As the coarser contribution decreases, the contribution of 2–6.32 µm particles (size bin 4; green) increases, while the contribution of the finest particles (0.063–2 µm; size bins 1–3; red, orange and yellow) remains low up to the top of the SAL, at less than 5%

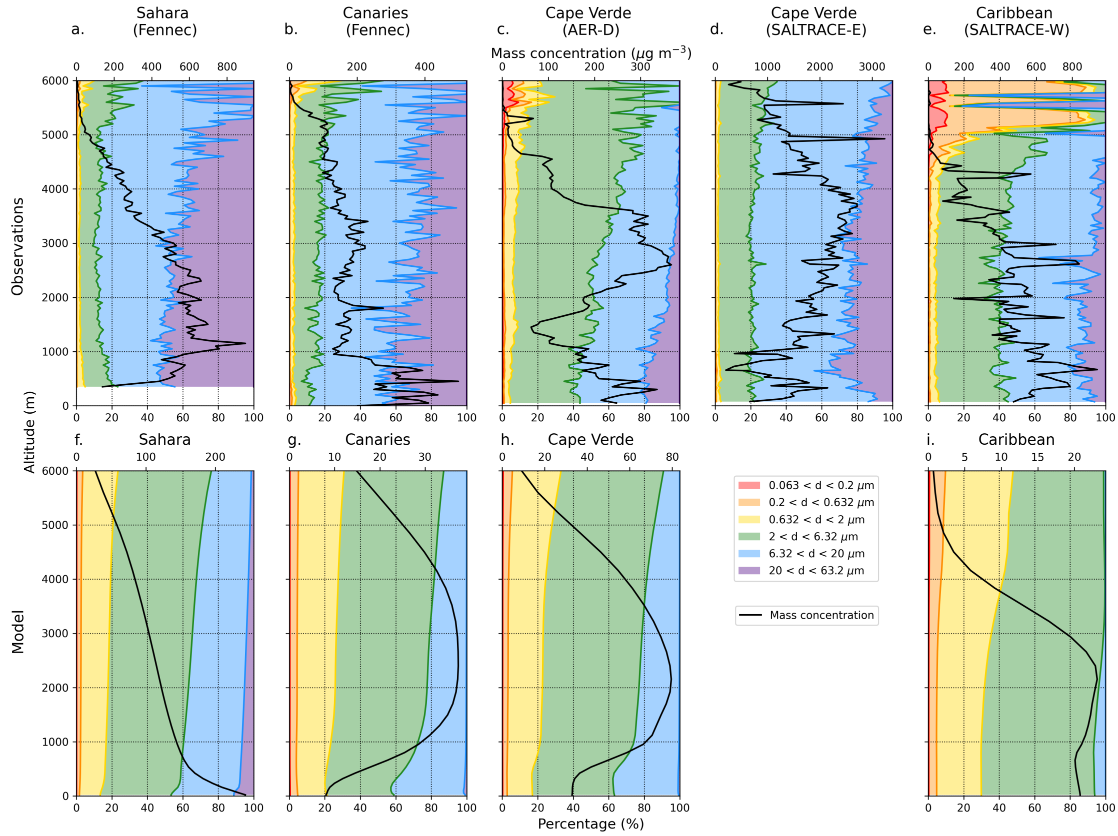

Figure 3.4: Dust mass concentration profiles, showing the total dust mass concentration in µg m^{-3} (black line) and the percentage contribution of dust mass in the six model size bins (coloured areas). Plots include the mean profiles from the observations (top) and from the model (bottom) at the Sahara (Fennec; a and f), Canaries (Fennec; b and g), Capbo Verde (AER-D and SALTRACE-E; c, d and h) and Caribbean (SALTRACE-W; e and i). Note that the mass concentration (black line) scales differ between panels.

at all locations except for Cabo Verde during AER-D (Fig. 3.4c). The coarse and super-coarse particles (6.32–63.2 µm; blue and purple) show a higher dependence on altitude in the AER-D data, whereby their mass contribution is highest in the lowest 1 km at up to 60% and decreases with altitude to half this contribution at 5 km. Fewer coarser particles were measured during the AER-D campaign, resulting in a higher contribution of 2–6.32 µm particles (size bin 4; green) compared to the other campaigns. The SALTRACE-E profile (Fig. 3.4d) shows a structure similar to the Fennec observations, suggesting that the AER-D campaign is the more anomalous of the two datasets.

In general, the model overestimates the mass contribution from 0.063–6.32 µm dust particles (size bins 1–4; red, orange, yellow and green) and underestimates the 6.32–63.2 µm particle (size bins 5 and 6; blue and purple) contribution at all locations. In the Sahara, the modelled dust mass between 6.32 and 63.2 µm between 2

Table 3.7: Mean percentage mass contribution to total mass between 2-3.7 km altitude from the three largest model size bins (2-6.32 µm, 6.32-20 µm and 20-63.2 µm; green, blue and purple in Figure 3.4) at the Sahara, Canaries, Cape Verde (AER-D (A) and SALTRACE-E (S)) and Caribbean in the observations (O) and model (M). Data relates to Figure 3.4.

	Sahara		Canaries		Cape Verde			Caribbean	
	O	M	O	M	O (A)	O (S)	M	O	M
Bin 4; 2-6.32 µm	10	46	14	52	48	19	55	35	64
Bin 5; 6.32-20 µm	43	31	54	21	40	55	22	50	2
Bin 6; 20-63.2 µm	44	4	28	0.2	5	24	0.1	10	9e-6

and 3.7 km accounts for 35% of total mass, less than half of the observed contribution of ∼87% (Fig. 3.4a and f). In the model, less than 15% of the contribution at the surface is made up of the coarsest particles (20–63.2 µm; size bin 6; purple), decreasing to ∼4% between 2 and 3.7 km altitude, which is 11 times less than the observed contribution. The mass contribution of 20–63.2 µm particles (size bin 6; purple) in the model decreases quickly beyond the Sahara to become negligible. In the Canaries and Cabo Verde, the vast majority of 20–63.2 µm particles have been removed between 2 and 3.7 km, leaving a contribution of less than 0.1%–0.2% from this size bin, 2 orders of magnitude less than the observed contribution measured during Fennec and SALTRACE (Fig. 4b, c, d, g and h; Table 3.7). Upon reaching the Caribbean, only a very small fraction of the mass comes from the 20–63.2 µm particles (size bin 6; purple), and the 6.32–20 µm (size bin 5; blue) contribution below 1 km is less than 10% and only 2% between 2 and 3.7 km. The rate at which the model loses coarse and super-coarse particles results in an increasing bias of particles smaller than 6 µm and thus an underestimation of the total dust mass remaining after long-range transport.

From the Sahara, the modelled contribution of particles smaller than 2 µm (size bins 1–3; red, orange and yellow) is overestimated by a factor of 10, with an overestimation of up to 13, 3–12 and 9 in the Canaries, Cabo Verde and the Caribbean, respectively. This overestimation of the fine-particle mass confirms that the model shows a bias towards fine particles over coarser particles.

In the two largest size bins, the model shows a decreasing percentage mass contribution with altitude (Fig. 3.4). In the Canaries, for example, the model 6.32–20 µm mass contribution (size bin 5; blue) drops from ∼30% at 1 km to ∼15% at 5 km, whereas, in the observations, only the coarsest size bin shows this altitude dependence, whereby the 20–63.2 µm particle contribution (size bin 6; purple) decreases with altitude from ∼50% at 1 km to ∼30% at 5 km in the Sahara and from ∼25%

at 1 km to ∼10% at 4 km in the Caribbean. Alternatively, the 6.32–20 µm contribution (size bin 5; blue) remains more consistent with altitude in the observations or shows an increasing relative contribution due to the decreased contribution of the 20–63.2 µm contribution (size bin 6; purple). Thus, where the model shows an altitude dependence in the percentage mass contribution of the coarse and super-coarse dust, the observations show this dependence only visibly affects the super-coarse mass contribution (i.e. 20–63.2 µm; purple).

The model represents the relative mass contribution of coarse and super-coarse particles as relatively height dependent, decreasing with altitude. However, the observations show little variation in coarse dust with height and a decreasing super-coarse-dust contribution with height. The model fails to retain the super-coarse dust during trans-Atlantic transport and incorrectly represents the vertical distribution of coarse dust, with a bias towards lower altitudes.

3.4.2 Size Distribution Evolution

The height-resolved modelled and observed volume size distributions have been normalised by total volume (Fig. 3.5). This highlights the peak of the size distribution and the difference in shape between the model and observations when the total concentrations are different. There are two things which are clear amongst all campaigns. Firstly, this is the shape of the distributions from the smallest size bin to the peak in volume; the model displays a broader shape, while the observations show a more steeply curved, peaking shape. Secondly, the model underestimates volume in the largest size bin at all locations. Beginning in the Sahara, the difference is around 1 order of magnitude. Moving downwind, the difference between the model and observations continues to grow by orders of magnitude such that the model volume distribution drops much more sharply to around 5 orders of magnitude less than the observations in size bin 6 (20–63.2 µm) by the Caribbean. At all locations (except for Cabo Verde during AER-D) the observed volume in the 2–6.32 µm range is very similar in magnitude to the volume in the 20–63.2 µm range (i.e. size bins 4 and 6), whereas, in the model, there is a notable drop from the fourth to the sixth size bin. The increasing difference between the model and observations at the coarsest range is an indication of the rapid deposition of the coarser particles in the model. Not only do we see a growing difference with distance from the Sahara, but also the underestimation of coarser-dust volume in the Sahara suggests there may be an issue with the model emissions and/or vertical transport, whereby not enough coarse and super-coarse particles are transported through the SABL. This underestimation is exacerbated through long-range transport by the overly swift deposition of the coarser particles.

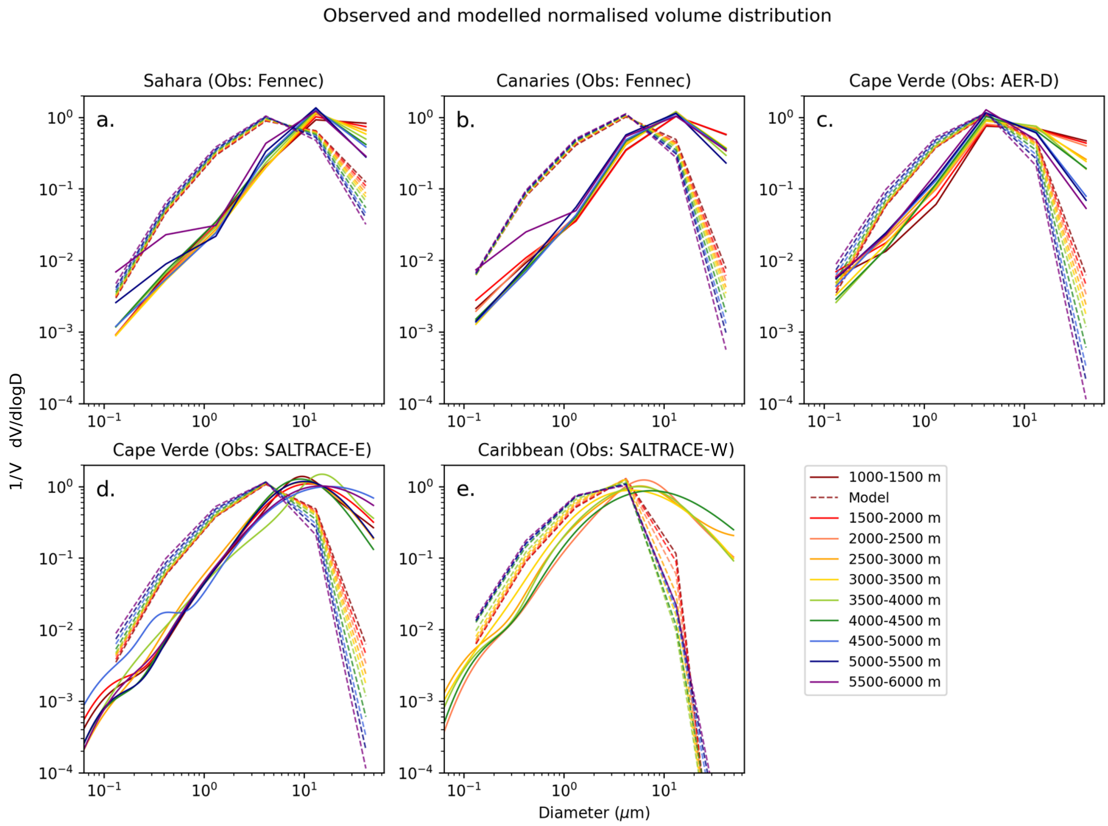

Figure 3.5: Vertically resolved modelled (dashed lines) and observed (solid lines) normalised volume distribution at the Sahara, Canaries (Fennec), Cabo Verde (AER-D and SALTRACE-E) and Caribbean (SALTRACE-W) at different altitudes. The volume distributions have been normalised by the total particle volume.

The model tends to peak in volume in the 2–6.32 µm bin, whereas the observations measured during the Fennec and SALTRACE campaigns peak in the next size bin up (6.32–20 µm). Contrary to the other campaigns, the volume distribution from the AER-D campaign in Cabo Verde peaks in the 2–6.32 µm bin. As mentioned previously when observing the different vertical structure, this difference could be a consequence of the different time of year in which this campaign occurred. Despite the differences between the data collected from the AER-D campaign and the Fennec and SALTRACE campaigns, the AER-D data remain consistent with the other campaigns, showing that the model underestimates coarser-dust-particle mass and transport.

When normalised, there is no particular pattern in relation to the altitude except for at the coarsest size ranges, where dust volume tends to decrease with altitude in the model and observations. Otherwise, the shape of the distribution remains consistent with altitude. The only other exception is at high altitudes in the smallest size bin in the observations in the Sahara, the Canaries and Cabo Verde (Fig. 3.5a, b and d). The volume distribution of fine 0.063–0.632 µm particles is greater above 5 km than at lower altitudes. This could be a signal of non-dust particles.

Figures 3.4 and 3.5 show that the model under-represents the coarser size distribution over the Sahara, as well as further downwind during transport. In this study, we focus on the impact of transport processes on the size distribution, rather than examining emission processes. The model emitted size distribution is dominated by size bin 6, although the atmospheric dust size distribution in the lowest model level is already dominated by size bin 4 (see Fig. 3.8). This suggests additional challenges in representing initial dust transport from emission into the very low atmosphere, which should be an area for future study. The aggregated Saharan observations presented here are from 500 m upwards, which prevents a detailed analysis of the near-surface emission size distribution.

In order to illustrate how the model represents the evolution of the dust size distribution during trans-Atlantic transport and the discrepancies between the model and observations over the Sahara, Fig. 3.6 shows the vertically resolved fractional model underestimate of the volume size distribution between the observations and the model in the Sahara, the Canaries, Cabo Verde and the Caribbean (i.e. observations/model of dV/dlogD). This figure shows that at all locations, the model underestimates the coarse fractions by greater orders of magnitude than the fine fraction. Additionally and most significantly, the magnitude of the coarse-fraction underestimate grows with transport from the Sahara; the fractional underestimate of size bin 6 increases from around a factor of 10 over the Sahara to over 1,000,000 in the Caribbean. Thus, we demonstrate that although there is an underestimation of the volume distribution at the source, this is significantly exacerbated by several orders of magnitude with westwards transport.

We have postulated previously that the model struggles to raise the coarse dust high enough, showing more altitudinal dependence than the observations. In Fig. 3.6c and d in Cabo Verde and the Caribbean, the model underestimate becomes worse at higher altitudes. In Cabo Verde in the SALTRACE-E comparison, there is an order-of-magnitude difference of the underestimate of size bin 6 between 1–1.5 and 5–5.5 km altitude.

While no observations of vertically resolved, size-resolved dust concentration

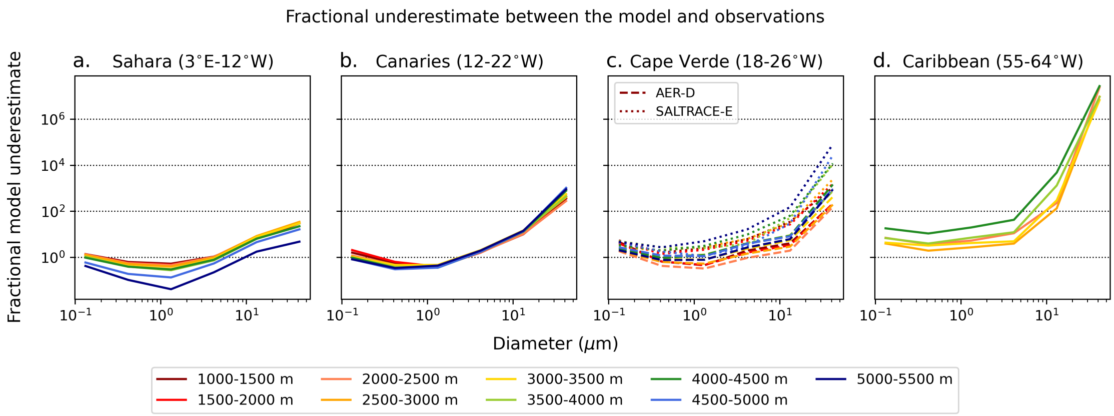

Figure 3.6: Fractional underestimate of the volume size distribution between the observations and model. The vertically-resolved difference is shown at the Sahara (a) and Canaries (b), using Fennec observational data, at Cabo Verde (c) using AER-D (dashed lines) and SALTRACE-E (dotted lines) data and at the Caribbean (d) using SALTRACE-W data.

over the mid-Atlantic exist, we are able to look at how the model simulates the concentration evolution across the Atlantic. Figure 3.7 shows the evolution of mass concentration in each size bin from the Sahara to the Caribbean. Figure 3.7a shows the modelled mean June AOD as well as stippling, which represents the 65th percentile of AOD between 1° S and 47° N at each degree longitude, which has been used to identify the mean latitudinal plume extent. The 65th percentile of AOD was chosen so as to cover an area including all the observed locations. Figure 3.7b shows the modelled mass concentration in each of the six size bins in the defined dust plume location and between the 2 and 3.7 km altitude range. The 2–3.7 km altitude range has been selected to analyse the dust plume to minimise interference from the MBL and free troposphere above the SAL, across the entire Atlantic. Figure 3.7b shows that the 2–6.32 μm particles (green) are the dominant contributors to dust mass across the Atlantic in the model, as in Fig. 3.4. Although the mass of 6.32–20 μm particles (blue) is double that of the 0.632–2 μm particles (red, orange and yellow) in the Sahara, these larger particles are removed more swiftly and have less mass than the finer particles west of Cabo Verde (∼25° W).

Figure 3.7c shows the normalised mass concentration transect in the six size bins. These have been normalised by their value in the Sahara (∼3° W) to allow for a direct comparison of the rate of change in mass concentration between each size bin. All size bins experience change in their mass concentration in two distinct regions, one over the entire African continent (15–3° W) and over the Atlantic, where each size bin loses mass at a size-dependent rate. These two distinct areas hint at the different processes which alter dust transport over land and ocean. The rate of loss

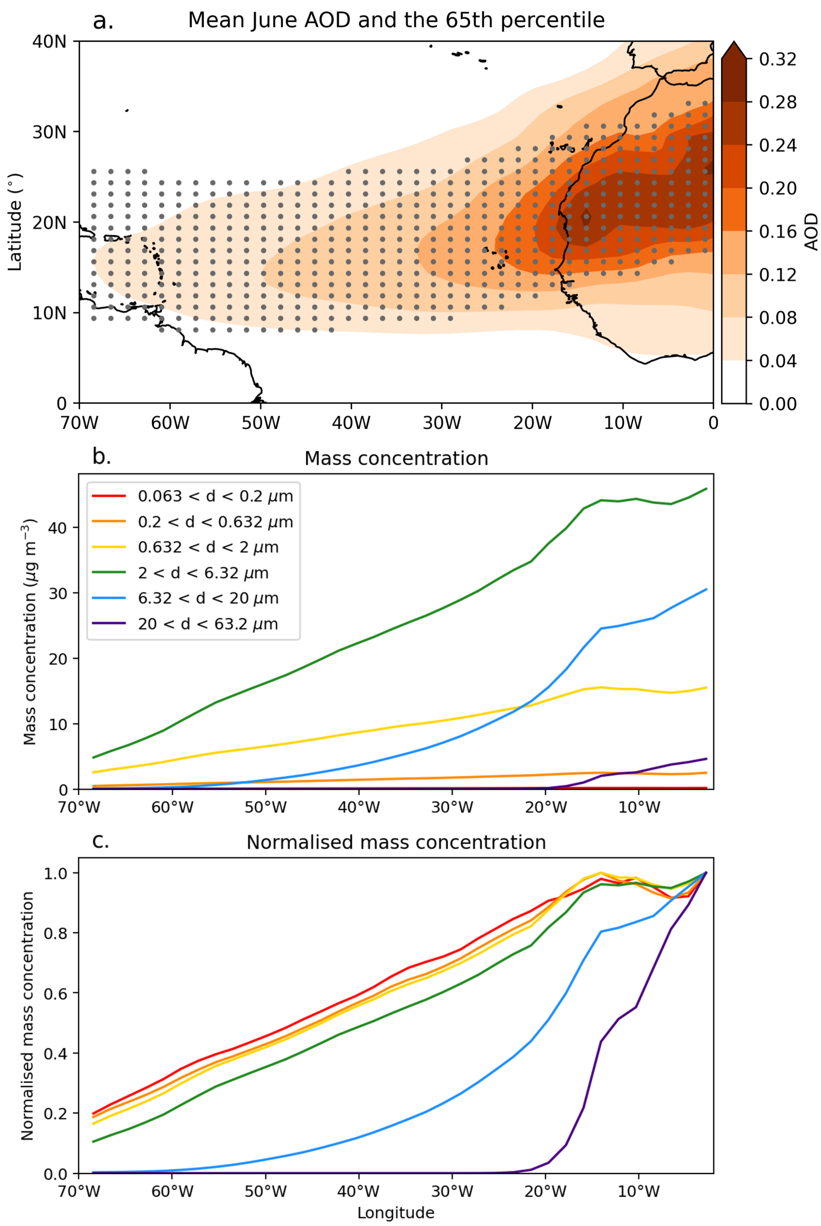

Figure 3.7: The 65th percentile (stippling) of mean June 2010-2014 AOD at 550 nm (orange shading) at each longitude has been used to locate the dust plume (a). The mean modelled dust mass concentration between 2.0-3.7 km altitude by longitude in the six CLASSIC size bins from the Sahara to the Caribbean (b). The binned concentrations have been normalised by the mass concentration in each bin at 3° W (c).

of the four finest size bins (0.063–6.32 μm; red–green) appears fairly linear; each size bin loses 70%–80% of its mass between the western African coast and the Caribbean. The rate of loss of the coarsest size bins (6.32–63.2 μm; blue and purple) is sharper. These much faster rates of loss result in a negligible mass of 20–63.2 μm particles remaining just west of Cabo Verde and of 6.32–20 μm particles remaining near the Caribbean.

3.5 Conclusions

Vertically resolved, in situ observations from three aircraft campaigns, Fennec, AER-D and SALTRACE, in the Sahara, the Canary Islands, Cabo Verde and the Caribbean are analysed together to understand the evolution of dust particle size distribution over long-range transport, with a particular focus on the coarser particles and their vertical distribution. The observations from these campaigns are used to evaluate the Met Office Unified Model (MetUM) HadGEM3-GA7.1 climate model representation of the dust size distribution across the Atlantic. This work presents the first time that all three of these campaigns have been used together and analysed at such a high vertical resolution in order to understand the size distribution evolution from the Sahara to the Caribbean, as well as being the most extensive evaluation of the MetUM HadGEM3-GA7.1 model representation of long-range dust size distribution evolution.

Aircraft observations from the Fennec, AER-D and SALTRACE campaigns show that coarser particles are further transported in the real world than in the model, in which coarser dust particles (6.32–63.2 µm) are underestimated in both mass and volume size distribution at all stages of long-range transport. In the Sahara, the model underestimates the normalised volume size distribution of the largest particles (20–63.2 µm) by more than 1 order of magnitude. The contribution of 20–63.2 µm particle mass to the total mass is only 4% in the model and 44% on average in the observations between 2 and 3.7 km over the Sahara, resulting in a model underestimation by a factor of 11. The particle mass contribution of size bin 5 is ∼43% in the observations and only 31% in the model. This results in a stark overestimation of the 2–6.32 µm mass contribution by 36%. These underestimations of the coarser particles suggest a challenge in representing the immediate transport upwards through the atmosphere after emission.

Observations suggest that the contribution of coarse-particle mass to the total mass is not strongly correlated with AOD, at least within a given campaign. The use of campaign periods with slightly higher-than-average AOD could therefore contribute to the poor representation of coarse particles in the model but is not a dominant driver. The model underestimation of coarse-particle concentration is so large that AOD variations within a campaign alone are not sufficient to explain the differences between the model and observations. We find that the model underestimates the coarser-particle volume distribution by increasing orders of magnitude with distance from the Sahara. The normalised volume size distribution in the largest model size bin (20–63.2 µm) is underestimated by 1 order of magnitude over the Sahara, up to 3 orders of magnitude in the Canaries, 5 orders of magnitude in Cabo Verde and 7 orders of magnitude in the Caribbean. This increasing disparity between the model and observations is a consequence of the overly swift removal of coarse and super-coarse particles from the modelled atmosphere, which is marked over the Sahara and is exacerbated during long-range transport. The majority of 20–63.2 µm particles have been removed from the Saharan air layer (SAL) just west of Cabo Verde, contributing only 0.1% of the total mass, where the observations show this size bin contributing up to 25% of the total mass between 2 and 3.7 km. The model's fifth size bin (6.32–20 µm) shows a slightly slower rate of removal from the model; however this still leaves a negligible concentration in the Caribbean, where the mass contributed by this size bin to the total dust mass is underestimated by a factor of 25 between 2 and 3.7 km. We suggest that the model is simulating far too swift a deposition of particles sized larger than 6.32 µm during the full course of long-range transport, leading to an increasing underestimation of dust mass with distance from the Sahara.

We have shown that the model generally agrees with the vertical distribution of total dust mass in the observations. We show that the mass centroid altitude (MCA) in the model is consistently within range of the observations. However, we find an underestimation in the super-coarse volume size distribution which increases with altitude, showing that the model increasingly struggles with coarser-particle representation over long-range horizontal and vertical transport and, despite representing the MCA of total dust mass, transports coarser dust particles too low in the atmosphere.

Our results are subject to some limitations. Firstly, it is noted that the aircraft observations used in this study cannot be fully representative of climatic conditions due to limitations in the temporal and spatial coverage of the observations. This makes our comparisons to the model more complex as the model provides daily mean data, covering each full 24 h period. Additionally, we find that the AER-D data have a slightly different vertical distribution of dust compared to SALTRACE-E in Cabo Verde, as well as a finer size distribution in comparison to the Fennec and SALTRACE campaigns, despite having instrumentation consistent with that of the Fennec campaign. It is not exactly clear what causes this disparity, but it could be a consequence of the measurements being taken in August compared to the other campaigns which were conducted in June. Additionally, we note that we excluded observations for which $d > 63.2$ µm since this is the maximum size represented by the model which was significant in the Sahara observations. Finally, we must consider that any biases in the model's representation of the dust vertical and horizontal distribution, as well as the size distribution, could be due to either the dust scheme or biases in the modelled climate. There is the potential for future research into the sensitivity of coarser-particle transport in the model regarding the numerical schemes which could provide additional valuable information for this research topic.

We have shown that the model has difficulty with representing the coarse-dust size distribution from the Sahara to the western Atlantic. This is consistent with other studies which have evaluated a range of models on more restricted spatial and vertical scales (Adebiyi and Kok 2020; Ansmann et al. 2017; O'Sullivan et al. 2020). Incorrect representations of dust size distributions in climate models will result in erroneous dust radiative effects, impacts on clouds, and deposition of nutrients within dust to the ocean and land surfaces (Adebiyi et al. 2023; Dansie et al. 2022; Kok et al. 2017). It is therefore important to understand and improve modelled dust size distributions. The discrepancy in the size distribution could be due to over-active processes affecting the dust deposition, such as sedimentation, wet deposition, and convective or turbulent mixing. It could also be a consequence of the dust not absorbing enough shortwave radiation (Balkanski et al. 2021; Colarco et al. 2014) and potentially affecting heating and therefore dust lofting after emission or plume height during transport. Alternatively, this long-range transport could be due to processes not considered in the model and not yet fully understood in practice, such as electric charging (Toth III et al. 2020; van der Does et al. 2018), asphericity (Huang et al. 2020; Huang et al. 2021; Saxby et al. 2018), turbulence (Cornwell et al. 2021; Denjean et al. 2016) and vertical mixing (Gasteiger et al. 2017). There is a need to better understand and observe dust size distributions during emission and in the lowest layers of the atmosphere over source regions. Whilst model dust concentration and size distribution near sources could be improved by re-tuning the emission scheme, this is unlikely to affect the evolution of the size distribution with transport, where additional processes are necessary to retain coarser particles, and should be investigated in further research along with size-resolved dust emissions.

This study presents an in-depth analysis of the evolution of the vertically resolved dust size distribution from the Sahara to the Caribbean from aircraft observations and the Met Office Unified Model. We show that the model underestimates super-coarse particles over the Sahara compared to observations, a difference which is exacerbated by up to 5 orders of magnitude during trans-Atlantic transport. As the presence and relative fraction of coarse particles is important for, among other processes, Earth's radiative budget and ice nucleation, it is imperative for the scientific community to obtain a better understanding of the physical processes which could be better understood and/or improved for models to improve simulations of super-coarse-dust transport. The work presented here demonstrates the need for a thorough analysis of processes affecting dust transport and deposition across the Atlantic in both observations and modelling in order to fully constrain models and to accurately simulate dust size changes during long-range transport and the diverse impacts on weather, climate and socio-economics dependent on this.

3.6 Supplementary material

This Section contains the Supplementary Material published with the journal article shown in this Chapter.

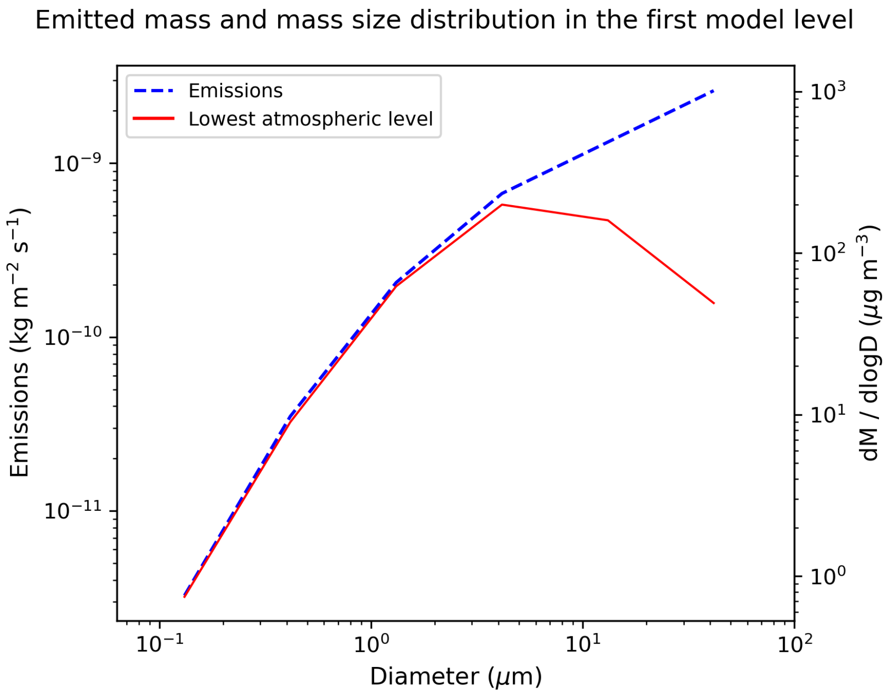

Figure 3.8: Model emitted dust mass (dashed blue line) and the mass size distribution (solid red line) in the lowest atmospheric level (0-36 m) at the Sahara (10° W-25° E, 18-29° N).

Table 3.8: Supplementary Table S1: Instrumental size bins used to construct equivalent number concentrations for comparison against model size bins. Diameter ranges are given in µm.

Model size bin	Fennec	AER-D	SALTRACE
Bin 1 (0.0632 to 0.2)	PCASP 0.132 – 0.198	PCASP 0.121 - 0.198	UHSAS 0.06949 – 0.20242 (bin 1 – bin 14)
Bin 2 (0.2 to 0.632)	PCASP 0.198 – 0.609	PCASP 0.198 – 0.609	UHSAS 0.20242 – 0.30687 (bin 15 - bin 25) + SkyOPC 0.3 – 0.615 (bin 2 - bin 6) + $\frac{1}{2}$ bin 7
Bin 3 (0.632 to 2)	PCASP 0.609 – 2.093	PCASP 0.609 – 2.093	SkyOPC 0.615 – 1.0 $\frac{1}{2}$ bin 7 + (bin 8 – bin 10) + CAS-DPOL 1.11 – 2.11 (bin 4 – bin 9) + $\frac{1}{2}$ bin 10
Bin 4 (2 to 6.32)	PCASP 2.093 – 3.492 + CDP 3.052 – 6.463	PCASP 2.093 – 3.492 + CDP 3.052 – 6.463	CAS-DPOL 2.11 – 6.43 $\frac{1}{2}$ bin 10 + (bin 11 – bin 15)
Bin 5 (6.32 to 20)	CDP 6.463 – 20.526	CDP 6.463 – 21.897	CAS-DPOL 6.43 – 20.11 (bin 16 – bin 22) + $\frac{1}{2}$ bin 23
Bin 6 (20 to 63.2)	CDP 20.526 – 39.600 + CIP15 37.5 – 67.5	2DS 20 – 65	CAS-DPOL 20.11 – 61.31 $\frac{1}{2}$ bin 23 + (bin 24 – bin 29)

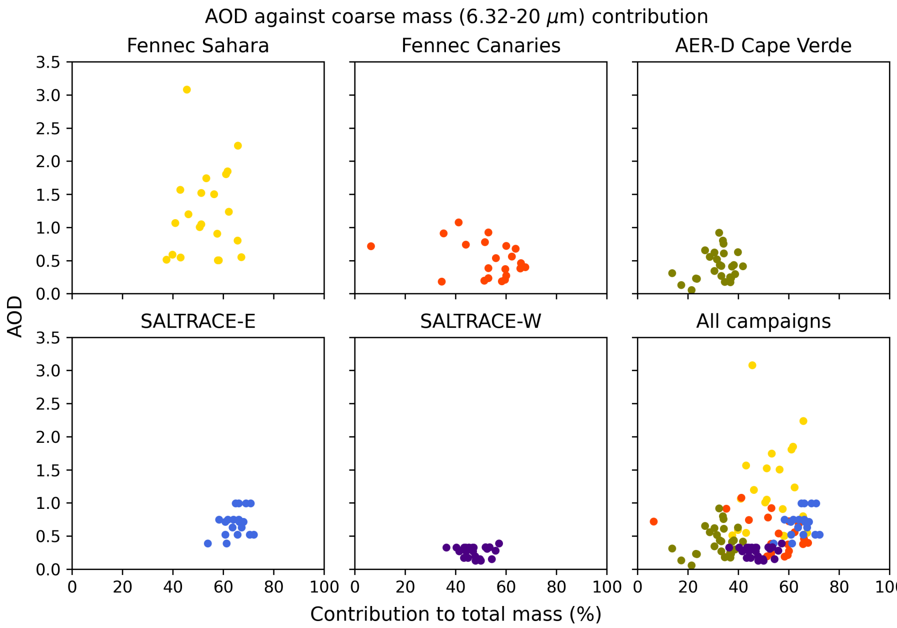

Figure 3.9: AOD against coarse mass (6.32-20 µm; size bin 5) contribution to total mass in each campaign. For Fennec and AER-D, AODs represent particles with diameters below 3 μm and mass contribution was averaged over profiles between 1-5 km at the Sahara, 0-5.5 km at the Canaries and 0-5 km at Cape Verde. For SALTRACE, AOD represents the full size range and mass contribution is taken from horizontal segments.

Chapter 4

Size Distribution Sensitivity to Transport and Deposition Mechanisms

After showing in Chapter 3 that the model consistently underestimates coarse dust mass at all locations but with increasing magnitude at increasing distance from the Sahara, this chapter aims to explore the sensitivity of coarse dust lifetime in the model to various transport and deposition processes. As previously discussed in Chapter 3 Section 1.1.7, there is the potential for mechanisms in the model to be altered which results in improved coarse particle lifetime. Here, I will remove or alter specific processes and analyse the impacts on the dust in an attempt to better understand any processes in the model which may be over- or under-active in altering the transport and deposition of coarse dust particles.

Section 4.1 will discuss the methods used and those which are specific to the experiments in this Chapter. Section 4.2 will present and discuss results from sensitivity experiments with radiative effects off in the model (sedimentation, impaction scavenging, convective mixing and turbulent mixing). Section 4.3 will present and analyse results from a sensitivity experiment with radiative effects on (tripled SW absorption). Finally, in Section 4.5 the chapter will be summarised and concluded.

4.1 Methods

In order to test the sensitivity of coarse dust transport in the model, I have removed, reduced or increased the impact of some modelled processes on dust. In this chapter, the methodology of these changes will be explained. All results in this chapter are averages of 20 June months (1995-2014) from the MetUM HadGEM3-GA7.1 model. If data is described as being at the Sahara, Canaries, Cape Verde and Caribbean, the model has been averaged over the box regions used in Chapter 3 Figure 3.1.

4.1.1 Tuning

From our findings in Chapter 3, we know that the HadGEM3-GA7.1 model simulation significantly underestimates the mass loading of dust, specifically coarse dust, at all stages of transport, including at emission. Thus, for these experiments where I wish to better understand how and where the coarse particles are being lost over long-range transport, the emissions have been tuned by the Met Office so that the model starts with the correct size distribution at the Sahara. The tuning applies only to trans-Atlantic dust transport and was not checked for its representation of emissions and resultant near-surface concentrations or AODs from other sources around the globe. A comparison of the VSD produced by the previous model configuration and the new, tuned configuration to the observations at the Sahara is shown in Figure 4.1. The tuning is based on observations of near-surface concentrations, AOD and size distributions between 77-130 m and 730-877 m altitude model levels. Due to this tuning, all simulations in this thesis after this point are no longer equivalent to the CMIP6 configuration. The new tuning provides a VSD with a greater coarse fraction and reduced fine fraction at the Sahara, bringing the VSD shape more into line with the observed VSD.

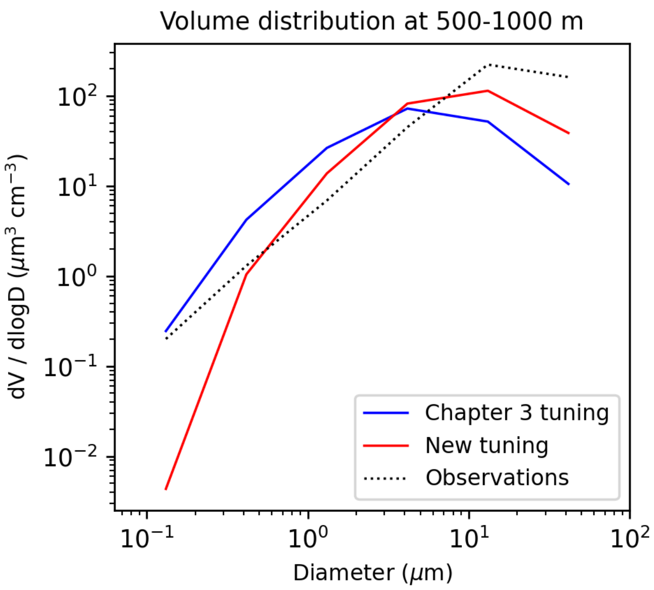

Figure 4.1: Volume size distribution (in μm^3 cm^{-3}) of dust over the Sahara between 500-1000 m in the Fennec Sahara observations, the model configuration used in Chapter 3 and the newly tuned configuration used in Chapters 4 and 5.

Emissions are tuned using three parameters in the model: a global multiplier of horizontal dust flux, a friction velocity multiplier and a soil moisture multiplier, as explained in Section 2.2. These have been changed from 2.25, 1.45 and 0.5 in the CMIP6 configuration to 30, 1.1 and 0.5 in the new configuration. The emissions were tuned to better match the size distributions measured at the Sahara during the Fennec aircraft campaign (Ryder et al. 2013b). This tuning was based purely on results from the Sahara and considered no other sources across the globe as it was specifically tuned for this research focusing on trans-Atlantic dust transport.

4.1.2 Radiative Effects

Radiative interactions with dust have been switched off for most of the simulations in this Chapter. Leaving radiative effects (RE) on results in changing emissions and atmospheric circulation as a result of the changes to deposition efficiency of dust. Thus, by switching RE off, the model simulations will be parallel in their meteorology, meaning the comparison between experiments shows the physical impact of the altered process for each experiment on the dust particles. By turning RE off, AOD has to be calculated offline using the calculations in Section 1.1.2 . RE are left turned on for only two experiments, a control simulation and one experiment where I have altered the SW absorption of dust.

4.1.3 Sensitivity Experiments

In this Section, I will describe the changes which are made for my sensitivity experiments on the model. Table 4.1 shows all of the experiments which will be discussed in this Chapter and the abbreviations by which they will be referred, as well as whether RE are switched on/off in those experiments.

Simulation name	Abbreviation	RE on
RE Off Control	Control	No
No sedimentation	NoS	
−95% sedimentation	S95	
−80% sedimentation	S80	
−50% sedimentation	S50	
No impaction scavenging	NoIS	
No convective mixing	NoCM	
Doubled convective mixing	2xCM	
No turbulent mixing (over the ocean)	NoTM	
RE On Control	REControl	Yes
Tripled SW absorption	3xSW	

Table 4.1: Sensitivity experiment names, name abbreviations used in the text and whether the experiment has radiative effects turned on.

Sedimentation

Recent research has suggested that certain processes not considered or effectively represented in many models, such as asphericity, electrical charging, and vertical and turbulent mixing, may increase coarse particle lifetime. Some studies have shown that by reducing the sedimentation velocity of dust particles, models have been brought into better agreement with observations of coarse particle transport (Drakaki et al. 2022; Huang et al. 2020; Maring et al. 2003; Meng et al. 2022). The changes made to Stokes settling velocities (V_S) or particle density are on the scale of orders of magnitude, for example, Drakaki et al. (2022) found agreement with observations when V_S was reduced by 40-80%. Here, I aim to test reductions in the sedimentation of dust in the HadGEM3-GA7.1 climate model configuration as well as a complete removal of V_S.

In order to alter the sedimentation, the Stokes deposition velocity, V_S in equation 1.13, is altered in both the UM and JULES code. Changes need to be carried out in the JULES code as V_S is used in the calculation of the Stokes number, an impaction parameter used in the calculation of the collection efficiency for when the dust hits a surface. One experiment tests the effect of 'turning off' sedimentation, in this case, V_S is overwritten to equal 0 at all times and locations in the model (Experiment NoS in Table 4.1). In other experiments, the sedimentation is reduced by 50% (S50), 80% (S80) and 95% (S95); in these cases, V_S is simply multiplied by values 0.5, 0.2 and 0.05, respectively.

Impaction Scavenging

In the model, wet deposition of dust is represented by impaction scavenging up to a cloud top. The rate of impaction scavenging is calculated using Equation 2.7 and controlled by a scavenging coefficient (Λ) which varies depending on particle size as shown in Table 2.2.

In these experiments, values of Λ are altered uniformly across bins in order to change the impact of impaction scavenging on dust. Specifically, to test the sensitivity of the dust to impaction scavenging, values of Λ are set to 0 for all size bins in a 'no impaction scavenging' experiment (NoIS).

Convective Mixing

Research such as that of Gasteiger et al. (2017), Takemi (2005), van der Does et al. (2018), and Xu et al. (2018) has hypothesised that convective mixing (CM) throughout the SAL could enhance particle lifetime. Here, I aim to test the impact of removing CM on dust, as well as the impact of amplifying the effect of CM.

Parameterised CM in the UM is responsible for both upwards and downwards movements of dust through the model atmosphere (described in Section 2.3). Dust is passed through the convection code as a tracer in the UM. In two experiments, I remove the impact of CM (NoCM) and double the impact of it (2xCM). To do this I either simply remove the code where the dust tracer is passed through the convective code, or multiply the tracer by a factor of two. Note that this does not mean meteorological convection is turned off completely in the model, only its interaction with dust.

Turbulent Mixing

Cornwell et al. (2021) and Denjean et al. (2016) have showed that turbulent mixing (TM) in the atmosphere could enhance coarse particle altitude and transport in the atmosphere. Additionally, the idea of self-lofting of dust, whereby the absorption of the dust heats the air around it, creating small turbulent motions could increase the transport of coarse particles (Colarco et al. 2014; van der Does et al. 2018).

TM is responsible for the lofting of dust after emission as well as downwards mixing of dust in the model. In the HadGEM3-GA7.1 model, it acts between the surface and just above the top of the BL (described in Section 2.3). In this experiment, I wish to test the impact of removing TM of dust from the model (NoTM). As TM is responsible for the uplift of dust over land, I use a gridbox land cover threshold to determine areas of land or ocean and keep TM turned on over land, but turned off over the ocean.

SW Absorption

Some research suggests that dust particles may be more absorbing than previously thought (e.g. Di Biagio et al. (2020)) which could create more in-plume heating, mixing dust particles to higher altitudes, thus improving transport (Colarco et al. 2014; van der Does et al. 2018). Therefore, my final sensitivity experiment will alter the SW absorption of dust in the model. In this experiment, I have tripled the SW absorption of dust as a drastic and large change to understand if there is any sensitivity (3xSW). A description of the model radiative effects of dust is in Section 2.5.

The spectral files for dust in the model have been altered for this experiment so that the original values for the SW absorption of dust have been tripled at all wavelengths. The original and new absorption values at 550 nm are shown in Table 4.2. The LW radiative effects remain unchanged.

Size bin	Mass absorption efficiency (m^2 kg^{-1})	
	Original	3xSW
1	16.94	50.83
2	28.19	84.56
3	29.99	89.97
4	21.70	65.09
5	15.32	45.96
6	8.65	25.96

Table 4.2: Mass absorption efficiency range (in m^2 kg^{-1}) at 550 nm from the model spectral file including the original values and those used in the 3xSW experiment.

The control simulation (REControl) used for the comparisons with the 3xSW experiment is not the same used in the previous experiments where RE were turned off. Therefore, this experiment will not be directly compared with the other sensitivity experiments due to the radiative interactions of dust affecting heating and cooling in the atmosphere which alter the meteorology and emissions.

4.2 Results of the RE Off Experiments

In this Section, the results from each of the RE off sensitivity experiments will be presented and discussed separately, before being compared collectively.

4.2.1 Control Simulation

In this section, the Control simulation will be introduced. This is the simulation that all RE off sensitivity studies are compared to. This simulation has been tuned so that the emissions are in better agreement with observations, as I found in Chapter 3 that the model underestimated the coarse dust size distribution at emission and this problem was exacerbated after long-range transport. Therefore the size distribution should be closer to observations at emission so that the difficulties faced by the model during transport are easier to analyse.

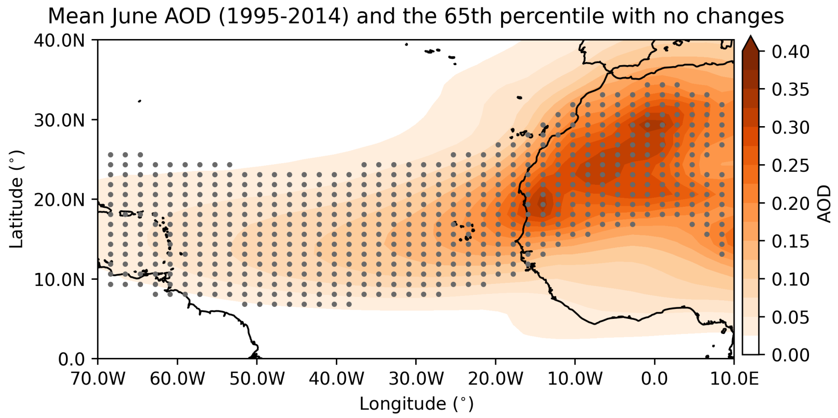

Figure 4.2: Mean June AOD (colour shading) and the 65th percentile of AOD values at each longitude (grey stippling) between 1995-2014 in the Control simulation.

Figure 4.2 shows the mean dust AOD from 20 Junes between 1995-2014 over the eastern Sahara and the tropical North Atlantic. The stippling on the plot shows the 65th percentile of AOD at each longitude between 1°S and 47°N. The mean AOD over the eastern Sahara extends up to 0.4, ∼0.05 higher than the simulation used in the previous chapter.

The dust plume follows the climatological trans-Atlantic path, suggesting that the mean of 20 June months that I am using in this study is representative of a climatology. The spatial distribution of dust is also representative of normal conditions.

Figure 4.3 shows the binned mass concentration profiles at the Sahara, Canaries, Cape Verde and Caribbean for the Control simulation. Mass is dominantly represented in the largest bins.

The profile at the Sahara peaks near the surface, whereas at the other locations, the concentration is greatest in the lofted SAL. Bins 4 and 5 have the greatest mass at all locations, except for at the Caribbean when the bin 5 mass decreases lower than the bin 3 mass. The greatest mass in bin 4 decreases by a factor of 5 from 150 µg m^{-3} at the Sahara to 30 µg m^{-3} at the Caribbean. Whereas the bin 5 maximum mass decreases by a factor over 40 from $>$ 230 µg m^{-3} at the Sahara to 5 µg m^{-3} at the Caribbean. Finally, bin 6 decreases from a concentration of close to 150 µg m^{-3} at the surface and 50 µg m^{-3} at 1 km at the Sahara to a negligible concentration at the Caribbean. Again, this shows the overly swift deposition

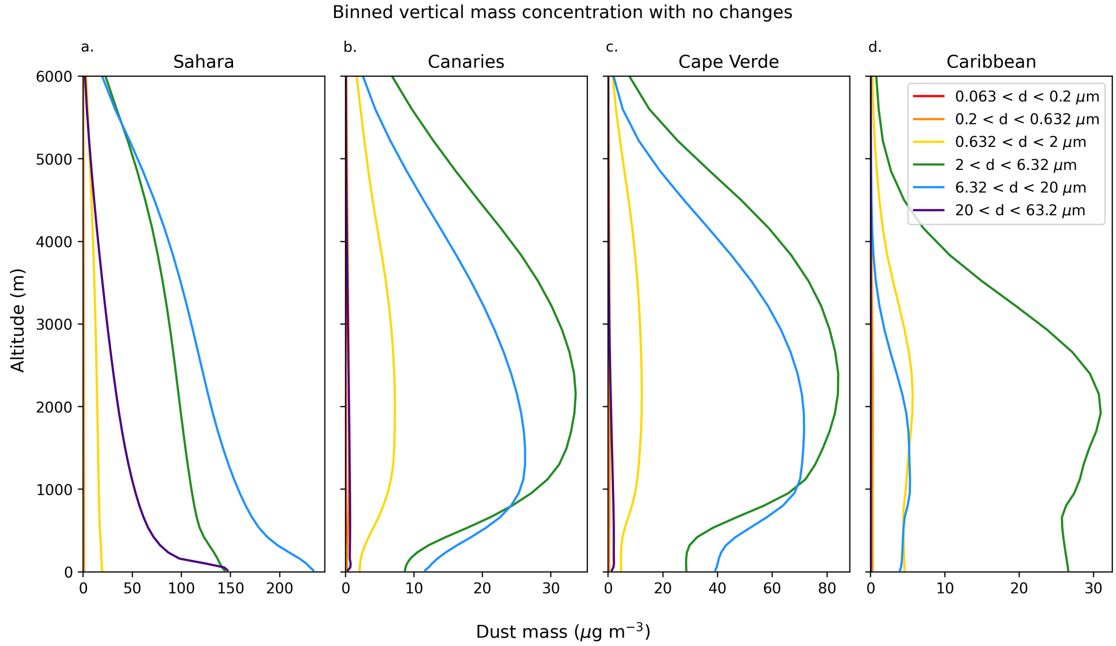

Figure 4.3: Binned mean June mass concentration profiles (in μg m^{-3}) at the Sahara, Canaries, Cape Verde and Caribbean between 1995-2014 in the Control simulation.

of the coarse bins even when the emissions are in better agreement with observations.

Figure 4.4 shows the vertically-resolved VSD of the Control simulation at the Sahara, Canaries, Cape Verde and Caribbean.

At the Sahara, all size bins are subject to an altitude dependence, whereby the VSD decreases with altitude. The coarser size bins are more dependent on altitude, with a greater difference between the VSD at the lowest and highest altitudes. At the Canaries and Cape Verde, the decreasing relationship of VSD with altitude is only seen above the peak in concentration in the SAL (between 2-3 km) in size bins 2-5 (0.2-20 μm), or at all altitudes in size bins 1 and 6. In the mid SAL (between 1-3 km), the VSD is fairly uniform in size bins 2-5, resulting in overlapping VSD lines. Below 1 km, the concentration decreases in the MBL, resulting in reduced VSD. At the Caribbean, the dust plume is much lower, as seen in Figure 4.3d, which results in overlapping VSDs between 0-2.5 km altitude in size bins 2-5.

Typically, the size bin 6 VSD is a similar or slightly lower value to size bin 3 at each altitude at the Sahara. Upon transport downstream to the Canaries or Cape Verde, the size bin 6 VSD is more comparable to VSD values from even finer particles. Additionally, the range in size bin 6 values has increased from less than one order of magnitude at the Sahara to nearly three orders of magnitude at Cape Verde,

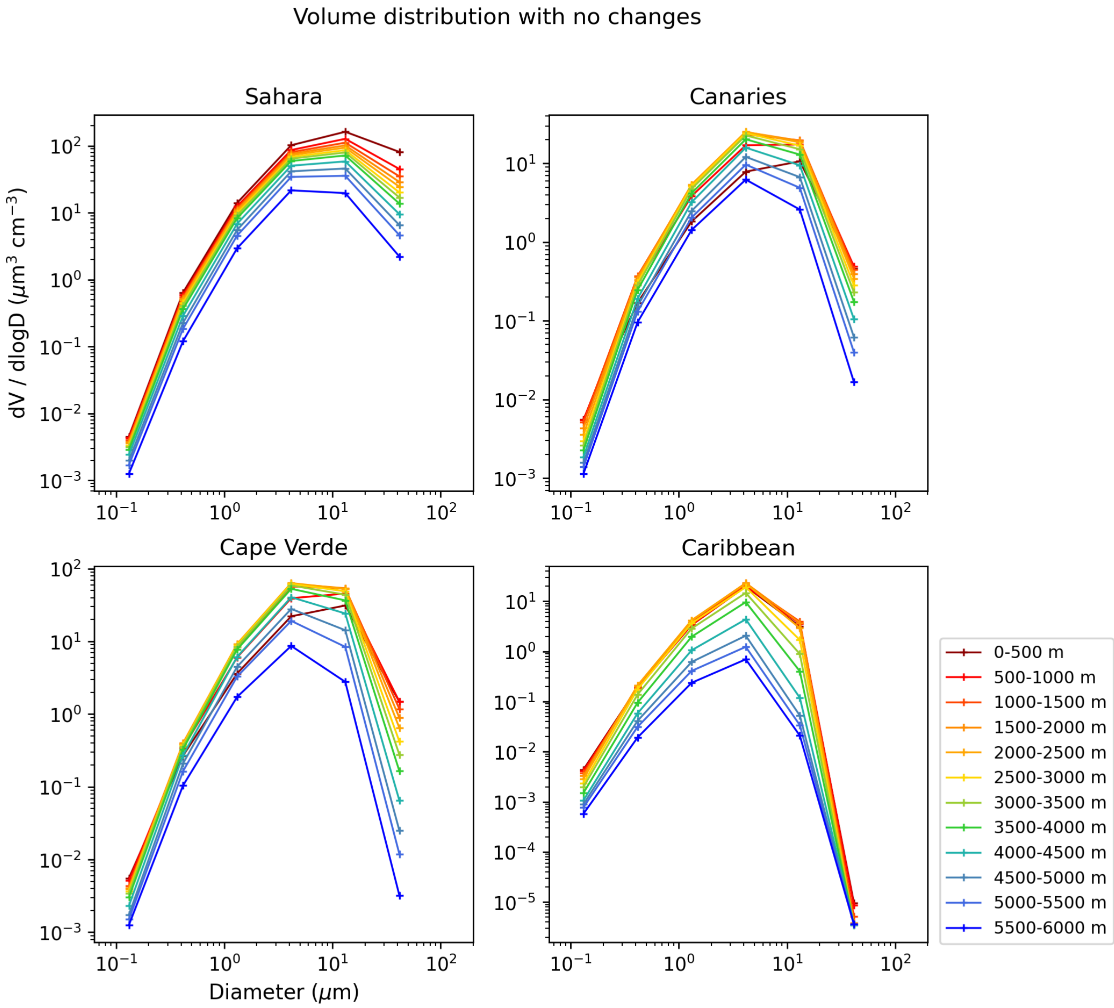

Figure 4.4: Vertically-resolved VSD (in $\mu m^3\ cm^{-3}$) of the Control simulation at the Sahara, Canaries, Cape Verde and Caribbean. The VSDs are shown as 0.5 km averages between 0-6 km.

with the high altitude VSD showing a greater difference between bin 5 and bin 6 than at lower altitudes. This suggests a swift deposition of the size bin 6 particles, not only by the much lower VSD values, but the amplified loss of VSD at altitude too.

Upon transport to the Caribbean, there is a significantly smaller range between the size bin 6 VSD at all altitudes compared to other locations, with all VSD values on the order of 10^{-6} μg m^{-3}. The low variability between altitudes is due to the low concentrations and the limited ability of the model to represent such low concentrations.

Thus, despite attempts made to improve the VSD with emissions tuning, the decrease in size bin 6 VSD with transport from the Sahara shows that there are still processes in the model which are inhibiting coarse particle transport.

4.2.2 Sedimentation

By reducing the settling velocity of dust in models, some studies have shown improved model representation with respect to observations (e.g. Drakaki et al. (2022), Huang et al. (2020), and Meng et al. (2022)). Thus, in these experiments, the sedimentation of dust in the HadGEM3-GA7.1 simulation will be reduced or completely turned off in order to assess the sensitivity of coarse dust transport to this mechanism.

No Sedimentation

In this experiment, the sedimentation of dust has been uniformly reduced to zero throughout the model atmosphere. Figure 4.5 shows the difference in total column mass across the six size bins between the NoS experiment and the Control simulation. In all size bins there is an increase in the atmospheric dust load both at the source and at distance from the source, towards the Caribbean. In size bins 2-6 (Figure 4.5bcdef), the greatest increase is seen over the Sahara, with a band extending out across the Atlantic in the location of the main dust plume. However, in size bin 1, the greatest difference occurs across the Atlantic with less change over the Sahara (Figure 4.5a).

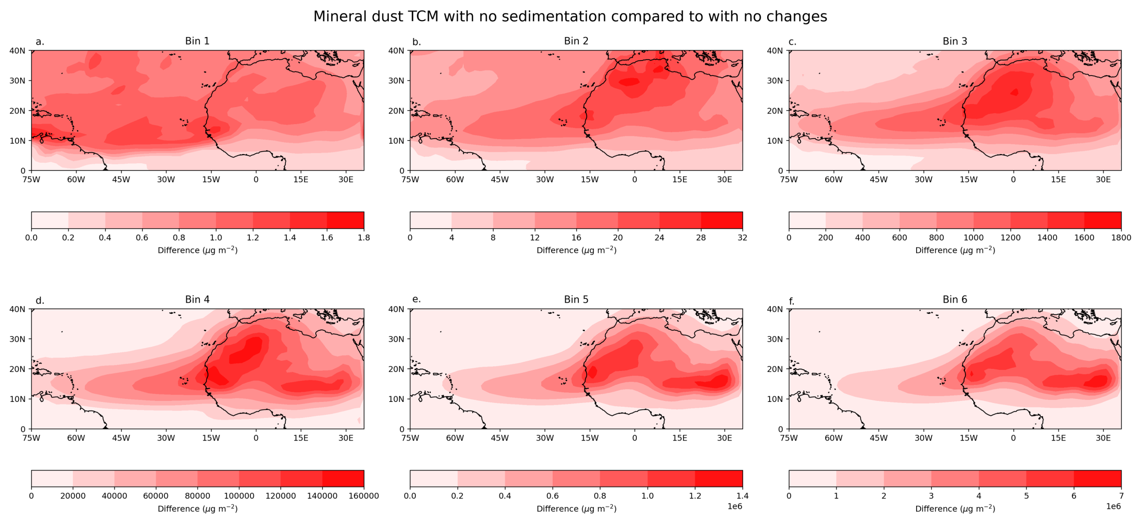

Figure 4.5: Difference in the total column mass (in µg m^{-2}) between the NoS experiment and the Control simulation. The six subplots represent the six size bins used in the model.

In the model, sedimentation is one of two mechanisms which controls the dry deposition of dust. Without this mechanism, there is increased dust loading in the atmosphere as seen in Figure 4.5. There is an increase in the AOD of up to 0.3 over the Sahara (not shown), which is nearly a doubling of the AOD in the Control simulation (Figure 4.2).

Figure 4.6 shows the percentage difference in the combined wet and dry deposition of dust in the model. In all size bins (Figure 4.6abcdef), the net change in deposition over the Sahara is negative, showing that in the NoS experiment, there is less deposition here than in the Control simulation. This indicates that dry deposition is usually the dominant cause of deposition over the Sahara. Outside of the main dust plume across the Atlantic, there is an increase in deposition in size bins 4-6 (Figure 4.6def) in the west Atlantic. This increase at distance ranges from increasing by 100% in size bin 4, 10000% in size bin 5 to 10^{12}% in size bin 6. These changes suggest an increase in particle transport, whereby the dust is allowed to travel further without sedimentation and so we see an increase in deposition. While the changes in size bin 6 appear large, they are only so extreme due to the very small quantity of particles over the Atlantic in the Control simulation. Any slight increase in particle quantity results in a huge percentage change, which is exactly what we see in the mid-Atlantic in Figure 4.6f.

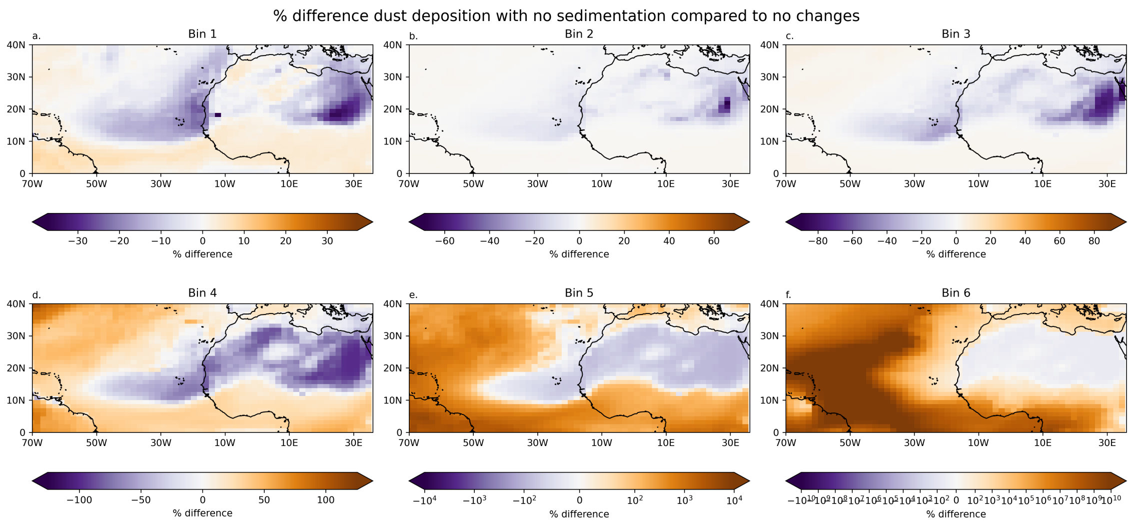

Figure 4.6: Percentage difference between the total dry and wet deposition of dust in the NoS experiment compared to the Control simulation. The difference is shown in the six size bins used in the model. The colour bar scales vary between bins. Size bin 5 and 6 are represented on a log scale.

In size bins 2 and 3 (Figure 4.6), away from the Sahara, there is very little change in the total deposition, suggesting that dry deposition by sedimentation is not normally very important for the deposition of these size particles. Alternatively, it appears that the size bin 1 dust is more impacted by the change in sedimentation than bins 2 and 3. This could be due to the dry deposition of particles in size bin 1 being dominantly controlled by Brownian diffusion, whereas particles in bins 2 and 3 are more dominantly controlled by turbulent processes (Bergametti and Foret 2014). Overall though, I postulate that the three smallest bins are the least affected by sedimentation and rely on other mechanisms for their deposition.

Figure 4.7 shows the changes in deposition broken down into wet and dry changes. The percentage change in wet and dry deposition is shown for each size bin. In size bins 1-5 (Figure 4.7acegi) and over the Sahara and in outflow regions close to the African coast in size bin 6 (Figure 4.7k), the dry total amount of deposition is lower in the NoS experiment; the degree of decrease varies between size bins. From size bin 1 to 5, the change in dry deposition is fairly uniform across the analysed domain and increases up to 100% reduction in size bin 5. By 'turning off' sedimentation, we have removed only one of two mechanisms which contribute to the total dry deposition; turbulent mixing in the model is also responsible. The changes in dry deposition of dust suggest that as size increases (up to size bin 5), the sedimentation becomes more important for the dry deposition than turbulent mixing, which is still responsible for dry deposition at the fine size range.

Theory suggests that we can separate our six size bins into three categories for understanding their settling velocities: the finest particles (< 0.1 µm; approximately size bin 1) which are dominantly impacted by Brownian diffusion, the mid-size particles (0.1-5 µm; size bins 2, 3 and 4) which are the slowest settling and dominantly controlled by turbulent processes and the coarser particles (> 5 µm; size bins 5 and 6) which are controlled by sedimentation (Bergametti and Foret 2014). Generally, the model corroborates this as there is an increase in dry deposition with size, showing that coarser particles are the in the size range most dominantly affected by sedimentation. Size bins 1 and 2 are the least impacted by sedimentation and thus show a decrease in dry deposition of less than 50%, due to alternative processes still contributing to their dry deposition. Particles in size bin 3 have a dry deposition $\sim$75% less than in the Control, suggesting some impact from turbulent processes. Whereas size bins 4 and 5 have nearly 100% reduction in dry deposition due to their large dependence on sedimentation.

For the most part, size bin 6 does not match the reaction of the other bins to removed sedimentation. Figure 4.7k shows that over the Sahara and in outflow regions close to the African coast, the amount of dry deposition has decreased, matching the other size bins. However, further from the source, over the mid and west Atlantic,

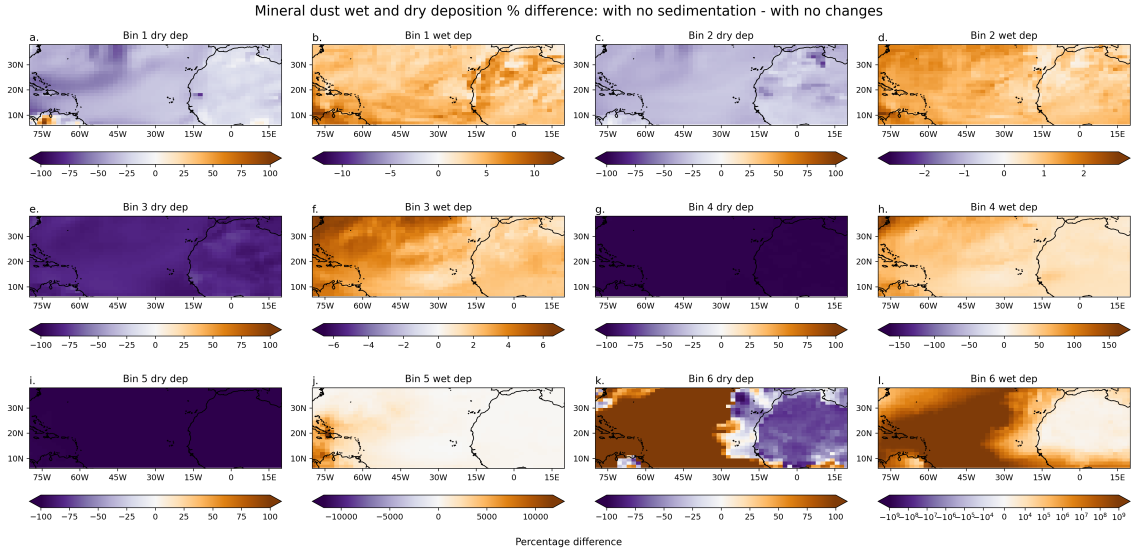

Figure 4.7: Percentage difference in the separate dry and wet deposition of dust in the NoS experiment and the control simulation. Each size bin has two plots showing the change in dry and wet deposition. Size bin 6 wet deposition is shown on a log scale.

the amount of dry deposition increases by more than 100%. In Figure 4.6f, there is increased total dust deposition in most size bins at distance from the Sahara, which I hypothesised to be caused by decreased deposition near the source, causing higher concentrations at distance which results in increased deposition at distance from the source by means other than sedimentation. For coarse size bins 4 and 5, the removal of sedimentation meant $> 99\%$ of the dust was removed through wet deposition, whereas for size bin 6, the presence of dust west of 30°W where there is usually no dust present results in an exaggerated increase in any deposition, wet or dry. Based on the nearly 100% decrease seen in size bin 5 dry deposition, we might expect to see this level of decrease over the Sahara in size bin 6. However, instead the dry deposition is reduced by $< 90\%$ across the Sahara suggesting that other processes must play a role in the dry deposition of size bin 6 particles, which doesn't seem to be the case for size bins 4 and 5.

With the removal of sedimentation and the reduced dry deposition efficiency, wet deposition becomes the main deposition mechanism for dust in all size bins (Figure 4.7). The change in wet deposition is less uniform than the changes in dry deposition, especially in size bins 1 and 2; this is likely due to wet deposition being caused by the presence of rain and clouds which are not uniformly distributed horizontally or vertically throughout the atmosphere. In the size bins which are more reliant on sedimentation for dry deposition (size bins 4, 5 and 6), the percentage change by which the wet deposition increases is more enhanced than the finer bins which are less reliant on sedimentation. For example, wet deposition in size bin 1 is only increased up to ∼15%, whereas wet deposition in bins 4, 5 and 6 is increased by up to 150%, 12000% and > 10^7%.

The analysis will now explore the more detailed vertically-resolved changes at individual locations as opposed to the total spatial changes. Figure 4.8 shows the volume size distribution (VSD) at the four locations in the NoS experiment. Additionally, the percentage difference between the NoS experiment and the Control simulation are shown on the same plot. The coloured lines represent 0.5 km vertical averages through the atmosphere.

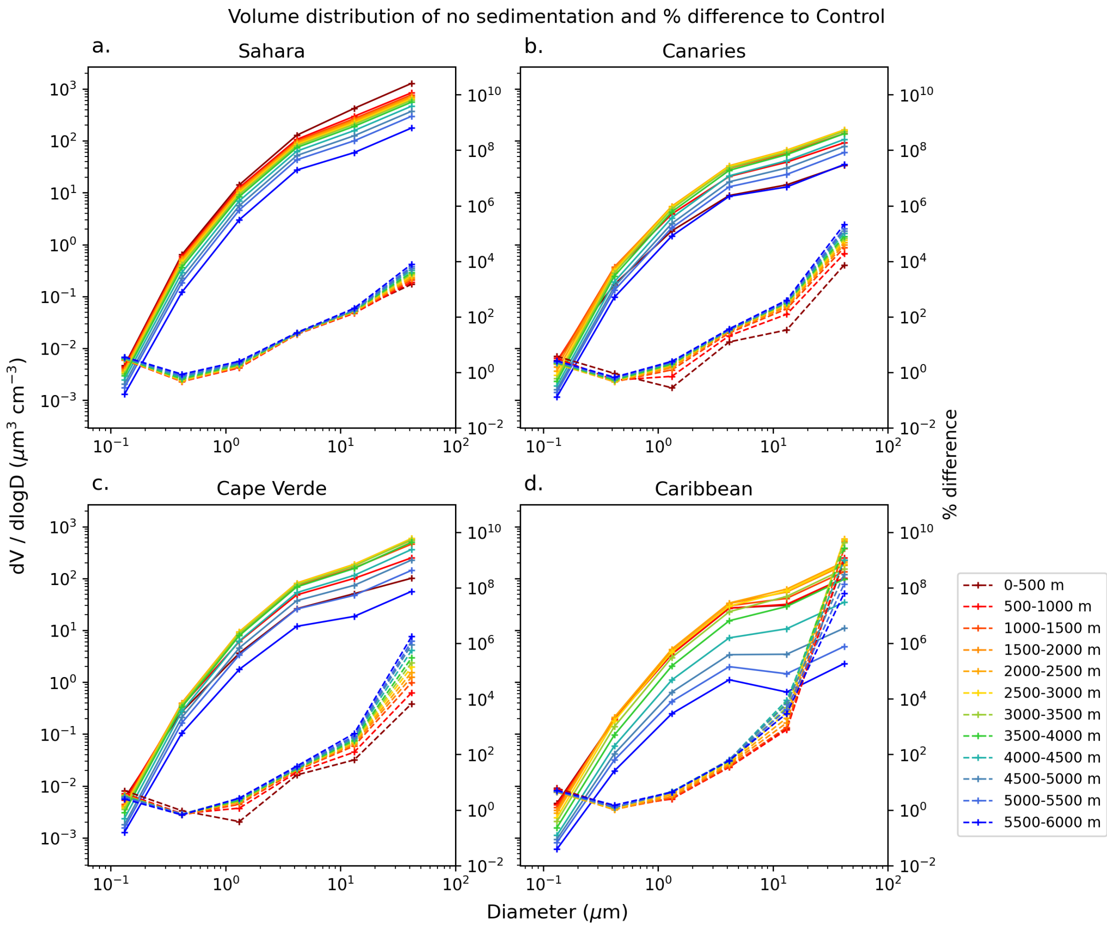

Figure 4.8: Absolute (solid lines; in $\mu m^3\ cm^{-3}$) and percentage difference (dashed lines) values of the VSD in the NoS experiment compared to the Control simulation. Plotted at the Sahara, Canaries, Cape Verde and Caribbean.

As explored previously, the coarser size bins (4, 5 and 6; 2-63.2 μm) are the most affected by changes to the sedimentation while there is little to no change at the fine size range (size bins 1, 2 and 3; 0.063-2 μm). The change in VSD is most exaggerated at coarser size ranges at all locations, increasing the 20-63.2 μm VSD by more than 2000% at the Sahara, 10000% at the Canaries and Cape Verde and up to 1e^{9}% at the Caribbean (Figure 4.8). Such large changes in size bin 6 result in completely changing the shape of the overall VSD, raising the coarse end of the distribution higher than all other bins. In terms of the shape of the new VSD, at the Canaries, Cape Verde and Caribbean, the curve is no longer completely smooth and consistent, with the a dip forming in the VSD between size bins 4 and 6 at bin 5 (Figure 4.8bcd). The VSD dips slightly between bins 4 and 6. This is likely due to size bin 6 being more affected by the changes to sedimentation than size bin 5. This effect becomes more exaggerated with distance from the Sahara. At the Sahara, there is not much change in the difference of the VSD gradient between size bins 4, 5 and 6. However, at the Caribbean, the difference between size bin 5 and 6 is always an increase, whereas between size bins 4 and 5, it is a much shallower gradient, occasionally turning negative.

The changes in the VSD shape are not uniform with altitude. At the Sahara, the greatest increase in size bins 4, 5 and 6 occurs between 0-0.5 km above the surface (Figure 4.8a). The amount of change then decreases with altitude to the highest level with the least increase in VSD. This agrees with our understanding of the changes we have made to the model. By turning off sedimentation, we have reduced the downward force on each coarse particle, reducing the removal of the coarse and super-coarse particles in the model, and allowing them to be raised higher into the atmosphere. Thus, we see an increase of coarser particles at altitude and an even greater increase near the surface where a lot of particles that would be removed within a couple of model time steps of emission are now retained for longer and the removal of one of the dry deposition mechanisms slows down the overall removal process, resulting in a 'pooling' of particles near the surface. Notably, the increased concentrations seen in the surface layer are no longer seen at the downstream locations (Figure 4.8bcd). Instead, the greatest increases in VSD are seen at central SAL altitudes (~0.5-4 km) at the Canaries, Cape Verde and Caribbean. The lower levels (0-1.5 km) are more comparable with change in the highest layers (4-6 km) at downstream locations. While the entire VSD increases at all levels, the greatest increase occurs within the SAL. This suggests that while the reduced sedimentation increases the horizontal and vertical transport of the coarse dust and its retention within the SAL, this change cannot overcome the processes which are active in the MBL that result in the removal of coarse particles.

Another thing to note is the enhanced altitudinal dependence at the Caribbean in the coarser size ranges compared to the fine size range (Figure 4.8d). At the fine size range, there is less than one order of magnitude between the VSD at 0-0.5 km as between 5.5-6 km, whereas at the coarsest end of the size range, there are two orders of magnitude difference between these same altitude ranges. This suggests that while we have removed sedimentation of dust particles, there is still some process in the model which is limiting the vertical distribution of the coarsest particles.

Figure 4.9 shows the difference in the size-resolved vertical mass concentration profiles at the Sahara, Canaries, Cape Verde and Caribbean between the NoS experiment and the Control simulation. These profiles allow us to see a higher resolution break down of the changes occurring in each size bin with altitude. Figure 4.8a revealed that the greatest changes in VSD at the Sahara occurred in the lowest layer between 0-0.5 km altitude. Figure 4.9 shows that the change in size bin 6 dust mass concentration peaks at the surface at an increase of more than 2000 µg m^{-3} and sharply decreases up to 0.5 km to an increase of ~1100 µg m^{-3} before decreasing at a more shallow gradient with altitude. These increases represent changes to the size bin 6 mass of 1300% at the surface up to 8000% at 5.5 km altitude (percentage change plots not shown). However large these changes are, they do not significantly impact the shape of the vertical profile which remains similar to the Control simulation (Figure 4.3a), but with slight exaggeration at the highest concentrations. This pattern is fairly similar for the other three locations analysed.

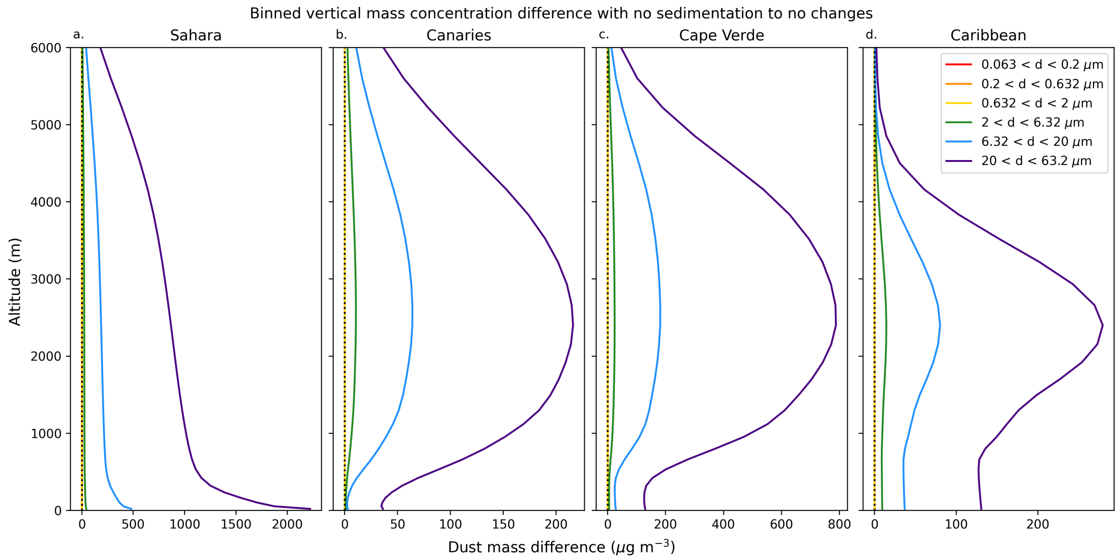

Figure 4.9: Mass concentration difference (in µg m^{-3}) between the NoS experiment and the Control simulation at the Sahara, Canaries, Cape Verde and Caribbean.

Reduced Sedimentation

After testing the impact of NoS of dust revealed that the coarse particles were retained for too long, I tested the sensitivity of the coarse dust to reducing the sedimentation by varying amounts in the S50, S80 and S95 experiments.

Figure 4.10 shows the mean dust VSD between 2-4 km in the observations and in the model in the Control simulation and multiple sedimentation experiments at the four analysed locations.

The first point to note is the increasing level of underestimation by the Control simulation compared to the observations in size bins 5 and 6 with increasing distance from the Sahara (Figure 4.10). At the Sahara, the Control simulation VSD is nearly within the range of the observed standard deviation in the coarse range (6.32-63.2 µm). At the Canaries, while the modelled size bin 5 is still within an order of magnitude of the observations, size bin 6 is underestimated by ~2 orders of magnitude. At the Caribbean, the difference has increased to 6 orders of magnitude, while bin 5 also shows more disparity with the model, with a difference of more than one order of magnitude. In Chapter 3, I showed that the difference between the observations and model grew with distance from the source. Here, I show that this occurs even with an improved size distribution at the source, that the overly swift deposition of coarse particles is not a consequence of a poor emitted distribution.

By looking at all these experiments together in Figure 4.10, we can get an idea of the coarse dust sensitivity to sedimentation. Without any sedimentation (NoS), the VSD is greatly increased in size bins 5 and 6 compared to the Control. The Control and NoS experiments represent the two extremes for which the other experiments sit between. Without sedimentation, the coarse end of the size distribution is raised higher than the Control simulation, with the S50, S80 and S95 experiments appearing with size bin 5 and 6 VSD in between. At the Sahara, all five experiments are within 2 orders of magnitude apart at size bin 6, whereas at the Caribbean, they are 8 orders of magnitude apart. In the space between the Control and NoS size bin 6 VSD, the S50, S80 and S95 experiments are nearly evenly spaced from each other on the log scale of Figure 4.10. This is despite the changes to sedimentation being varying in magnitude, i.e. there is only a 5% change in sedimentation between NoS and S95, and a 30% change between S80 and S50. This suggests that the impact of sedimentation is not linear. The difference between the bin 6 VSD in the NoS and S95 experiments (a change of only 5% sedimentation) is just less than half of the difference from the NoS to the S80 experiment (a change of 30%, 6 times the change

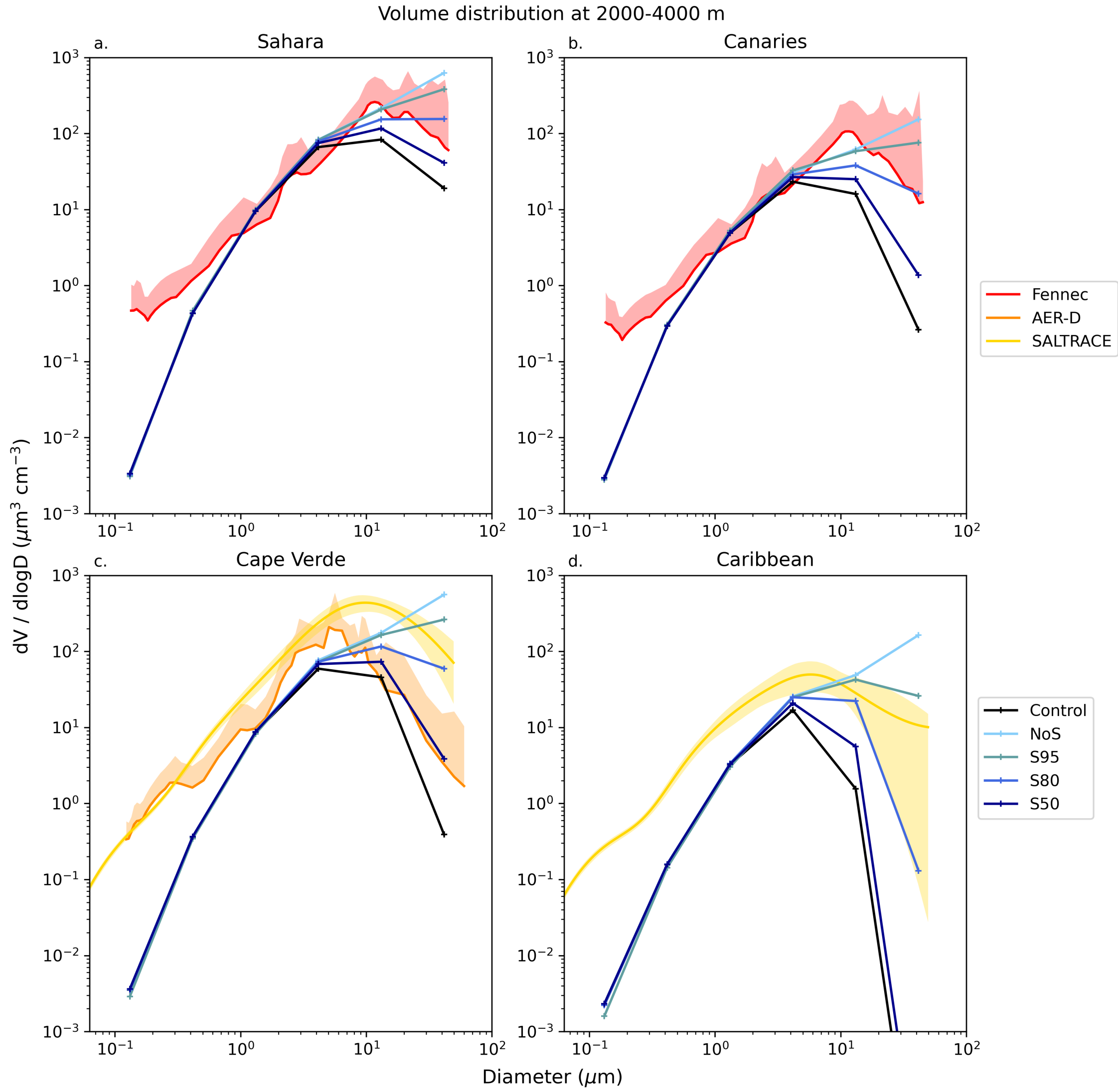

Figure 4.10: Mean VSD (in μm^3 cm^{-3}) between 2-4 km altitude at the Sahara, Canaries, Cape Verde and Caribbean. The observed VSDs from Fennec, AER-D and SALTRACE East and West are shown. One standard deviation is shown for the Fennec, AER-D and SALTRACE data by the shaded areas. Only upwards shading is shown for clarity. The 10th and 90th percentiles of the SALTRACE data are shown. The Control simulation is shown alongside the NoS, S50, S80 and S95 experiments. The Control simulation terminated at $3.57e^{-6}$ μm^3 cm^{-3} in size bin 6 at the Caribbean.

in sedimentation). Alternatively, the difference between the Control simulation and the S50 experiment is much smaller than with the S80 experiment. This is especially notable at the Caribbean, where the 50% reduction in sedimentation results in an insignificant change to the bin 6 VSD where the model is still underestimating the observations 6 orders of magnitude. Whereas a 30% more reduction (S80) in the sedimentation reduces the underestimation to only 2 orders of magnitude. Reducing by only a further 15% (S95) raises the VSD above the observations. This means that large reductions in sedimentation are required to alter the magnitude of the bin 6 VSD by the amount which is required to match the observations.

In terms of recreating the observed VSDs, depending on the location, some experiments have better success at matching the observations at the coarse size range. By comparing the shapes of the modelled size distributions to the observations, we can gain a better understanding of which experiments are better matched. At the Sahara, the absolute values of the VSD at size bin 6 are relatively close between the Control and the observations. However, the shape of the observed size distribution shows that size bin 4 and size bin 6 have similar dV/dlogD values, whereas the Control simulation has a size bin 6 value lower than size bin 4. Thus, S50 is better fitted to the observations as the size bin 4 and size bin 6 values are more similar, though I suggest a reduction of more than 50% is needed to fully bring the shape of the modelled VSD into better agreement with the Fennec observations as S80 raises the coarse end of the VSD too high.

At the Canaries, the size bin 4 and size bin 6 values are again similar in the observations, showing fairly little change from the Sahara (Figure 4.10b). However, due to the swift deposition of the coarse particles in the model, neither the Control or S50 simulations are suitably matched to the observations with low size bin 5 and size bin 6 values. In the S50 experiment, the size bin 5 value is nearly equivalent to the size bin 4 value where it should be greater than this. Instead, the S80 experiment shows a better VSD shape, peaking in size bin 5 and dropping only slightly to size bin 6. Here, the S80 experiment achieves a VSD most similar to the observations. However, at Cape Verde, the disparity in the AER-D and SALTRACE-E observations results in a less certain comparison with the model experiments. The SALTRACE-E observations have a more similar VSD shape to the Fennec observations, peaking in size bin 5, whereas the AER-D observations peak at a smaller size range approximately within size bin 4. Similarly to at the Canaries, the S80 experiment appears best fitted to the SALTRACE-E observations, with a peak in size bin 5, though the observations show less of drop to size bin 6, suggesting that a reduction greater than 80% could be more appropriate. Alternatively, the AER-D observations are much more closely represented by the Control and S50 experiments. Further downstream at the Caribbean, the Control, S50 and S80 experiments all have a VSD which drops off too swiftly at the coarse size range with size bin 6 values significantly lower than the observations (Figure 4.10d). This suggests that a reduction in sedimentation of more than 80% and less than 95% is required for coarse particles to reach the Caribbean in quantities seen in the observations.

The VSD in the Control simulation and all four sedimentation experiments appears to underestimate the fine VSD by 1-2 orders of magnitude at every location (Figure 4.10). This could be an artefact of the tuning which has been carried out to improve the coarse end of the size distribution. Alternatively, it could be due to contamination of the observations. The fine tail of the observed size distribution (< 0.3 µm) at all locations shows a slight bump or more gentle decline compared to the distribution 0.3-5 µm, this could be due to anthropogenic pollution increasing the concentration of sub-micron particles.

Figure 4.11 shows the normalised total mass profile in the Control simulation and the four sedimentation experiments at the Sahara, Canaries, Cape Verde and Caribbean. Having been normalised by their total mass between 0-7 km, the plots show changes in the shape of the vertical distribution of dust due to changes in the sedimentation.

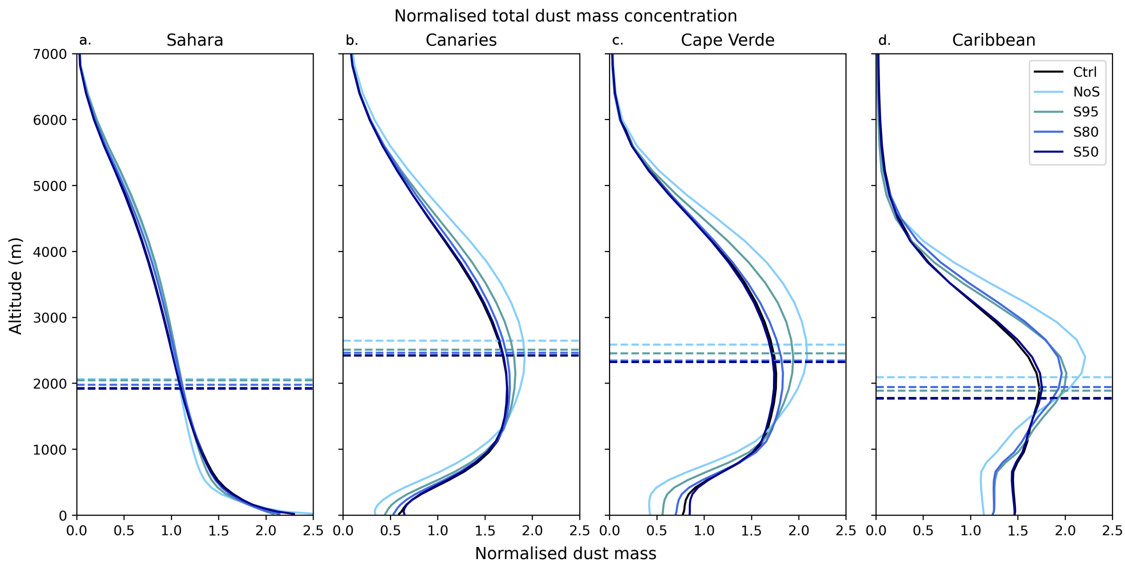

Figure 4.11: Total mass concentration profiles normalised by the total 0-7 km mass in the Control and four sedimentation experiments: NoS, S95, S80 and S50. Dashed lines show the position of the MCA for each simulation.

At the Sahara (Figure 4.11a), there is not much change in the overall profile shape between the different simulations, especially between the Control, S95, S80 and S50. The NoS simulation stands out the most. Below 0.1 km, near the surface layer, the NoS mass is greater than that in the other experiments, due to the reduced removal efficiency. Between 0.3-1.7 km, there is relatively less NoS mass and a signal suggesting there is slightly more mass between 3.5-5.5 km; this suggests that there is a slight vertical shift in the dust mass, with more in the top half of the SABL and right at the surface, and less in the lower half of the SABL (0.1-3.5 km). As the distance from the source increases, the disparity between the profile shape in each simulation also increases. Excluding the increase at the surface seen at the Sahara, the sedimentation-altered profiles at the subsequent locations follow a similar pattern of decreased concentration in the lower profile and increased mass at higher altitudes, with the NoS simulation having the greatest impact. At the Canaries, Cape Verde and Caribbean, the peak in mass concentration in the SAL raises higher with decreasing sedimentation. At Cape Verde, the peak in mass concentration in the Control simulation at ∼2 km is ∼0.5 km lower than in the NoS simulation. Both the S50 and S80 simulations have their peak concentration at very similar altitudes, showing the least change in vertical profile, whereas the S95 simulation is raised higher. The difference in profile shape is the greatest at the Caribbean, suggesting an exacerbated deformation of the profile with transport. The NoS profile has a greater increase in relative mass concentration in the SAL (2-4 km) than the other simulations. As was seen in Figure 4.9, the greatest changes in absolute mass concentration profiles was in the SAL, which has resulted in this exaggerated profile seen in Figure 4.11d. The increased concentration in the SAL reduces the relative concentration in the MBL, resulting in a sharper change in mass concentration in the lower SAL. At all locations, to varying degrees, reducing sedimentation raises the peak in mass concentration to higher altitudes. Figure 4.10 showed that changes to the sedimentation only affected particles greater than 2 µm diameter, thus suggesting that the changes to sedimentation result in increased vertical dispersion of coarse particles. There is not much change in mass at the top of the SABL/SAL at each location. Each simulated profile at each location tends towards zero at the same altitude. This suggests that though reducing the sedimentation encourages vertical transport, the dust is kept from mixing into the free atmosphere above the SABL/SAL by the same meteorological process in each simulation and reduced sedimentation does not overcome this interaction.

Figure 4.12 shows the normalised size bin 6 mass concentration profiles in the Control and four sedimentation experiments at the Sahara, Canaries and Cape Verde, as well as the related MCA values. Only mass concentrations greater than 0.001 µg m^{-3} are shown to remove analysis of negligible concentrations. Therefore, only profiles from the NoS, S95 and S80 experiments are plotted at the Caribbean.

While Figure 4.11 showed that with reduced sedimentation, the dust plume and MCA rose higher, Figure 4.12 shows that size bin 6 mass is more impacted by reducing sedimentation than the total mass. At the Sahara, the NoS size bin 6 MCA is more than 0.8 km higher than the Control, with more mass above 1 km altitude in NoS. At the Canaries and Cape Verde, the NoS MCA is above 2.6 km, while the Control MCA is more than 1 km lower than this at the Canaries and 1.5 km lower

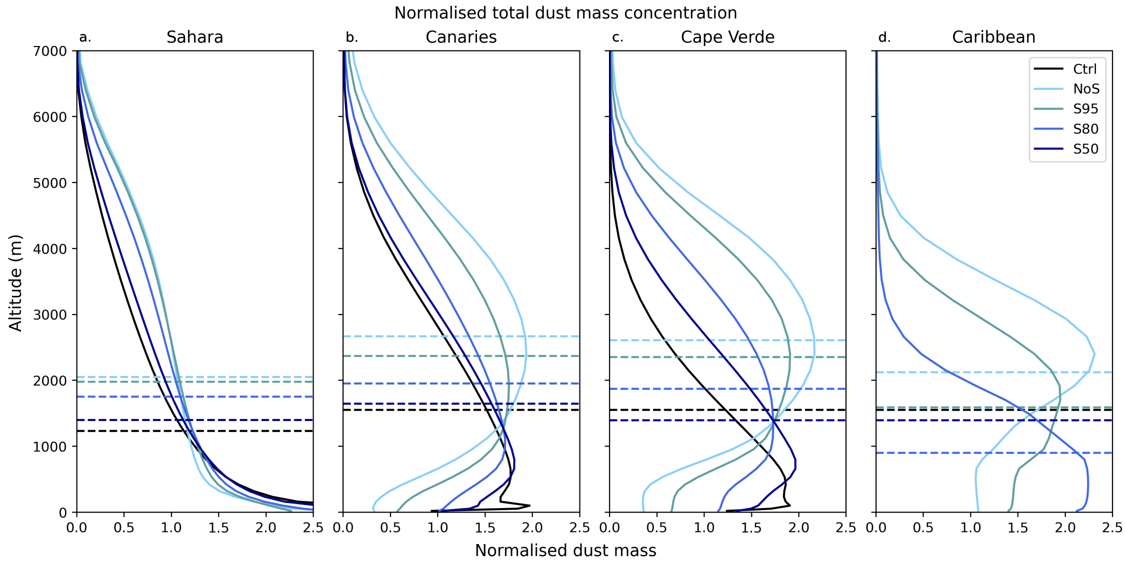

Figure 4.12: Size bin 6 mass concentration profiles normalised by the total 0-7 km size bin 6 mass in the Control and four sedimentation experiments: NoS, S95, S80 and S50. Dashed lines show the position of the MCA for each simulation. A mass concentration threshold has been applied at 0.001 µg m^{-3} to remove noise from negligible mass concentrations, thus, only NoS, S95 and S80 are shown at the Caribbean.

at Cape Verde. Thus, with transport the difference in MCA between the Control and NoS grows.

The shape of the size bin 6 mass profile changes between the Control and sedimentation experiments, especially away from the Sahara (4.12). At the Sahara, the main shape of the profiles is relatively similar between these experiments, with a peak at the surface, followed by a sharp decrease up to 0.5 km, then a gentle decrease up to 7 km. However, at the Canaries and Cape Verde, there is a more substantial difference in the mass profiles caused by the reduction in sedimentation. In the Control, the size bin 6 dust mass is focused much closer to the surface, with no discernible MBL in the profile structure. However, as the sedimentation decreases, the MCA rises, creating a profile more akin to the total mass profiles (Figure 4.11) with a peak in concentration above 2 km and a more distinct MBL. The NoS and S95 size bin 6 mass profiles are the most similar to the total mass profile, suggesting that these changes result in size bin 6 behaviour most comparable to the other dust size bins. The S80 size bin 6 mass profiles still have the dust transported lower than the total dust profile, suggesting that this experiment does not produce the best improvement in coarse particle transport altitude.

At the Caribbean, only three of the five experiments have a non-negligible mass concentration above 0.001 µg m^{-3}; NoS, S95 and S80. The S80 size bin 6 mass is centered fairly low, with an MCA just below 1 km altitude. Whereas in the NoS experiment, the size bin 6 dust mass is retained at a higher altitude throughout transport so that at the Caribbean, the MCA is over 2 km altitude. Compared to the total mass concentration profile in Figure 4.11, the NoS experiment, pulls the dust mass too high, disturbing the profile structure at the MBL-SAL interface, whereas the S95 experiment shows a more similar profile in both total dust concentration and size bin 6 concentration.

As shown in Chapter 3, the model has a fairly good representation of total vertical mass distribution. The coarse particles, however, were found to be transported too low in the atmosphere. Figure 4.11 showed that by reducing sedimentation, the MCA of total dust concentration could be raised by up to 250 m at Cape Verde. In terms of the height of the SAL, this is a minor change to the MCA and therefore would not mean that the model representation of vertical total dust distribution would be significantly depreciated. However, these same changes to sedimentation have much greater impacts on the vertical distribution of size bin 6 dust mass, which would result in an improvement of the model relative to the observations.

These experiments have shown the sensitivity of dust to sedimentation in the HadGEM3-GA7.1 model configuration. So far, the NoS experiment has been looked at in depth and compared with three experiments which reduced the sedimentation by 95%, 80% and 50%. The comparison of these four experiments with observations has shown that greater reductions in sedimentation with distance are required in order to bring the model into better agreement with the observations. At the Sahara, a reduction of up to 50% is required to bring the VSD into better agreement with the observations. However, at Cape Verde, a reduction of between 50-80% is required and finally, at the Caribbean, between 80-95% is required. This would suggest that huge reduction of between 80-95% in sedimentation is required to achieve a better shaped VSD after long-range transport, though if this were implemented, the VSD at the Sahara would have too great of a coarse size distribution. Thus, I suggest a flexible approach for future testing whereby sedimentation velocity decreases with distance from the source.

4.2.3 Impaction Scavenging

In this experiment, removal of dust particles through wet deposition in the model is turned off. Where the previous sedimentation experiments impacted the dry deposition of dust, this experiment looks at the sensitivity of dust deposition to the alternative, wet deposition. As before, I analyse the impact of the experiment on the large-scale distribution of the dust, before looking at the vertical changes in the dust size characteristics at specific locations.

Figure 4.13 shows the percentage difference in the binned total column mass between the no impaction scavenging (NoIS) experiment and the Control simulation. Without wet deposition, the removal efficiency of dust is depleted globally, resulting in an increase in TCM in all six size bins. Size bins 1-3 (Figure 4.13abc) show fairly uniform changes across the plotted domain, while size bins 4 and 5 (Figure 4.13de) shows less uniformity, with the greatest increase occurring outside of a trans-Atlantic band extending into the continents at either side at ∼10°N, south of the trans-Atlantic dust plume. Finally, in size bin 6 (Figure 4.13f), the changes to TCM are limited by others factors controlling the dust lifetime, whereby TCM is increased, but does not appear to have changed the typical TCM shape/pattern of the summer trans-Atlantic dust plume from the Control simulation. In size bin 6, the greatest changes to TCM in the NoIS experiment occur over the Sahara (Figure 4.13). As I have found that size bin 6 dust is very dependent on dry deposition, it is not surprising that there are not large changes to the TCM of size bin 6 dust.

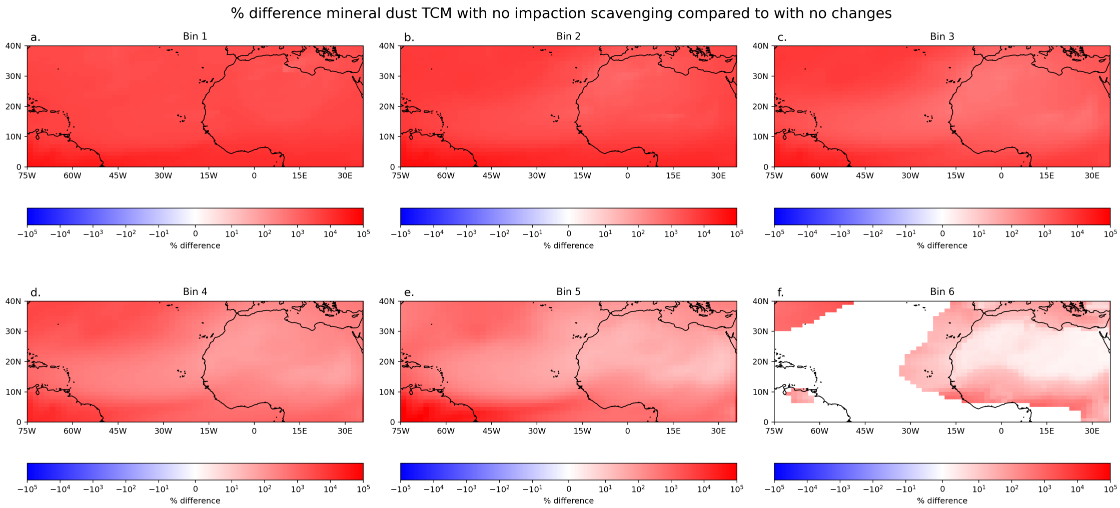

Figure 4.13: Percentage difference in the size-resolved TCM in the NoIS experiment compared to the Control simulation. Each plot uses the same scale on the colour bar. Gridpoints with a TCM value below a threshold of 0.1 µg m^{-2} in both simulations have been removed to reduce noise.

The greatest changes in TCM in size bin 4 occur in regions of typically high June precipitation south of the trans-Atlantic dust plume (Figure A.1 in Appendix A) which is related to the location of the ITCZ; it is likely that the precipitation results in dust removal in the Control simulation in these regions. Therefore without impaction scavenging, the most change is seen in those regions of high precipitation. Size bin 5 also shows some co-location with the location of the ITCZ, where the dust TCM is increased across the Atlantic, south of the dust plume. In size bins 1-3, the change is much less spatially dependent, instead uniformly spreading across the whole of the plotted domain. Size bins 4 and 5 have their lifetime extended, but only in regions where impaction scavenging is more dominant, outside of this, they are removed by other mechanisms. Whereas in size bins 1-3, their lifetime is extended and they are not dominantly removed by other mechanisms and disperse across the globe without significant removal mechanisms remaining.

The large widespread changes in size bins 1-4 results in a global change of dust AOD (not shown), with AOD increasing by more than 0.6 across the tropical Atlantic, where the Control simulation has an AOD less than 0.05 in the West Atlantic, less than 0.2 in the East Atlantic and no more than 0.45 over the Sahara (Figure 4.2). At some points over the Sahara, the AOD nearly doubles in the NoIS experiment compared to the Control simulation. This is the greatest amount of change to the AOD in any of the sensitivity experiments.

By turning off the wet deposition of dust, I have removed an important removal mechanism of dust in the atmosphere. As the only other diagnostic causing dust deposition, the dry deposition of dust is expected to increase in response to the decreased removal efficiency. Figure 4.14 shows the percentage difference in total deposition of dust between the NoIS experiment and the Control simulation. The percentage change of total deposition is shown on a logarithmic colour bar in order to capture the range of magnitude changes. Figure 4.15 shows the percentage difference in the dry and wet deposition separately between the Control and NoIS experiment. Every size bin shows 100% decrease in the amount of wet deposition in this experiment in comparison to the Control simulation. This is counteracted by an increase in the amount of dry deposition occurring in each bin, which increases by up to 100000% in every size bin. The increase in dry deposition is typically weakest at the Sahara and under the track of the trans-Atlantic SAL across the Atlantic. This is likely due to dry deposition being dominant in these locations in the Control simulation, resulting in not much change when removing the wet deposition. Where wet deposition is normally dominant – in the North Atlantic and south of the trans-Atlantic dust path – there is typically a greater increase in dry deposition. This is likely a consequence of the decreased removal efficiency creating higher dust concentrations in these locations, as suggested by Figure 4.13, increasing the pool of dust available for dry deposition.

The percentage changes in total deposition shown in Figure 4.14 are a sum of the dry and wet deposition. In the westward outflow regions from the Sahara, total

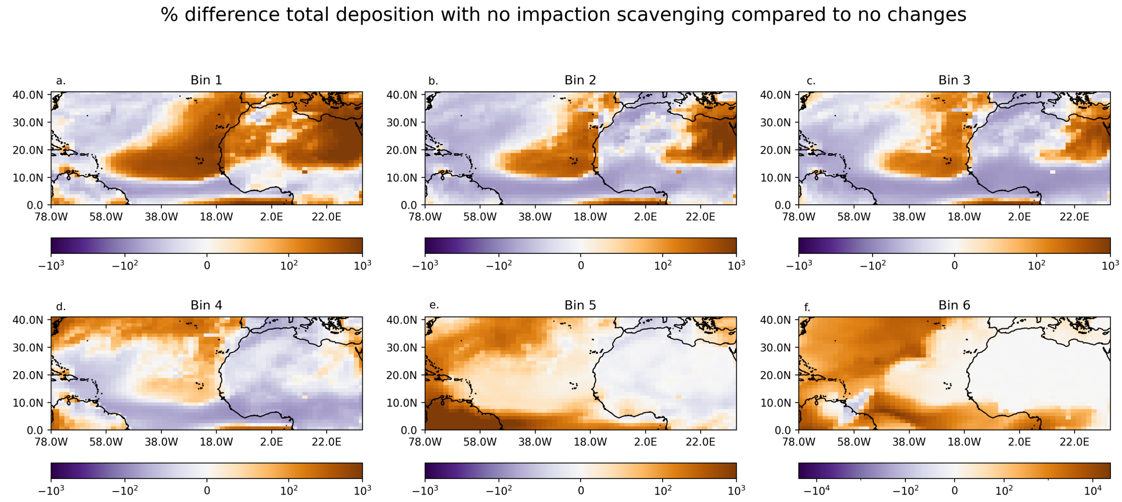

Figure 4.14: Percentage difference of the total deposition in NoIS compared to the Control simulation. The scales are logarithmic and different for each size bin.

deposition increases in the NoIS experiment, despite this being the location of weakest, but still positive, change in dry deposition. In all size bins, there is an increase in the total dust deposition off the northeast and east coast of Africa in the East Atlantic, which extends westwards towards the West Atlantic (Figure 4.14). This area of increased deposition is strongest in bin 1, with an increase of up to 10000%, and weakest in the coarsest size bins, with an increase of less than 100%. It could be that particles in the MBL are typically deposited by wet deposition in this outflow region, and thus without wet deposition, the particles, which are unlikely to be mixed back up into the SAL, are more likely to succumb to dry deposition to the ocean.

Size bins 1-4 show a decrease in deposition in the region of the ITCZ of nearly 100% (Figure 4.14abcd). This change in the total deposition is mostly driven by the removal of wet deposition, despite the increase in dry deposition of up to 100000%. Though the percentage increase in dry deposition is by orders of magnitude at this location, the relative amount of dust deposition by dry methods is significantly smaller than by wet deposition as this still represents the dominant change in the percentage change of total deposition. In size bins 5 and 6, the percentage change in total deposition is positive across the majority of the Atlantic (Figure 4.14ef). This increase in deposition could be a consequence of reduced particle loss/deposition, resulting in increased lifetime and transport of dust. This process dominantly impacts size bins 5 and 6 which are usually subject to swift deposition and negligible transport outside of the trans-Atlantic plume.

Figure 4.16 shows the absolute difference and percentage difference mass con-

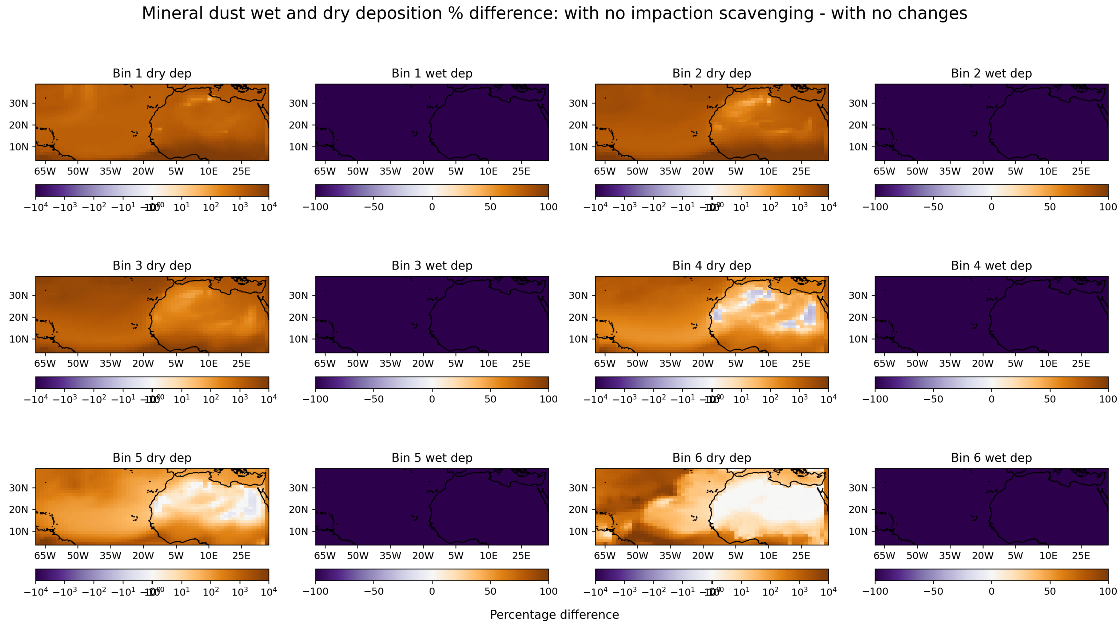

Figure 4.15: Percentage difference of the dry and wet deposition in NoIS compared to the Control simulation. The scales are logarithmic and different for dry deposition of each size bin.

centration profiles between the NoIS experiment and the Control simulation. The profiles are shown at four locations in the six CLASSIC size bins. In this experiment, dust mass concentration is increased in all bins at all locations.

In terms of the absolute difference, there is greatest change in concentration at each location below 2 km and in size bins 3, 4 and 5 (Figure 4.16). Despite this, the greatest percentage changes occur above the SAL and in bins 1, 2 and 3. This disparity between the two difference metrics is due to the use of mass concentration; the coarser bins will have a greater mass and therefore an increase relative to the original concentration will appear greater. Thus, the absolute change in size bins 1 and 2 appears small, but relative to the initial concentration, it creates a large percentage change. Thus, the absolute difference provides insight to the change in total profile mass concentration, whereas the percentage change shows the relative change to each bin compared to the Control simulation. Despite the scavenging coefficients being larger for coarser particles, the finer particles experience the greatest percentage change in concentration. However, the large percentage changes in fine particle mass at all locations suggests that it is an important and dominant removal mechanism for the finer particles; without wet deposition, the lifetime of the fine particles is dramatically extended.

In terms of the altitudinal changes at all locations shown in Figure 4.16, the absolute differences experience the greatest change at lower altitudes with the greatest

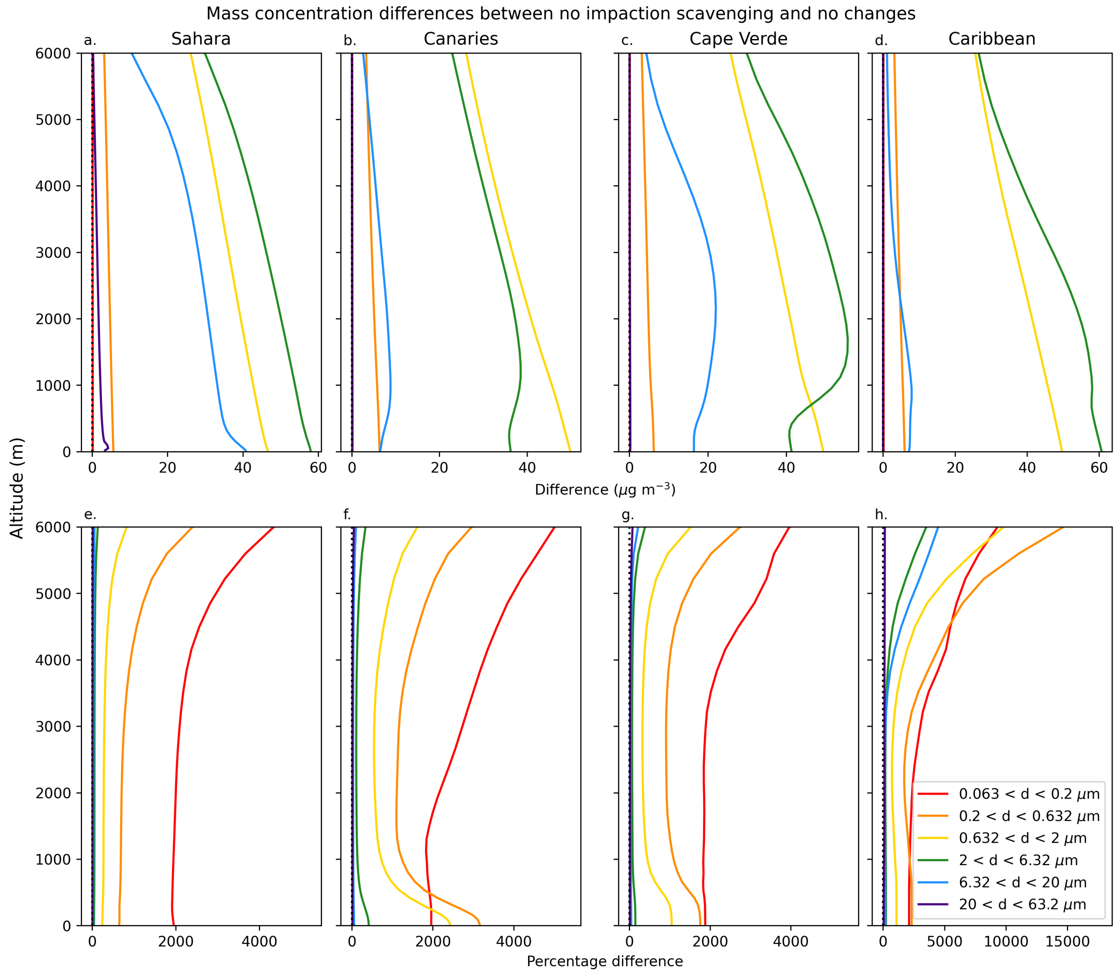

Figure 4.16: Absolute (top; in µg m^{-3}) and percentage (bottom) difference mass concentration profiles between the NoIS and Control experiments. Profiles shown in the six CLASSIC size bins at four locations.

absolute concentrations in the Control (< 2 km). However, the greatest percentage change in particle concentration is most pronounced at altitude (> 5 km) where the absolute concentration is much smaller and so the percentage change is much more significant. This suggests that impaction scavenging is important for controlling and capping the vertical transport of dust particles beyond the SAL top. This is appears especially important for fine particles which are less impacted by sedimentation which counteracts their vertical transport.

There is a difference in the percentage concentration change between dust in the MBL, SAL and free troposphere at the Canaries and Cape Verde (Figure 4.16fg). In the SAL, the change in concentration with height is fairly constant (~1-4 km). Below 1 km altitude, the percentage change is greater than in the SAL, with a 0.2-0.5 km layer extending up from the surface of constant difference, which then decreases sharply to the bottom of the SAL. At the top of the SAL and into the free troposphere (4.5-6 km), the difference of the NoIS simulation the Control simulation increases in all size bins. At the Sahara, the lack of a MBL results in a uniform profile of change from the surface to the top of the SAL, where the percentage change steadily increases (Figure 4.16e). Similarly to the Sahara, at the Caribbean, the MBL does not appear to impact the percentage change in mass concentration, resulting in a uniform percentage change from the surface to the top of the SAL (~3.5-4 km; Figure 4.16h). As the top of the SAL is lower than in the East Atlantic, there is increased divergence from the Control simulation at a lower altitude at the Caribbean than in the other locations. Where we see increased percentage difference between the NoIS experiment and the Control simulation in the MBL and towards the top of the SAL, it could be related to locations in the atmospheric profile at which we might expect cloud formation. As we do not expect to see cloud forming in the dry, dusty SAL, changes in the SAL represent reductions in below-cloud scavenging as opposed to in-cloud scavenging. Clouds can form at the top of the MBL and the top of the SAL (Carlson 2016), thus, the exaggerated percentage increase of dust is likely higher in the MBL and top of the SAL due to the removal of both in-cloud and below-cloud scavenging.

Now I have observed the general pattern among all size bins, I will analyse changes specific to individual or groups of size bins. While mass concentrations of all size bins has been increased at all locations by removing impaction scavenging, the changes at the coarse range are less substantial, especially in size bin 6. At the Sahara, the maximum difference in size bin 6 mass concentration occurs at ~0.1 km altitude and represents a change of only ~5 µg m^{-3} (Figure 4.16a). At all other locations, the change in size bin 6 mass is close to 0. Similarly, in terms of the percentage difference to the Control, the NoIS simulation results in very small changes in the size bin 6 mass. The greatest changes occur at high altitude.

Where in the absolute difference we saw the greatest change near the source (Figure 4.16a), the percentage change in bin 6 mass grows with distance from the source as the reduced removal increases transport distance (Figure 4.16h). Though this means that by removing impaction scavenging coarse particle lifetime has been improved, it is not on the order of magnitude scale which is required for the model to better match the observations. While the increase in size bin 6 transport is not significant enough to match the observations, the changes in size bin 5 are more promising for increasing coarse particle lifetime. At 6 km there is 4000-5000% more size bin 5 mass at the Caribbean and an increase of approximately 10 µg m^{-3} at 1 km altitude. Thus despite only small changes in size bin 6, increases in size bin 5 are still important due to the models great underestimation of these particles too at the Caribbean (as seen in Chapter 3).

Previously, I looked at the percentage difference changes in the MBL in Figure 4.16efgh. Interestingly, fluctuations based on different layers in the atmosphere only occur in the coarser size bins in the absolute difference profiles in Figure 4.16abcd. For example, the three finest size bins show a gentle decrease in difference to the Control with increasing altitude at all locations. However, the coarsest three bins tend to show more variation in the difference profile dependent on the different atmospheric layers, for example showing enhanced difference in the SAL and reduced difference in the MBL (e.g. size bin 4 in Figure 4.16c). This suggests that the finer particles are less susceptible to stratification in the atmosphere, being able to be mixed freely, while the coarser particles are more dependent on other meteorological processes for their vertical dispersion.

Figure 4.17 shows the vertically-resolved VSD at the Sahara, Canaries, Cape Verde and Caribbean in the NoIS experiment. The solid lines indicate the absolute values of the NoIS experiment VSD and the dashed lines indicate the percentage change to the Control simulation.

As seen previously, the effect of removing impaction scavenging is mostly seen at the fine size range. On the NoIS VSD, the fine size range (0.063-2 µm) is most impacted and has shifted to greater VSD at all locations compared to the Control VSD (Figure 4.17). In the Control simulation, the size bin 1 VSD ranges between 0.001-0.006 µm^3 cm^{-3} between 0-6 km altitude at the Sahara, whereas in the NoIS simulation, the VSD has been increased by 2000-4000% to between 0.05-0.1 µm^3 cm^{-3}. At the Canaries, Cape Verde and Caribbean, the size bin 1 VSD is consistently increased by more than 1700% compared to the Control simulation. At each altitude, size bin 1 is typically more different to the Control than the successive size bins. Each successive size bin is less affected by the removal of impaction scavenging, with decreasing VSD difference to the Control with increasing size. There are some exceptions to this general pattern which will be discussed shortly.

As the finer size ranges are more impacted by the removal of impaction scavenging, a lot of changes are therefore only seen at these finer size ranges. For example, there is a decreased dependence on altitude in the finer size bins at all locations i.e. that there is less variation in each bins absolute VSD values between all altitude levels. This is showing the same phenomenon which was observed in the mass concentration difference profiles (Figure 4.16) where the profile was smoothed in the finer bins and showed less stratification between the MBL, SAL and free troposphere.

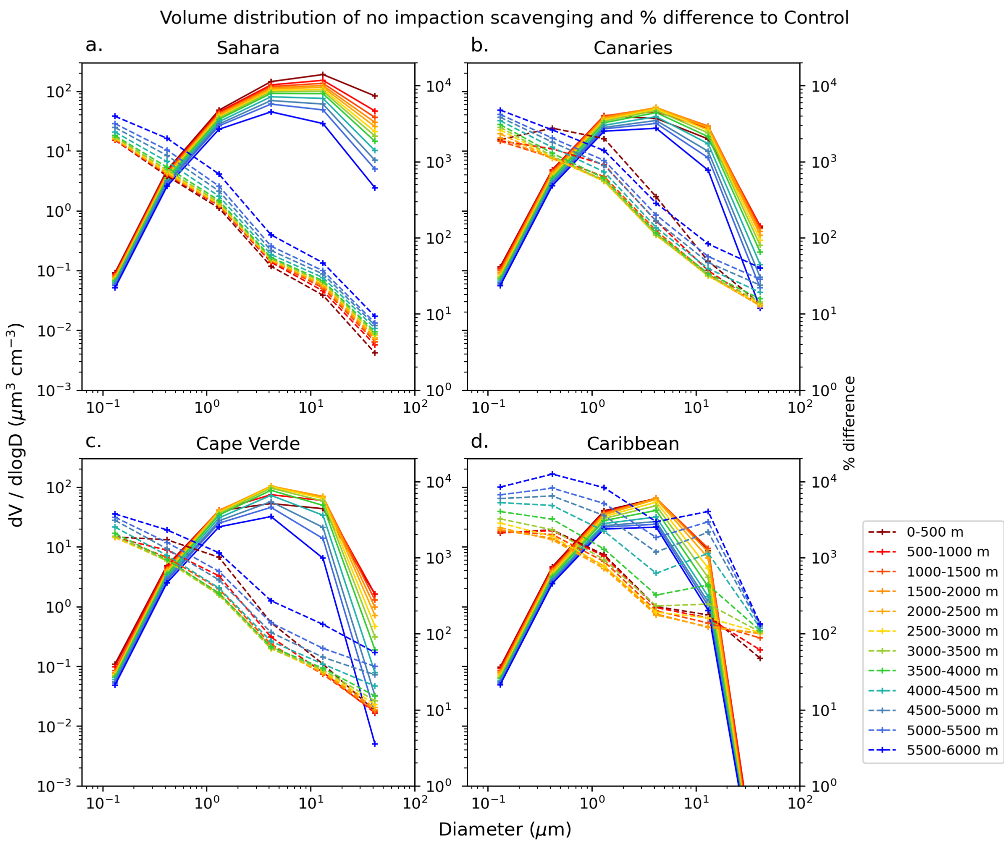

Figure 4.17: Vertically-resolved VSD (in μm^3 cm^{-3}) of the NoIS experiment (solid lines) and the percentage difference of the NoIS experiment to the Control simulation (dashed lines) at the Sahara, Canaries, Cape Verde and Caribbean.

Perhaps unsurprisingly, the greatest changes to the VSD are seen at distance from the Sahara (Figure 4.17d). The maximum difference to the Control simulation occurs at the Caribbean, with an increase of 0.2-0.632 μm (size bin 2) particles by 13000% between 5.5-6 km altitude. The enhanced increase in VSD at distance from the Sahara could be an artifact of two processes; firstly, at distance from the source, the impact of removed impaction scavenging has had longer to affect the dust plume, resulting in greatest relative change. Or, specifically relating to the removed process, wet deposition is more likely to happen away from the relatively dry Sahara, so the removal of this process sees the most difference in the moister regions, away from the Sahara.

Previously, I have noted the lack of altitudinal dependence shown in the finer size bins in the NoIS experiment; the percentage change in VSD continues to corroborate this (Figure 4.17). Firstly, I will analyse the changes between 0-1 km altitude at the Canaries and Cape Verde, which is typically where we see decreased dust concentration due to turbulent mixing and wet deposition within the MBL. However, the smoothing of the vertical profile, as shown by the tightly packed VSD altitude lines, means that there is a greater percentage difference in the two lowest 0.5 km layers, as seen in Figure 4.17bc. At the Caribbean, the already sunken dust plume does not show there is not a large percentage change below 1 km in the NoIS experiment VSD (Figure 4.17d). At the Canaries and Cape Verde, particularly in size bins 2, 3 and 4, the increase in the 0-0.5 km layer is on a similar magnitude to the increase in VSD occurring above 5.5 km. Alternatively, in size bin 1, the percentage change is not as exaggerated; this is due to the altitude dependence of size bin 1 in the Control simulation. In the Control simulation, there is a uniform decrease in size bin 1 VSD with altitude, as opposed to the VSD peaking between 2-4 km in size bins 2-5. Thus, in the NoIS experiment, size bin 1 VSD does not increase as much as other bins in order to form the same pattern.

By plotting the vertically-resolved percentage change to VSD in the NoIS experiment, we can see that the highest altitudes (above 4.5-6 km) tend to show the greatest difference from the Control simulation at all locations (Figure 4.17). Similar to changes below 1 km, these enhanced increases are indicative of a smoothing of the vertical profile in a location where concentrations tend to decrease into the free troposphere (as seen in the Control simulation; Figure 4.3).

These discussed changes to the NoIS VSD show that removing impaction scavenging results in a smoother, more uniform vertical profile. We can therefore hypothesise that impaction scavenging and wet deposition are more important for the vertical distribution of fine dust particles than processes such as turbulent and convective mixing which tend to have a stratifying effect on the atmosphere around the SAL, as will be shown later in Sections 4.2.4 and 4.2.5.

From this experiment, I have found that impaction scavenging in the model is a strong removal mechanism for the four finest size bins (0.063-6.32 µm) in the model. Without impaction scavenging, these particles have a significantly longer atmospheric lifetime, impacting the global atmospheric dust mass and AOD. Without wet deposition, these particles are more evenly vertically dispersed in the atmosphere, showing a much more uniform vertical dispersion. While I have found that wet deposition does decrease coarse particle lifetime, removing wet deposition results in only minor improvement of the transport of coarse dust particles.

4.2.4 Convective Mixing

In this section, I will explore two experiments which were carried out in relation to the convective mixing (CM) of dust in the atmosphere. It is hypothesised that increased vertical mixing could enhance the lifetime of coarse dust particles in the atmosphere (Gasteiger et al. 2017; Takemi 2005; Xu et al. 2018). To understand the impact of CM of dust on transport and deposition, CM is turned off and doubled in two different experiments, NoCM and 2xCM, respectively.

No Convective Mixing

Figure 4.18 shows the percentage difference of the TCM between the no convective mixing experiment (NoCM) and the Control simulation in the models six dust size bins. The impact at the finer size ranges appears to be mostly negative, where removing CM has decreased TCM in size bins 1 and 2 across nearly the entirety of the plotted domain (Figure 4.18ab). With increasing particle size, the magnitude of reduction decreases. This suggests that there is a greater reliance on CM for the transport and mixing through the atmosphere of the finer particles. As the TCM is reduced across nearly the whole domain, it suggests that CM is important for transport of the finest particles at all scales, including short-range transport. The reliance on CM for short-range transport decreases with size as decreases in TCM are seen at greater distances from the source in the coarser size bins.

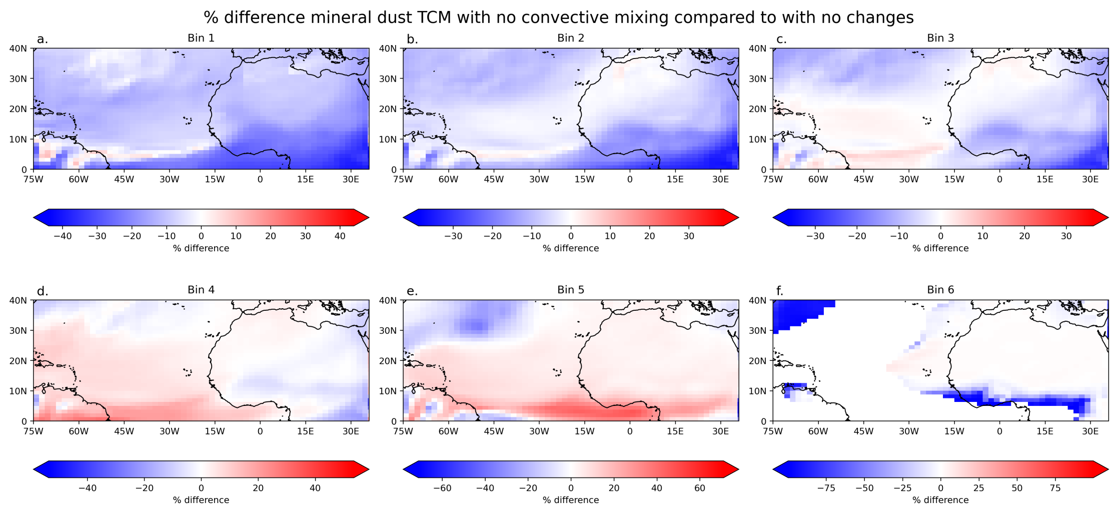

Figure 4.18: Size-resolved dust TCM percentage difference between the NoCM experiment and the Control simulation. A different scale is used for each plot. TCM values below 1 µg m^{-3} have been removed in order to reduce noise.

In size bins 1-4, there is a decrease in TCM over the Sahel by up to 40% (Figure 4.18abcd). This likely suggests that by removing CM, transport away from the dust source outside of the normal trans-Atlantic pathway is reduced, resulting in decreased TCM to the south of the Sahara, i.e. in these regions, CM sustains transport for size bins 1-4. Alternatively in size bin 5 (Figure 4.18e), the TCM increases over the entirety of north Africa, including over the Sahel where there is a percentage increase of up to 10%, i.e. CM has a net removal effect for size bin 5.

In size bins 5 and 6 (Figure 4.18def), there is an increase in TCM over the Sahara and in the trans-Atlantic dust plume and a decrease in TCM in the north Atlantic, away from the plume. The changes in size bin 4 combine the decrease of TCM over the Sahel and east Sahara seen in the finer bins, and an increase in TCM in the trans-Atlantic dust plume, extending to the northeast of the Sahara. These increases of TCM in the central dust plume suggest a decrease in dust dispersion to the north and south of the dust plume, increasing the dust mass retained in the plume.

Patterns between the equator and 10°N are likely driven by the presence of the ITCZ. As the ITCZ is a convective phenomenon, it is understandable that by turning off the CM of dust, there would likely be great changes to the distribution of dust here. In size bin 5, the greatest percentage change occurs south of the normal trans-Atlantic dust path, in line with the ITCZ; an increase in TCM of up to 60% over the Gulf of Guinea and up to 50% in the west tropical Atlantic shows that the removal of CM positively impacts the lifetime of coarse (size bin 5) dust in moist convective regions. Whereas in size bins 1-3, the removal of CM typically reduces their lifetime and transport distance.

Figure 4.19 shows the percentage difference in mass concentration between the NoCM and Control simulations in a transect across the Atlantic in each bin. The transect crosses through the trans-Atlantic dust plume at 16.9°N. The positioning of this transect means it is placed centrally in the dust plume over the Atlantic, but is further south than the highest concentrations of dust over the Sahara.

In all size bins, there is a decrease of dust mass above $\sim$5 km altitude east of $\sim$50°W. This is likely signifying a sharpening of the boundary between the SAL and the free atmosphere with a decrease in the mixing of dust up out of the SAL. As dust radiative effects are turned off, the meteorology in the simulations is parallel and only the way the dust interacts with meteorology is changed, thus the decrease of dust at altitude cannot represent a change in the SAL-top height. East of 50°W, there is reduced dust concentration above the main plume down to 4 km in size bins

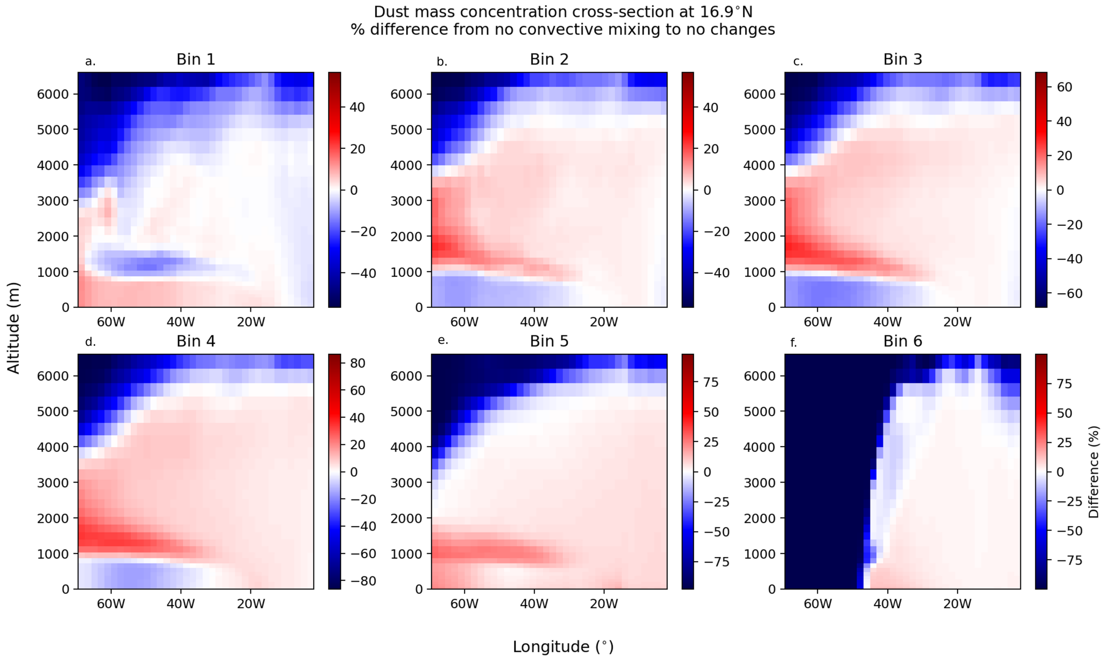

Figure 4.19: Binned cross section of percentage difference in the mass concentration between the NoCM experiment and the Control simulation. The scale used for each size bin is different. The cross section is at approximately 16.9°N and runs from 0° at the Sahara to 70°W at the Caribbean up to 6.7 km altitude.

2-4, 3 km in size bins 1 and 5 and down to the surface in size bin 6. It appears that the removal of CM in this experiment limits the vertical transport of dust to within the SAL, reducing transport above the SAL into the free troposphere by up to 100%. Especially in size bin 6, where transport beyond 50°W at the surface, 40°W at 5 km altitude and above 6 km between 40°W and the meridian is negligible in the NoCM experiment.

The reduced vertical transport is paired with increased mass concentrations within the SAL in size bins 2-6 (Figure 4.19bcdef). Additionally, in size bins 2-4, there is a decrease of mass concentration in the MBL between 70-30°W from the surface up to 0.8-1 km (Figure 4.19bcd). Without CM, it seems that the dust becomes less well-mixed throughout the depth of the SAL, instead settling into the lower SAL as shown by the exaggerated increase in concentration above the MBL in the west Atlantic (1-2 km altitude and 30-70°W).

Together, the decreased vertical transport out of the plume shown in Figure 4.19 and the decreased horizontal transport to the north, east and south of the trans-Atlantic plume shown in Figure 4.18 suggests overall decreased mixing of dust out of the dust plume, increasing the concentration of dust in the plume and the mass of dust transported to the west Atlantic.

Interestingly, size bins 1, 5 and 6 actually show increased dust mass concentrations in the MBL where the other bins show a decrease (Figure 4.19). The size bin 2-4 particles are kept in the SAL by the strong inversion at the SAL-MBL interface, but the mass of the coarsest particles is strong enough to overcome this, resulting in size bin 5 and 6 particles settling through the MBL and increasing the mass concentration relative to the Control simulation. In size bin 1, there is an opposite reaction to the removal of CM between 0-2 km and 30-70°W (Figure 4.19a). There is an increase in dust mass in the MBL and decrease in the lower SAL. This suggests that the size bin 1 particles interact with the convective mixing in a different way to the other size particles, the reasons for which are not clear.

In all size bins, the greatest points of increased concentration are seen in the west Atlantic at distance from the Sahara. This suggests that while there is some dependence on location and local meteorology (as seen in Figure 4.18 at the ITCZ), the removed CM has an almost cumulative impact, building up over distance.

Figure 4.19 showed the changes in vertical profile across the Atlantic and revealed a general pattern of decreasing concentration at high and low altitudes (< 1 km and > 5 km), as well as increasing concentrations throughout the SAL and particularly in the lower SAL (1-2 km). Figure 4.20 shows the absolute vertical mass concentration profiles at the Sahara, Canaries, Cape Verde and Caribbean in the six size bins.

In Figure 4.19 the greatest amount of change to the dust mass occurred in the West Atlantic or at the SAL-top (∼6 km). Similarly, Figure 4.20 shows that the Sahara, Canaries and Cape Verde profiles in the NoCM experiment are very similar to the Control simulation (Figure 4.3) in terms of the shape. The mass concentrations only vary from the Control by $\pm$ 10% below 5 km altitude. However, at the Caribbean, the shape of the vertical profile becomes more different to the Control. The result of having no CM creates a clearer difference between the MBL and SAL with a sharp concentration gradient from the MBL into the SAL forming in the west Atlantic. The decreased MBL concentrations and increased lower SAL concentrations are indicative of reduced vertical mixing. Without CM, the dust in the SAL is not mixed through the full-depth of the SAL and settles down to the lower SAL, where reduced mixing decreases the amount of dust mixed down into the MBL too.

Figure 4.21 shows the absolute VSD at the Caribbean in the NoCM experiment, as well as the percentage difference VSD to the Control simulation, also at the

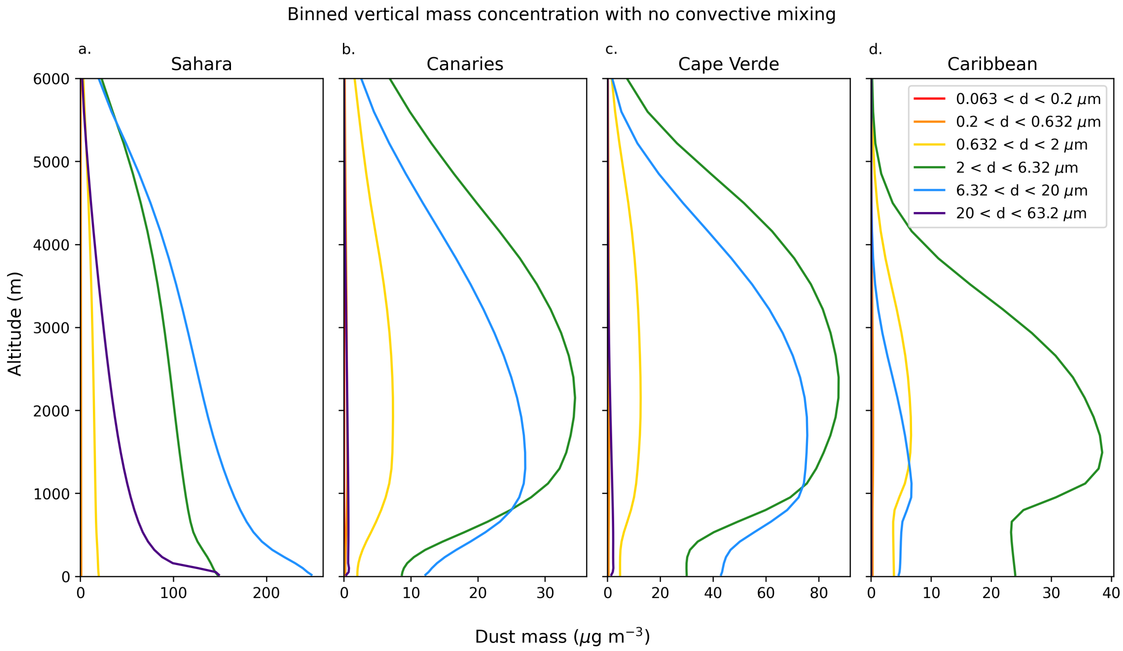

Figure 4.20: Absolute vertical mass concentration (in μg m^{-3}) profile in the NoCM experiment. The size-resolved profiles are plotted at the Sahara, Canaries, Cape Verde and Caribbean.

Caribbean. As changes at the Sahara, Canaries and Cape Verde were minimal (between −15% and +8%) and the most extreme changes were seen at distance from the Sahara, I have opted to focus purely on changes at the Caribbean here.

As has been noted in previous figures, Figure 4.21b is consistent in showing a decrease in VSD at all size ranges at high altitudes; between 4-6 km, the VSD shows a decrease of 5-100% in all size bins compared to the Control. This decrease at altitude is counteracted by an increase in size bins 2-4 VSD between 1-4 km, with the greatest increase between 1-1.5 km. This again corroborates the findings from Figure 4.19 which showed increased concentrations within the lower SAL. Finally, there is decreased VSD in the MBL (0-1 km) in size bins 2-4 and 6, representing the decreased downwards mixing of dust from the SAL into the MBL.

This general overview of Figure 4.21b does not stand for all size bins. I will now discuss the more intricate details and changes. In size bin 5, rather than decreasing VSD below 1 km and above 4-5 km like size bins 2-4, the VSD increases. As discussed previously, I postulate that this is to due enhanced concentrations of bin 5 particles in the SAL being more affected by sedimentation than the finer bins due to its greater mass. Thus, the particles are able to overcome the stratifying meteorology at the MBL-SAL interface, unlike the finer particles, and are transported towards the surface via sedimentation. Unlike the coarse particles with strong depo-

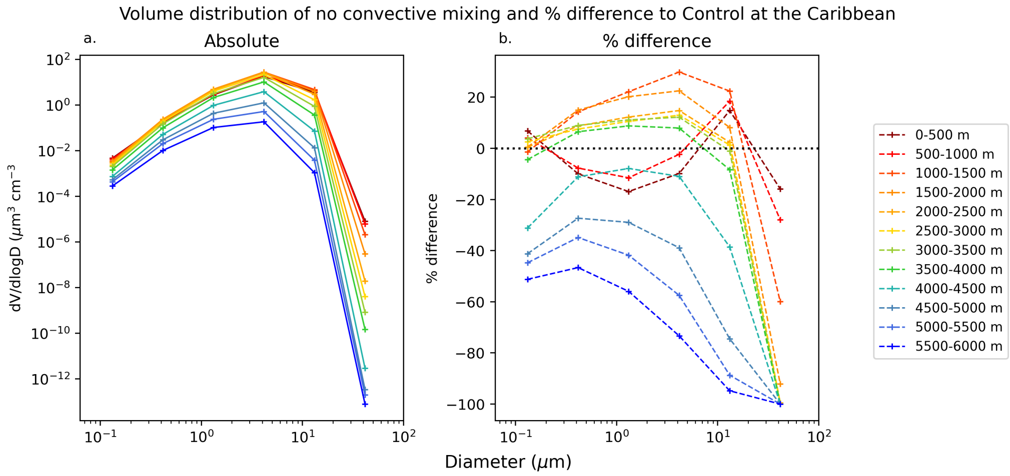

Figure 4.21: Vertically-resolved VSD (in μm^3 cm^{-3}) of the NoCM experiment at the Caribbean (a) and the percentage difference of the NoCM experiment to the Control simulation at the Caribbean (b). The black dotted line on signifies no change at 0%.

sition velocities, the finer particles are not able to overcome the inversion separating the MBL and SAL without the CM, and thus remain in the SAL. Size bin 6 has the greatest percentage VSD loss of all the bins, decreasing by ∼15% between 0-0.5 km altitude and ∼100% from 3-6 km altitude. Despite no CM acting, the sedimentation of size bin 6 particles is strong enough that these particles are deposited anyway, resulting in such a strong decrease in size bin 6 VSD at the Caribbean. The effect of sedimentation on size bins 5 and 6 results in a more altitude-dependent VSD, whereby VSD decreases with altitude from the surface, unlike size bins 2-4 which only show decreasing VSD with altitude above 3.5 km (Figure 4.21a). Size bin 1 shows the same altitude dependence of VSD as size bins 5 and 6, despite having the greatest difference in particle diameter. This is likely to due to only small changes of less than ± 10% to the VSD below 4 km altitude not significantly changing the VSD significantly from the Control simulation.

By turning off CM, I have found decreased dust transport away from the trans-Atlantic dust plume, both to the north and south, as well as above and below the main plume. I postulate that by removing any convective mixing of dust in the model, the dust remains contained within the SAL for longer, generally increasing dust concentrations between 1-4 km at the Caribbean. Without CM, the dust tends to settle into the lowest km of the SAL, unable to be mixed up above the SAL or down into the MBL. Unlike the finer particles which rest above the MBL-SAL inversion, size bin 5 and 6 (6.32-63.2 μm) particles continue to settle through the inversion. Initially, the coarsest particles are transported further due to decreased downwards mixing and subsequent deposition with increases in mass concentration of up to 10% at Cape Verde. However, they are then deposited prematurely in the mid and west Atlantic without the CM to counteract their settling out of the SAL.

Thus, while CM has both upwards and downwards mixing effects on the dust, could enhanced convective mixing within the SAL result in improved retention of coarse particles within the SAL?

Doubled Convective Mixing

In this experiment, I aim to test the effect of increasing the amount of CM of dust in the model atmosphere. The hypothesis being that by increasing CM of dust, the swift settling velocity of the coarser particles will be more heavily counteracted by increased upwards mixing, extending their atmospheric lifetime. To test this, I have doubled the CM of dust throughout the model atmosphere.

Figure 4.22 shows the difference in the TCM in the six size bins between the doubled CM experiment (2xCM) and the Control simulation.

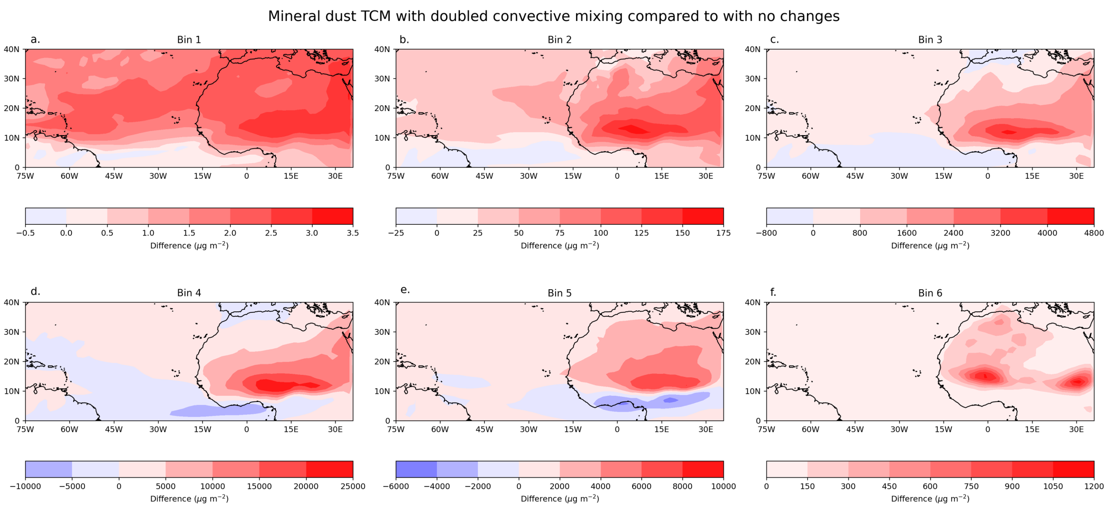

Figure 4.22: Absolute difference of the binned TCM (in μg m^{-2}) between the 2xCM experiment and the Control simulation. Each plot uses a different scale on the colour bar.

I might expect that the impact of doubling CM of dust might be the inverse of the previous experiment where I removed all CM of dust in the model. At the finer size range, this is not far from the truth; in size bin 1, where previously there had been a widespread decrease in TCM with NoCM, there is instead a widespread increase by up to 3.5 μg m^{-3} or 25% in the 2xCM experiment, with only a slight decrease in TCM at the ITCZ of up to 4% (Figure 4.22a). As the particle size increases, the area of greatest change shrinks, becoming more focused over the Sahara and Sahel (Figure 4.22). Despite the area of greatest change shrinking with size, the net change over the plotted domain remains positive, with predominantly increasing TCM across north Africa and north Atlantic in all bins. This suggests an increase in the horizontal transport of dust in the model, except for to the south of the trans-Atlantic dust plume.

Size bins 1-5 experience some magnitude of decreased TCM at the ITCZ (Figure 4.22abcde). These changes are driven by the convective ITCZ, having more CM removal potential in this experiment, i.e. the doubling of CM of dust at the ITCZ increases dust removed in this region. At smaller size ranges, the area of decreased TCM is over the north of the South American continent, and across the tropical Atlantic. Whereas as the particle size increases, the area of decreased TCM spreads further east to partially cover tropical Africa. Additionally, by area, size bin 4 has the greatest decrease in TCM with regard to the Control simulation. Extending up to nearly 30°N in the west Atlantic, the larger area of decreased size bin 4 TCM suggests a different relationship with the CM process in comparison to the other bins.

Size bin 6 is the only size bin to experience an increase in TCM across the whole of the plotted domain (Figure 4.22f). The greatest changes are focused near the Sahara and over the Sahel at ∼15°N. As seen in the previous experiment (NoCM; Section 4.2.4), TCM over the Sahel appears to be very responsive to changes in CM. There is a greater change to the doubling of CM in the western Sahara.

Figure 4.23 shows the mean June horizontal and vertical winds in the model at specific level heights. As the RE of dust are turned off in these experiments, the meteorology is parallel i.e. the winds shown in Figure 4.23 are the same in all experiments in Section 4.2. At 1.8 km, over the Sahara, there are significant vertical updrafts directly over the Sahel, as well as sporadically across the western Sahara. The location of these Saharan and Sahelian updrafts coincides with the location of the increased size bin 6 TCM in Figure 4.22f. These updrafts must be associated with convective processes that by doubling the CM has resulted in increased lofting of the dust particles, and thus, the mass of coarse dust retained in the atmosphere. In Figure 4.22f, the greatest changes to TCM over the Sahel is broken into two regions, between 10°W-5°E and the east of 20°E. Whereas in Figure 4.23, the vertical w winds are strong across the entirety of the Sahel with no breaks. However, the horizontal winds are stronger in the 5°-20°E area (Figure 4.23); these stronger horizontal winds could be reducing the impact of the strong vertical winds on the size bin 6 particles and removing them from the updraft line over the Sahel too quickly, resulting in a reduced increase of TCM.

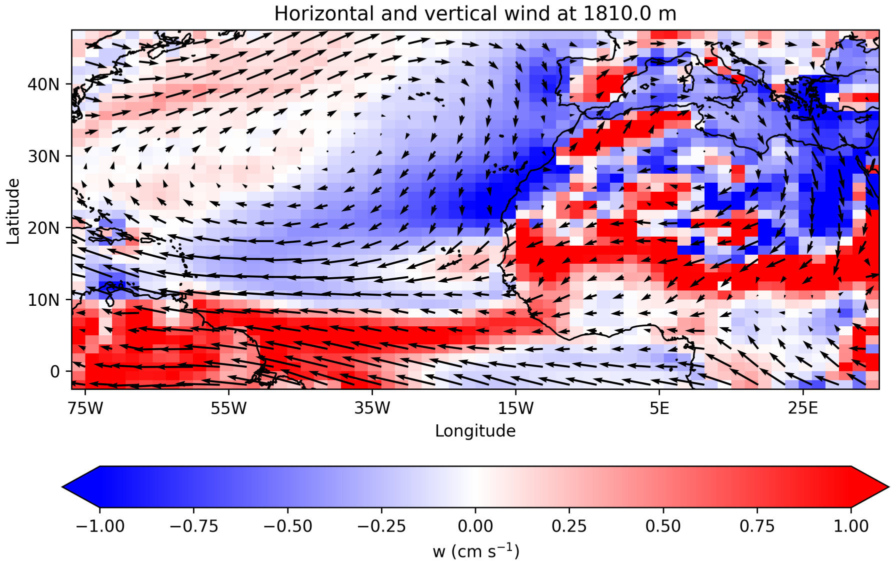

Figure 4.23: Model horizontal (u and v; arrows) and vertical (w; coloured shading; cm s−1) wind speeds at 1.8 km altitude. The meteorology is consistent throughout the experiments.

In size bins 1-5, it appears that the region of increased TCM which I have associated with convection over the Sahel in size bin 6 (Figure 4.22f), is shifted further south with decreasing particle size (Figure 4.22abcde). It could be that while the additional vertical transport at the Sahel results in increased size bin 6 dust loading directly overhead, once transported further away, it quickly drops out again, resulting in the large change in TCM only being visible over the Sahel. However, lighter particles could be lofted over the Sahel in the same way and moved to the south or west, then, their slower settling velocity means they are not deposited as quickly as the bin 6 particles and so are transported further south of the Sahel. This results in the southwards shifting of the area of greatest TCM increase.

Despite the ITCZ consisting of strong and spatially consistent updrafts (Figure 4.23), there is a decrease in the dust TCM in size bins 1-5 corresponding to its location (Figure 4.22abcde). I hypothesise that this could be a consequence of the strong easterly winds in the ITCZ; possibly they could be counteracting the effect of the increased CM.

Figure 4.24 shows the percentage difference of total (dry and wet) deposition in the 2xCM and the Control simulations. The percentage difference has been chosen here to better understand changes further from their source and the relative change in each model gridbox.

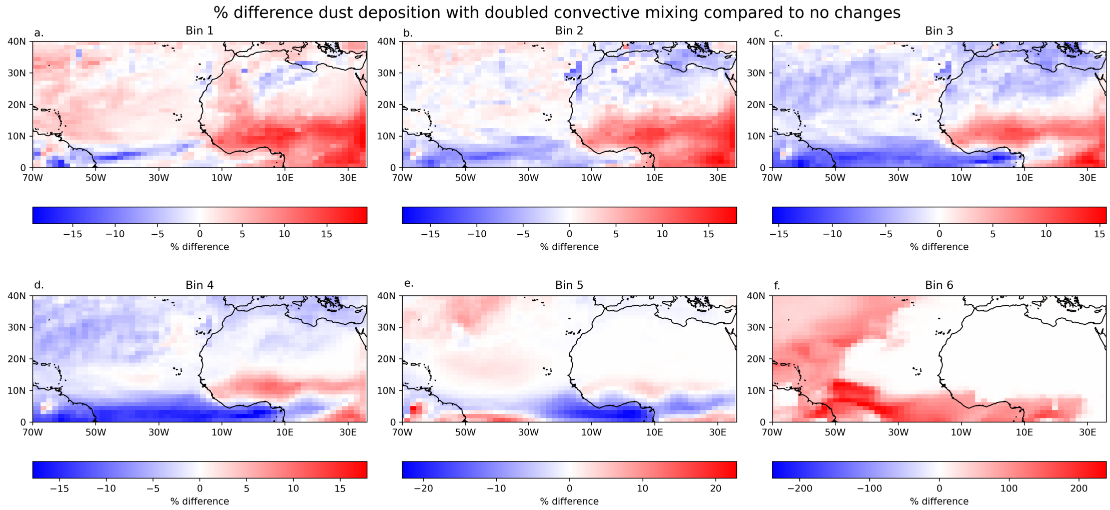

Figure 4.24: Percentage difference of the total (dry and wet) deposition of dust in the 2xCM experiment and the Control simulation. Each plot uses a different scale on the colour bar.

Figures 4.22 and 4.24 can be compared; where there is increased TCM, we might expect to see increased deposition as there is more dust available for deposition and vice versa. This is true for some areas. At the ITCZ, for example, there is a consistent match in size bins 1-5 between decreased TCM and decreased deposition (Figures 4.22 and 4.24 abcde).

Over the Sahara, there is a decrease in dust deposition in size bins 2-5 (Figure 4.24bcde). This would align with my hypothesis that convective updrafts over the Sahara (vertical winds shown in Figure 4.23) loft the dust away from the surface where it is transported elsewhere, reducing the total deposition close to these positive vertical winds near the source. The strong vertical winds over the Sahel aided in dust transport to the south of the Sahel. This has ultimately created a pathway for more dust to be deposited at, and to the south of, the Sahel in all size bins (Figure 4.24).

For the model to improve its representation of coarse dust transport, more coarse dust needs transporting west, towards the Caribbean. As Figure 4.22 showed increased dust TCM in all size bins in the West Atlantic and as Figure 4.24cd shows decreased dust deposition too, this suggests that the dust is travelling further and not being deposited, thus remaining in the atmosphere for longer. While size bins 5 and 6 do not show a decrease in deposition in the west Atlantic, this does not mean that the transport is not improved. In fact the increased deposition in Figure 4.24 suggests that the dust has travelled further than normal, creating a greater mass of dust available for deposition further form the source. Similarly, size bins 1 and 2 (Figure 4.24ab) show increased deposition in regions of the Atlantic. This could again be due to increased dust loading (as seen in Figure 4.22ab) creating the potential for more dust deposition.

This experiment has shown so far that by doubling CM, the dust loading of coarse particles in the atmosphere can be increased and that these particles are able to travel further from the source than in the Control simulation. I will now analyse the impact of doubled CM on the vertical transport of the dust. Figure 4.25 shows the difference in the binned vertical dust profile up to 11 km in the six size bins with each line corresponding to a different box between the Sahara and Caribbean. This plot has been shown with absolute difference values to show the changes relative to the rest of the profile.

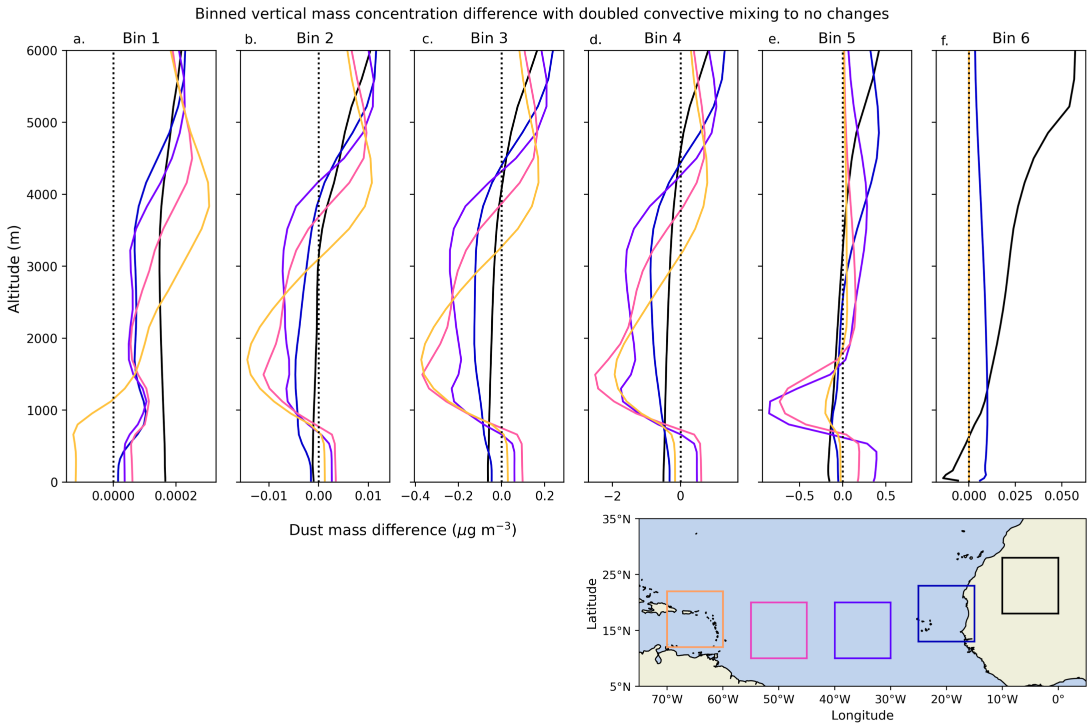

Figure 4.25: Mass concentration difference profiles (in μg m^{-3}) at five different regions from the Sahara to the Caribbean (shown on map) between the 2xCM experiment and the Control simulation. Each plot represents a different size bin. The black dotted line shows the point of no change at 0. The colour of the line corresponds to the box colour on the map. The coordinates of the boxes from east to west are: 0-10W 18-28N, 15-25W 13-23N, 30-40W 10-20N, 45-55W 10-20N, 60-70W 12-22N.

At all locations in all bins, there is an increase in the mass of dust in the upper SAL (above 4 km) and into the free atmosphere above the SAL suggesting that increased CM has increased the vertical transport of dust (Figure 4.25). In size bins

2-5, the increase of dust at altitude is paired with a decrease of dust mass in the lower SAL (2-4 km). The magnitude of the positive and negative changes are very similar at the point of greatest change. However, the vertical depth of the changes are very different; typically there is only a loss of mass over 2-3 km of altitude, whereas there is increased dust in at least 6 km of the atmosphere. This creates the net increase in atmospheric dust that was so widespread in Figure 4.22. The decrease in mass concentration begins at ∼0.7 km altitude in locations with a MBL present; this is likely a consequence of both enhanced mixing into the MBL and due to the additional mixing up through the SAL.

Where the changes in each box in size bins 1-4 are of a similar magnitude, in size bins 5 and 6, the changes are greatest near to the source and then decrease, rapidly in the case of size bin 6, with distance from the source (Figure 4.25ef). As we have seen in other experiments, the swift deposition of the coarser size bins results in this decreasing difference from the Control simulation. In size bin 6, the swift decrease to negligible concentrations means we can only see changes in the first two regions extending to 25°W. The swift settling velocity of the size bin 5 and 6 particles results in a more sunken profile of change when compared with the finer size bins. The region of decrease in the lower SAL which I have associated with enhanced mixing in the other size bins is significantly shorter in size bin 5, only extending 1 km vertically. This suggests that while 2xCM enhances vertical transport, the impact on the amount of coarse dust reaching the West Atlantic is still not significant enough to match the observations.

The decrease in the impact of the increased CM with transport from the Sahara and Sahel is evident in the smaller size bins too. At the Sahara, the peak in increased mass concentration occurs at ∼7 km in size bins 2, 3 and 4 (Figure 4.25bcd). Moving away from the Sahara, this peak decreases in altitude by 0.5-1 km with each box to the west; finally in the most westerly box, the peak is at ∼4 km altitude. This lowering of the dust profile suggests a shift back towards the Control experiment and a reduction in the impact of the increased CM change.

As seen in previous figures, size bin 1 has a more widespread reaction to the 2xCM change. Figure 4.25a reveals increased mass concentration throughout the depth of the atmosphere up to 11 km in all regions except for the most westerly box. At 6 km altitude, at the top of the SAL, this corresponds to an increase in the size bin 1 dust mass of between 15-25% in the five box regions. The increased dust at all altitudes explains the widespread increase in size bin 1 dust mass seen in Figure 4.22a. As the dust is transported higher and suffers very little negative effects on the mass concentration, the dust is able to travel further horizontally, and experience reduced removal efficiency. the only location where the size bin 1 vertical mass profile experiences a decrease in mass is in the MBL (< 1 km) in the West Atlantic. This could be due to the 'reintroduction' of land into the dust's pathway, changing the convective regime in the boundary layer. This is a very speculative hypothesis as this specific change is fairly unique to this bin and is only evident in this figure. As I am mostly focused on the changes to the coarse sized dust in these experiments, I will not speculate further into the cause of this change.

Figure 4.26 shows the absolute VSD of the 2xCM experiment and the percentage difference of the 2xCM experiment to the Control simulation at the Caribbean. The size bin 6 VSD is not as small as the NoCM experiment (Figure 4.21. Instead, the size bin 6 VSD experiences an increase of more than 10% between 0-0.5 km and more than 80% above 5 km altitude. Despite these relatively large changes, the VSD remains very small and close to the Control simulation at approximately 10^{-5} µm^3 cm^{-3}.

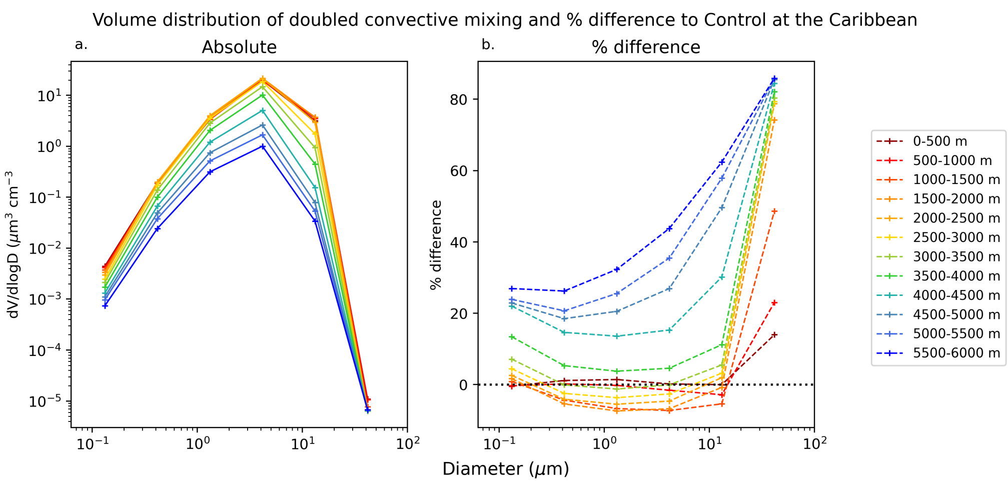

Figure 4.26: Vertically-resolved VSD (in µm^3 cm^{-3}) at the Caribbean of the 2xCM experiment (a) and the percentage difference to the Control simulation (b). The black dotted line on signifies no change at 0%.

The changes to the VSD in Figure 4.26 shows again the loss of size bin 2-5 dust between 1-3 km, and an increase of dust in all size bins at altitude, especially at the top of the SAL.

While this experiment does result in additional vertical transport of dust throughout the SAL, the extension of mixing beyond the SAL top is too great, making it a rather unrealistic simulation, as in reality we know that dust transport is capped by a strong inversion at the top of the SAL. What has been learnt from this experiment is that the increased CM over the Sahel and Sahara in regions of relatively high vertical wind velocity resulted in increased coarse dust mass in the atmosphere. Transport beyond these areas of increased updrafts is significantly decreased. Figure 4.27 shows a cross section at 16.9°N between 25°W and 5°E of the vertical wind speed and the size bin 6 mass concentration. This Figure more clearly shows the hypothesised relationship between decreasing vertical velocity and coarse dust mass. Where the vertical velocity is shown to be higher over the African continent (east of 15°W), the mass concentration is spatially fairly constant at ∼30-35 µg m^{-3}. However, beyond the African coast, both the vertical velocity and the bin 6 mass concentration drop off swiftly, with the bin 6 mass concentration dropping to a negligible concentration by 22°W, shortly west of Cape Verde.

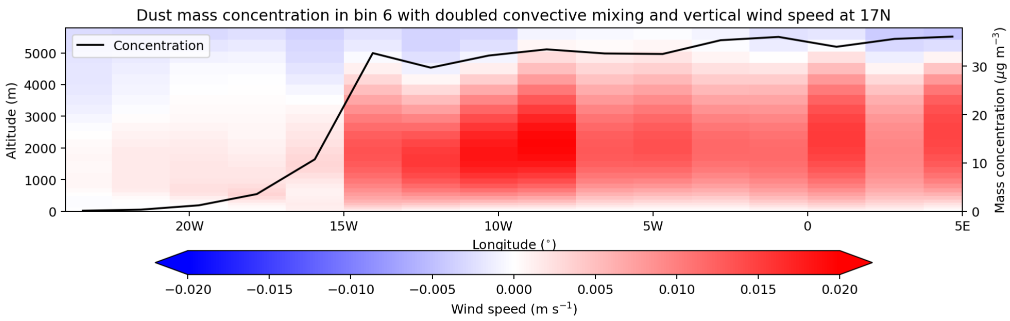

Figure 4.27: Dust mass concentration in the sixth size bin (black line; in µg m−3) and the vertical wind velocity (coloured shading; in m s^{-1}) are shown in a cross section at approximately 16.9°N between 25°W and 5°E up to 6 km altitude.

There are two potential causes which could be the reason for the swift drop-off in size bin 6 mass concentration at the African coastline. Firstly, is as hypothesised above, that the strong vertical wind velocity is no longer counteracting the fast deposition velocity of these heavy coarse particles, resulting in an increased fall rate. Or secondly, that the concentration is only heightened and steady over the continent due to emissions from the surface constantly replacing the swiftly deposited particles. Once over the ocean, this constant resupply of coarse dust is lost, resulting in the swift decrease to negligible concentrations that we see in Figure 4.27. It is likely that both of these explanations are important in the processes involved in this cross section of size bin 6 concentration. Both of these explanations continue to present the issue of overly swift deposition of coarse particles in the model that was made abundantly clear in Chapter 3. However, I propose that in lieu of these results, the vertical winds within the SAL and at the Sahara in the model should be investigated further. I believe I have presented evidence to suggest that increased vertical winds have the potential to enable coarse particle transport. In depth study could be carried out where the vertical winds are altered within the SAL, as opposed to throughout the atmosphere as has been tested here, to test whether a more directed experiment could improve the retention of coarse particles in the model.

4.2.5 Turbulent Mixing

Recent results show that turbulent mixing (TM) in the air could be used to explain long-range transport of coarse dust particles (Rodakoviski et al. 2023). Thus, in this experiment, I will test the sensitivity of coarse dust transport to TM in my climate model simulation. In this experiment, NoTM, I will test the impact removing turbulent mixing from the model. TM remains turned on over land so that dust is still raised and mixed into the SABL. However, I have turned off the effects of TM over the oceans so that I can assess whether this has a dominant impact on the removal of dust from the atmosphere. Thus, I expect greater changes at distance from the source.

Figure 4.28 shows the average profile of the potential temperature (PT) and relative humidity (RH) at five locations along the trans-Atlantic dust plume (shown in Figure 4.29). Each subplot also shows the mean altitudes of the top of the boundary layer (BL top) and the maximum turbulent mixing height (TM max). Most importantly, Figure 4.28 shows that TM in the model occurs up to and beyond the BL top at all locations.

At the Sahara, the model BL is $\sim$1.25 km in depth, with the TM max at 1.8 km (1.69-2.01 km) altitude, suggesting that TM exceeds the BL top by more than 40% of the BLs depth (Figure 4.28). The BL is deepest in this box due to the extensive convective heating and mixing of the air over the Sahara. The air here has the lowest RH and the highest PT which are both fairly constant with height; this is very typical of a deep, well-mixed SABL (Garcia-Carreras et al. 2015; Marsham et al. 2013). Upon transport over the ocean, the BL top height drops to below 1 km and an inversion in the RH and PT forms between 0.4-0.75 km altitude (Figure 4.28bcde). The MBL is differentiated from the SAL by a lower PT and a higher RH. The BL top and TM max altitudes are lower over the ocean by at least a half compared to the Sahara. The extension of TM max beyond the BL top is decreased too. With westwards transport, the gap between the TM max and the BL top decreases and the inversion weakens.

Considering that the TM has remained 'turned on' over land to avoid inhibiting dust transport completely, I will now analyse spatial changes to the trans-Atlantic

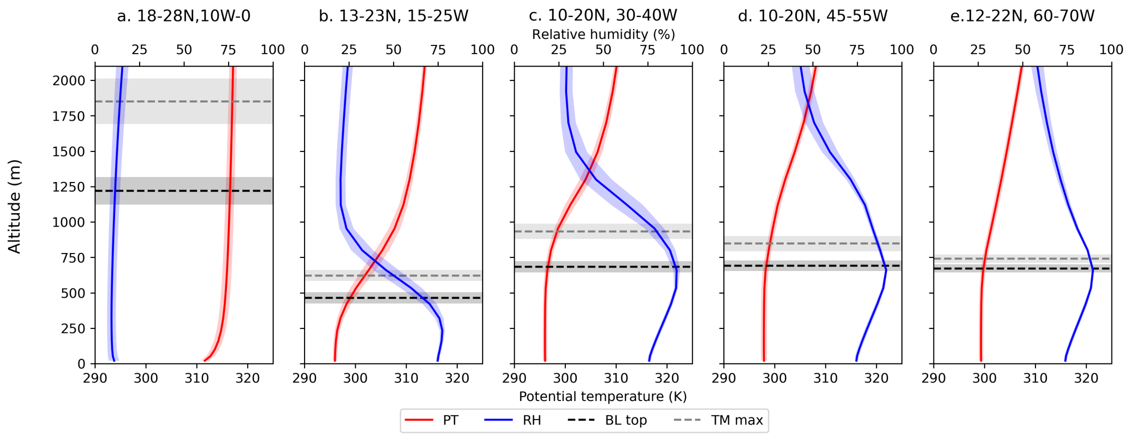

Figure 4.28: Boundary layer profiles from 0-2.1 km showing the average potential temperature (PT; red line; in K) and the relative humidity (RH; blue line). The boundary layer top height (BL top; black dashed line; in m) and the maximum turbulent mixing altitude (TM max; grey dashed line; in m) are plotted horizontally. Standard deviation of the PT, RH, BL top and TM max is shown by the shaded colouring. All plots use the same horizontal and vertical scales. Box regions used here shown in Figure 4.29, where a) is at the Sahara, b) includes the west African coast and Cape Verde, c) is in the mid-Atlantic, d) is in the mid-west Atlantic and e) is at the Caribbean.

dust path in the NoTM experiment. Figure 4.30 shows the absolute change between the NoTM experiment and the Control simulation of the binned TCM.

Generally, without TM, there is an increase in TCM over the Atlantic in all size bins (Figure 4.30). Over the Sahara in size bins 2-6, the TCM decreases; as the NoTM experiment should be parallel with the Control simulation at the Sahara, this result suggests that there is a decrease in 'recirculated' dust, i.e. dust which is first transported out to the ocean, not deposited due to the decreased TM and is then transported back to the Sahara. This change is rather small though and is a decrease of less than 2% in size bins 2-6. In size bin 1 however, there is an increase in TCM over the Sahara which is likely due to increased concentrations throughout the atmosphere increasing the amount of recirculated dust (Figure 4.30a).

Changes of a similar magnitude are more widespread in size bins 1-3, whereas the greatest changes in size bins 4 and 5 are limited to a band across the Atlantic, corresponding to the trans-Atlantic dust plume. In size bin 6, the changes are even more spatially limited, peaking strongly off the African west coast. The widespread nature of changes to the fine size bins suggests that TM is an important process for the transport of the finer particles, with decreasing importance with increasing size. With increasing size, the greatest changes appear to be limited with their distance from the Sahara; bin 1 changes are very widespread across the Atlantic, bin

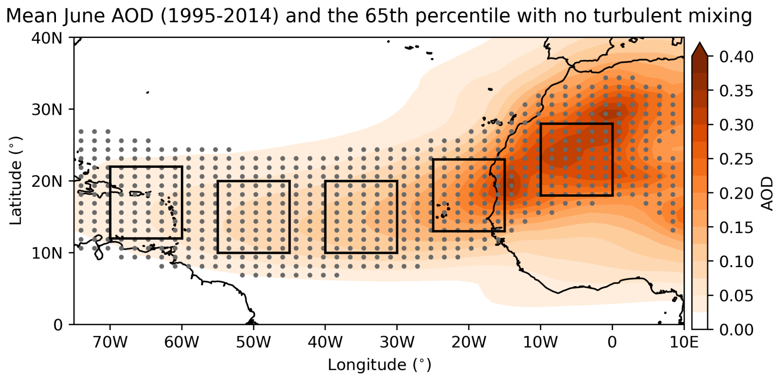

Figure 4.29: Five regions (black boxes) which are used in the analysis of this experiment. Average AOD in the NoTM simulation is shown by the coloured shading and the 65th percentile of the AOD between 1°S and 47°N is shown by the grey stippling. the location of these boxes is chosen based up the location of the 65th percentile of AOD to ensure the 'central' dust plume is captured.

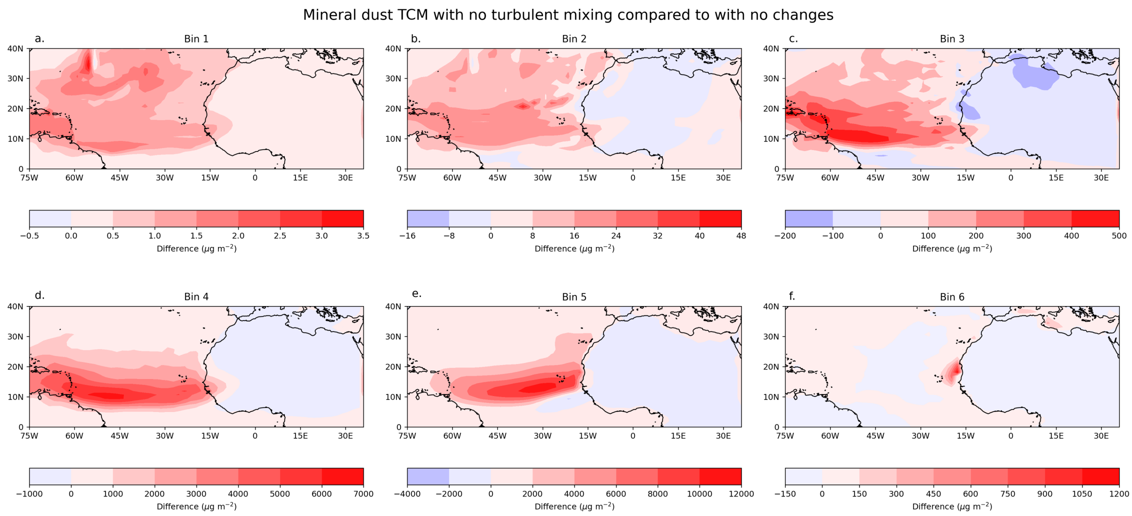

Figure 4.30: Difference in the TCM (in µg m^{-2}) of each model size bin between the NoTM experiment and the Control simulation. Each plot uses a different scale on the colour bar.

4 changes span the Atlantic, bin 5 changes are centered further east in the Atlantic and bin 6 changes are limited to just off the African coast. Thus, it appears that sedimentation is still the dominant process in controlling the long-range transport of the coarser particles. However, removing TM has somewhat increased the TCM of these coarsest particles, suggesting that it has had improved the lifetime of the coarse particles in comparison to the much longer lived coarse dust seen in the observations.

Interestingly, the changes to the TCM in size bins 3, 4 and 5 are greatest on the southern edge of the dust plume (Figure 4.30cde dust plume shown by the 65th percentile of AOD in Figure 4.29). To investigate this further, Figure 4.31 shows cross sections of the TM max height at various longitudes along the trans-Atlantic dust path between the east and west Atlantic. The orange shading indicates the location of dust plume, with the darker areas representing the latitudes where dust is always present and the lighter areas representing north and south shifts in the SAL position across the Atlantic. Except for the first transect at 22°W, the TM max decreases in altitude with distance from the Sahara. It appears that where there is exaggerated increase in dust TCM on the southern edge of the dust plume in Figure 4.30, the transects in Figure 4.31 at 52°W, 44°W, 37°W and 29°W all show a peak in TM max between 10-15°N. Where the TM max extends further into the atmosphere, it could be reasoned that the mixing actions remove more dust from the lower SAL, enhancing dust deposition. Thus, in this experiment, where I have removed TM, I postulate that the cause of the exaggerated increase in dust TCM at the southern edge of the plume is due to enhanced removal of dust in the Control simulation at this location due to TM occurring higher into the atmosphere.

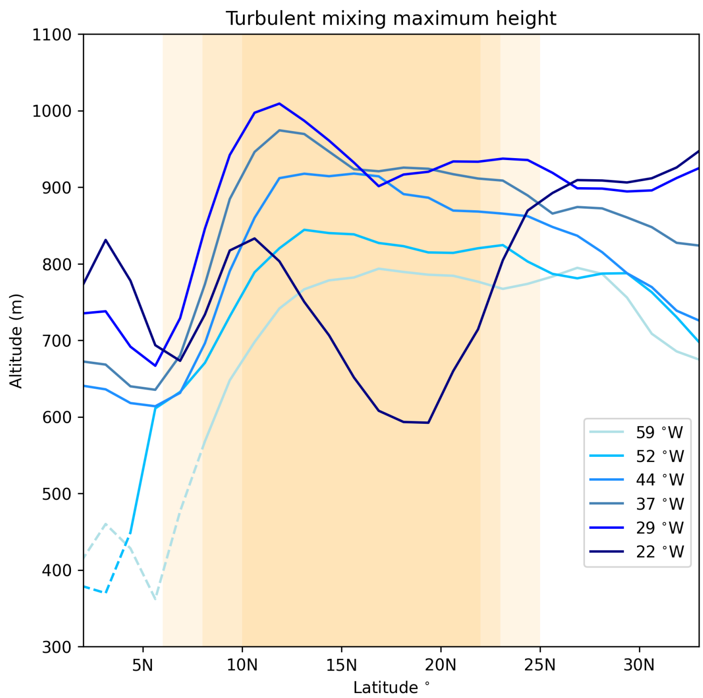

Figure 4.31: Cross sections of the turbulent mixing maximum altitude (in m) from 2-35°N shown at various points along the trans-Atlantic dust path. The orange shading represents the dust plume, which due to its changing latitude across the Atlantic, is shown by a darker area which always contains dust, and the lighter shaded areas are latitudes which are not always containing dust. A dashed line represents where the cross section intersects with land.

Additionally to note in the TM max cross sections shown in Figure 4.31 is the very different shape of the first transect at 22°W. The cross section shows a drop in

TM max centrally in the dust plume between 12-24°N. This drop explains why the TM max is so much lower in Figure 4.28b than the other averages of TM max across the Atlantic. The drop in TM suggests a very different series of processes occurring in this region compared to either TM in the west Atlantic and even over the Sahara, where TM max values are much higher. As I have suggested that higher TM max heights result in enhanced dust deposition, this dip likely does not pose a concern to coarse particle transport, rather it likely assists in leaving dust within the SAL.

It should also be noted that where the TM max transects intersect with land, shown by dashed lines in Figure 4.31, the TM max appears to drop considerably lower than any other latitude in the respective transect and lower than the other transects. Dropping to between 0.35-0.45 km altitude where the 69°W and 62°W transects intersect the South American continent, the TM max is approximately half of the transects between 2-6°N.

Taking the changes to the TCM into consideration, I will now analyse changes to the dry and wet deposition of dust in the NoTM experiment. Figure 4.32 shows the percentage difference of the separated dry and wet deposition of dust in the NoTM experiment to the Control simulation. Focusing first on dry deposition, a clear dependence on size is visible whereby the size bin 1 particles show a uniform ∼100% decrease across the ocean where TM has been turned off, while as the particle size increases, the decrease in dry deposition becomes weaker and less uniform. Consequently, the changes in wet deposition reflect the changes in dry deposition and increase most at finer sizes to compensate for the decreased dry deposition efficiency. Decreasing by nearly 100%, the changes in dry deposition of size bins 1 and 2 reveal a high dependence of these particles on TM for removal from the atmosphere by dry deposition. Unsurprisingly, as I have shown the high dependence of coarse particles on sedimentation for dry deposition, these particles are the least impacted by changes to TM in terms of the dry deposition. Additionally, size bins 3 and 4 show a similar spatial dependence to Figure 4.30, whereby decreased TM seems to result in increased TCM in the southern sector of the trans-Atlantic dust plume and here, we see a decrease in dry deposition in this same region.

In response to the removal of TM and the decrease in dry deposition of particles in the main Atlantic dust plume, size bins 1-5 show an increase in the wet deposition of dust (Figure 4.32). In size bins 1-4, the most exaggerated change occurs in the East Atlantic, southwest of the Cape Verde islands, whereas in size bin 5, the greatest changes to wet deposition spread northeast from the South American continent. The changes in size bins 1-4 are likely related to the previously discussed TM max

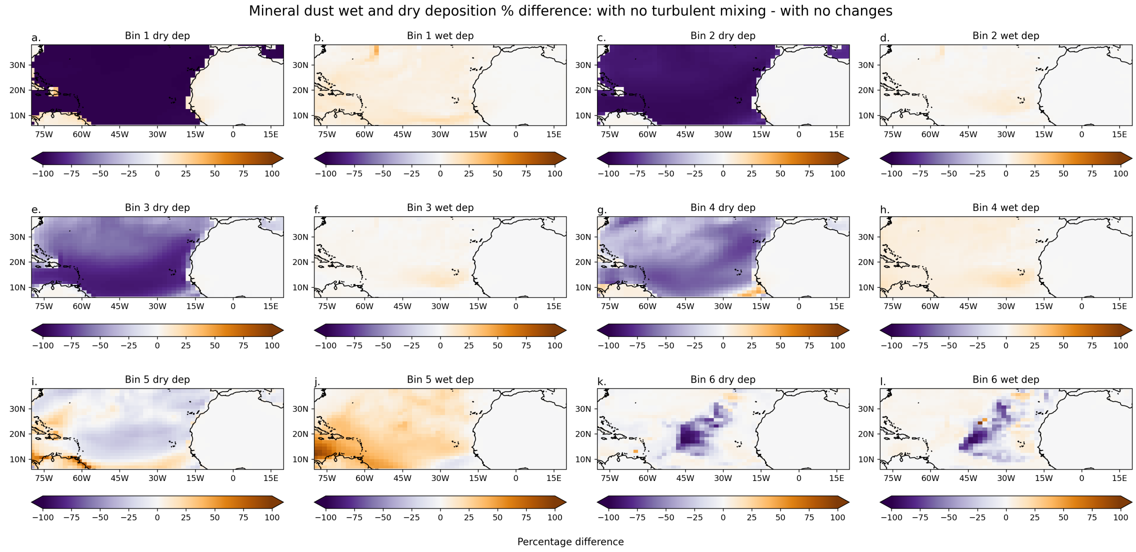

Figure 4.32: Percentage difference in the dry and wet deposition in each bin between the NoTM experiment and the Control simulation. All plots share the same scale.

values in the southern part of the trans-Atlantic dust plume. Whereas in size bin 5, it seems the changes are more related to the pattern of precipitation and that due to the decreased dry deposition, the dust is transported further than normal, making it more available for wet deposition processes. The changes in size bin 6 are largely occurring in locations with very small mass concentrations of dust and so are not statistically significant changes. However, close to the African coast, where there is an increase in size bin 6 TCM (Figure 4.30f), there is an increase in both dry and wet deposition, suggesting again that the lengthened transport provides a higher availability of dust for deposition.

So far, I have shown that by removing TM in the model, the TCM of dust in all size bins increases, suggesting increased transport distance and atmospheric lifetime. I will now analyse the vertically-resolved changes. Figure 4.33 shows the difference in the mass concentration between the NoTM experiment and the Control simulation along a transect at ∼16.9°N. As expected due to the limited vertical range of TM in the model atmosphere, the greatest changes are below 2 km altitude in all size bins.

In size bins 2-4, there is a dipole effect whereby between 0-0.3 km, there is a significant decrease in mass concentration by up to 80%, whereas above this, there is an increase in mass concentration by up to 40%. It should be noted that the altitude of the change from negative to positive occurs at ∼0.3 km, up to 0.4 km below the TM max over the Atlantic, thus it is not as simple as decreased concen-

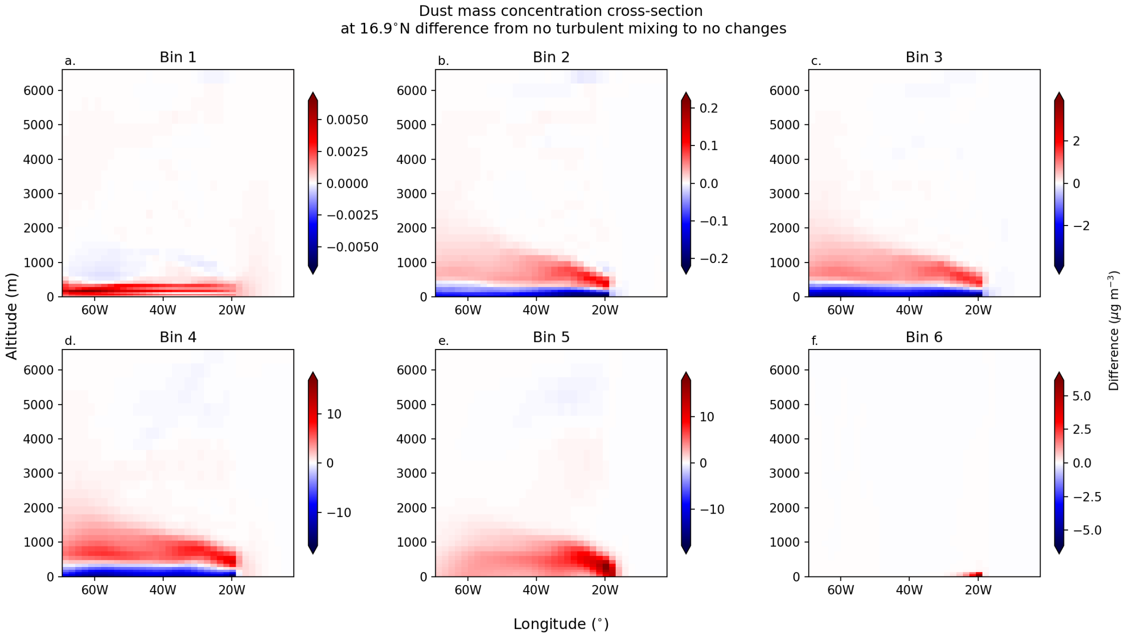

Figure 4.33: Absolute difference between the NoTM experiment and the Control simulation of the dust mass concentration (in µg m^{-2}) in a transect across the Sahara and Atlantic at ∼16.9°N. The colour bar scale is different for each plot.

tration within the TM zone or MBL. Instead, approximately halfway through the MBL, the change in mass concentration changes sign. This suggests that without TM, the sharp concentration inversion normally seen at the MBL-SAL interface is smoothed out as the SAL bottom is not eroded by TM, and the dust is brought into the upper MBL by CM and sedimentation instead. However, the TM is usually responsible for the further mixing down to the surface and thus without TM, the dust, not susceptible enough to the sedimentation, is less well-mixed into the lowest 0.3 km of the models atmosphere.

In size bin 5, there is not the same dipole pattern in the MBL (Figure 4.33e). Instead, there is a 'plume' of increased concentration extending from the west African coast. There is no decrease at the surface, unlike in size bins 2-4 where the decrease at the surface is caused by the absence of TM. In size bin 5, due to the greater particle mass, the faster sedimentation of these coarse particles results in increased mass all the way down to the surface. Despite this, there is still a darker coloured area between ∼0.3-0.7 km in the mid Atlantic (40-60°W). This is in the same location as the greatest increase seen in bins 2-4, suggesting that while the sign of change does not flip below 0.3 km, the signal becomes weaker. This shows that the same process is happening to result in increased concentrations within the upper MBL, but the greater settling velocity is enough to pull the particles shown into the lowest 0.3 km. The removal of TM has increased the amount of size bin 5 dust reaching the mid and west Atlantic; at the Caribbean, the mass concentration is 50-100% greater between 0-0.9 km altitude. However, there is only a 10-25% increase in size bin 5 mass concentration between 1-2 km.

With increasing distance from the Sahara, the vertical depth over which the mass concentration is changed becomes deeper in size bins 2-5. For example, in size bin 4, at 20°W, only the lowest 1 km of the atmosphere is significantly affected, however, at 70°W, this has extended up to 2 km. This suggests that when the changes are newly introduced to the dust plume at the African coast, the impact is below the TM max (∼0.6 km between 15-25°W; Figure 4.31b) and extending into the lower SAL. However, with time and transport, the effects of the removed TM are propagated further up into the SAL, especially for smaller size bins where the settling velocities are much smaller.

In size bin 6 in the Control simulation, the even greater settling velocity means that the concentration drops to near negligible concentrations very swiftly after being transported off the African coast. By turning off TM, the model is able to transport the coarsest dust marginally further, producing an increase of up to 6 µg m^{-3}, or 125% at ∼20°W. However, the concentrations quickly become negligible again with westwards transport.

As the aircraft observations collected at the Caribbean which revealed the extent of the model underestimation at long distances from the Sahara (shown in Chapter 3) are focused between 2-4 km, we know that the mass concentration at these altitudes needs to be significantly improved. Although this experiment shows improved coarse particle (size bin 5; 6.32-20µm) transport to the Caribbean, however, it does not provide the improvements in concentration at altitude that are necessary for bringing the model in line with the observations. Instead this experiment gives insight into the downward mixing within the MBL.

4.3 Results of the RE On Experiments

4.3.1 Tripled SW Absorption

Uncertainties in the size distribution and the mineralogical composition of emitted dust results in uncertainty in the absorptivity of dust. Recent research has suggested that the SW absorption of dust is too low (Di Biagio et al. 2020; Li et al. 2021) and that increasing the it can improve meteorology in models (Balkanski et al.

2021). Thus, as an extreme experiment, I will triple the SW absorption of dust in all size bins to test the sensitivity (3xSW). Unlike the previous experiments, in this experiment, the RE are turned on in order to understand the impact of increasing the SW absorption of dust in the model. This means that the meteorology and dust emissions are no longer parallel between simulations. In this Section, I will compare a control simulation with RE turned on (REControl) and the 3xSW experiment.

Before analysing any changes in the dust transport and lifetime, I determine how different the dust emissions are in the two simulations (REControl and 3xSW) to confirm whether being non-parallel affects the comparability of the simulations. Figure 4.34 shows a timeseries of the mean dust emission rate across the whole Sahara (a) and separated into the west (c) and east (d) Sahara in both simulations. The standard deviation of the two simulations is also shown in the shaded colours.

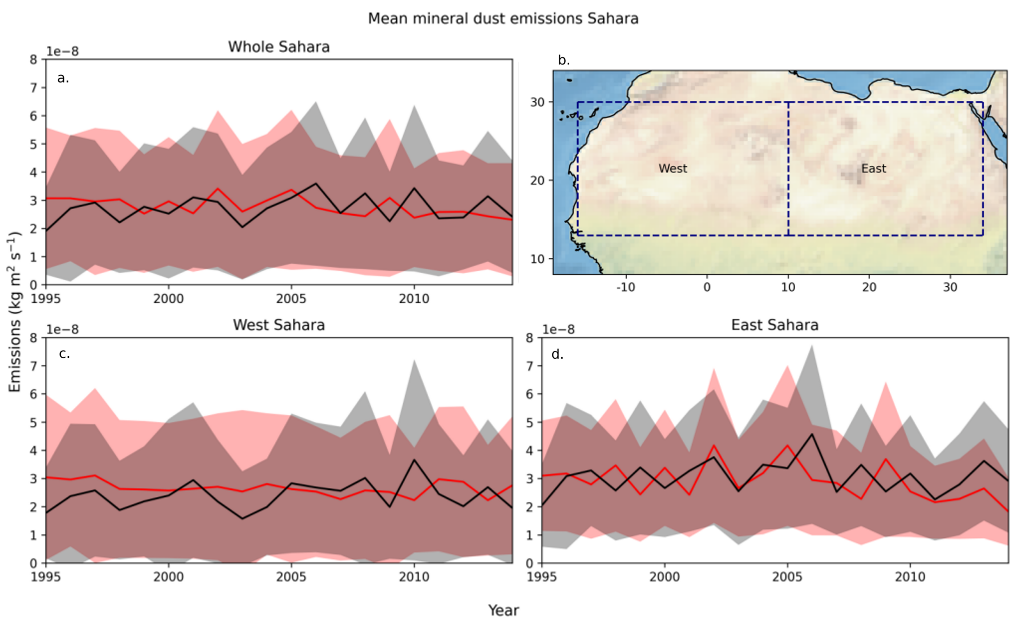

Figure 4.34: Timeseries of the mean dust emissions (in kg m^2 s^{-1}) from the Sahara in both the REControl (black) and the 3xSW (red) simulations (a). The emissions are also plotted from the west (c) and east (d) Sahara. The location of the analysed areas are shown on a map (b).

Exact peaks and troughs in the Figure 4.34 timeseries are not matched between the two simulations as the model is free-running. However, there is a great amount of overlap between the standard deviation of the emissions in both simulations, suggesting that the 3xSW experiment is still within a comparable range of the REControl simulation.

There is no discernible trend in the REControl emissions in any of the three analysed regions. Alternatively, in the east Sahara in the 3xSW experiment, there is a slight trend towards decreasing emissions from 2005 onwards (Figure 4.34d). The spread of the standard deviation remains overlapping with the REControl simulation to a reasonable extent. Due to the end of the simulation in 2014, it is hard to tell whether this trend is significant and real, or just within reasonable variability. Fortunately, the downwards trend does not take the 3xSW experiment out of the range of the REControl experiment, so I can maintain that the two experiments are within a comparable range of each other.

In the west Sahara, in the first half of the period (1995-2005), the upper spread of the standard deviation appears to show higher emissions in the 3xSW experiment compared to the REControl simulation (Figure 4.34). The mean dust emissions are still within the REControl standard deviation however, so I will continue to assume that the two simulations are comparable. As there are no strong trends in the data, I can assume that changes to the dust (i.e. tripled SW absorption) are not significantly driving changes in the meteorology associated with dust emissions. Therefore, I will now analyse changes to the dust abundance and lifetime.

Figure 4.35 shows the percentage change in the size-resolved dust TCM between the 3xSW experiment and the REControl simulation. At the Sahara, there is a percentage decrease in TCM in size bin 1 in the west of up to 50% (Figure 4.35a). Size bin 2 shows an increase across the majority of the Sahara, except for a band of negative percentage difference at $\sim$18°N between 0-15°W of up to 50%. In size bins 3 and 4 over the Sahara, TCM is increased with percentage changes of up to 50%. These changes could be related to the differences in emissions; 3xSW has marginally higher emissions than REControl in the west Sahara (Figure 4.34) which could be why we are seeing an increase in TCM here, especilly in size bin 5 which only increases over the Sahara in the west. However, the magnitude of the changes to TCM (up to 50%) are on average larger than the difference between the emissions in the two experiments, i.e. not all of the difference in TCM at the Sahara can be explained by differences in the emissions. This suggests that by tripling absorption, the TCM over the Sahara generally increases in size bins 2-4.

In size bins 2-5, there is a decrease in TCM to the south of the Sahel, extending out in a WSW direction over the tropical Atlantic in Figure 4.35. This area of decrease is strongest in size bin 5, with a decrease of up to 50%. This could be caused by slight changes in the transport pathway of the dust, with less dust transported southwards at the Sahara, and then this decrease is propagated to the west. Size bin 5 also shows a fairly strong decrease in TCM in the Mediterranean, which again

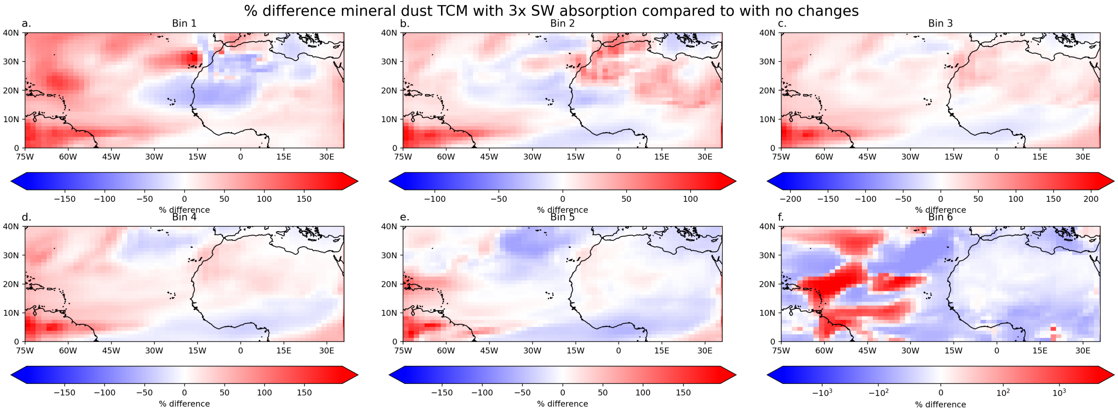

Figure 4.35: Percentage difference in the size-resolved TCM in the 3xSW experiment and the REControl simulation. The scale differs between each plot. Size bin 6 is shown on a log scale. Gridpoints with a TCM value below a threshold of 0.1 µg m^{-2} in both simulations have been removed to reduce noise.

could be due to altered transport pathways. It does not seem to be due to a decrease in lifetime and transport of the particles as there is an increase in TCM in the west Atlantic in all size bins. This suggests that while some minor transport pathways (to the north and south) have decreased in magnitude or frequency, the main trans-Atlantic dust pathway appears to have improved transport of dust to the west Atlantic.

Size bin 1 has a different reaction to the tripling of SW absorption, with sporadic decreases in TCM in the west and north Sahara and off the west African coast in a small plume (Figure 4.35). However, the fairly strong increase across the rest of the domain is indicative of increased dispersion of the very fine size bin 1 particles in the 3xSW experiment. The decrease near the source and increase elsewhere suggests that the particles are very swiftly moved away, leaving less mass at the source than in REControl, but with more further away. This could be due to changes in the meteorology induced by additional heating from the tripled SW absorption. I will further explore this possibility later in the Section by looking at how the meteorology of the two simulations differ.

Size bin 6 shows a widespread decrease in TCM at the Sahara, which shows up to a halving of the TCM and greater decreases beyond the Sahara (Figure 4.35f). At distance from the Sahara, in the Atlantic, there are some patches of increased TCM, with increases of more than 4000%. These changes occur in locations of very low size bin 6 concentration in the REControl, resulting in the large magnitude of changes. This suggests that size bin 6 dust is more able to reach the west Atlantic in the 3xSW simulation compared to the REControl. However, the decrease in TCM at the Sahara hints that the dust may not be transported from there, but that we are seeing improved transport from different sources (maybe in North America or South America). As the model outputs the data here as monthly means, I cannot analyse in more depth the transport of this size bin 6 dust and where it originated from. As the Sahara is the largest dust source within the vicinity and within the transport range of the coarsest dust, I will assume that a significant portion of this increased size bin 6 TCM comes from the Sahara.

Figure 4.36 shows the total dust mass profile, standard deviation and MCA of both the REControl simulation and the 3xSW experiment. At the Sahara, the greatest change to the total profile is at the surface where the concentration is increased by ∼200 µg m^{-3} (Figure 4.36). With increasing altitude, the 3xSW total profile falls back into line with the REControl simulation. The increased dust concentration near the surface in the 3xSW experiment reduces the total dust MCA lower than the REControl simulation by ∼100 m. Additionally, the spread of the standard deviation of the 3xSW experiment is about half that of the REControl simulation. This could be a result of the fairly stable mean emissions in the west Sahara (Figure 4.34c), which still shows a similar spread in the standard deviation to the REControl, but with a less variable mean.

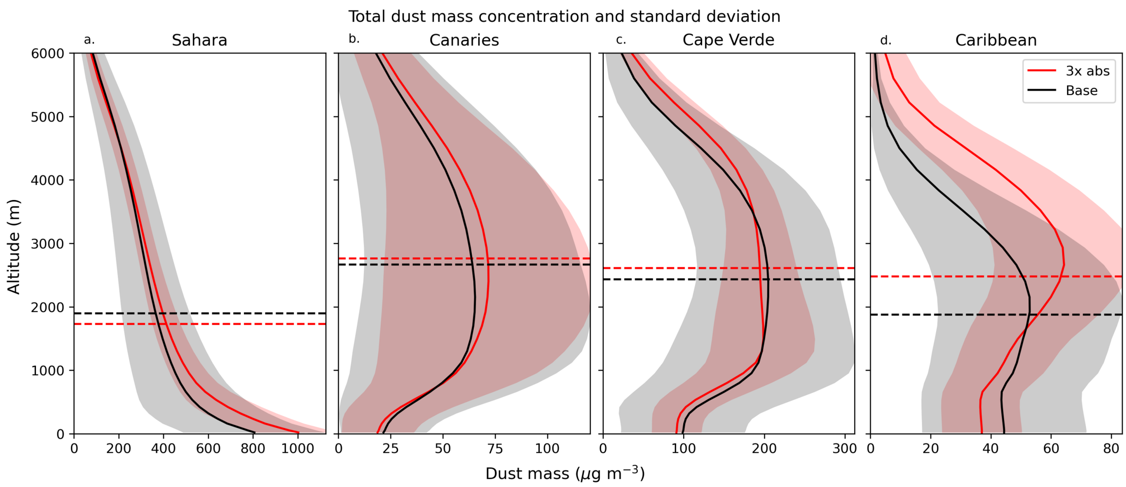

Figure 4.36: Total dust mass concentration profile (solid line; in µg m^{-3}) and standard deviation (shaded area) of the REControl simulation (black with grey shading) and 3xSW experiment (red with light red shading). The MCA is shown by the dashed lines at each location.

At the Canaries, there is an increased mass concentration in the dust profile in the 3xSW experiment, especially above 1.5 km altitude. This increase of dust in the SAL results in a slightly heightened MCA.

At Cape Verde, a decrease of dust in the MBL and SAL between ~1.5-3.5 km, and an increase of dust above 3.5 km compared to REControl results in a heightened MCA again (Figure 4.36c). Similar to previous experiments which lofted dust higher, the increase at altitude is paired with a decrease lower down. Like at the Sahara, the standard deviation of the total mass concentration is much less than the REControl simulation. This could again be a result of the more stable mean emissions rate in the west Sahara. Or this could also be the consequence of different vertical mixing processes as a result of the different absorption.

Finally, at the Caribbean, the difference between the two total mass profiles is the greatest in terms of the overall shape. The dust has been raised much higher at the Caribbean, with an MCA more than 500 m higher than the control. Above 3.3 km altitude, the profile mean from each experiment is no longer within the standard deviation of the other experiment, suggesting a significant change in the vertical structure of the dust profile. The standard deviation of the REControl profile between 5-6 km is very small in comparison to that of the 3xSW experiment. This suggests that while dust rarely exceeds 5.5 km in the REControl simulation, in the 3xSW experiment, it is more regularly transported to this altitude and above.

Now looking at the vertically-resolved changes by size, Figure 4.37 shows the change in VSD between the 3xSW experiment and the REControl simulation. At the Sahara, there is an increase in size bins 2-6 VSD in the lowest layer (0-500 m; Figure 4.37), corroborating the increase in mass concentration seen in Figure 4.36a. Moving upwards, the VSD of size bin 6, and from 3 km up, size bin 5 particles decreases compared to the REControl simulation. Alternatively, size bins 2-4 show increased VSD compared to the REControl at the Sahara at all altitudes. So although the total mass concentration of dust at the Sahara is greater in the 3xSW experiment, it is made up of more finer particles, rather than coarser particles.

At the Caribbean, all size bins show increased VSD above 2.5 km altitude, with size bins 2-6 decreasing at some level below this altitude (Figure 4.37). This agrees with the total mass profile which showed decreased mass concentrations below 1.8 km at the Caribbean (Figure 4.36d). The greatest changes occur at altitude, for example in size bin 5, the VSD has increased by ~400% between 4-5 km. This again agrees with the sentiment that the increased absorption has raised the dust higher, increasing the changes seen at altitude.

Figure 4.38 shows the vertically-resolved percentage difference of VSD from Cape Verde to the Caribbean in the REControl simulation (a) and the 3xSW experiment

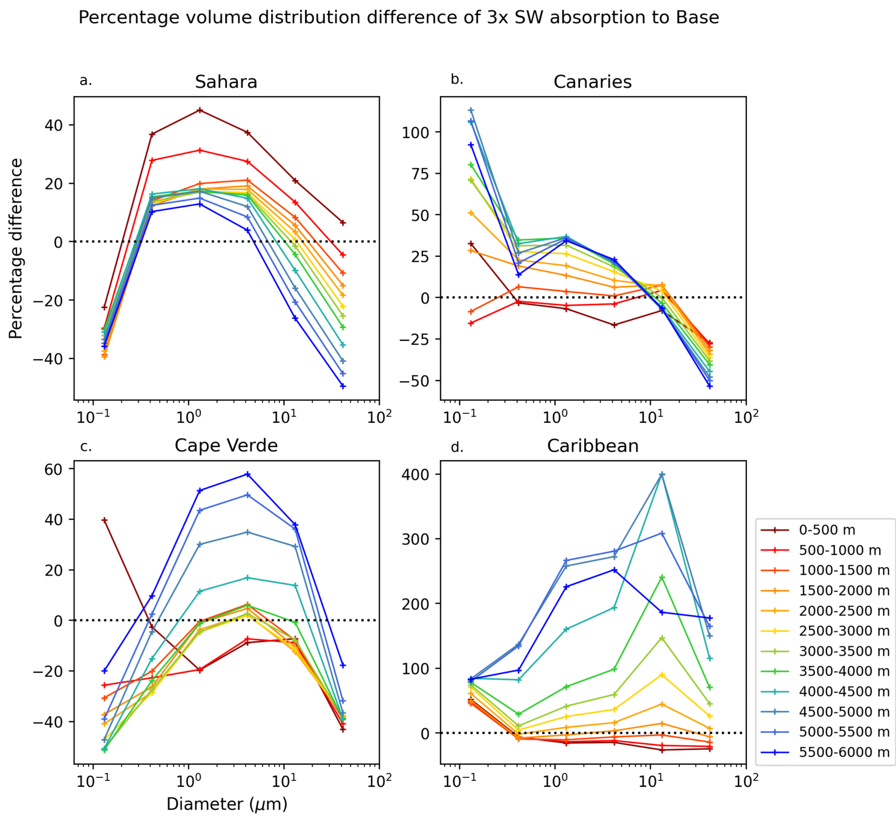

Figure 4.37: Vertically-resolved VSD percentage difference between the 3xSW and REControl simulations. The black dotted line is at 0 and represents no change in VSD.

(b). 4.38c shows the difference between the two differences shown in 4.38a and 4.38b.

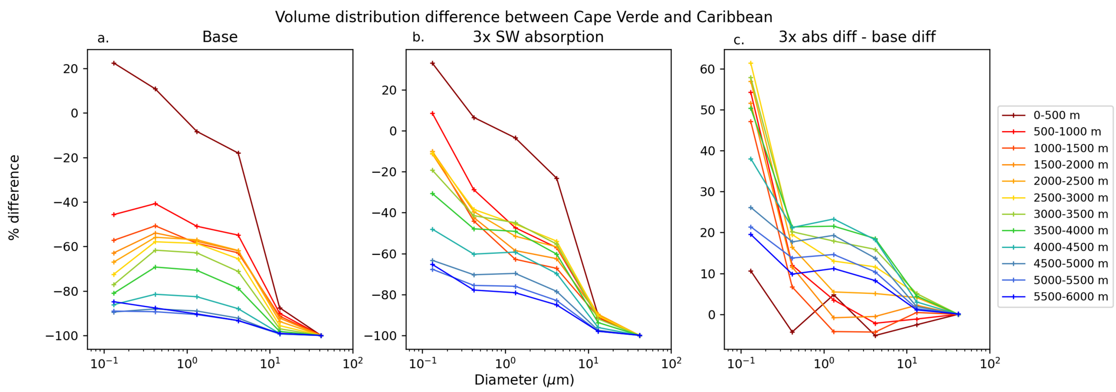

Figure 4.38: Change of VSD between Cape Verde and the Caribbean in the REControl (left) and the 3xSW (middle) experiments. The difference between the two experiments of the change over transport is shown (right); i.e. the additional VSD retained as a result of higher absorption.

In the REControl simulation, there is a loss of 40% of the VSD in all bins from Cape Verde to the Caribbean, except for between 0-0.5 km (Figure 4.38a). The highest altitudes are subject to the greatest percentage loss in all size bins in both experiments. As the dust plume is transported west, the gradual sinking of the SAL will result in reducing concentration of all particles from 6 km altitude (the top of the SABL/SAL at the Sahara/East Atlantic) down to 4/5 km (SAL top in the West Atlantic). As the plume is transported, dispersion mechanisms and deposition will reduce the concentration within the plume, hence why we see a minimum of 40% loss above 1 km here. However, in the 3xSW experiment, there is a reduced magnitude of particle loss between Cape Verde and the Caribbean, with size bin 1 particles only losing between 10-35% between 1-4 km altitude. There is also less loss at altitude; in size bins 1-4, there is no loss greater than 86%, compared to most size bins losing more than this above 5 km in the control.

Comparing the two percentage difference plots shows that there is less VSD loss over long-range transport between Cape Verde and the Caribbean in the 3xSW experiment, this is shown by the mostly positive values on Figure 4.38c. While the increased SW absorption dominantly impacts the VSD of fine particles, there is still an increase in the VSD of size bin 6 particles reaching the Caribbean. Approximately 1% more size bin 6 particles reach the Caribbean at every height level in the 3xSW experiment. There is an increase of size bin 5 particles reaching the Caribbean of up to 5% above 1 km altitude. The finer the size bin, the smaller the loss of particles between Cape Verde and the Caribbean.

There is a reduced altitude-dependent reaction to transport in the 3xSW experiment. In the REControl simulation, the percentage VSD loss increases with altitude. However, in the 3xSW experiment, the loss of VSD between 0.5-2.5 km is greater than at higher altitudes. This results in a similar percentage loss in size bin 3 between 4.5-5 km and 1.5-2 km where, in REControl, the two losses were separated by nearly 40%.

While this experiment has improved the amount of coarse particles reaching the Caribbean with respect to observations (not shown), it has not resulted in the magnitude of change required to match the observations. Changes to the VSD at size bin 6 need to be more than 5 orders of magnitude to be brought into agreement with the observations. The changes to SW absorption have a greater impact on size bins 2-4 due to their size and thus, their interaction with SW radiation. However, the intention is that by creating a dust plume that absorbs more radiation as a whole, the dust plume will be heated, heightening transport and extending the lifetime of all sized particles. Delving further into the meteorology of this experiment, I will show how it differs to the REControl simulation.

Figure 4.39 shows the maximum dust mass concentration and 75th percentile of mass dust concentration at each longitude; this is used here as a proxy for the location of the dust plume. Both the REControl and 3xSW plumes are shown between 0-6.6 km (top) and 3-6.6 km (bottom). Over the whole profile (0-6.6 km), the two are not discernibly different in their general location. Differences in the maximum concentration over the Sahara are likely due to dust sources being activated in different ways due to the tripling of absorption, altering small- and large-scale meteorology, for example the location and strength of the SHL. Caton Harrison et al. (2019) discusses the movement of the SHL throughout the summer and shows the changing wind speeds and direction, and deep convective cloud cover associated with this seasonal movement. With slightly altered meteorology, either caused by the models internal variability or the increased dust absorption, the position and strength of the SHL could be the cause of the changes to mass concentration distribution in the 3xSW experiment compared to the REControl.

In the mid and west Atlantic between 60-40°W, the 3xSW total depth of the plume shifts further south of the REControl plume with the maximum concentration occurring up to two grid boxes further south (Figure 4.39 top). However, the 75th percentile of dust concentration does not show this same southerly drift, instead remaining mostly overlapped with the control simulation. This suggests a shift of the latitudinal distribution of dust within the plume.

There are similarly few discrepancies between 0-3 km (not shown) as to between 0-6.6 km (Figure 4.39 top). However, there are more changes in the plume location at 3-6.6 km in the upper SAL between REControl and 3xSW (Figure 4.39 bottom). The maximum concentration location extends further north in the east Atlantic at Cape Verde and further south in the mid Atlantic (35-55°W). This hints at changes to large-scale meteorology as a consequence of the additional SW absorption, which alter the dust higher, closer to the free troposphere, i.e. the three-dimensional structure of the SAL.

Figure 4.40 shows the temperature and relative humidity (RH) profiles in the control and 3xSW simulations. The approximate locations of the plots are at the Sahara, Cape Verde and Caribbean, however, the latitudinal extent of the previously used boxes has been extended to account for any north/south latitudinal shifting of the dust plume. The air temperature is analysed here in order to ascertain the impact of tripling the dust absorption. As Figure 4.36d showed, the 3xSW dust profile was higher than the control dust plume. I postulate that this is due to additional SWheating within the dust plume caused by the enhanced absorption, which is re-

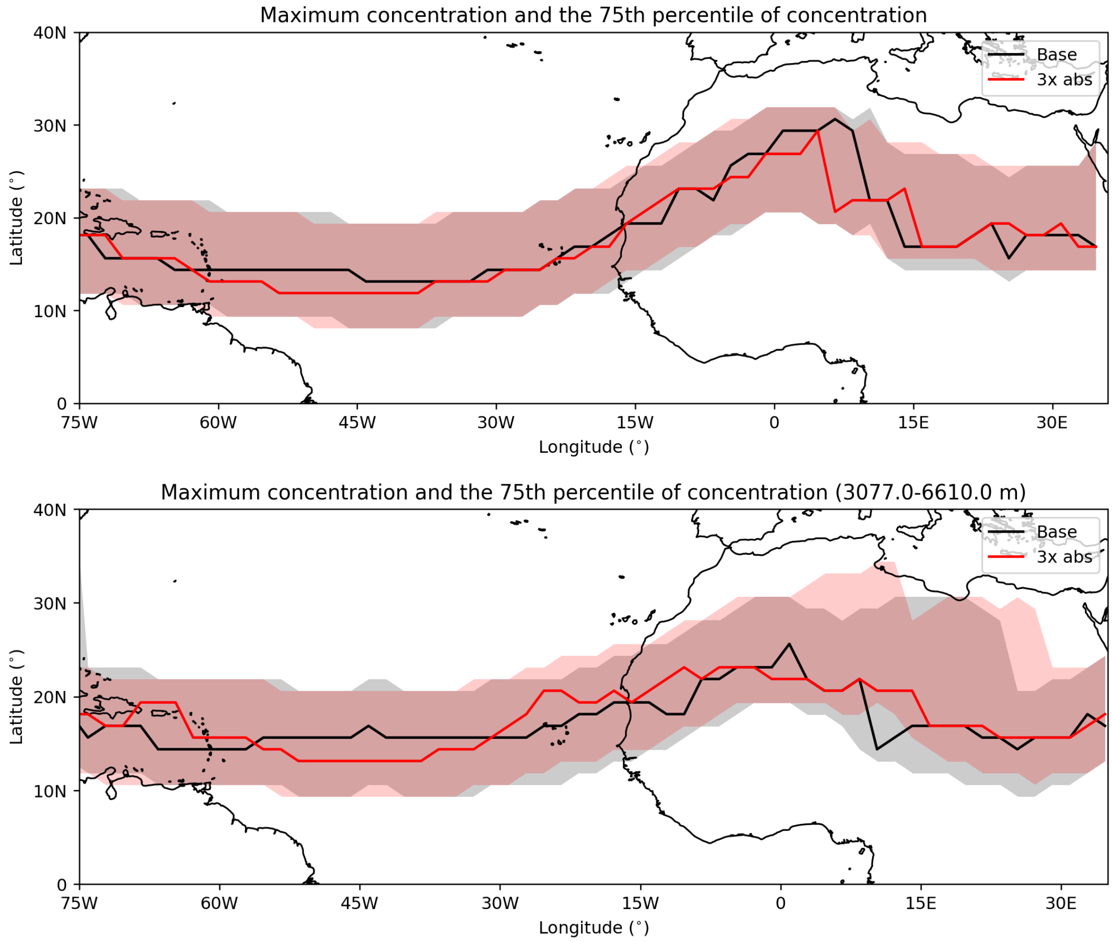

Figure 4.39: Maximum mass concentration of total dust mass concentration (solid line) and the 75th percentile of total dust mass concentration (shaded area) in the REControl (black) and 3xSW (red) simulations. The maximum and percentile data is averaged over 0-6.6 km (top) and 3.0-6.6 km (bottom).

sulting in a lofting effect, raising the dust higher into the SAL. Figure 4.40 shows that at each location, there is an increase in the air temperature by up to 1 K within the SAL.

Despite the largest changes to the dust mass concentration occurring near the surface at the Sahara, the temperature changes are the smallest here and increase with height (Figure 4.40). Between 3.5-7 km, the temperature change remains steady at about +1 K. At Cape Verde, the structure of the MBL appears to have changed slightly in 3xSW, becoming weaker due to the increased altitude of the dust. This results in a negative temperature difference between 0.5-1.4 km altitude compared to REControl. Above this, the air temperature in the 3xSW experiment increases beyond the REControl simulation, to a maximum difference of around +1 K at ~4 km altitude. This peak in difference occurs in the upper SAL. This is likely caused by a feedback loop of increased heating within the dust plume, resulting in

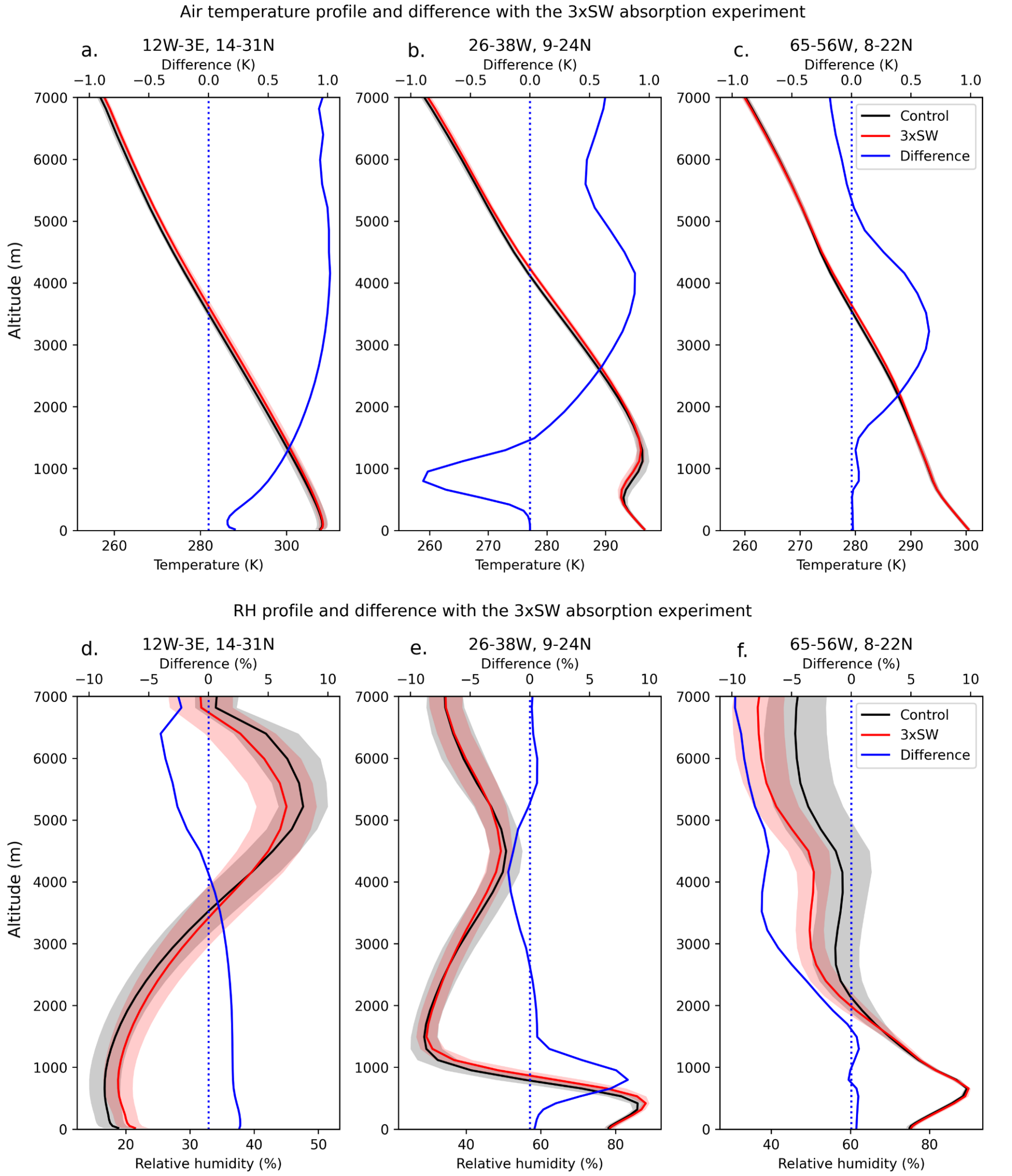

Figure 4.40: Vertical profiles of air temperature (in K) in the REControl (black line) and 3xSW (red line) experiments and the difference between the two (blue line; in K).Vertical profiles of relative humidity (as a %) in the REControl (black line) and 3xSW (red line) experiments and the difference between the two (blue line; in %).

dust lofting and increased dust concentrations at altitude, which then results in further heating, exacerbating the heating effect in the upper SAL. At the Caribbean, the increased absorption leads to increased air temperature within the central dust plume between 2-5 km altitude. Below 1.7 km, there is much less change (< 0.1 K) in the air temperature. This could be due to the decreased dust concentration in the MBL (Figure 4.37d) resulting in decreased additional heating relative to the rest of the dust profile.

I have also analysed the RH changes at the three locations too. This analysis was motivated by research by (Balkanski et al. 2021), which suggested that when they improved the representation of dust SW absorption, more water vapour was advected from the ocean into the Sahel region. Additionally, changes to the water vapour mixing ratio (WVMR) of the air will influence heating and cooling in the LW.

At the Sahara, the 3xSW experiment shows an increase in RH below 4 km of up to 3%, and an decrease in RH of up to 5% in the upper SAL (Figure 4.40a). This suggests that the profile could be more well-mixed. In the REControl simulation, where there is higher RH in the top of the SAL, there will likely be more warming as a result of this moisture. Ryder (2021) found that a higher water vapour mixing ratio at the top of the SAL induced heating at the plume top. With lower RH, the 3xSW may not be benefiting from additional heating that would otherwise raise the plume even higher. In the West Atlantic, the difference between the RH in the REControl and 3xSW experiments grows with altitude. Below 2 km, the difference is less than 1%, but with increasing altitude, this grows to 10% at 7 km altitude. This is the largest change in RH of the analysed locations.

4.4 Discussion

4.4.1 Impact of RE Off Transport and Deposition Mechanisms

In this Section, I will compare all of the experiments which ran with RE turned off, i.e. they follow the same meteorology evolution with the same dust emissions. Figure 4.41 shows the normalised total mass profile from each experiment and the Control simulation at the Sahara, Canaries, Cape Verde and Caribbean. Each experiment has also had the mass centroid altitude (MCA) calculated – the altitude at which 50% of the dust mass is above and 50% is below – which are shown in Table 4.3. At the Sahara, there is not a great amount of change between the shapes of the profiles in each experiment. With distance from the Sahara, the differences between the profiles become more prominent; the greatest range in MCA values occurs at the Caribbean.

The NoIS experiment shows the most significant change to the shape of the vertical profile as well as the MCA at each location. Initially at the Sahara, the NoIS experiment already shows an increase of dust at altitude compared to the other experiments, showing a different profile shape from 5 km up, resulting in an MCA 0.176 km higher than the next highest MCA. Moving downstream to the Canaries,

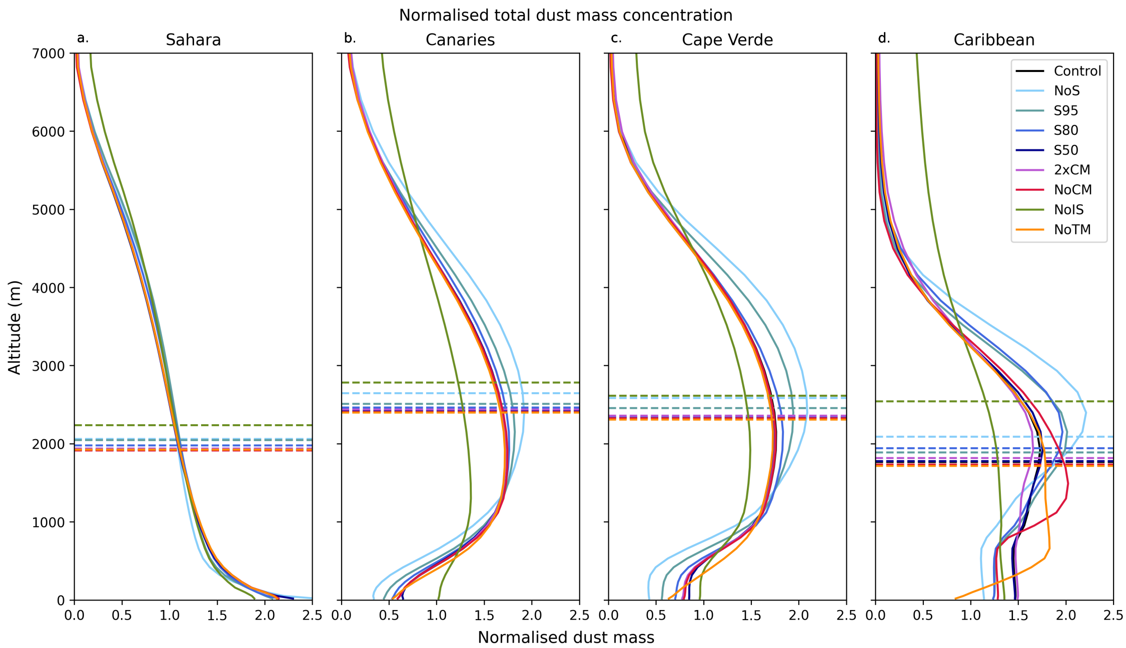

Figure 4.41: Normalised profiles of the total mass concentration at the Sahara, Canaries, Cape Verde and Caribbean in the Control simulation and 8 experiments; NoS, S95, S85, S50, 2xCM, NoCM, NoIS and NoTM. The dashed lines represent the MCA. The profiles have been normalised by the average concentration over altitude.

the profile is much more well-mixed than the others, with a much straighter normalised profile shape. The profile shape at Cape Verde is marginally more similar to the other experiments, but still showing a heightened MCA at 2.8 km and increased concentration above the SAL top. Finally, at the Caribbean, the profile no longer resembles any of the other experiments, with an MCA ~0.5 km higher than any other. The vertical dust profile produced by the NoIS experiment is the least like what we see in the observations. As seen in Chapter 3, the model profiles often struggle to capture the sharp inversions in concentration throughout the profile, thus, these changes from the NoIS experiment exacerbate and make this issue worse, taking the model further from the observations.

Similarly, the NoTM experiment changes the vertical profile of dust for the worse, though this time by lowering the profile. At all locations, the NoTM MCA is the lowest of the experiments. This is likely because of the loss of the MBL structure in the dust profile, which is seen most significantly at Cape Verde and the Caribbean. Not only is there increased concentration of dust below 1 km altitude in the MBL, but there is typically decreased concentration relative to the other experiments in the upper SAL (3-7 km at the Sahara and Canaries, and 3-5 km at Cape Verde and Caribbean). Thus, the NoTM experiment also has a negative impact on the representation of the vertical dust profile in comparison to the observations.

	Total dust mass centroid altitude (m)			
Experiment	Sahara	Canaries	Cape Verde	Caribbean
Control	1928	2421	2344	1771
NoS	2065	2651	2588	2093
S95	2048	2514	2459	1893
S80	1980	2465	2345	1945
S50	1922	2429	2327	1779
NoIS	2241	2786	2617	2546
2xCM	1941	2442	2362	1821
NoCM	1916	2408	2331	1738
NoTM	-	2402	2313	1719

Table 4.3: Total dust MCA values (in m) for each experiment at each location. No data is shown at the Sahara for the NoTM experiment as no changes were made to the model at the Sahara.

The NoCM and 2xCM experiments have a vertical profile which is very similar to the Control at the Sahara, Canaries and Cape Verde. In the NoCM experiment at the Caribbean, the dust settles within the SAL, creating a peak in concentration between 1-2 km altitude, though leaving the MBL intact. Alternatively, the 2xCM experiment has a more well-mixed MBL and lower SAL, removing the distinct shape of the MBL from the dust profile.

The sedimentation experiments (NoS, S95, S80 and S50) show a large amount of variability between the normalised concentration within the SAL, with the greatest differences appearing between 2-3 km at each location. The NoS experiment extends the most, with the highest concentration in the SAL. Relative to the other experiments, these changes are the most realistic to real-world representation. There is an exaggeration of the features of the vertical dust structure seen in the observed profiles.

Decreasing the sedimentation increases the distance travelled by coarse particles in the model, as well as increasing the total dust MCA, whereby the NoS experiment has the highest coarse mass concentration and the highest MCA at the Caribbean out of the sedimentation experiments. However, the S80 experiment has a higher MCA at the Caribbean than the S95 experiment by $\sim$50 m. This could be because S95 has a greater coarse dust loading at the Caribbean than S80, but doesn't have the same level of reduced sedimentation as the NoS experiment, so the dust settles lower than NoS, but with a greater mass than S80, the MCA value is skewed lower.

Figure 4.42 shows the absolute VSD values from every experiment as well as the observed VSD between 2-4 km altitude. This allows us to see the changes relative to the observations, allowing me to assess which experiments produce realistic and representative outputs. A normalised VSD could be used to understand changes to the shape, but I have chosen to focus on the magnitude of the changes here instead.

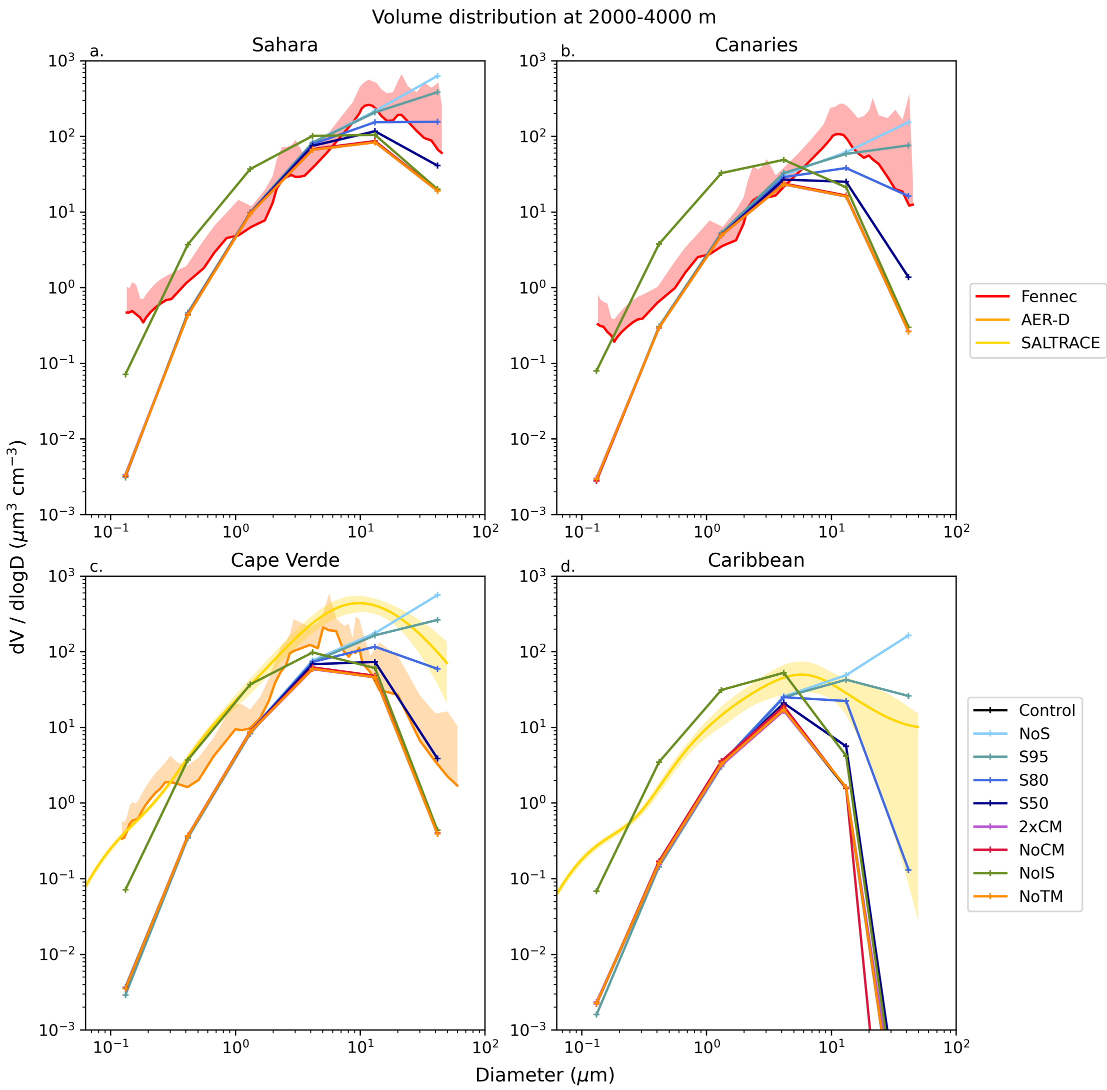

Figure 4.42: Mean VSD (in μm^3 cm^{-3}) between 2-4 km at the Sahara, Canaries, Cape Verde and Caribbean in the Control simulation and the 8 experiments; NoS, S95, S85, S50, 2xCM, NoCM, NoIS and NoTM. The Control simulation terminated at $3.57e^{-6}$ μm^3 cm^{-3} in size bin 6 at the Caribbean. VSDs from the aircraft campaigns (Fennec, AER-D and SALTRACE) are also shown between the same altitude. Shading above the Fennec and AER-D campaign VSDs represents one standard deviation. Shading above and below the SALTRACE VSDs represents the 10th and 90th percentiles of the measurements.

Changes to the VSD from the NoCM, 2xCM and NoTM experiments are minimal in nearly all locations and size bins, except for a 2 order of magnitude decrease in the size bin 6 VSD at the Caribbean in the NoCM experiment. Though these experiments have produced interesting results and an insight into the processes controlling dust transport and its vertical distribution, as discussed in previous sections, they do not result in great enough changes to alter the model in ways significant enough to result in better agreement with the observed VSD. At the Caribbean, the size bin 6 VSD is underestimated by at least 6 orders of magnitude still, the same as the Control simulation.

The NoIS experiment is the only experiment to affect the finer size bins, increasing the size bin 1-4 VSD by up to an order of magnitude at all locations. This exacerbates the fine particle bias which is in the model and raises the model VSD above the observed VSD in size bins 2-4 at all locations. At the Caribbean, the increased fine VSD does raise the model into better agreement with the absolute values measured during the observations and improve agreement in size bins 1-4. However, it should be remembered that the SALTRACE campaign measured high concentrations, and so just because the absolute values match does not result in an overall improvement, especially when the overall shape of the VSD is still too low at the coarse size range.

Finally, the sedimentation experiments are the only experiments to greatly change the coarse VSD in the direction of the observations. As found in Section 4.2.2, the coarsest size bins are most impacted by sedimentation, with decreasing dependence with decreasing diameter. With no sedimentation, the coarse VSD at the Caribbean was increased by nearly two orders of magnitude at the Sahara and more than 7 orders of magnitude at the Caribbean compared to the Control. Compared to the observed VSD at the Caribbean, the NoS VSD was too great by more than one order of magnitude. From these sedimentation experiments, I showed that a decrease in sedimentation of up to 50% is required at the Sahara to bring the model into line with the observations, whereas at the Canaries and Cape Verde, this increased to between 50-80%. Finally, to match the observations at the Caribbean, a reduction of between 80-95% was required. Additionally, with decreasing sedimentation, the dust MCA increased by up to 300 m with dust transported higher and for longer. The sedimentation experiments created the most realistic changes to form a model VSD which is more fitted to the observations.

In Chapter 3, I showed that the model underestimated coarse VSD at the Sahara, and that this underestimation was exacerbated with transport. In this chapter I then used a configuration of the model which had been tuned by the Met Office in order to improve the initial size distribution and to better understand what causes the increasing underestimation with transport. It is necessary to note that despite tuning the model configuration used in this Chapter (Figure 4.1), the model still suffers an exacerbated underestimation of coarse particle mass concentration and VSD after long-range transport. This confirms an issue with transport and deposition processes over long-range transport of coarse mineral dust particles in the model and shows that simply tuning the model emissions is not enough to fix the issue of coarse mass underestimation in models.

Future work could look at making changes to sedimentation of size bins 5 and 6 (6.32-20 µm and 20-63.2 µm) only as these are the two size bins which suffer the greatest underestimations in mass concentration contribution and VSD (as shown in Chapter 3). Additionally, differing percentage reductions could be applied to the two bins, for example, at the Caribbean, size bin 6 requires a reduction of sedimentation by 80-95%, whereas size bin 5 requires only ∼80%. Additional testing could be carried out to find an appropriate value for these two size bins. Using a simple change to the sedimentation, such as I have done in this Chapter, is a computationally-inexpensive, temporary fix for models to improve coarse particle transport without having to include complex processes such as triboelectrification and asphericity. However, matching a model to observations without understanding the physical explanation can be difficult as the model is then purely based on a limited set of conditions measured during the campaigns.

The changes of up to between 50-95% of the sedimentation of coarse particles are similar to the findings of Drakaki et al. (2022) who found that a reduction in sedimentation of between 40-80% was required at the Sahara and East Atlantic to bring a forecast model into line with observations. The WRF-Chem model configuration used by Drakaki et al. (2022) has a higher resolution horizontal grid (15 km) than that used in this thesis (210 km) and with higher order advection schemes in the horizontal and vertical. On a more similar model scale to that in this thesis, Meng et al. (2022) find that particle density needs to be reduced by an order of magnitude as well as marginally reducing the sedimentation in a coarse resolution climate model to bring the model into agreement with observations near source. Thus, despite using a model configuration with greater spatial resolution, the results from Drakaki et al. (2022), Meng et al. (2022) and the sedimentation sensitivity studies in this thesis Chapter are remarkably similar in requiring order of magnitude changes and suggest an overarching issue in our understanding of the processes acting on coarse dust particles in the atmosphere. As the equations associated with dry deposition of particles are well understood, this suggests that processes not considered in the model, or not well understood in practice are required to lengthen coarse particle transport by such significant distances. My work adds to the growing body of evidence that this is the case.

Figure 4.43 shows a very simple schematic of the impacts of CM and TM over the ocean in the model. Without CM, dust was shown to be confined within the SAL, settling to the lower SAL, except for when sedimentation was strong enough to pull dust down into the MBL. Alternatively, TM was found to be a driving force for mixing dust in the MBL to the surface and without TM, particles in middle size bins has significantly reduced concentrations near the surface.

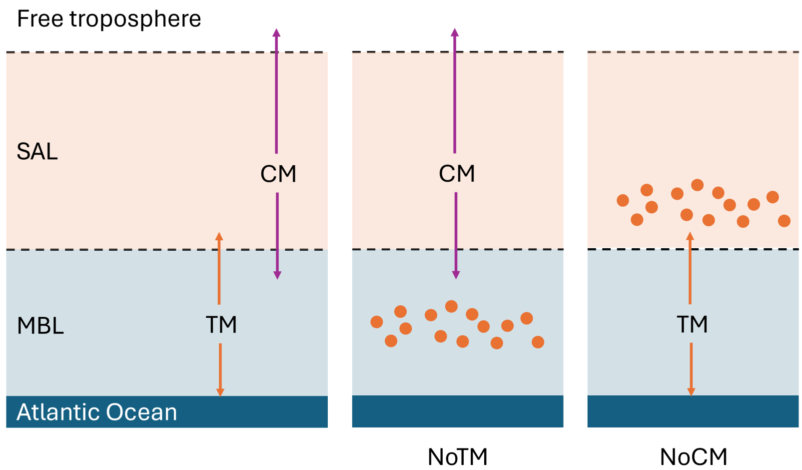

Figure 4.43: Schematic showing the vertical processes associated with convective mixing (CM) and turbulent mixing (TM) in the model over the Atlantic Ocean (left). Where dust collects in the NoTM (middle) and NoCM (right) experiments.

In the NoTM experiment, dust is mixed throughout and out of the SAL, like normal, by the CM. However, in the MBL, the dust isn't affected by TM and collects in the middle of the MBL, not being mixed to the surface, as shown in the Figure 4.43 central panel. In the NoCM experiment, this is reversed, the dust is mixed through the MBL like normal, except the dust is not mixed up through the SAL as normal and collects in the lower SAL (Figure 4.43 right). The No CM and NoTM experiments have revealed important information about the vertical transport and mixing of dust in the atmosphere.

One suggestion for a future experiment could be to look at the impacts of reduced sedimentation and reduced or removed CM. In the NoCM experiment, dust tended to settle low into the SAL (Figure 4.43 right), however, I hypothesise that a reduction of sedimentation additional to the reduced CM would mean dust would not as readily settle into the lower SAL, producing a vertical dust profile more similar to observations. In the NoCM experiment, size bin 5 VSD was increased, but only below 3 km, exacerbating the coarse particle low-altitude bias explored in Chapter 3. Thus, though the experiment suggested here could plausibly provide interesting results and further clarify understanding of particle transport sensitivity, it could produce results exacerbating a current problem, creating further disparity between the model and observations.

Alternatively, I also suggest an experiment series with spatially variable increased CM, i.e. increased CM just over the Sahara or just in the SAL. This is based on results that suggested coarse dust concentration increased in areas associated with positive vertical wind in the 2xCM experiment. Additionally, previous research suggests that updrafts and convective mixing could be important for fully understanding the long-range transport of coarse particles (Cornwell et al. 2021; Denjean et al. 2016; Gasteiger et al. 2017; Takemi 2005; van der Does et al. 2018; Xu et al. 2018). I suggest this as the 2xCM experiment uniformly doubled CM across the globe and thus mixed dust too far above the plume as well as too far horizontally from the plume to the north. This will be difficult to implement in a model.

4.4.2 Impact of Tripled Absorption

In this Section, I will discuss results from two experiments run with RE turned on; REControl and 3xSW. In the 3xSW experiment, I aimed to test the sensitivity of coarse particle transport in the model to the SW absorption properties of dust. To do this, I tripled the absorption of dust in each of the six size bins as a strong, albeit unrealistic change. However, the large change resulted in a relatively small reaction in terms of the coarse particles. Only 1% more size bin 6 particles reached the Caribbean from Cape Verde with tripled absorption, relative to the sedimentation experiments in Section 4.2.2 which changed the size bin 6 VSD by multiple orders of magnitude to bring it into agreement with the observations.

The key changes as a result of the tripled SW absorption of dust are in the changes to the plume altitude and meteorology. The dust plumes were up to 1 K hotter in the SABL and SAL in the 3xSW experiment compared to the REControl. As a result of this additional heating, the MCA of the dust plume was higher, especially at the Caribbean, where the dust was transported more than 500 m higher than in the REControl.

There were not large changes in the coarse particles in this experiment, however, further work should be carried out on simulations which retain coarse particles for longer range transport. The changes to plume height and coarse particle VSD were most pronounced at distance from the Sahara. Thus, if the coarse particles were retained for slightly longer (for example due to reduced sedimentation), then they may be more susceptible to the changes caused by increased absorption. Altering the SW absorption therefore cannot be ruled out as a mechanism which could improve the lifetime of coarse particles along with other processes and mechanisms.

It is, however, likely that the SW absorption could be more important for improvements in general circulation in the model as opposed to coarse particle transport.

4.5 Conclusions

In this Chapter, I carried out a series of sensitivity tests on a HadGEM3-GA7.1 climate model setup in order to better understand the dominance of processes involved in the transport and deposition of mineral dust particles. There were five processes tested: sedimentation, impaction scavenging, convective mixing, turbulent mixing and SW absorption. The key findings from this chapter are:

1. The experiments in which sedimentation was altered showed the most change to the coarse size distribution.
    (a) With distance from the Sahara, the greater the reduction of sedimentation required to bring the model into agreement with observations: at the Sahara, a reduction of 50% brought the VSD into agreement, but a reduction of at least 80% was needed at the Caribbean.
    (b) Assuming the equations for dry deposition are well-understood, the need for a large reduction in sedimentation to bring the model into line with observations suggests the presence of processes not considered in the model which can counteract sedimentation by more than 80%.
    (c) The results from these experiments were the most comparable with the observations out of all the sensitivity studies.
2. Impaction scavenging has the greatest effect at the fine particle size range.
    (a) Without wet deposition, the lifetime of the finest particles was extended significantly due to uninhibited transport beyond the SAL top.
    (b) Coarse particle transport was not greatly affected in this experiment.
3. Convective and turbulent mixing have been shown to be important for maintaining the vertical structure of the MBL and lower SAL across the Atlantic.

   (a) Turbulent mixing is key for mixing dust through the MBL and down to the surface, whereas convective mixing is more important in determining the vertical structure throughout the SAL.

4. Increased coarse particle concentration was associated with strong, positive vertical winds in experiments altering convective mixing.
   (a) When convective mixing was doubled, the coarse particles were lofted higher and remained in the atmosphere for longer.
   (b) Coarse particle VSD was still 1-2 orders of magnitude too small at Cape Verde and up to 6 orders of magnitude too small at the Caribbean.
5. Tripling the SW absorption of dust raised dust higher, improving transport to the West Atlantic.
   (a) Increased heating within the SABL/SAL by up to 1 K.
   (b) Long-range transport of size bin 6 VSD was marginally improved by approximately 1%, and size bin 5 was improved by up to 6%.

Chapter 5

Dust Transport Sensitivity to Plume Altitude

5.1 Introduction

As found in the previous two Chapters (Chapters 3 and 4), coarse dust is deposited too quickly in the HadGEM3-GA7.1 model compared to observations. Additionally, in Chapter 3, I showed that coarse dust was often transported too low in the atmosphere. Results from Chapter 4 indicated that the concentration of coarse dust in westwards transport decreased very quickly at the west African coast (e.g. Figure 4.27). In this Chapter, I hypothesise that this could be in part due to the introduction of the marine boundary layer (MBL). I will now use Figure 5.1 to explain my hypothesis. Over the Sahara, the fine particles are well-mixed throughout the Saharan atmospheric boundary layer (SABL), whereas the coarsest particles are concentrated in the lower SAL (as found in Chapter 3 Section 3.4.1). The particles are transported west towards the Atlantic Ocean. At the coast, the MBL begins to form and grows in depth with further westwards transport. As the dry, dusty air of the SAL meets the MBL, the bottom of the SAL is eroded by turbulent and convective mixing, as well as wet deposition processes in the MBL. Thus, I postulate that particles below a threshold altitude (approximately the height of the MBL or turbulent mixing maximum height over the ocean) are likely to be mixed out of the SAL and deposited to the ocean surface close to the African coast, especially those which have such large sedimentation that they depart from the isentropic uplift of the SABL. Those particles which are lofted above the threshold altitude over the Sahara, are more likely to have extended horizontal transport.

Previous research has shown that some models have difficulty raising dust to the correct altitude. O'Sullivan et al. (2020) found that the MetUM NWP model and ECMWF models placed dust on average 0.5-2.5 km too low in the atmosphere. Similarly, Koffi et al. (2016) found a low-altitude bias in aerosols below 1.5 km over North Africa in most models in the AeroCom II model intercomparison project.

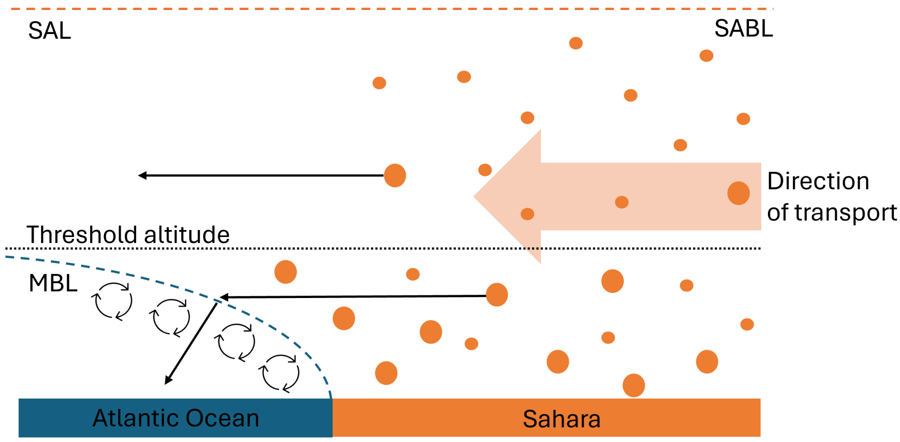

Figure 5.1: Schematic showing a hypothesised cause of coarse particle loss at the west African coast. Particles are the Sahara are blown westwards by the prevailing winds over the Atlantic Ocean. Particles above a hypothetical threshold altitude – the approximate height of the MBL – will continue westwards transport, whereas particles below the threshold altitude will be swiftly deposited upon reaching the turbulent MBL.

Meng et al. (2022) found that when they improved the dust emission scheme at the Sahara, the surface concentrations were more akin to observations, however, the new scheme did not improve concentrations between 2-4 km altitude, suggesting an issue with the vertical lofting of coarse dust particles. Not only could this mean that dust is not lofted above the MBL/a threshold altitude as I have hypothesised, but as wind speed and direction are very altitude dependent, it could mean that the model dust might not be reaching higher, faster, more easterly winds that the coarse dust reaches in the real world. Additionally in Chapter 4, I have shown the altitudes that turbulent mixing acts up to in the model; if the dust is not lofted high enough, then it will still be under the influence of turbulent mixing, which could speed up deposition.

Some mechanisms for raising dust higher have been proposed by previous research. Heisel et al. (2021) showed that more detailed representations of subgrid-scale topography can enhance upward transport of coarse, super-coarse and giant dust particles up through the BL. As the model grid resolution used in this thesis is run at N96 (∼210 km wide grid boxes at the equator), it is not likely that the topography will be detailed enough to achieve the small, subgrid-scale perturbations in the wind required to raise the dust further in this way. The topography used in the Heisel et al. (2021) study is on the scale of 50 or 100 m elevations; only very high resolution models can include this level of detail, meaning it is not possible to consider this in the current generation of global climate models. O'Sullivan et al.

(2020) suggest that the boundary layer height at the source, large-scale winds (also suggested by Chouza et al. (2016)) or the models convection scheme could be the cause of inhibiting the vertical transport of coarse dust.

Thus, I pose the following question: If coarse particles are lofted higher at the Sahara, will they travel further across the Atlantic? This could be caused by deficiencies in the Saharan meteorology which result in Saharan dust not being lofted high enough.

5.2 Methodology

In order to test my hypothesis, I needed to make sure coarse dust was transported throughout the depth of the SABL at the Sahara with high enough concentrations at the upper SABL edge. To achieve this, I have run a series of experiments with altered model initialisation that move the entire dust column at the Sahara up to the top of the SABL. This will reveal whether this does have a significant impact on coarse dust transport. A positive result could lead to future work to improve the meteorology and vertical distribution of dust at the source.

These experiments use the same emissions tuning as described in Chapter 4 and also keep the radiative effects of dust turned off to ensure that meteorology is not affected by differences in modelled dust.

5.2.1 Altered Model Initialisation

At initialisation, the model reads in a series of ancillary files which provide the starting conditions. For this experiment, I have altered the dust prognostic initialisation fields for each size bin.

The model was initially run from the simulation start-date in December 1994 up to the end of May 1995, which produces restart dumps for the beginning of June 1995. The restart dumps were converted from mass mixing ratio to mass concentration, then to total column mass. The entire total column mass was then concentrated into one model level at the top of the SABL. This was converted back to a mass mixing ratio and saved as an ancillary file. Redirecting the model initialisation to my new ancillary files, the model runs using the altered files. A control simulation was set up in the same way, except for the dust at the Sahara was left with the original vertical distribution (REControl). All dust in the whole profile was moved into one model level in order to conserve the total column mass. This does mean that mass previously above the SAL was brought down into the SAL, however, it was deemed that this was not of a significant magnitude to skew the results (as shown by the relatively small values above 5 km in Figure 5.2).

This process was carried out with dust in a box over the Sahara (12°W-8°E, 14-27°N). Everywhere else, the dust concentrations were set to 0 so there would be no background interference and I could analyse changes to the raised dust only. Similarly, to remove noise from 'background' dust, dust emissions were turned off from the start of the simulation (June 1995). Figure 5.2 shows the size bin 6 vertical mass concentration profiles of the REControl simulation and the Raised simulation at model initialisation. This Figure is used to demonstrate the significant changes which have been made to dust at the Sahara in the Raised simulation, whereby dust is only present between 4.7-5 km altitude. This altitude was chosen based on analysis of the horizontal wind patterns, and an inversion in the profiles of relative humidity, potential temperature and water vapour mixing ratio (Figure A.2 in Appendix A). Between 5-6 km altitude, the horizontal winds above the west Sahara and African coast are more easterly than the central SAL winds below 5 km which blow eastnortheast.

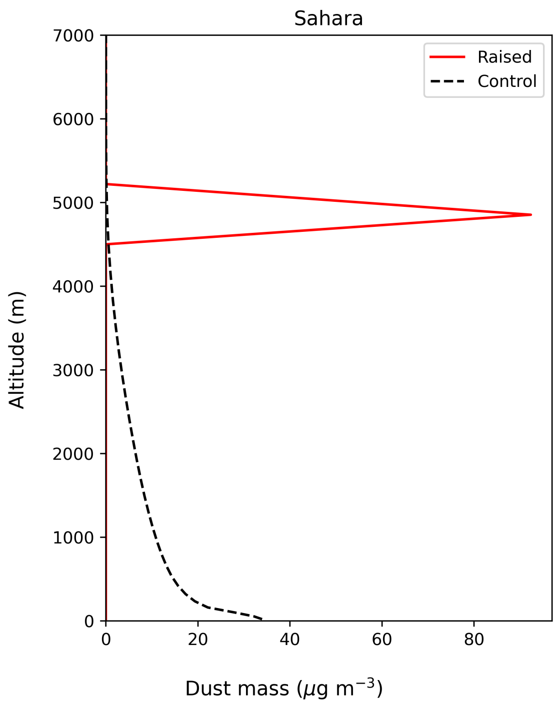

Figure 5.2: Size bin 6 mass concentration profiles (μg m^{-3}) at the Sahara at model initialisation in the REControl (dashed black line) and Raised (solid red line) simulations.

Due to the unrealistic manner of the changes being made to the vertical profile of dust, the radiative effects of dust will remain turned off in these experiments to avoid any unintentional changes to the models meteorology.

5.2.2 Sensitivity Testing

I ran two additional sensitivity simulations with the Raised setup; an 80% reduced sedimentation experiment (RS80) and a 10x convective mixing experiment (R10xCM). The methodology for these is as in Chapter 4 Section 4.1.3.

5.2.3 Model Output

The simulations are run for 15 days at 3 hourly output. The 3-hourly output is instantaneous.

As the model is free-running and I am not interested in a specific event or date, these experiments use June 1995 as this was the earliest available summer month and thus reduced unnecessary computational cost of running to later months or years. As this is the case and I am not using a large average of many months, I cannot guarantee that the dust will exactly follow the usual mean trans-Atlantic dust path. Therefore, rather than analysing the transport of the dust (for example the mass of dust reaching the Caribbean), I will use the global atmospheric dust mass as a proxy for understanding the lifetime of the dust. This allows for transport of the dust in any direction. Where I do look at trans-Atlantic transport specifically, the boxes in Figure 5.3 are used to average the data. The box over the Sahara matches the area which contains the dust at initialisation.

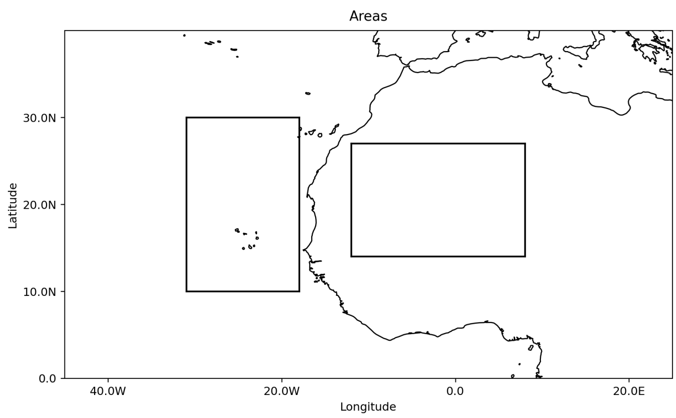

Figure 5.3: The box areas used for averaging data in this series of experiments. The Sahara box represents the only area with dust at initialisation.

5.3 Results

In this Section, I will first compare the differences between the Raised simulation and the REControl. I will then analyse the further sensitivity experiments with raised dust before summarising my findings from all of these experiments.

5.3.1 The Impact of Raised Dust

In this section, I will compare the REControl and raised dust (Raised) simulations to understand how raising dust, especially coarse dust, at the Sahara can impact atmospheric lifetime and transport in the model. The two simulations have conserved mass. Figure 5.4 shows the evolution of TCM in the REControl and Raised simulations over a week, as well as the difference between the two.

Starting at 24 hours in, the REControl simulation appears to have a more dispersed TCM than the Raised simulation with dust extending further north and southwest in the REControl simulation (Figure 5.4). Instead, in the Raised simulation, the difference plot shows that there is an increase in TCM to the east (between 20-25°N) and west of the dusts initial location, suggesting a different wind pattern at the upper edge of the SAL where the Raised dust has been placed. As time continues, the Raised dust continues to flow in a different way to the REControl dust, extending further north into the Mediterranean as well as transporting west at a higher latitude.

The difference TCM plots in Figure 5.4 show a decrease in general dispersion of dust outside of the main dust plume. In the REControl simulation, small fractions of the dust are transported to the south, east and northeast of the plume resulting in differences of TCM in east Africa of up to -100% after 24 hours and up to -50% after 168 hours.

These changes to the dispersion and transport of the dust are specific to the meteorology of this simulation. Unlike in previous Chapters where I have used a long term mean to look at changes in dust transport, this example experiment cannot be used as a blanket example of what will happen every time, rather it is specific to this time. Therefore, rather than looking at the changes to dust concentration at specific location I will now look at the lifetime of the dust. Figure 5.5 shows the evolution of global atmospheric dust mass in the REControl simulation and the Raised experiment as a time series.

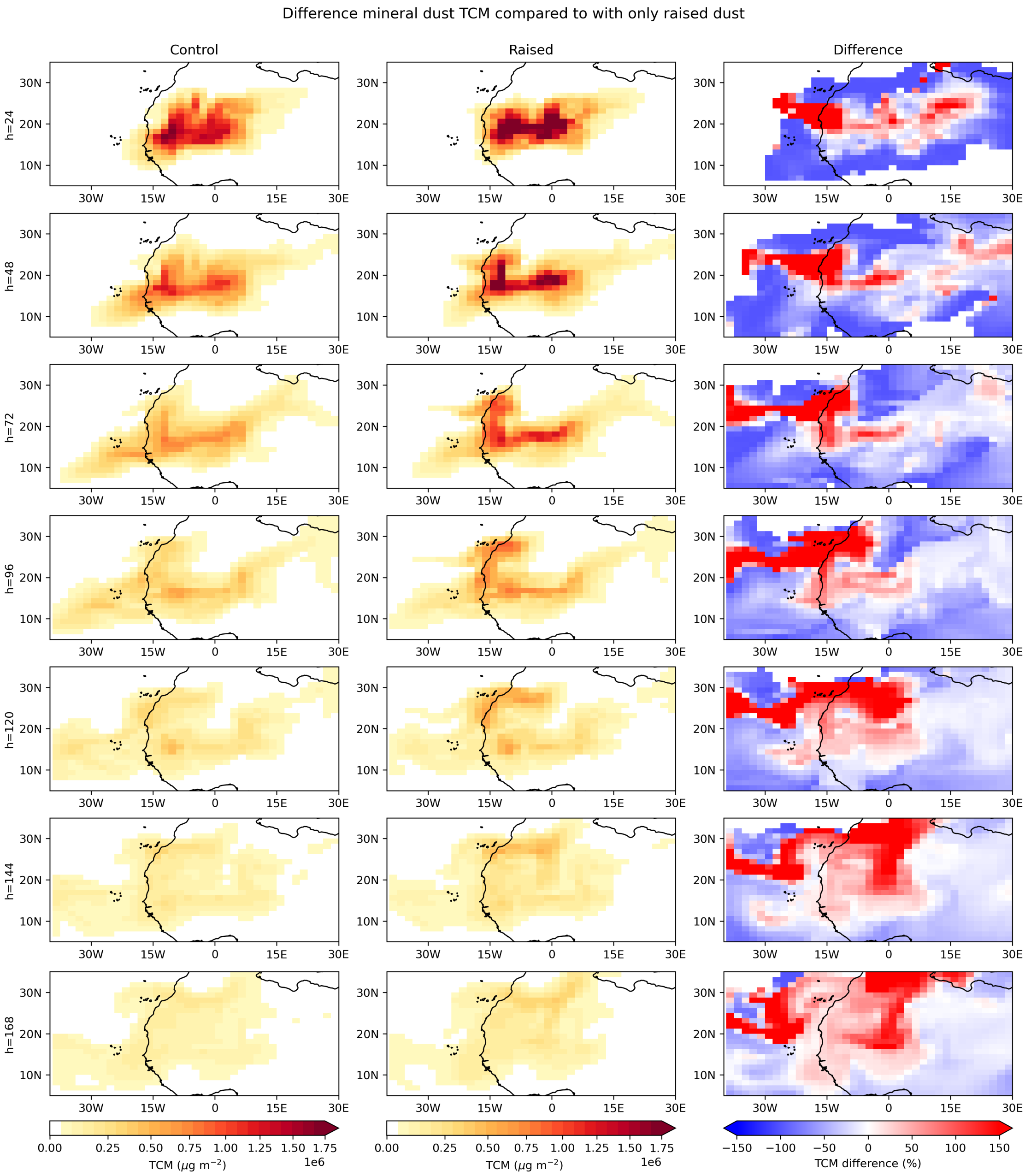

Figure 5.4: TCM in the REControl (left) and Raised (centre) dust simulations at 24 hour intervals over 7 days and the percentage difference (right) between the two simulations. A threshold has been applied to the TCM where only grid boxes with more than 1 μg m^{-3} in both simulations are used to reduce noise.

In every size bin, the Raised experiment loses global dust mass at a slower rate than the REControl simulation so that, in the cases of size bins 1-5, there is more dust left at 96 hours in the Raised simulation compared to the REControl. In size bin 6, both simulations lose all dust mass quickly within the 4 day period shown on Figure 5.5, however, more time passes in the Raised simulation before the bin 6 dust mass becomes negligible. Thus, raising the dust at initialisation has increased

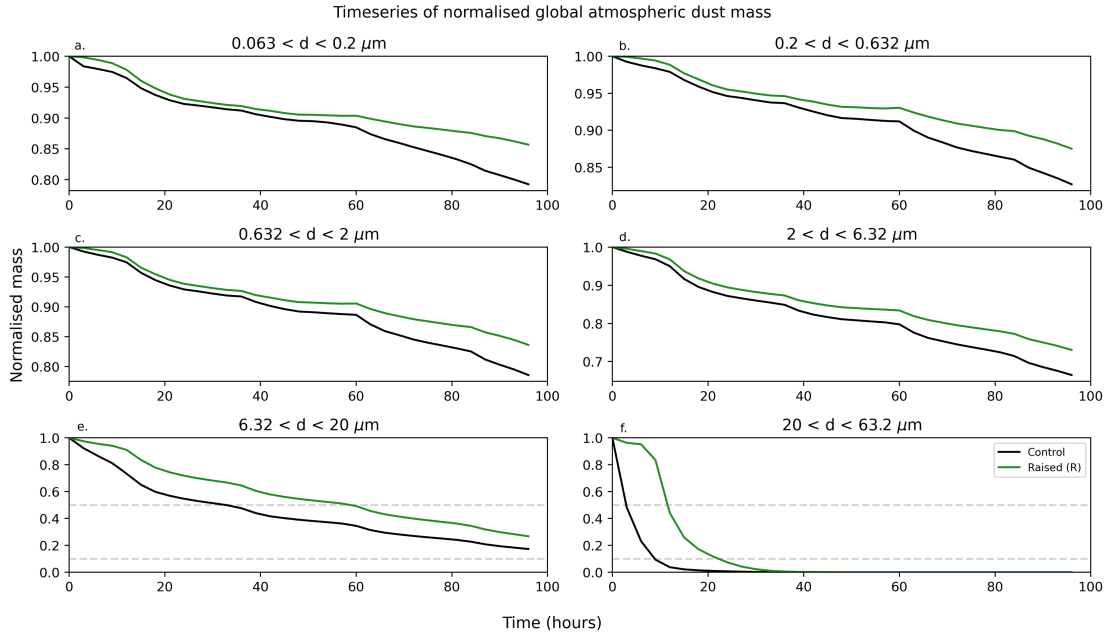

Figure 5.5: Normalised global atmospheric dust mass in the REControl (black line) and Raised (green line) simulations in the six model size bins over 96 hours. Grey dashed lines are shown at 0.5 and 0.1, representing a loss of 50% and 90% of the original dust mass.

the lifetime of all size bins. This is variable between different size bins and different meteorological conditions on different days. I will now analyse these differences in more depth.

In size bins 1-4, the two simulations follow a fairly similar pattern, though slowly diverge up to 96 hours where up to 6% more of the original mass remains per bin in the Raised simulation (Figure 5.5abc). The divergence particularly increases after 60 hours suggesting a change in the meteorology causing an increased loss of particles in the REControl simulation. This is likely a consequence of the different vertical distributions of dust in the two simulations; where the dust was present from the surface upwards in the REControl simulation, it was only present at the top of the SAL. Thus, as these finer particles are less affected by sedimentation (as found in the previous Chapters work), it could be that these particles remain relatively lofted in the Raised simulation and a low-level meteorological phenomenon acted to remove some of the lower particles in the REControl simulation after 60 hours.

Table 5.1 shows the time in hours at which the REControl and Raised simulations have lost 50% and 90% of their original bin 5 and bin 6 mass.

In size bin 5, there is an initial disparity between the two simulations of ∼15% 10 hours into the simulations, increasing close to 20% at 20 hours. Interestingly, as

Simulation	50% lost (hours)		90% lost (hours)
	Size bin 5	Size bin 6	
REControl	32.75	2.85	8.85
Raised	58.54	11.56	22.2

Table 5.1: Time (in hours) taken for the global atmospheric dust mass in size bins 5 and 6 to decrease by 50% and 90% in the REControl and Raised experiments. Only size bin 6 is calculated for 90%.

time increases, the difference between the two simulations decreases to below 10% of the original mass at 96 hours. This initial difference is likely caused by deposition of the dust closer to the surface in the REControl simulation. It takes nearly 33 hours for the REControl simulation to lose half of its original bin 5 mass, whereas in the Raised simulation, it takes nearly twice as long at 58.5 hours (Table 5.1).

Finally, in size bin 6, the REControl simulation very quickly loses a high proportion of its mass, with 50% left 2.85 hours in and with only 10% left less than 9 hours into the simulation (Figure 5.5; Table 5.1). In the Raised simulation, it takes 3 times as long to lose 50% of the original mass and twice as long to lose 90%. The rate of change of the global atmospheric dust mass in size bin 6 is very similar in the REControl (from 1 hour in) and Raised (from 10 hours in) simulations.

In size bins 1-5, a 24 hour repeating pattern appears, most clearly in size bins 2-4. Starting at 12h, then repeating at 36h, 60h and 84h, the rate of change of global atmospheric dust mass briefly increases before plateauing or slowing again before the cycle repeats at midday the next day. This effect is seen in size bin 5 but not with as sharp of a change as seen in the three smaller bins; in size bin 6, the rate of particle loss is too great to see this pattern at all. The behaviour of size bins 5 and 6 suggest that strong sedimentation counteracts the force creating this repeating cycle observed in the finer size bins.

Despite the dust being lofted higher into the SAL, the global atmospheric size bin 6 mass depletes to negligible amounts within 40 hours with 90% of the original mass lost after ~23 hours. Figure 5.6 shows a mean cross section between 12-25°N of the size bin 6 mass concentration between 3 and 15 hours in the simulation. This cross section shows the fast rate at which the dust falls to the surface. Three hours into the simulation, the dust is still relatively clustered together and the main mass has dropped below 4 km altitude. The main dust plume continues to drop. After 12 hours, the main size bin 6 dust clouds begins to reach the surface; this agrees with the time series in Figure 5.5 which shows a loss of less than 20% of the original mass up until ∼12 hours, then the rate of change of global mass increases. Beyond 12 hours, Figure 5.5 suggests that about a quarter of the original dust mass remains in the atmosphere, and based on Figure 5.6, this dust appears to be fairly uniformly spread throughout the depth of the SAL.

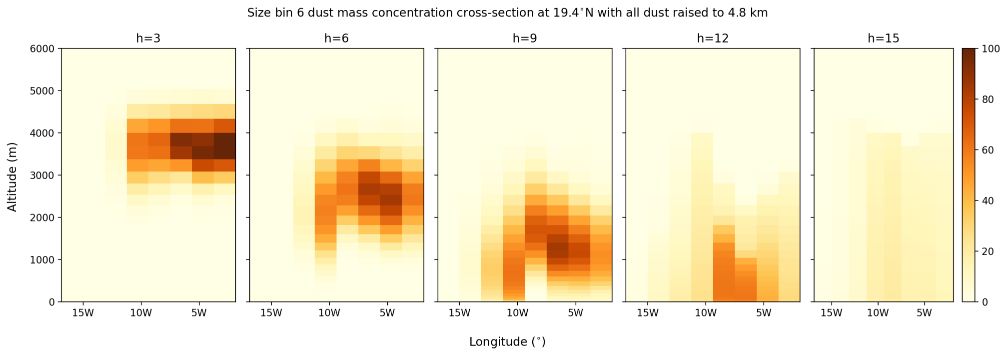

Figure 5.6: Longitudinal cross section of size bin 6 mass concentration (in µg m^{-3}) between 17-0°W averaged between 12-25°N and up to 6 km altitude. Shown at 3 hourly intersections from 0300 on the first simulation day, up to 1500.

Using Equation 1.13 (Chapter 1), the Stokes velocity (V_S) of size bin 6 particles (D_{rep} = 35.6 µm) is calculated to be 10.1 cm s^{-1} at 288 K and 1013.25 hPa. Based on Figure 5.6, it seems that a lot of the dust drops at a rate whereby it begins to reach the surface after ∼12 hours. Using a simple distance-time equation, this suggests that the size bin 6 dust is falling at ∼10.6 cm s^{-1} at its fastest. Thus, the size bin 6 particles are reaching the ground at a marginally faster rate than calculated. This could be due to differences in the calculations, such as the fact that my estimation of V_S is based on air density at average surface conditions. Alternatively, the faster falling speed could be caused by model processes such as downdrafts or numerical diffusion between vertical levels. This difference is not large enough to be concerning. Either way, this velocity suggests that there is little counteracting the deposition velocity of the majority of size bin 6 particles seen settling to the surface in Figure 5.6, such as convective and turbulent mixing. Additionally, we can consider processes not in the model which could be counteracting their deposition in the real world, such as electrical charging and asphericity.

As Figure 5.5 shows though, not all of the size bin 6 dust is removed at or shortly after 12 hours. The existence of mass in the atmosphere after 12 hours suggests the presence of processes counteracting the V_S of a small fraction of the size bin 6 particles, keeping them mixed within the SABL. However, these processes are not acting strongly enough to maintain the particles within the atmosphere for long enough to encourage longer range transport.

Figure 5.7 shows the size-resolved fractional difference in the total deposition over a 7 day period between the REControl simulation and the Raised experiment.

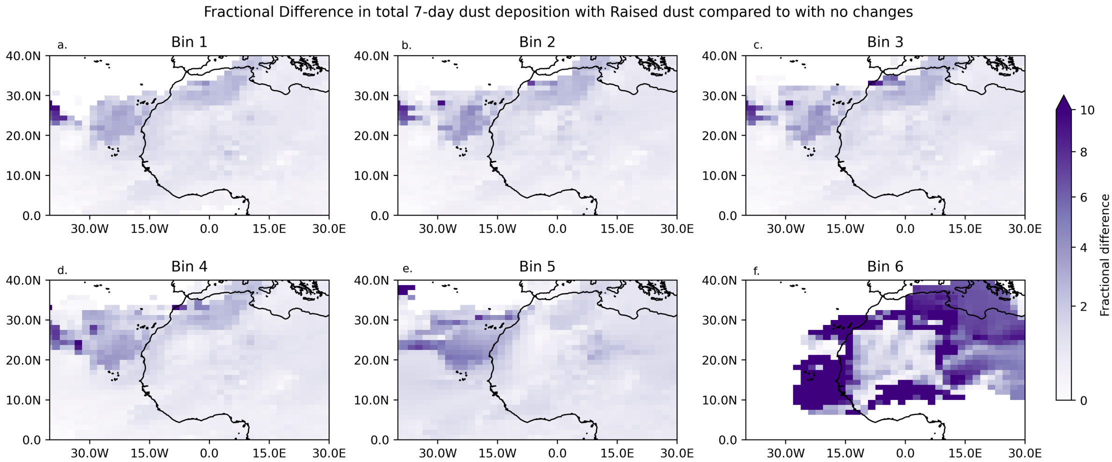

Figure 5.7: Fractional difference between the Raised and REControl experiments (i.e. Difference = Raised/REControl) of the total deposition of dust over 7 days. A threshold has been applied to the deposition, which is a sum of 3-hourly instantaneous values over the week long period, removing values smaller than 10^{-16} kg m $^{-2}$ to reduce noise.

Size bins 1-5 show a fractional increase in deposition in the Atlantic between 20-30°N by a factor of between 2 and 8 (Figure 5.7), this agrees with the increased TCM in this location (Figure 5.4). This band of increased deposition is also visible across the northwest of Africa and stretching into the Mediterranean. Elsewhere, over central Africa and the tropical Atlantic, there tends to be a fractional difference close to 1, suggesting only a minor degree of difference between the two simulations. In size bins 1-4, further from the African coast in the tropical Atlantic, the fractional difference goes below 1 and close to 0, suggesting a decrease in deposition in the Raised simulation. This decrease could hint at two possibilities, first, that by raising the dust to a different level, the main transport route has changed and resulted in more north and northeastwards transport, and second, that by lofting the dust, it remains in the atmosphere for longer during trans-Atlantic transport, reducing deposition. Based on the absolute TCM in Figure 5.4, we know that there is increased transport at a higher latitude across the Atlantic in the Raised simulation. Thus, decreased deposition on the southern edge of the Atlantic plume could be due to transport at a higher latitude.

As the size bin 6 dust is deposited from the model so quickly, the fractional changes in deposition shown in Figure 5.7 are dominantly from the first 24 hours of the simulation and the majority of the deposition occurs within or near to the box region where the dust was initialised. Figure 5.7 shows a strong decrease in the deposition within the initialised dust region and a shadow of increased deposition surrounding this area. The fractional change in this area extends significantly beyond the limit of the colour bar, extending up to a factor of more than 400. This unique pattern of change suggests that the lifetime of the dust has been extended, as was suggested by the increased lifetime in Figure 5.5, this reduces the deposition near the source and increases it further away. However, this shows the lack of long-range transport achieved in this simulation still by the fractional difference only showing change just slightly further west of Cape Verde. To the northeast of the initialised dust box, there is a fractional increase of dust by a factor of up to 8 in the Mediterranean which has been able to be transported a greater distance from the source. This could be due to the specific meteorology modelled during this time period, but still proves that raised dust can improve transport by greater distances. It is worth noting that the changes to dust transport distance are still not enough when considering the long-range transport of coarse particles to the Caribbean seen in the observations (Chapter 3).

Due to the relatively short lifetime of the size bin 6 particles, even after raising them to the top of the SAL, it does not seem appropriate to look for changes in the coarse size distribution given that I have shown the time scale with which these particles are lost on.

In order to understand how the vertical distribution of dust is changed by lofting the dust at the Sahara, I need to look at some vertical profiles. As mentioned previously, it is difficult to analyse specific locations given the altered transport pathways of the dust. Additionally, given the relatively short-range transport achieved in this simulation, concentrations far from the Sahara will be low and very sensitive to small fluctuations and thus I will only look at the Sahara and just off the west coast of Africa. Figure 5.8 shows the size bin 5 absolute mass concentration profiles and percentage difference between the REControl and Raised simulations in the Sahara and east Atlantic. I am only focusing on size bin 5 here to best understand the impact on coarse mode particles. Due to the consistently short lifetime of size bin 6 particles, I have not shown them here as any results after 24 hours are based on very small mass concentrations (less than 10% of the starting mass).

At 24 hours, the vertical profile of size bin 5 particles at the Sahara is fairly uniform from the surface up to 4.5 km. This suggests that the size bin 5 particles are mixed down through the depth of the SABL, though some upward mixing occurs as

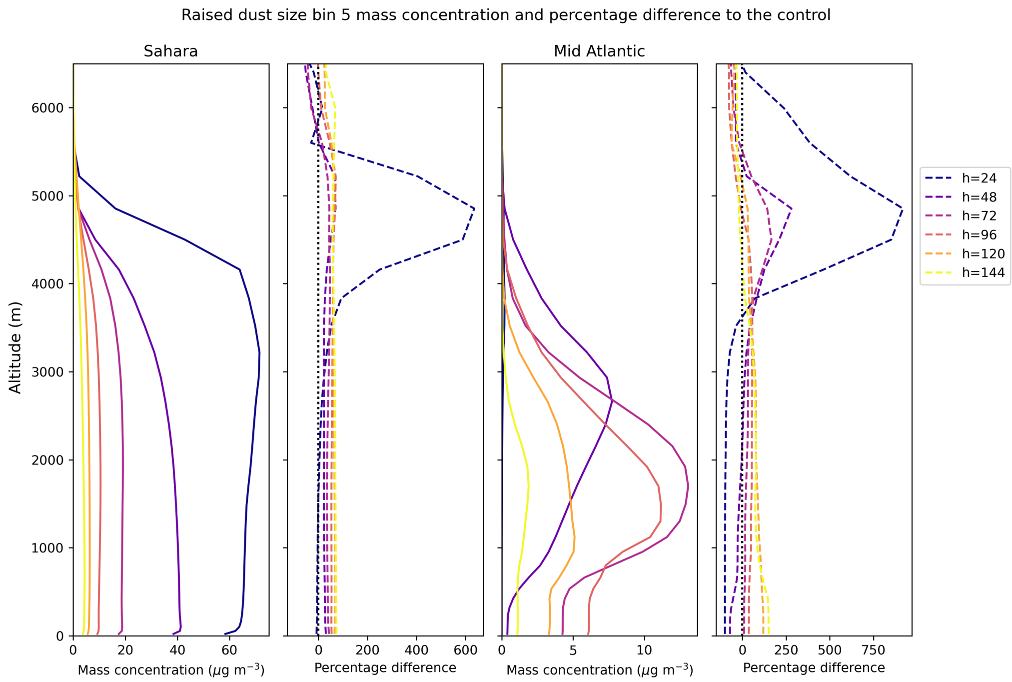

Figure 5.8: Size bin 5 (6.32-20 µm) mass concentration profile (in µg m^{-3}) in the Raised simulation (solid lines) at the Sahara and east Atlantic and the percentage difference (dashed lines) to the REControl simulation at 24 hour intervals.

the dust is present up to 5.2 km altitude. the downwards transport of the size bin 5 particles is likely dominantly controlled by the sedimentation. Throughout the next few days, the total concentration decreases as the dust is transported elsewhere, but the uniformity up to ∼4 km persists, suggesting the size bin 5 particles are continually mixed both up and down throughout the SABL, unlike the size bin 6 particles which were much more dominantly affected by sedimentation. The percentage difference plot shows the large initial perturbation to the vertical profile is still affecting the profile at the Sahara 24 hours after initialisation with an increase of 635% at 4.8 km. At 48 hours, the difference profile is much more vertically uniform and the large perturbation is not as clear anymore only reaching a percentage difference of 70%. By 144 hours, the percentage difference is very uniform with altitude at ∼70% up to 6 km altitude. This suggests that after the large initial perturbation, the size bin 5 dust eventually becomes uniformly mixed throughout the SABL and therefore, by raising the dust higher, I have increased the coarse dust loading at the Sahara for longer after emission.

In the east Atlantic, 24 hours after initialisation, there is a only a very small mass concentration of size bin 5 dust, peaking at 0.7 µg m^{-3} due to it not having been transported westwards from the Sahara yet. Despite only being a very small amount transported, this results in a 920% increase in mass concentration at 5 km showing an increase in transport at altitude. This is likely a result of the westwards transport of dust further north of the normal dust plume between 20-25°N. By 48 hours, the dust has arrived in a larger amount with a maximum concentration of ∼8 µg m^{-3} at ∼2.6 km, resulting in a change of 280%. As time passes, the peak in concentration initially increases in magnitude before decreasing after 72 hours, but consistently lowers in altitude with each 24 hour period. This aligns with my previous findings that suggest sedimentation is one of the most important mechanisms affecting size bin 5 transport (Chapter 4) and gradually pulls the coarse dust mass lower through the atmosphere. Despite the mass of dust being centered between 1-3 km between 48-72 hours, the greatest percentage changes to the profiles occurs between 4.5-5 km altitude. With increasing time, the altitude of greatest percentage change lowers until at 144 hours, the peak is at ∼500 m altitude at 150%.

5.3.2 Impact of the Diurnal Wind Cycle

In Figure 5.5, I noted the presence of a 24 hour repeating cycle which resulted in increased loss of dust particles at midday each day. I hypothesise that this is in relation to the diurnal cycle of vertical wind at the Sahara. Figure 5.9 shows mean 3-hourly wind profiles at the Sahara during the third model day (i.e. 48-72 hours on previous figures). I have chosen to show the third model day here as this showed the sharpest change in rate of dust loss in Figure 5.5bcd. Negative w wind values denotes wind blowing down towards the Earth surface and a positive w value denotes wind blowing upwards, away from the surface.

Beginning at 0300, this is when the vertical winds are strongest, with a speed of more than +1.25 cm s^{-1} between 2-3 km altitude, and a positive profile up to 6 km. As time continues further into the morning, the positive winds decrease in both magnitude and altitude, with negative vertical winds appearing as low as 3.3 km at 0900. At midday, the profile up to 6 km mostly consists of negative vertical winds, with weak positive winds only in the lowest 1.5 km of the SABL. As the day continues, the positive w winds grow in strength and vertical depth again. Despite only showing the third model day here, this pattern occurs on each day in the model simulation.

To summarise, after midday each day, the rate of loss of global atmospheric dust mass increases in most size bins. Additionally, the vertical wind velocity is weakest and most negative at midday and the early afternoon. Thus, I postulate the two are related and that the increased vertical wind velocity aids the suspension of dust

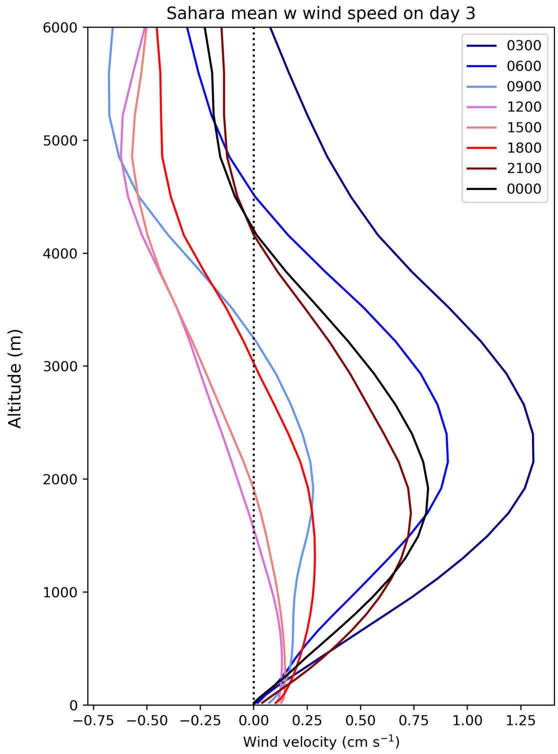

Figure 5.9: 3-hourly instantaneous vertical (w) wind profiles (cm s^{-1}) averaged at the Sahara throughout the third model day. The meteorology is parallel between all simulations in this Chapter.

particles in the model atmosphere and when it reduces during the day, the particles are more susceptible to deposition.

Though the winds are strong enough to counteract the deposition of the smallest four size bins, at the coarse range, especially bin 6, much stronger winds are required in order to counteract the much faster deposition velocity (around 10 cm s^{-1}).

More in-situ observations are required of the vertical wind velocities over the Sahara and in the SAL across the Atlantic in order to better understand whether the model is accurately representing the correct range of values. If the model is underestimating vertical wind velocity, further testing to fully understand the impact of increased w velocity could provide an answer to why the model struggles to retain its coarse particles so significantly. Unfortunately, a comparison with the vertical wind velocities measured by the aircraft during the Fennec and AER-D campaigns is not suitable due to poor calibrations and high sensitivity to inputs.

5.3.3 Testing Transport Processes With Raised Dust

To further test how the raising of the dust aids the lifetime of coarse particles, I have carried out two sensitivity experiments with the raised dust. In the first additional Raised experiment, I have reduced sedimentation by 80% (RS80), as this was deemed to be the minimum reduction needed to bring the coarse size distribution into agreement with the observations after long-range transport (Chapter 4). Secondly, I have multiplied the convective mixing (CM) by 10 (R10xCM); in the previous chapter, a doubling of the CM was not enough to greatly alter coarse particle transport, thus, I have gone for a much more extreme approach with the hope that it may produce a more extreme reaction in coarse particle transport given the potential relationship with vertical wind velocity. From here on, the sensitivity experiments will be compared to the Raised experiment.

Figure 5.10 shows the TCM every 24 hours for 7 days in the Raised simulation on the left. In the central and right columns are the percentage difference of the R10xCM and RS80 simulations from the Raised simulation over the same time period. Though some of the percentage changes are quite large (>1000%), the absolute values of the TCM reveal that these changes result in relatively low TCM still.

In the R10xCM experiment, the percentage difference with the Raised simulation reveals that there is an increase in transport to the east of the location of the initialised dust (Figure 5.10 central column). At 24 hours, there is an increase in TCM by more than 1000% in northeast and east Africa. This increase in TCM is paired with a decrease in TCM at locations where dust is usually transported westwards. This suggests that the CM increases transport to the east. As time continues, the percentage difference between the R10xCM and Raised simulations tends to being positive in the east of the plotted domain and shifting southwards so that the increase is focused in the southeast of the plotted domain.

Using the TCM in the Raised experiment to identify the main dust plume (Figure 5.10 left column), we can see that there is a decrease in the TCM in the main dust plume over the east Atlantic in the R10xCM experiment. The magnitude of the percentage decrease grows with time; for example at 48 hours, there is a change of less than 5% in the TCM around Cape Verde. Whereas by 168 hours, this has substantially increased to up to 50%, suggesting that the increased transport to the east is gradually depleting the dust available for transport across the Atlantic.

Interestingly at 168 hours, there is a localised increase in TCM northwest of

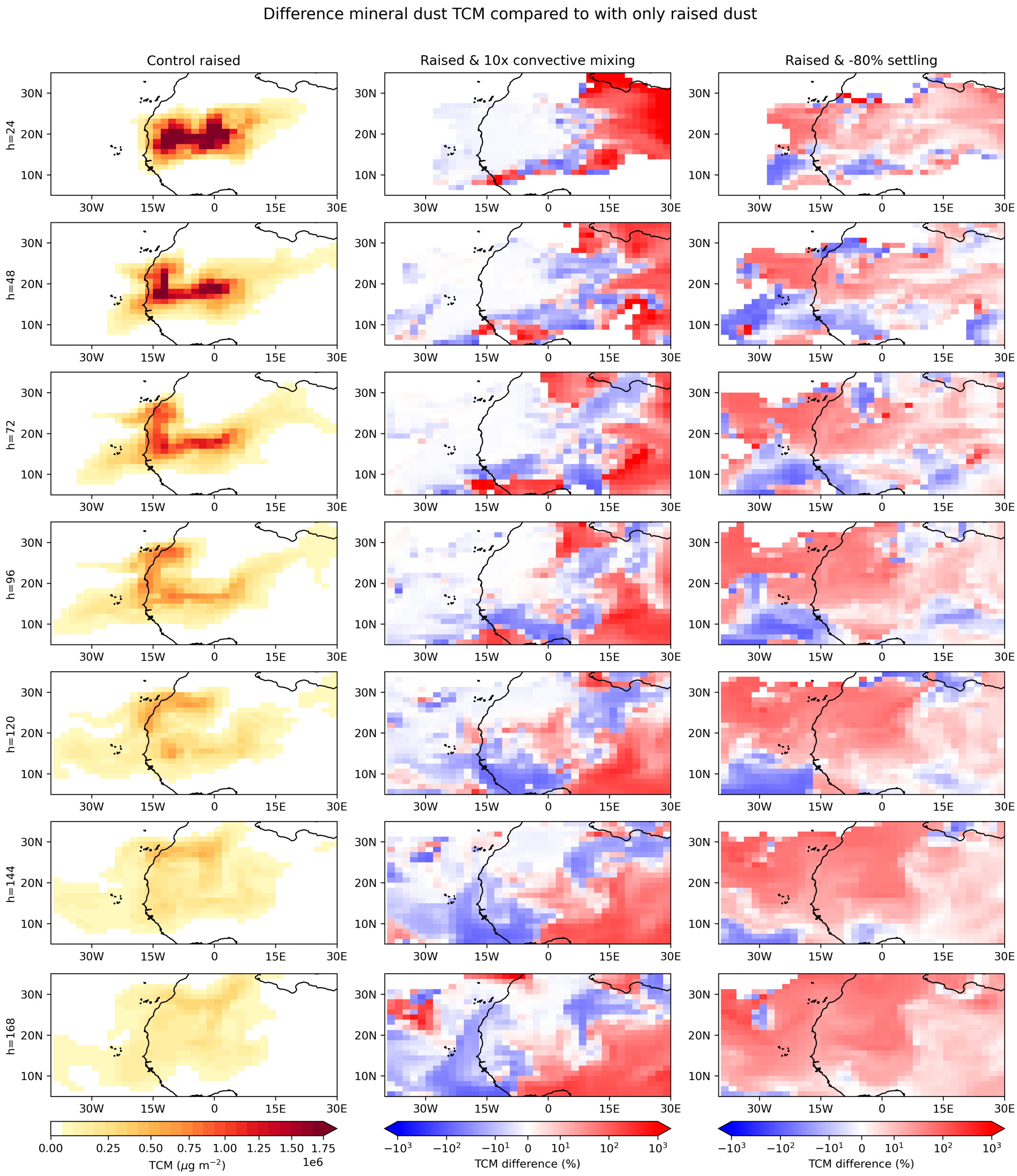

Figure 5.10: The absolute TCM (in μg m^{-2}) of the Raised simulation is shown every 24 hours from 24 hours into the simulation (left). The percentage difference of the R10xCM (centre) and the RS80 (right) to the Raised simulation are shown. The percentage difference plots use the same scale and colour bar, which is linear between −10 and 10 and logarithmic below −10 and above 10. A threshold has been applied to the TCM where only grid boxes with more than 1 μg m^{-3} in both simulations are used to reduce noise.

the Cape Verde islands between 20-30°N and 25-40°W in the R10xCM experiment (Figure 5.10). This increase in TCM appears to grow over the two preceding days in the model; at 120 hours, four grid boxes show a percentage increase of between 2-80% in this area. At 144 hours, the number of grid boxes in this region showing a positive difference has increased to ∼15. This region of positive change could be indicative of a convective meteorological system which, with the increased CM, retains dust more effectively than the Raised simulation. This suggests that while there is generally a decrease in TCM over the east Atlantic, there is evidence that increased CM could result in increased dust lifetime, but the specific meteorology of this event would need to be further explored to better understand this mechanism.

Moving onto the RS80 experiment, at 24 hours, the changes to the TCM appear to have a lower magnitude than in the R10xCM experiment (up to 100%), but tend to be more localised to the dusts location (as shown by the absolute TCM of the Raised simulation; Figure 5.10). Over the Sahara, there are patches of both increased and decreased percentage change between the Raised and RS80 simulations, though as time continues, the area of positive change increases to cover nearly the entirety of north Africa, with the same pattern over the east Atlantic. This suggests an increase in the atmospheric mass (relative to the Raised simulation caused by reduced deposition) which is slowly mixed throughout the plotted domain until there is an increase at nearly all locations.

At 48 hours, there is an increase in the TCM transported the more northerly westward route between Cape Verde and the Canaries in the RS80 experiment, compared to the Raised experiment which shows dust transport both on this route and to the south of Cape Verde (Figure 5.10). This could be indicative of the wind flow at higher altitudes in the SABL transporting along the more northwards route, so that the dust, which is falling more slowly because of the reduced sedimentation, is taken on this higher latitude route. Transport on this higher latitude plume continues throughout the RS80 simulation, though from 144 hours, the increased TCM stretches down to lower latitudes (10°N at 144 hours and 5°N at 168 hours) in the east Atlantic.

The changes to the TCM in both the R10xCM and RS80 experiments reveal changes in the dust transport pathways which confirm that analysis at specific locations will be biased towards certain experiments. Analysis at Cape Verde would be biased towards higher dust concentrations in the Raised experiment compared to the R10xCM experiment where significant portions of dust were transported to the east, or the RS80 experiment where dust was transported westwards at higher latitudes. Thus, the majority of my analysis will continue to focus on the global lifetime of the dust or when looking at specific areas, the averaged regions will be larger to account for different transport pathways.

Figure 5.11 shows the normalised global atmospheric dust mass of the REControl, Raised, R10xCM and RS80 experiments in the six model size bins. This plot is similar to Figure 5.5, except for this new figure contains the lifetimes of the R10xCM and RS80 experiments. Table 5.2 contains the times taken for the global atmospheric mass at initialisation to reduce by 50% and 90% in the two simulations (i.e. where the the normalised TCM intersects the grey dashed lines).

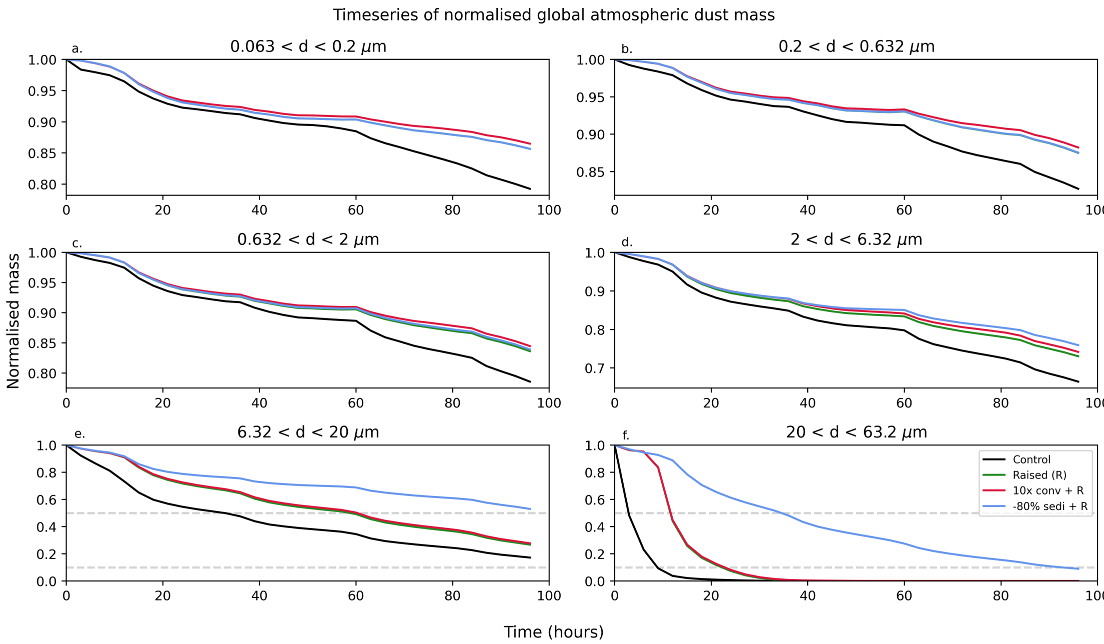

Figure 5.11: Normalised size-resolved global atmospheric dust mass in the REControl, Raised, R10xCM and RS80 experiments. Grey dashed lines are shown at 0.5 and 0.1, representing a loss of 50% and 90% of the original dust mass.

Simulation	50% lost (hours)		90% lost (hours)
	Size bin 5	Size bin 6	
REControl	32.75	2.85	8.85
Raised	58.54	11.56	22.2
R10xCM	61.1	11.61	22.8
RS80	96+	34.5	92.7

Table 5.2: Hours taken to lose 50% and 90% of the original bin 5 (only 50%) and bin 6 dust mass in the REControl, Raised, R10xCM and RS80 experiments.

At finer size ranges (size bins 1-3), the R10xCM experiment has a greater impact in terms of lengthening the atmospheric lifetime of these particles than the RS80 experiment (Figure 5.11). However, the difference between these two experiments and the Raised experiment are minimal and show that raising the dust has the dominant impact on the lifetime of these particles. In size bin 4, the RS80 experiment has the greatest effect with the R10xCM experiment only extending the lifetime marginally from the Raised experiment. Finally, in size bins 5 and 6, there is a significant difference between the RS80 and R10xCM experiment with significant extensions to the size bin lifetime in the RS80 experiment. The R10xCM experiment at this size range has a minimal impact, remaining very similar to the Raised experiment with minimal improvements to the coarse particle lifetime.

In size bin 6, the reduction in sedimentation has resulted in a reduced rate of change to the total atmospheric mass (Figure 5.11). The RS80 simulation takes more than 12 times longer to lose 50% of its original size bin 6 mass and more than 10 times longer to lose 90% than the REControl (Table 5.2). With this extension of lifetime, the diurnal pattern which I had previously only noted in finer size bins begins to appear in size bin 6. The hastening of mass loss every day at 1200 in size bin 6 suggests a relationship with the vertical wind velocity, as I have hypothesised for the finer bins. If this is the case, then this is more evidence to suggest that vertical winds could be an important factor in lengthening the lifetime and transport of coarse mode particles.

As the R10xCM experiment is not very dissimilar to the Raised simulation, I will not discuss the results from it any further and will instead focus on the RS80 experiment. Replicating Figure 5.8, Figure 5.12 shows the RS80 size bin 5 vertical profiles and the percentage difference with the Raised simulation.

Unlike in the Raised simulation, the size bin 5 dust does not lose altitude as quickly in the RS80 experiment, meaning that at 24 hours, the dust profile at the Sahara still resembles the initialisation profile with a sharp peak near 4.8 km (Figure 5.12). This results in a much larger percentage difference of nearly 6000% just over 5 km above the Sahara. After 48 hours, the profile shape looks much more similar to the Raised profile at the Sahara, however, the percentage difference continues to be larger in the RS80 experiment.

In the east Atlantic, the vertical profiles show that the dust is lofted higher in the RS80 experiment than in the Raised simulation (Figure 5.12), with peaks in the concentration between 2-5 km altitude in RS80. The percentage difference between the RS80 and Raised simulations grows with each day, from a peak of ∼5200% at 24 hours up to ∼46000% after 144 hours. This shows that the reduced sedimentation is important for maintaining the higher altitude of the dust achieved by raising it at the Sahara. With only raising the dust, it still drops quickly to a lower altitude with transport from the Sahara, thus additional mechanisms are required for maintaining the dusts altitude and improving long range transport.

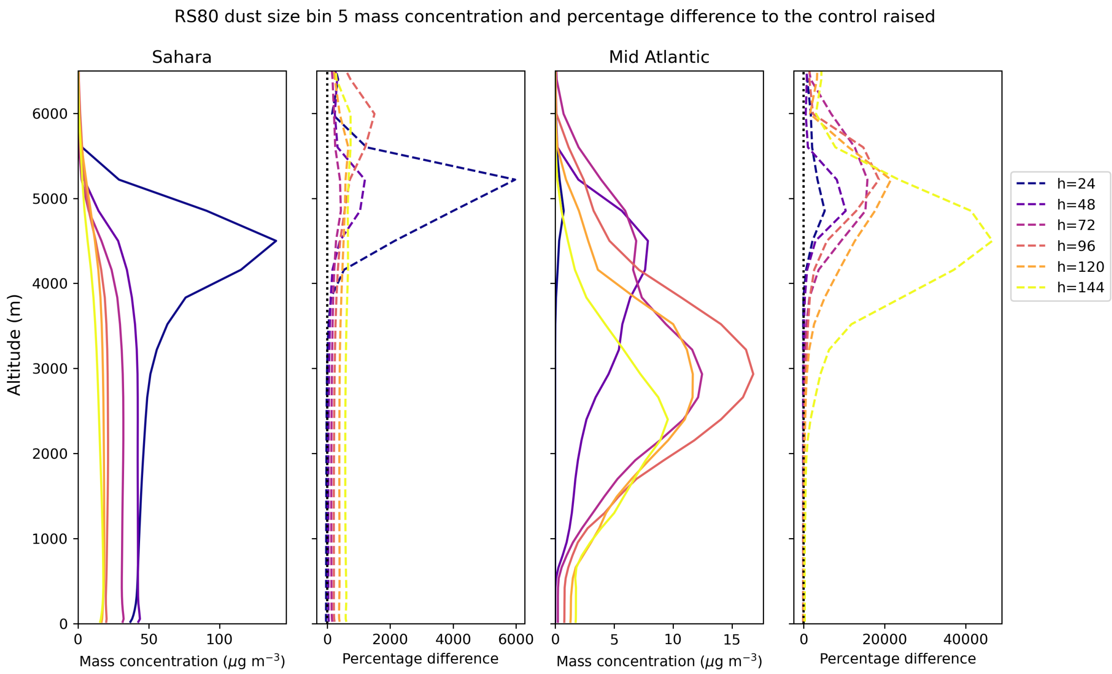

Figure 5.12: Size bin 5 mass concentration profiles (in µg m^{-3}) at the Sahara and West Atlantic of the RS80 experiment and the percentage difference to the Raised experiment. Given at 24 hourly intervals from 24 hours into the simulation up to 144 hours.

5.4 Discussion and Conclusions

5.4.1 Discussion

In Chapter 3, I found that coarse dust was often transported too low in the model atmosphere when compared with observations. In Chapter 4, I found that size bin 6 mass concentration rapidly decreased in westwards transport after leaving the African continent. Using these two findings, I created a hypothesis which suggested that low particles at the Sahara were likely to be rapidly mixed out of the atmosphere shortly after westwards transport to the MBL over the Atlantic. Thus, if coarse particles reached a higher altitude at the Sahara, would they be transported greater distances from the source?

In this Chapter, a series of experiments were run where dust in the model has been raised to the top of the SABL at the Sahara to test how this alters the transport of coarse dust particles. A control simulation (REControl) has been tested against a raised dust simulation (Raised), and two sensitivity experiments with raised dust, 10x convective mixing (R10xCM) and sedimentation reduced by 80% (RS80) have been compared against the Raised experiment.

I have shown that by raising dust at the Sahara, the lifetime of dust at all size ranges increases. In the coarsest size bin, the time taken to lose more than 90% of the original starting mass more than doubles from 8.85 hours to 22.2 hours. In size bin 5, it takes nearly twice as long to lose half of the original starting mass. Thus, raising dust higher at the Sahara, improves the lifetime of coarse particles. However, the magnitude of these changes are not great enough to result in long-range transport on the scale required (i.e. transport to the Caribbean over multiple days). The sedimentation of these coarse bins is too great. This suggests that other mechanisms must be involved.

If the raising of dust in this experiment represents vertical mixing which is not being effectively modelled, it could be that this process is missed throughout the whole dust lifetime. I have represented an initial perturbation to the the dust mass concentration profile in the Raised simulation, however, this does not account for a process that continually acts on the dust for the rest of its lifetime. For example, if it is the vertical winds at the Sahara that are misrepresented in the REControl and is not mixing the coarse dust up through the depth of the SABL, then a temporally longer perturbation would have more realistic results representative of continual meteorology. This would be akin to that suggested by Gasteiger et al. (2017), who hypothesised and proved that repeated diurnal convective mixing within the SAL enhanced coarse particle lifetime.

The question remains as to what the raising of dust actually represents in the real-world. I have suggested that the coarse dust is not lifted high enough at the Sahara, but the exact reason for the misrepresented vertical profile remains uncertain. As mentioned at the beginning of this Chapter, it could be the cause of underestimated vertical winds and updrafts, or perturbations to the wind by unresolved topography. Additionally, particle asphericity and electrical charging could also be responsible for enhanced vertical transport of coarse particles. All of these processes are beyond the capabilities of a climate model to represent without parameterisation, especially such a coarse model as is used here. More work will need to be put into working out why the dust is not transported high enough at the Sahara.

In the finer size bins, a daily cycle in atmospheric mass loss appears, by which the rate of mass lost every 3 hours increases after midday each day. I have hypothesised that this pattern is related to a diurnal wind cycle in the model, whereby vertical winds decrease and become more negative around midday. The loss of the upward winds could result in dust falling faster, increasing the deposition rate. From this potential correlation, I postulate whether increased magnitude upward vertical winds could enhance and prolong the lifetime of dust particles in the atmosphere. Some previous research has shown cases where updrafts were stronger than models predicted (Denjean et al. 2016). Therefore, it is not unreasonable to suggest that the model may struggle to represent sub-gridscale updrafts in convective and turbulent motions which could be vital for extending the lifetime of dust particles.

A 10x CM experiment (R10xCM) and an 80% reduced sedimentation (RS80) experiment were run to understand the compound effects with the raised dust, as raised dust by itself improved coarse dust lifetime but not by the extent needed to match the observations. Both experiments resulted in varied changes to the transport pathways of the dust: the R10xCM experiment resulted in greater transport to east and southeast Africa, and the RS80 experiment increased transport to both the east and west of the Sahara.

The R10xCM experiment did not significantly increase the lifetime of size bin 5 or 6 dust compared to the Raised experiment. There was some evidence to suggest that increased CM may have increased dust TCM in localised convective events. However, changing the CM did not have changes which would be desired to improve the representation of dust compared to the observations with very little change to dust in the trans-Atlantic plume. Instead changes from the R10xCM experiment compared to changes in the RS80 experiment show that the nature of convective mixing and convection are too spatially variable to be altered in this way where is it globally multiplied. Instead, experiments where localised CM is altered, for example in the west Sahara and SAL, would likely provide better insight.

The RS80 experiment showed improvements to the Raised experiment, extending the lifetime of the size bin 6 dust beyond 90 hours compared to less than 9 hours in the REControl experiment. This more closely aligns with observations where coarse dust reaches the Caribbean (can take 120 hours (Huang et al. 2010)). With this extension in lifetime, the diurnal cycle which was visible in the finer bins, begins to appear for size bin 6. Though not affecting the dust loss rate as much, the slight fluctuations in loss rate every 24 hours indicate some dependence on the diurnal feature. As it seems that the coarse particles might have some dependence on the vertical wind, then it is plausible to suggest that stronger, positive vertical winds could substantially counteract the sedimentation of these coarsest particles.

There is the potential for future experiments which only change the altitude and sedimentation of the coarsest particles as this is where the model struggles most with horizontal and vertical transport. Additionally, a more realistic enhanced vertical distribution of coarse dust through the SABL could produce a more realistic latitudinal distribution of dust transport.

5.4.2 Conclusions

At the start of this Chapter, I hypothesised that if coarse dust were raised higher at the Sahara, then it may have an increased transport distance. To test this, I ran a series of model experiments which used an altered restart dump to loft the dust to the top of the SABL. I also ran two experiments which tested the sensitivity of this raised dust to convective mixing (CM) and sedimentation. The key findings from this Chapter are:

1. Raising dust higher at the Sahara does improve coarse particle lifetime.
   (a) Raising the dust approximately doubled the lifetime of size bin 5 and 6 (6.32-63.2 µm) particles; lifetime would need to be multiplied by 13 at least to remain in the atmosphere for the expected travel to Caribbean.
   (b) The coarse size bin 6 dust still falls at the rate expected by Stokes settling suggesting that other model processes are relatively inactive in counteracting the deposition velocity.
2. A diurnal cycle in the rate of atmospheric dust loss appears to be related to the vertical winds in the model.
   (a) A correlation appears with increased dust loss when the vertical winds are negative or only weakly positive suggesting that larger positive vertical winds provide an upwards force on the dust, reducing its fall speed.
   (b) I suggest a more in-depth evaluation of the summertime Saharan meteorology in the model.
3. Multiplying the CM of dust by 10 in a raised dust simulation did not greatly increase the coarse particle lifetime.
   (a) Dust transport was enhanced to the east and southeast, away from the regular transport path across the Atlantic.
   (b) There was some evidence to suggest that localised changes to CM, for example in the SAL only, may provide some enhancement to particle lifetime.
4. Decreasing the settling velocity of dust by 80% in a raised simulation improved coarse particle transport and lifetime.

(a) Dust was transported to the west from the Sahara, but at a higher latitude due to more easterly winds at the SABL top, as opposed to northeasterly winds in the SABL/SAL centre.

(b) The initial lofting of the dust plus the reduced settling velocity meant coarse particles had a longer lifetime and were kept higher up in the SAL.

Chapter 6

Conclusions

Coarse mineral dust particles have been observed being transported significantly further than expected based on our understanding of theory. Coarse dust particles impact the Earth system in different ways to fine particles, which are better understood and represented in climate models. Modelling coarse particles can, among other effects, decrease the top-of-atmosphere cooling effect from dust, pose different effects on human health and act differently as cloud condensation and ice nuclei.

In this thesis, I aimed to improve understanding of the transport and deposition mechanisms affecting coarse particle transport from the Sahara to the Caribbean. I first analysed the difference between the size distribution evolution in observations and a climate model. I then carried out sensitivity testing on the model to better understand the dependence of coarse particle lifetime on different transport and deposition mechanisms.

This thesis has shown the relatively high retention of coarse particles over long-range transport in observations that is not reproduced in a specific climate model. I have also shown a very strong dependence of coarse particle transport on sedimentation in the model. Additional testing of the convective mixing, turbulent mixing, impaction scavenging and SW absorption shows a small dependence with minimal impact on long-range transport. Finally, I have shown that releasing the dust at altitude can increase coarse particle transport, though not by the order of magnitude required to bring the model into agreement with the observations.

This Chapter provides further discussion on these findings. In Section 6.1, the results of this thesis are summarised in the form of answers or insights to the research questions set out in Chapter 1 Section 1.2. A further discussion of the scope and limitations is in Section 6.2. Finally, suggestions for future research are given in Section 6.3.

6.1 Research Questions Revisited

1. How does dust size distribution evolve over long-range transport in both observations and a climate model?

   In this thesis, coarse and super-coarse dust particles (6.32-63.2 µm diameter) have been shown transported much further from the Sahara in observations than in the HadGEM3-GA7.1 climate model. The model underestimates dust mass at all stages of transport, including at emission, and the underestimation is exacerbated by orders of magnitude with westwards trans-Atlantic transport. 20-63.2 µm dust is shown in the observations to contribute 10% of the total dust mass at the Caribbean. Whereas in the model, the coarsest particles are deposited too quickly, resulting in negligible concentrations reaching the Caribbean. The model was able to represent the vertical structure of the total dust mass profile, but has difficulty with the coarse mass vertical distribution, showing a low altitude bias.

2. How sensitive are coarse dust particles to different transport and deposition processes in the model?

   Sedimentation rate, convective mixing, turbulent mixing, impaction scavenging and SW absorption were tested to understand the impact on coarse particle transport and deposition in a climate model. Coarse dust particles have been shown in this thesis to be most sensitive to changes in sedimentation. A reduction in sedimentation of between 80-95% is required to bring the modelled volume size distribution at the Caribbean into agreement with the observations. Convective mixing, turbulent mixing, impaction scavenging and increased SW absorption of dust in the model were shown to have an impact on the transport of coarse particles which resulted in a VSD that was still up to 6 orders of magnitude too small compared to the observations. Turbulent mixing controlled vertical transport of dust in and out of the MBL, and convective mixing controlled mixing in and out of the SAL. Increased SW absorption raised the altitude at which the dust travelled. But none of these processes (convective and turbulent mixing, SW absorption and impaction scavenging) were able to counteract the fast sedimentation of the coarse particles by enough to improve their long-range transport. This work reinstates the overarching importance of sedimentation for controlling the retention of coarse dust particles.

3. Does plume altitude at the Sahara impact coarse particle transport?

   In a model experiment, dust was raised up to the top of the Saharan atmospheric boundary layer at the Sahara. This was done partly as coarse dust was found to have a low-altitude bias in the model and concentration declined rapidly at the west African coast. I hypothesised that the low bias may result in inhibited horizontal transport for two reasons: the dust not reaching higher horizontal wind speeds present in the central SAL, and swift removal at the MBL-SAL interface when the coarse, heavy particles cannot rise above the MBL. Thus, this experiment was to test if the coarse dust was raised higher initially, whether it would be more likely to travel over the MBL. I found that raising dust higher at the Sahara improves the lifetime of coarse particles but not significantly enough to achieve full trans-Atlantic transport. The sedimentation of the coarse particles was too great as the coarsest mass was still nearly completely removed from the atmosphere within 24 hours. The coarsest dust was found to fall at approximately the expected Stokes settling velocity, suggesting a lack of counteracting processes. In addition to raising the dust, reducing the sedimentation by 80% improved coarse particle lifetime to multiple days, enough to allow for long-range transport. I discovered a diurnal cycle affecting the finer particles in the model, which I hypothesise is caused by a diurnal cycle in the vertical wind velocity. The coarse particles have too high sedimentation to show this diurnal cycle strongly. However, I suggest that strong, positive vertical winds could be important for counteracting sedimentation of the coarsest model dust particles.

6.2 Discussion and Limitations

One of the key processes in dust modelling to get right alongside transport and deposition is the emissions. As I found in Chapter 3, the model underestimated the total mass of dust near the source by an order of magnitude, as well as showing a fine bias in the emitted size distribution. In Chapter 4, the version of the model used had been tuned to improve the shape of the size distribution and encourage emissions of coarse particles. However, even with this new tuning, there is still an underestimation in the emissions of the coarsest particles. This tuning additionally only benefited emissions from the Sahara (as it was tuned specifically for the trans-Atlantic transport analysed in this thesis), and would likely have different impacts in different emissions sources across the globe. Thus, while tuning can be used to improve an emitted size distribution based on observations, the scarcity (temporally and spatially) of these observations results in large error margins which can only be narrowed by the collection of more observations and improved understanding of the complex associated mechanisms. Despite the improvements to emitted size distribution that can come from tuning a model's dust emissions, I have shown in Chapters 3 and 4 that the underestimation of coarse particles in the atmosphere grows by orders of magnitude with transport. This signifies difficulties in modelling of the coarse particle transport and deposition mechanisms.

The results from the sedimentation sensitivity experiments revealed that a reduction in sedimentation of more than 80% is required to bring the model into agreement with observations at the Caribbean. The sedimentation experiments produced the largest improvements in coarse particle model representation out of all the sensitivity tests. Reasonably assuming that the equations for dry deposition are well understood, this suggests the presence of processes in the real-world which are counteracting the sedimentation of the coarse particles by in excess of 80%. This 80% reduction in sedimentation is of a similar magnitude to the changes implemented by Drakaki et al. (2022) in their study, where they found reductions in sedimentation by 40-80% were required to bring a higher resolution NWP model into agreement with observations. Meng et al. (2022) also showed that particle density needed to be reduced by an order of magnitude (from 2500 kg m^{-3} to 250 kg m^{-3}) to bring a nudged climate model into agreement. These reductions to particle settling act as proxies for other processes or mechanisms which counteract the dust sedimentation rate; these counteracting processes were discussed in Chapter 1 Section 1.1.7 as mechanisms which could extend coarse particle lifetime. Some of the mechanisms which have been suggested include asphericity, electrical charging, turbulent motions in the atmosphere, convective mixing and self-lofting.

Asphericity was one of these mechanisms that has been suggested to extend the lifetime of coarse particles in the atmosphere. However, Huang et al. (2020) suggest that to account for asphericity in models, particle settling should be reduced by only 13%. In this case, asphericity would only account for a small portion of the counteracting forces acting upon coarse particle sedimentation. However, in Huang et al. (2020), the particles are assumed to be randomly oriented in the atmosphere. If the particles oriented so that the longest axis was horizontal, then the sedimentation could be greater than calculated by Huang et al. (2020) and thus account for more than 13%.

Electrical charging of dust particles can enhance the number of particles emitted (Esposito et al. 2016) and can be used to partially explain the long-range transport of coarse dust particles (Méndez Harper et al. 2022; Renard et al. 2018; Toth III et al. 2020; van der Does et al. 2018). However, it is not known by how much dust charging would impact coarse particle lifetime by, but it is possible that it can be used here to explain some of the counteraction of sedimentation in the observations.

Another potential mechanism that has been hypothesised previously is in relation to convective and turbulent mixing in the atmosphere. In the ChArMEx/ADRIMED field campaign, Denjean et al. (2016) measured updrafts that were greater than the settling velocity of 8µm particles. Thus, this could be an important mechanism for keeping coarse particles lofted in the atmosphere for longer. Super-coarse particles, with a greater sedimentation, would need much larger updrafts to completely counteract their sedimentation, however, they could still slow down sedimentation. Additionally, Marsham et al. (2011) found that global models with parameterised convection greatly underestimated dust uplift compared to a simulation permitting convection. Roberts et al. (2018) have gone on to show that explicit convection improved the diurnal wind cycle at the Sahara in a MetUM simulation. When tested in Chapters 4 and 5, removing or increasing the convective mixing in the model had minimal impact on coarse particles. Re-running these experiments with altered convective mixing rates in a convection-permitting simulation would potentially show more impact.

Gasteiger et al. (2017) proposed a theory which suggested that diurnal cycles in convective mixing could re-loft coarse particles each day after they sank through the stable atmosphere overnight. This repetitive mechanism could result in enhanced coarse particle lifetime. It is worth noting that size bin 6 particles (20-63.2 µm) in the model are dominantly removed within the first 24 hours of being lofted as I showed in Chapter 5. Thus, without any additional mechanisms to counteract sedimentation in the model, it is not likely that this alone can explain the extended super-coarse particle transport. Other results within this thesis, however, did suggest that altered vertical mixing in the atmosphere could extend coarse particle lifetime when combined with other mechanisms.

Although changes to turbulent mixing in Chapter 4 did not show significant changes to coarse particle lifetime, this should not rule out its importance for coarse dust transport. As turbulence is parameterised, it could be that the impacts of turbulent mixing on dust in the real-world is on too small of a scale to be resolved in current global climate models. However, Rodakoviski et al. (2023) found that in a large-eddy simulation (LES), turbulent mixing could be used to explain long-range coarse particle transport. This suggests that with better representation of fine-scale turbulent mixing, models could represent coarse particle transport more accurately. However, as mentioned previously, these detailed model representations of atmospheric mixing are very expensive and hard to achieve on the scale of a global model as appropriate parameterisations muct be developed.

When sedimentation was reduced by 80% in Chapter 5 Section 5.3.3, a diurnal force counteracting the sedimentation was shown, which appeared to be related to the vertical winds at the Sahara. Thus, once the dust is able to stay in the atmosphere for longer, it becomes susceptible to more mechanisms which can further extend its lifetime.

In June 2022, the DAZSAL (Diurnal vAriation of the vertically resolved siZe distribution in the Saharan Air Layer; Marenco et al. (2023)) field campaign (paired with the ASKOS campaign Marinou et al. (2023)) and using unmanned aerial vehicles (UAVs) measured diurnal fluctuations in the dust size distribution throughout the depth of the SAL at Cape Verde in order to test the Gasteiger et al. (2017) theory. Results from this campaign will be key to better understand the processes involved in long-range transport of coarse mineral dust particles.

In Chapter 5, I analysed the impacts of raising all the atmospheric dust at the Sahara up to the top of the Saharan atmospheric boundary layer. In a partner experiment, I also reduced the sedimentation by 80% as a result of my experiments in Chapter 4. This experiment showed again that a reduction in sedimentation of at least 80% is required to improve coarse particle transport by enough to transport particles of a significant quantity to the Caribbean to come into agreement with observations. In this experiment, one tenth of the 20-63.2 µm dust mass remained in the atmosphere after 4 days. With transport to the Caribbean taking approximately 5 days, this means that coarse particles are more capable of long-range transport to the Caribbean in this experiment.

Despite being essential, observations come with various limitations and potential issues. One of the main issues with the aircraft campaign observations used in this thesis is the limited spatial and temporal coverage. Intensive observations are often limited to only measure, at best, up to a month and not continuously throughout this time, meaning they are often at the mercy of the prevailing meteorological conditions during that time, which can result in results not representative of normal or climatological conditions despite the best of planning. The SALTRACE campaign, for example, used in this thesis occurred during relatively dusty conditions, with higher than average AODs measured at Cape Verde and the Caribbean. In

Chapter 3, I discussed the relationship between AOD and coarse mass fraction and showed results from the three campaigns (Fennec, AER-D and SALTRACE) that suggested AOD and coarse mass fraction are not strongly correlated with each other within a given campaign. This suggests that although the campaigns may fluctuate in the magnitude of dust event observed, for this thesis, the findings would not be significantly impacted by these campaigns having higher than average AODs.

The AER-D campaign analysed in this thesis often showed different dust plume characteristics compared to the other aircraft campaigns: the coarse fraction tended to be smaller and the profile shape was more stratified. This could be down to the observations occurring in August unlike the Fennec and SALTRACE campaigns which measured Saharan dust in June. Based on this limited set of results, this might suggest a significant change in dust plume characteristics throughout the summer season (JJA). The change in latitude of the ITCZ throughout the year is known to affect the magnitude of dust uplift, as well as activating different dust source locations, though these results hint that changes within seasons could be more significant than is often considered. I have carried out my model assessments on the month of June in this thesis, my comparisons with the Fennec and SALTRACE observations are therefore aligned. Results from the Fennec, AER-D and SALTRACE campaigns are frequently used in model validation elsewhere (e.g. Di Biagio et al. 2020; Drakaki et al. 2022; Meng et al. 2022; O'Sullivan et al. 2020). Further work to understand the root cause of differences between the Fennec and SALTRACE, and AER-D campaigns would be beneficial. This month-to-month variation should be considered in future model-observations comparisons, and additional assessment of these variations should be carried out to understand the validity of comparisons with these campaigns beyond their observed month. This is a core motivation for increasing the number of observational datasets throughout the summer months and rest of the year. With increased observations, the ability we have to improve model representations can only improve. I will discuss potential future field campaigns which could provide fruitful datasets in the next Section.

One issue that remains on the modelling side even if the question to the coarse particle transport is answered is that the processes likely controlling the transport are sub-grid scale, even at sub-km grid scale modelling. Mechanisms such as turbulent and convective mixing can occur on very fine scales and are therefore very expensive to model, and are parameterised. As Drakaki et al. (2022) found that similar reductions in sedimentation were required in a finer 15 km NWP model, this suggests that the model grid resolution is not a key factor in their underestimation of coarse particle transport. Additionally, Meng et al. (2022) carried out their research in a nudged climate model, which still required order of magnitude changes to the particle density to improve coarse particle transport representation. Thus, nudging a model would also not improve the representation. The variety of models used in these experiments suggests that the models are not the problem and it is instead a fundamental limitations in our understanding of the processes associated with coarse particle transport and deposition in the atmosphere.

Though current climate models are fairly coarse and tend to include parameterised convective and turbulent mixing, there is currently a move towards producing higher resolution models (Slingo et al. 2022; Stevens et al. 2024) with better representations of convective and turbulent mixing. However, due to the computational expense of aerosols, it is likely that sophisticated aerosol schemes will not be used. Though there is still the potential for improved convective mixing in high resolution models to be tested with higher resolution dust schemes in order to improve our understanding of what controls the lifetime of coarse particles. Similarly to Rodakoviski et al. (2023), testing dust transport in a higher resolution model could prove fruitful for our understanding.

6.3 Future Work

6.3.1 Suggested Research Resulting From This Thesis

I have shown that reductions in sedimentation of more than 80% are required to bring the HadGEM3-GA7.1 model into better agreement with observations (in terms of the coarse volume size distribution). However, at the Sahara, only reductions of 50% were required. Thus, I propose more testing is required to optimise the changes that could be made to dust schemes in models. For example, would a more flexible change where the reduction in sedimentation increases with distance from the dust source and only in the coarsest size bins produce a simulation with even higher agreement with the observations. Until there is better understanding as to the physical processes resulting in counteracting sedimentation by 80%, some climate models could apply a simple reduction to coarse particle sedimentation, as I have done here, in order to quickly and cheaply improve the significant issue of coarse particle transport.

Despite my results in Chapter 4 suggesting that convective and turbulent mixing had little impact on the coarse particle transport, I do not believe that they can be ruled out for further study. In all likelihood, the coarse resolution of the climate model used and the fact that both mixing processes are parameterised means that the relationship between the mixing and dust are not representative of real-world interactions. Especially as Marsham et al. (2011) showed that parameterised convection did not have the same effect as explicit convection on dust in a climate model. Rodakoviski et al. (2023) has shown that turbulent mixing could be used to explain coarse particle transport in a much higher resolution large-eddy simulation. Additionally, I have shown evidence in this thesis that suggests vertical winds may be an important process for counteracting coarse particle sedimentation. Convective and/or turbulent mixing could play an important role in coarse particle transport, but a low-resolution model with extensive parameterisations may have limitations for understanding the interaction with dust. Thus, I suggest experiments in higher resolution models are they way forwards in understanding the relationship between convective and turbulent mixing, and dust.

Even if convective meteorology at the Sahara is explicitly represented, it is not likely enough to fully counteract sedimentation of the coarsest particles. Instead other mechanisms are likely to be dominant. Further research into the mechanisms counteracting lifetime will be important for furthering our understanding of coarse particle lifetime. More high-resolution modelling, akin to the work of Rodakoviski et al. (2023), analysing the impact of the processes (e.g. asphericity and electrical charging) one at a time will reveal the individual impact. Then, further understanding of the way the mechanisms interact with each other would be beneficial. For example, understanding how asphericity and charging of particles would interact; would charging and orientation of aspherical particles actually result in faster sedimentation. With these further experiments, it should become clearer which processes are dominant in counteracting sedimentation. This knowledge will assist in designing dust schemes and parameterisations which can better model coarse dust transport in the future.

6.3.2 Field Campaign Proposal

As touched on in the previous Section, observational datasets are key to improving our understanding of real-world processes and ability to improve model representation.

I propose a field campaign utilising a research vessel fitted with remote sensing instruments and UAVs, which will follow the path of the trans-Atlantic dust plume during JJA. It would also be paired with aircraft observations and satellite overpasses. Figure 6.1 shows a schematic of the proposed components of the field campaign and the measurements which they would provide. This proposed campaign takes inspiration and builds on multiple previous campaigns which I will credit throughout this description. The overarching aim of this field campaign would be to better understand coarse particle transport and the mechanisms extending their lifetime.

Results from Chapter 4 suggest that a reduction in the sedimentation of coarse particles by around 80% would bring the model into agreement with the observations. This suggests the presence of processes counteracting the sedimentation of dust which aren't represented effectively, or at all, in the model. This includes the potential effects of asphericity, turbulent mixing, electrical charging of dust, particle orientation, and vertical wind velocity. Thus, in the proposed field campaign, these processes will be observed alongside particle size distribution in order to improve our understanding of the relationship between these processes and coarse particle lifetime.

This campaign is proposed to follow a dust plume from the source at the Sahara, all the way to the Caribbean, following a dust plume and collecting lagrangian-style observations. The SALTRACE campaign managed to observe the same dust plume at both Cape Verde and the Caribbean (Weinzierl et al. 2017). The campaign proposed here will go further, measuring the plume across the Atlantic, giving a more detailed understanding of the plume evolution. The first measurements will be made using an aircraft near the source. Similar to the Fennec campaign, a research aircraft will take measurements of the full size distribution vertical profile at the Sahara during summer (Ryder et al. 2013b). These measurements will be useful for confirming those taken during the Fennec campaign as well as providing the initial conditions of the dust plume which will be tracked across the Atlantic. Scientific flights will also be observed at Cape Verde and the Caribbean.

The research vessel will travel across the Atlantic, from the west coast of Africa to the Caribbean with various equipment on-board. This is reminiscent of a campaign in Spring 2013 (Ansmann et al. 2017) which used the Meteor research vessel with a lidar on-board to measure the springtime trans-Atlantic Saharan dust plume. This was a successful campaign providing vertical dust profiles from a lidar across the Atlantic ocean over a period of 1 month. The field campaign I am proposing plans to build on the Ansmann et al. (2017) campaign by a) occurring in the summer under the dust plume's strongest conditions, b) travelling from east to west to track the same dust emission over long-range transport and c) combining remote-sensing

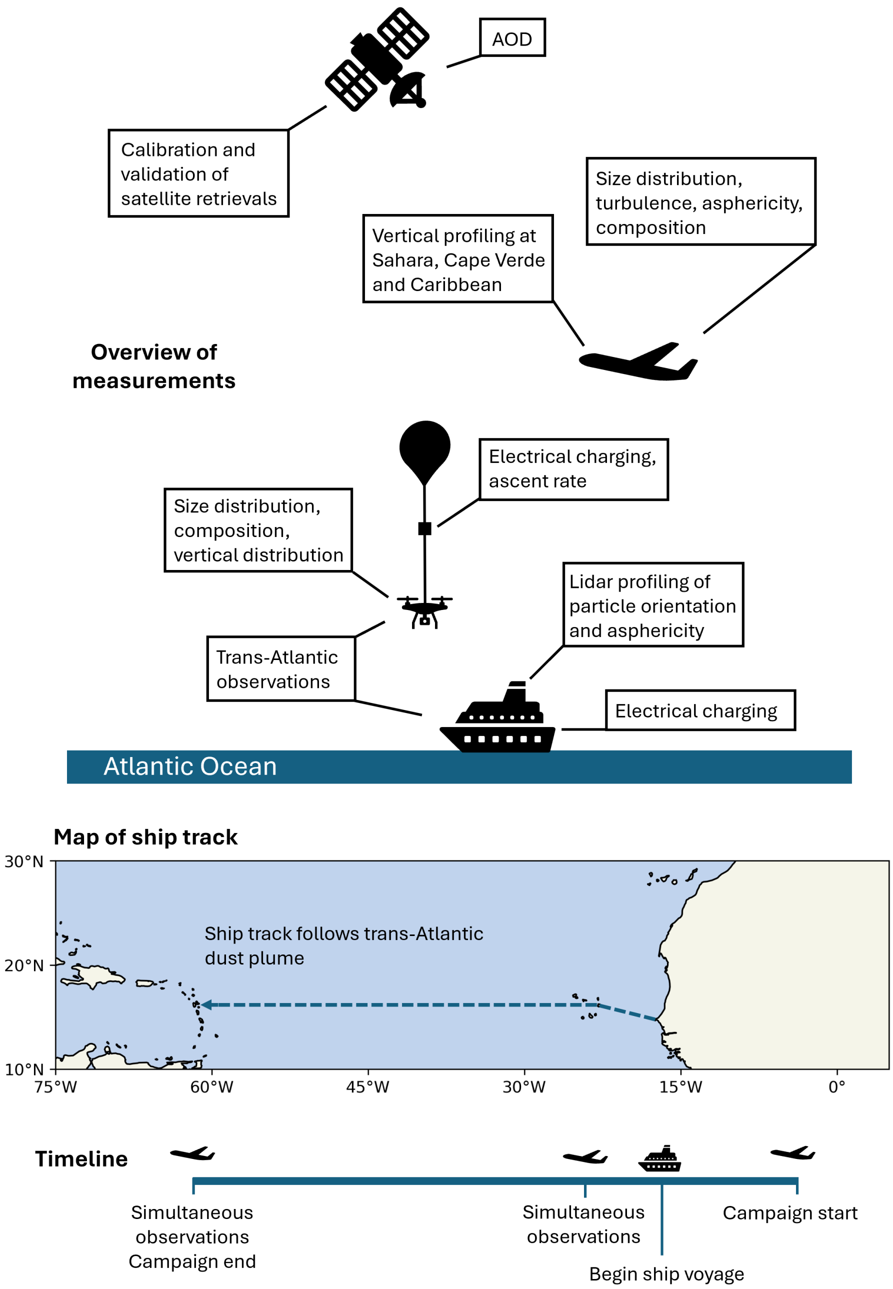

Figure 6.1: Schematic of the field campaign proposed in this thesis. A series of observations will be made following a dust plume from the Sahara, across the Atlantic, to the Caribbean. Aircraft observations will be made at the Sahara, Cape Verde and Caribbean. A research vessel equipped with remote-sensing equipment will traverse the Atlantic from east to west underneath the SAL. Radiosondes and UAVs tethered to weather balloons will be periodically released from the vessel. Satellite overpasses will be used. A map of the proposed ship track is shown.At the bottom, a timeline relating to the map shows the location of aircraft measurements (indicated by the plane graphic) and the start of the ship voyage relative to the campaign start (indicated by the boat graphic).

observations taken on-board with additional in-situ observations of the dust plume. Remote-sensing observations retrieved from instruments such as a lidar and sun photometer would be used to provide information on the orientation and sphericity of dust particles in the atmosphere, which are characteristics potentially important for coarse particle lifetime (Colarco et al. 2014; Huang et al. 2020; Mallios et al. 2020; Ulanowski et al. 2007; Yang et al. 2013). These characteristics will also aid in characterising dust and non-dust particles. Aboard the ship, an electric field mill could also measure any charging at the surface too. The ship will make simultaneous measurements with the aircraft at Cape Verde and the Caribbean.

From the ship, weather balloons tethered to radiosondes and small UAVs can be released to retrieve vertical profiles of the SAL across the Atlantic, unlike the aircraft, which is limited by its distance to airports on land. The weather balloons serve two purposes, a) observing vertical meteorological profiles, including variables such as electrical charging, and b) lofting UAVs to the top of the SAL where they will be piloted back to the ship, taking measurements of the dust on the way (as in Marenco et al. (2023)). A small electrical charging sensor can be tethered to weather balloons (akin to one used in the ASKOS campaign (Daskalopoulou et al. 2022)) to understand charging through the SAL associated with the dust. Additionally, variation in the ascension rate of the balloon could be used to infer updrafts in the SAL which could be affecting particle lifetime. Hanging below these instruments, UAVs, such as those used during the DAZSAL campaign, can carry equipment to measure the full size distribution and vertical distribution of dust throughout the SAL. The UAVs can also carry impactors which can later be analysed to understand the particle composition; van der Does et al. (2016) suggests composition could alter the charging ability of dust.

Finally, satellites can a) undergo product calibration and validation of products with comparison to the intensive observations, and b) provide retrievals of AOD which can used alongside the observations to understand how tuning models to AOD affects model dust representation.

Without field campaigns providing in-situ observations in typically hard-to-measure locations, we are unlikely to ever fully understand the processes which are affecting dust transport and deposition processes. Thus, continued efforts to measure in-situ dust are vital for upgrading our understanding and taking current generation models into the next generation.

6.4 Closing Remarks

Through this thesis I have shown that the cause of long-range transport of coarse particles in observations remains largely a mystery and is not represented in a climate model. An 80% reduction in the sedimentation of coarse particles in the model can improve agreement with observations. Thus, in the real-world some processes are counteracting the sedimentation by a significant amount; this could include asphericity or electrical charging of dust particles. I have shown evidence to suggest vertical winds may play some role in counteracting the coarse particle sedimentation. However, further observational datasets are required to fully understand the processes affecting these particles during trans-Atlantic transport.

Appendices

Appendix A

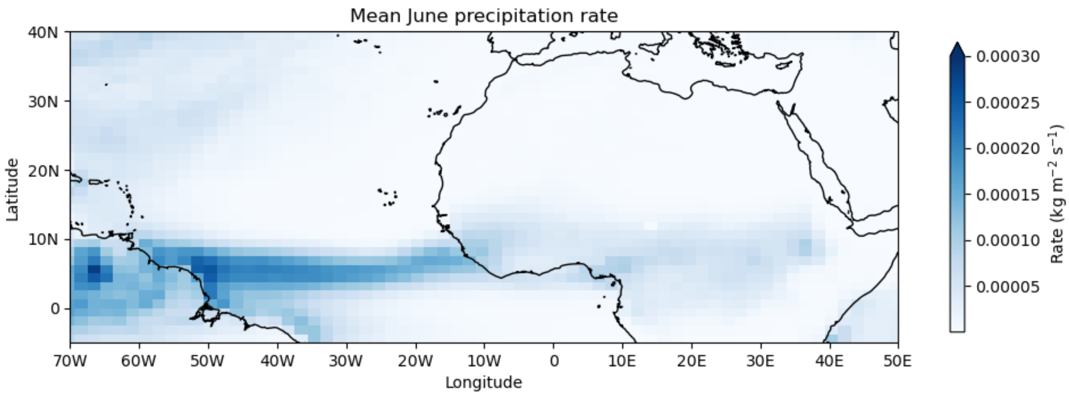

Figure A.1: Mean June precipitation rate in kg m^{-2}s^{-2} between 1995-2014 across North Africa and the north Atlantic.

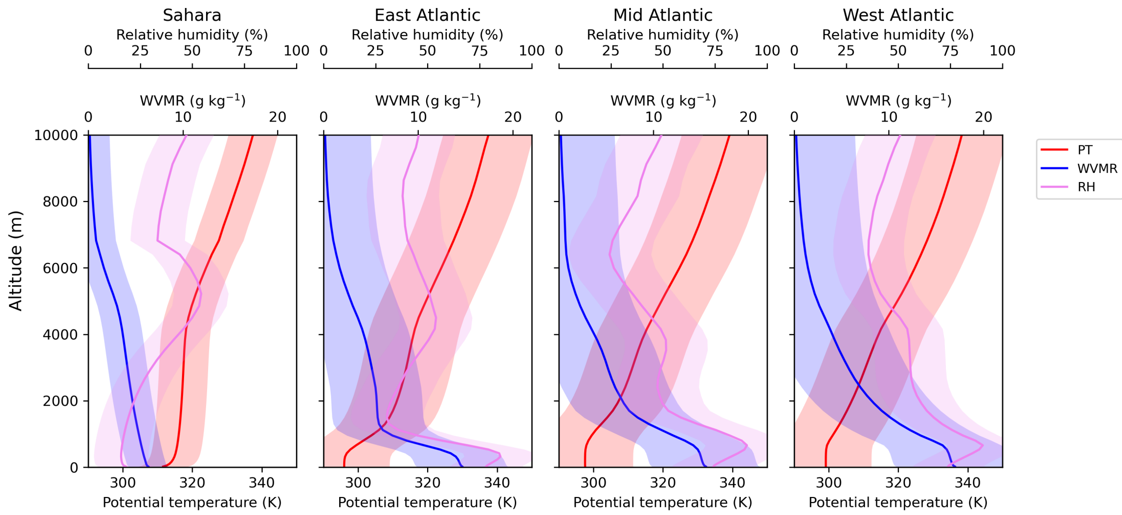

Figure A.2: Profiles of water vapour mixing ratio (WVMR in g kg^{-1}; blue), relative humidity (RH in %; pink) and potential temperature (PT in K;red) at the Sahara (14-27N, 12W-8E), east Atlantic (10-25N, 31-16W), mid Atlantic (10-25N, 60-35W) and west Atlantic (12-27N, 70-55W). The shading shows the standard deviation.

Bibliography

Adebiyi, A. A. and J. F. Kok (2020). "Climate models miss most of the coarse dust in the atmosphere". *Science Advances* 6.15. DOI: 10.1126/sciadv.aaz9507.

Adebiyi, A. et al. (2023). "A review of coarse mineral dust in the Earth system". *Aeolian Research* 60, p. 100849. DOI: 10.1016/j.aeolia.2022.100849.

Ansmann, A. et al. (2017). "Profiling of Saharan dust from the Caribbean to western Africa - Part 2: Shipborne lidar measurements versus forecasts". *Atmospheric Chemistry and Physics* 17 (24), pp. 14987–15006. DOI: 10.5194/acp-17-14987-2017.

Arias, P. et al. (2021). *Technical Summary. In Climate Change 2021: The Physical Science Basis. Contribution of Working Group I to the Sixth Assessment Report of the Intergovernmental Panel on Climate Change.* Ed. by V. Masson-Delmotte et al. Cambridge University Press, Cambridge, United Kingdom and New York, NY, USA, pp. 33–144. DOI: 10.1017/9781009157896.002.

Atkinson, J. D. et al. (2013). "The importance of feldspar for ice nucleation by mineral dust in mixed-phase clouds". *Nature* 498 (7454), pp. 355–358. DOI: 10.1038/nature12278.

Bagnold, R. A. (1941). *The Physics of Blown Sand and Desert Dunes.* New York; Metheun.

Baker, A. R., T. D. Jickells, M. Witt, and K. L. Linge (2006). "Trends in the solubility of iron, aluminium, manganese and phosphorus in aerosol collected over the Atlantic Ocean". *Marine Chemistry* 98 (1), pp. 43–58. DOI: 10.1016/J.MARCHEM.2005.06.004.

Balkanski, Y., R. Bonnet, O. Boucher, R. Checa-Garcia, and J. Servonnat (2021). "Better representation of dust can improve climate models with too weak an African monsoon". *Atmospheric Chemistry and Physics* 21 (14), pp. 11423–11435. DOI: 10.5194/acp-21-11423-2021.

Barkley, A. E. et al. (2021). "Atmospheric Transport of North African Dust-Bearing Supermicron Freshwater Diatoms to South America: Implications for Iron Transport to the Equatorial North Atlantic Ocean". *Geophysical Research Letters* 48.5, e2020GL090476. DOI: 10.1029/2020GL090476.

Bellouin, N. et al. (2013). "Impact of the modal aerosol scheme GLOMAP-mode on aerosol forcing in the hadley centre global environmental model". *Atmospheric Chemistry and Physics* 13 (6), pp. 3027–3044. DOI: 10.5194/ACP-13-3027-2013.

Benedetti, A. et al. (2009). "Aerosol analysis and forecast in the European Centre for Medium-Range Weather Forecasts Integrated Forecast System: 2. Data assimilation". *Journal of Geophysical Research: Atmospheres* 114.D13. DOI: 10.1029/2008JD011115.

Bergametti, G. and G. Foret (2014). "Dust Deposition". In: *Mineral Dust: A Key Player in the Earth System*. Dordrecht: Springer. DOI: 10.1007/978-94-017-8978-3.

Boyd, P. W. and M. J. Ellwood (2010). "The biogeochemical cycle of iron in the ocean". *Nature Geoscience* 3 (10), pp. 675–682. DOI: 10.1038/ngeo964.

Braun, S. A. (2010). "Reevaluating the Role of the Saharan Air Layer in Atlantic Tropical Cyclogenesis and Evolution". *Monthly Weather Review* 138 (6), pp. 2007–2037. DOI: 10.1175/2009MWR3135.1.

Brown, A. R. et al. (2008). "Upgrades to the boundary-layer scheme in the Met Office numerical weather prediction model". *Bound.-Lay. Meteorol.* 128, pp. 117–132.

Bullard, J. et al. (2016). "High-latitude dust in the Earth system". *Reviews of Geophysics* 54.2, pp. 447–485. DOI: 10.1002/2016RG000518.

Carlson, T. N. (2016). "The Saharan Elevated Mixed Layer and its Aerosol Optical Depth". *The Open Atmospheric Science Journal* 10 (1), pp. 26–38. DOI: 10.2174/1874282301610010026.

Caton Harrison, T., R. Washington, and S. Engelstaedter (2019). "A 14-Year Climatology of Saharan Dust Emission Mechanisms Inferred From Automatically Tracked Plumes". *Journal of Geophysical Research: Atmospheres* 124.16, pp. 9665–9690. DOI: 10.1029/2019JD030291.

Checa-Garcia, R. et al. (2021). "Evaluation of natural aerosols in CRESCENDO Earth system models (ESMs): Mineral dust". *Atmospheric Chemistry and Physics* 21 (13), pp. 10295–10335. DOI: 10.5194/acp-21-10295-2021.

Chouza, F., O. Reitebuch, A. Benedetti, and B. Weinzierl (2016). "Saharan dust long-range transport across the Atlantic studied by an airborne Doppler wind lidar and the MACC model". *Atmospheric Chemistry and Physics* 16 (18), pp. 11581–11600. DOI: 10.5194/acp-16-11581-2016.

Claquin, T., M. Schulz, Y. Balkanski, and O. Boucher (1998). "Uncertainties in assessing radiative forcing by mineral dust". *Tellus B* 50 (5), pp. 491–505. DOI: 10.1034/j.1600-0889.1998.t01-2-00007.x.

Clift, R. and W. H. Gauvin (1971). "Motion of entrained particles in gas streams". *The Canadian Journal of Chemical Engineering* 49 (4), pp. 439–448. DOI: 10.1002/cjce.5450490403.

Colarco, P. R. et al. (2014). "Impact of radiatively interactive dust aerosols in the NASA GEOS-5 climate model: Sensitivity to dust particle shape and refractive index". *Journal of Geophysical Research* 119 (2), pp. 753–786. DOI: 10.1002/2013JD020046.

Cornwell, G. C., H. Xiao, L. K. Berg, and S. M. Burrows (2021). "Simulated dust transport in the convective boundary layer". *Journal of Geophysical Research: Atmospheres* 126.5. DOI: 10.1029/2020jd033429.

Cuesta, J., J. H. Marsham, D. J. Parker, and C. Flamant (2009). "Dynamical mechanisms controlling the vertical redistribution of dust and the thermodynamic structure of the West Saharan atmospheric boundary layer during summer". *Atmospheric Science Letters* 10 (1), pp. 34–42. DOI: 10.1002/asl.207.

Dansie, A., D. Thomas, G. Wiggs, M. Baddock, and I. Ashpole (2022). "Plumes and blooms – Locally-sourced Fe-rich aeolian mineral dust drives phytoplankton growth off southwest Africa". *Science of The Total Environment* 829, p. 154562. DOI: 10.1016/j.scitotenv.2022.154562.

Dansie, A., G. Wiggs, and D. Thomas (2017). "Iron and nutrient content of wind-erodible sediment in the ephemeral river valleys of Namibia". *Geomorphology* 290, pp. 335–346. DOI: 10.1016/j.geomorph.2017.03.016.

Daskalopoulou, V., V. Spanakis-Misirlis, G. Hloupis, S. Mallios, and V. Amiridis (2022). "A low-cost Miniature Field Mill (MiniMill) Electrometer for Atmospheric Electric field Profiling Measurements". In: *44th COSPAR Scientific Assembly. Held 16-24 July*. Vol. 44, p. 1039.

Denjean, C. et al. (2016). "Size distribution and optical properties of mineral dust aerosols transported in the western Mediterranean". *Atmospheric Chemistry and Physics* 16.2, pp. 1081–1104. DOI: 10.5194/acp-16-1081-2016.

Di Biagio, C., Y. Balkanski, S. Albani, O. Boucher, and P. Formenti (2020). "Direct Radiative Effect by Mineral Dust Aerosols Constrained by New Microphysical and Spectral Optical Data". *Geophysical Research Letters* 47 (2), pp. 1–12. DOI: 10.1029/2019GL086186.

Di Mauro, B. et al. (2015). "Mineral dust impact on snow radiative properties in the European Alps combining ground, UAV, and satellite observations". *Journal of Geophysical Research* 120 (12), pp. 6080–6097. DOI: 10.1002/2015JD023287.

Di Tomaso, E., N. A. J. Schutgens, O. Jorba, and C. Pérez García-Pando (2017). "Assimilation of MODIS Dark Target and Deep Blue observations in the dust aerosol component of NMMB-MONARCH version 1.0". *Geosci. Model Dev.* 10, pp. 1107–1129. DOI: 10.5194/gmd-10-1107-2017.

Diedhiou, A., S. Janicot, A. Viltard, and P. de Felice (1998). "Evidence of two regimes of easterly waves over West Africa and the tropical Atlantic". *Geophysical Research Letters* 25 (15), pp. 2805–2808. DOI: 10.1029/98GL02152.

Doherty, O. M. and A. T. Evan (2014). "Identification of a new dust-stratocumulus indirect effect over the tropical North Atlantic". *Geophysical Research Letters* 41 (19), pp. 6935–6942. DOI: 10.1002/2014GL060897.

Drakaki, E. et al. (2022). "Modeling coarse and giant desert dust particles". *Atmospheric Chemistry and Physics* 22 (18), pp. 12727–12748. DOI: 10.5194/acp-22-12727-2022.

Dumont, M. et al. (2020). "Accelerated Snow Melt in the Russian Caucasus Mountains After the Saharan Dust Outbreak in March 2018". *Journal of Geophysical Research: Earth Surface* 125.9, e2020JF005641. DOI: 10.1029/2020JF005641.

Dunion, J. and C. Velden (2004). "The Impact of the Saharan Air Layer on Atlantic Tropical Cyclone Activity". *Bulletin of the American Meteorological Society* 85 (3), pp. 353–366. DOI: 10.1175/BAMS-85-3-353.

Edwards, J. M. and A. Slingo (1996). “Studies with a flexible new, radiation code, part 1: Choosing a configuration for a large-scale model”. *Q. J. Roy. Meteor. Soc.* 122, pp. 689–719. DOI: 10.1002/qj.49712253107.

Emerson, E. W. et al. (2020). “Revisiting particle dry deposition and its role in radiative effect estimates”. *Proceedings of the National Academy of Sciences of the United States of America* 117.42, pp. 26076–26082. DOI: 10.1073/pnas.2014761117.

Esposito, F. et al. (2016). “The role of the atmospheric electric field in the dust-lifting process”. *Geophysical Research Letters* 43 (10), pp. 5501–5508. DOI: 10.1002/2016GL068463.

Evan, A. T., C. Flamant, S. Fiedler, and O. Doherty (2014). “An analysis of aeolian dust in climate models”. *Geophysical Research Letters* 41.16, pp. 5996–6001. DOI: 10.1002/2014GL060545.

Eyring, V. et al. (2016). “Overview of the Coupled Model Intercomparison Project Phase 6 (CMIP6) experimental design and organization”. *Geoscientific Model Development* 9 (5), pp. 1937–1958. DOI: 10.5194/gmd-9-1937-2016.

Fan, S. M., L. W. Horowitz, H. Levy, and W. J. Moxim (2004). “Impact of air pollution on wet deposition of mineral dust aerosols”. *Geophysical Research Letters* 31 (2). DOI: 10.1029/2003GL018501.

Fecan, F., B. Marticonera, and G. Bergametti (1998). “Parametrization of the increase of the aeolian erosion threshold wind friction velocity due to soil moisture for arid and semi-arid areas”. *Annales Geophysicae* 17, pp. 149–157. DOI: 10.1007/s00585-999-0149-7.

Foret, G., G. Bergametti, F. Dulac, and L. Menut (2006). “An optimized particle size bin scheme for modeling mineral dust aerosol”. *Journal of Geophysical Research Atmospheres* 111 (17). DOI: 10.1029/2005JD006797.

Garcia-Carreras, L. et al. (2015). “The turbulent structure and diurnal growth of the Saharan atmospheric boundary layer”. *Journal of Atmospheric Sciences* 72.2, pp. 693–713. DOI: 10.1175/JAS-D-13-0384.1.

Gasteiger, J. and M. Wiegner (2018). “MOPSMAP v1.0: a versatile tool for the modeling of aerosol optical properties”. *Geoscientific Model Development* 11.7, pp. 2739–2762. DOI: 10.5194/gmd-11-2739-2018.

Gasteiger, J. et al. (2017). “Particle settling and vertical mixing in the Saharan Air Layer as seen from an integrated model, Lidar and in situ perspective”. *Atmospheric Chemistry and Physics* 17, pp. 297–311. DOI: 10.5194/acp-17-297-2017.

Gillette, D. A. (1979). *Environmental factors affecting dust emission by wind erosion, in: Saharan Dust.* Ed. by M. C. John Wiley, New York.

Ginoux, P. (2003). “Effects of nonsphericity on mineral dust modeling”. *Journal of Geophysical Research: Atmospheres* 108 (D2), p. 4052. DOI: 10.1029/2002JD002516.

González-Flórez, C. et al. (2023). “Insights into the size-resolved dust emission from field measurements in the Moroccan Sahara”. *Atmospheric Chemistry and Physics* 23 (12), pp. 7177–7212. DOI: 10.5194/acp-23-7177-2023.

Greeley, R. and J. D. Iversen (1985). *Wind as a Geological Process on Earth, Mars, Venus and Titan.* Cambridge University Press.

Greenfield, S. M. (1957). "RAIN SCAVENGING OF RADIOACTIVE PARTICULATE MATTER FROM THE ATMOSPHERE". *Journal of Atmospheric Sciences* 14 (2), pp. 115–125. DOI: 10.1175/1520-0469(1957)014%3C0115:RSORPM%3E2.0.CO;2.

Gregory, D. and S. Allen (1991). "The effect of convective downdraughts upon NWP and climate simulations". In: *Nineth conference on numerical weather prediction*, pp. 122–123.

Gregory, D. and P. R. Rowntree (1990). "A massflux convection scheme with representation of cloud ensemble characteristics and stability dependent closure". *Monthly Weather Review* 118, pp. 1483–1506. DOI: 10.1175/1520-0493(1990)118\%3C1483:AMFCSW\%3E2.0.CO;2.

Hallegraeff, G., D. M. Anderson, A. Cembella, and A. Wegener (2003). *Manual on Harmful Marine Microalgae.* 2nd ed. Paris, France, UNESCO. DOI: 10.25607/OBP-1370.

Harrison, R. G., K. A. Nicoll, G. J. Marlton, C. L. Ryder, and A. J. Bennett (2018). "Saharan dust plume charging observed over the UK". *Environmental Research Letters* 13.5. DOI: 10.1088/1748-9326/aabcd9.

Haywood, J. M. et al. (2011). "Motivation, rationale and key results from the GERBILS Saharan dust measurement campaign". *Quarterly Journal of the Royal Meteorological Society* 137.658, pp. 1106–1116. DOI: https://doi.org/10.1002/qj.797.

Heisel, M., B. Chen, J. F. Kok, and M. Chamecki (2021). "Gentle Topography Increases Vertical Transport of Coarse Dust by Orders of Magnitude". *Journal of Geophysical Research: Atmospheres* 126 (14). DOI: 10.1029/2021JD034564.

Hess, M., P. Koepke, and I. Schult (1998). "Optical Properties of Aerosols and Clouds: The Software Package OPAC". *Bulletin of the American Meteorological Society* 79 (5), pp. 831–844. DOI: 10.1175/1520-0477(1998)079<0831:Opoaac>2.0.Co;2.

Highwood, E. and C. L. Ryder (2014). "Mineral Dust: A Key Player in the Earth System". In: Springer, Dordrecht, Heidelberg, New York, London. Chap. Radiative Effects of Dust.

Hillger, D. et al. (2013). "First-Light Imagery from Suomi NPP VIIRS". *Bulletin of the American Meteorological Society* 94.7, pp. 1019–1029. DOI: 10.1175/BAMS-D-12-00097.1.

Hoose, C. and O. Möhler (2012). "Heterogeneous ice nucleation on atmospheric aerosols: a review of results from laboratory experiments". *Atmospheric Chemistry and Physics* 12, pp. 9817–9854. DOI: 10.5194/acp-12-9817-2012.

Hsu, N. C. et al. (2013). "Enhanced Deep Blue aerosol retrieval algorithm: The second generation". *Journal of Geophysical Research Atmospheres* 118 (16), pp. 9296–9315. DOI: 10.1002/jgrd.50712.

Huang, J., C. Zhang, and P. Joseph M. (2010). "African dust outbreaks: A satellite perspective of temporal and spatial variability over the tropical Atlantic Ocean". *Journal of Geophysical Research Atmospheres* 115 (5). DOI: 10.1029/2009JD012516.

Huang, Y. et al. (2020). "Climate models and remote sensing retrievals neglect substantial desert dust asphericity". *Geophysical Research Letters* 47.6. DOI: 10.1029/2019GL086592.

Huang, Y., A. A. Adebiyi, P. Formenti, and J. F. Kok (2021). "Linking the Different Diameter Types of Aspherical Desert Dust Indicates That Models Underestimate Coarse Dust Emission". *Geophysical Research Letters* 48.6. DOI: 10.1029/2020GL092054.

Huneeus, N. et al. (2011). "Global dust model intercomparison in AeroCom phase I". *Atmospheric Chemistry and Physics* 11.15, pp. 7781–7816. DOI: 10.5194/acp-11-7781-2011.

Javanmard, Z. et al. (2020). "Soil dust effects on morphological, physiological and biochemical responses of four tree species of semiarid regions". *European Journal of Forest Research* 139 (3), pp. 333–348. DOI: 10.1007/s10342-019-01232-z.

Jickells, T. D. et al. (2005). "Global Iron Connections Between Desert Dust, Ocean Biogeochemistry, and Climate". *Science* 308.5718, pp. 67–71. DOI: 10.1126/science.1105959.

Jones, A. C. et al. (2022). "Below-cloud scavenging of aerosol by rain: a review of numerical modelling approaches and sensitivity simulations with mineral dust in the Met Office's Unified Model". *Atmospheric Chemistry and Physics* 22 (17), pp. 11381–11407. DOI: 10.5194/acp-22-11381-2022.

Karydis, V. A., P. Kumar, D. Barahona, I. N. Sokolik, and A. Nenes (2011). "On the effect of dust particles on global cloud condensation nuclei and cloud droplet number". *Journal of Geophysical Research Atmospheres* 116 (23). DOI: 10.1029/2011JD016283.

Koffi, B. et al. (2016). "Evaluation of the aerosol vertical distribution in global aerosol models through comparison against CALIOP measurements: AeroCom phase II results". *Journal of Geophysical Research* 121 (12), pp. 7254–7283. DOI: 10.1002/2015JD024639.

Kok, J. F. (2011). "Does the size distribution of mineral dust aerosols depend on the wind speed at emission?" *Atmospheric Chemistry and Physics* 11.19, pp. 10149–10156. DOI: 10.5194/acp-11-10149-2011.

Kok, J. F. et al. (2017). "Smaller desert dust cooling effect estimated from analysis of dust size and abundance". *Nature Geoscience* 10, pp. 274–278. DOI: 10.1038/ngeo2912.

Kok, J. F., D. S. Ward, N. M. Mahowald, and A. T. Evan (2018). "Global and regional importance of the direct dust-climate feedback". *Nature Communications* 9.241. DOI: 10.1038/s41467-017-02620-y.

Kok, J. F. et al. (2023). "Mineral dust aerosol impacts on global climate and climate change". *Nature Reviews Earth & Environment 2023*, pp. 1–16. DOI: 10.1038/s43017-022-00379-5.

Kotsyfakis, M., S. G. Zarogiannis, and E. Patelarou (2019). "The Health Impact of Saharan Dust Exposure". *International Journal of Occupational Medicine and Environmental Health* 32.6. DOI: 10.13075/ijomeh.1896.01466.

Laakso, L. et al. (2003). “Ultrafine particle scavenging coefficients calculated from 6 years field measurements”. *Atmospheric Environment* 37, pp. 3605–3613. DOI: 10.1016/S1352-2310(03)00326-1.

Lavaysse, C. et al. (2009). “Seasonal evolution of the West African heat low: a climatological perspective”. *Climate Dynamics* 33, pp. 313–330. DOI: 10.1007/s00382-009-0553-4.

Levy, R. C. et al. (2013). “The Collection 6 MODIS aerosol products over land and ocean”. *Atmospheric Measurement Techniques* 6 (11), pp. 2989–3034. DOI: 10.5194/amt-6-2989-2013.

Li, L. et al. (2021). “Quantifying the range of the dust direct radiative effect due to source mineralogy uncertainty”. *Atmospheric Chemistry and Physics* 21 (5), pp. 3973–4005. DOI: 10.5194/ACP-21-3973-2021.

Lock, A. P. (2001). “The numerical representation of entrainment in parametrizations of boundary layer turbulent mixing”. *Monthly Weather Review* 129, pp. 1148–1163.

Lock, A. P., A. R. Brown, M. R. Bush, G. M. Martin, and R. N. B. Smith (2000). “A new boundary layer mixing scheme. Part I: Scheme description and single-column model tests”. *Monthly Weather Review* 128, pp. 3187–3199.

Lohmann, U. and J. Feichter (2005). “Global indirect aerosol effects: a review”. *Atmospheric Chemistry and Physics* 5.3, pp. 715–737. DOI: 10.5194/acp-5-715-2005.

Lu, Z. et al. (2023). “First Mapping of Monthly and Diurnal Climatology of Saharan Dust Layer Height Over the Atlantic Ocean From EPIC/DSCOVR in Deep Space”. *Geophysical Research Letters* 50 (5). DOI: 10.1029/2022GL102552.

Mahowald, N. et al. (2014). “The size distribution of desert dust aerosols and its impact on the Earth system”. *Aeolian Research* 15, pp. 53–71. DOI: 10.1016/j.aeolia.2013.09.002..

Mahowald, N. et al. (2008). “Global distribution of atmospheric phosphorus sources, concentrations and deposition rates, and anthropogenic impacts”. *Global Biogeochemical Cycles* 22 (4). DOI: 10.1029/2008GB003240.

Mahowald, N. M. et al. (2005). “Atmospheric global dust cycle and iron inputs to the ocean”. *Global Biogeochemical Cycles* 19 (4). DOI: 10.1029/2004GB002402.

Mahowald, N. M. et al. (2009). “Atmospheric iron deposition: Global distribution, variability, and human perturbations”. *Annual Review of Marine Science* 1, pp. 245–278. DOI: 10.1146/annurev.marine.010908.163727.

Mahowald, N. M. et al. (2018). “Aerosol trace metal leaching and impacts on marine microorganisms”. *Nature Communications* 9 (1). DOI: 10.1038/s41467-018-04970-7.

Mailler, S., L. Menut, A. Cholakian, and R. Pennel (2023). “AerSett v1.0: A simple and straightforward model for the settling speed of big spherical atmospheric aerosols”. *Geoscientific Model Development* 16 (3), pp. 1119–1127. DOI: 10.5194/GMD-16-1119-2023.

Mallet, M. et al. (2016). "Overview of the Chemistry-Aerosol Mediterranean Experiment/Aerosol Direct Radiative Forcing on the Mediterranean Climate (ChArMEx/ADRIMED) summer 2013 campaign". *Atmospheric Chemistry and Physics* 16.2, pp. 455–504. DOI: 10.5194/acp-16-455-2016.

Mallios, S. A., E. Drakaki, and V. Amiridis (2020). "Effects of dust particle sphericity and orientation on their gravitational settling in the earth's atmosphere". *Journal of Aerosol Science* 150. DOI: 10.1016/j.jaerosci.2020.105634.

Manners, J., J. Edwards, P. Hill, and J. Thelen (2015). *SOCRATES (Suite Of Community RAdiative Transfer codes based on Edwards and Slingo) Technical Guide, Met Office, UK.* Tech. rep.

Marenco, F. et al. (2023). "Unmanned Aerial Vehicles for the Joint Aeolus Tropical Atlantic Campaign". In: *EGU General Assembly Conference Abstracts.* EGU General Assembly Conference Abstracts, EGU-17089, EGU–17089. DOI: 10.5194/egusphere-egu23-17089.

Maring, H., D. L. Savoie, M. A. Izaguirre, L. Custals, and J. S. Reid (2003). "Mineral dust aerosol size distribution change during atmospheric transport". *Journal of Geophysical Research: Atmospheres* 108 (19). DOI: 10.1029/2002jd002536.

Marinou, E. et al. (2023). "An Overview of the ASKOS Campaign in Cabo Verde". *Environmental Science Proceedings* 26 (1), p. 200. DOI: 10.3390/environsciproc2023026200.

Marsham, J. H., D. J. Parker, C. M. Grams, C. M. Taylor, and J. M. Haywood (2008). "Uplift of Saharan dust south of the intertropical discontinuity". *Journal of Geophysical Research Atmospheres* 113 (21). DOI: 10.1029/2008JD009844.

Marsham, J. H. et al. (2013). "Meteorology and dust in the central Sahara: Observations from Fennec supersite-1 during the June 2011 Intensive Observation Period". *Journal of Geophysical Research: Atmospheres* 118 (10), pp. 4069–4089. DOI: 10.1002/JGRD.50211.

Marsham, J. H., P. Knippertz, N. S. Dixon, D. J. Parker, and G. M. S. Lister (2011). "The importance of the representation of deep convection for modeled dust-generating winds over West Africa during summer". *Geophysical Research Letters* 38.16. DOI: 10.1029/2011GL048368.

Marticorena, B. (2014). "Dust Production Mechanisms". In: *Mineral Dust: A Key Player in the Earth System.* Dordrecht: Springer. DOI: 10.1007/978-94-017-8978-3.

Marticorena, B. and G. Bergametti (1995). "Modeling the atmospheric dust cycle: 1. Design of a soil-derived dust emission scheme". *Journal of Geophysical Research* 100 (D8), pp. 415–431. DOI: 10.1029/95JD00690.

Méndez Harper, J. et al. (2022). "The lifetime of charged dust in the atmosphere". *PNAS Nexus* 1 (5). DOI: 10.1093/pnasnexus/pgac220.

Meng, J. et al. (2022). "Improved Parameterization for the Size Distribution of Emitted Dust Aerosols Reduces Model Underestimation of Super Coarse Dust". *Geophysical Research Letters* 49 (8). DOI: 10.1029/2021GL097287.

Middleton, N. J. (2017). "Desert dust hazards: A global review". *Aeolian Research* 24, pp. 53–63. DOI: 10.1016/j.aeolia.2016.12.001.

Miller, R. L. and I. Tegen (1998). "Climate Response to Soil Dust Aerosols". *Journal of Climate* 11.12, pp. 3247–3267. DOI: 10.1175/1520-0442(1998)011<3247:CRTSDA>2.0.CO;2.

Mona, L. et al. (2023). "Observing Mineral Dust in Northern Africa, the Middle East, and Europe: Current Capabilities and Challenges ahead for the Development of Dust Services". *Bulletin of the American Meteorological Society* 104 (12), E2223–E2264. DOI: 10.1175/BAMS-D-23-0005.1.

Morcrette, C. J. (2012). "Improvements to a prognostic cloud scheme through changes to its cloud erosion parametrization". *Atmospheric Science Letters* 13.2, pp. 95–102. DOI: https://doi.org/10.1002/asl.374.

Mulcahy, J. P. et al. (2020). "Description and evaluation of aerosol in UKESM1 and HadGEM3-GC3.1 CMIP6 historical simulations". *Geoscientific Model Development* 13 (12), pp. 6383–6423. DOI: 10.5194/GMD-13-6383-2020.

Nenes, A., B. Murray, and A. Bougiatioti (2014). "Mineral Dust and its Microphysical Interactions with Clouds". In: *Mineral Dust: A Key Player in the Earth System.* Dordrecht: Springer. DOI: 10.1007/978-94-017-8978-3.

Nickovic, S. et al. (2021). "Cloud icing by mineral dust and impacts to aviation safety". *Scientific Reports* 11.6411. DOI: 10.1038/s41598-021-85566-y.

Nicoll, K., G. Harrison, G. Marlton, and M. Airey (2020). "Consistent dust electrification from Arabian Gulf sea breezes". *Environmental Research Letters* 15.8, p. 084050. DOI: 10.1088/1748-9326/ab9e20.

Nowottnick, E. et al. (2010). "Online simulations of mineral dust aerosol distributions: Comparisons to NAMMA observations and sensitivity to dust emission parameterization". *Journal of Geophysical Research: Atmospheres* 115.D3. DOI: https://doi.org/10.1029/2009JD012692.

O'Sullivan, D. et al. (2020). "Models transport Saharan dust too low in the atmosphere: a comparison of the MetUM and CAMS forecasts with observations". *Atmospheric Chemistry and Physics* 20, pp. 12955–12982. DOI: 10.5194/acp-20-12955-2020.

Otto, S., T. Trautmann, and M. Wendisch (2011). "On realistic size equivalence and shape of spheroidal Saharan mineral dust particles applied in solar and thermal radiative transfer calculations". *Atmospheric Chemistry and Physics* 11 (9), pp. 4469–4490. DOI: 10.5194/acp-11-4469-2011.

Painter, T. H. et al. (2007). "Impact of disturbed desert soils on duration of mountain snow cover". *Geophysical Research Letters* 34.12. DOI: 10.1029/2007GL030284.

Piedra, P. G., L. R. Llanza, and H. Moosmüller (2018). "Optical losses of photovoltaic modules due to mineral dust deposition: Experimental measurements and theoretical modeling". *Solar Energy* 164, pp. 160–173. DOI: 10.1016/j.solener.2018.02.030.

Price, H. C. et al. (2018). “Atmospheric Ice-Nucleating Particles in the Dusty Tropical Atlantic”. *Journal of Geophysical Research: Atmospheres* 123.4, pp. 2175–2193. DOI: 10.1002/2017JD027560.

Prospero, J. M. and P. J. Lamb (2003). “African Droughts and Dust Transport to the Caribbean: Climate Change Implications”. *Science* 302.5647, pp. 1024–1027. DOI: 10.1126/science.1089915.

Prospero, J. M. et al. (2020). “Characterizing and Quantifying African Dust Transport and Deposition to South America: Implications for the Phosphorus Budget in the Amazon Basin”. *Global Biogeochemical Cycles* 34 (9), e2020GB006536. DOI: 10.1029/2020GB006536.

Pruppacher, H. and J. Klett (2010). *Microphysics of Clouds and Precipitation.* Dordrecht, Netherlands: Springer.

Räisänen, P. et al. (2013). “Impact of dust particle non-sphericity on climate simulations”. *Quarterly Journal of the Royal Meteorological Society* 139.677, pp. 2222–2232. DOI: https://doi.org/10.1002/qj.2084.

Ratcliffe, N. G. et al. (2024). “Long-range transport of coarse mineral dust: an evaluation of the Met Office Unified Model against aircraft observations”. *Atmospheric Chemistry and Physics* 24.21, pp. 12161–12181. DOI: 10.5194/acp-24-12161-2024.

Renard, J. B. et al. (2018). “In situ measurements of desert dust particles above the western Mediterranean Sea with the balloon-borne Light Optical Aerosol Counter/sizer (LOAC) during the ChArMEx campaign of summer 2013”. *Atmospheric Chemistry and Physics* 18 (5), pp. 3677–3699. DOI: 10.5194/acp-18-3677-2018.

Roberts, A. J. et al. (2018). “Can explicit convection improve modelled dust in summertime West Africa?” *Atmospheric Chemistry and Physics* 18.12, pp. 9025–9048. DOI: 10.5194/acp-18-9025-2018.

Rodakoviski, R., J. Kok, and M. Chamecki (2023). “Dust Settling From Turbulent Layers in the Free Troposphere: Implications for the Saharan Air Layer”. *Journal of Geophysical Research: Atmospheres* 128 (6). DOI: 10.1029/2022JD037724.

Rosenberg, P. D. et al. (2014). “Quantifying particle size and turbulent scale dependence of dust flux in the Sahara using aircraft measurements”. *Journal of Geophysical Research: Atmospheres* 119 (12), pp. 7577–7598. DOI: 10.1002/2013JD021255.

Rosenfeld, D. et al. (2008). “Flood or Drought: How Do Aerosols Affect Precipitation?” *Science* 321.5894, pp. 1309–1313. DOI: 10.1126/science.1160606.

Ryder, C. L. (2021). “Radiative Effects of Increased Water Vapor in the Upper Saharan Air Layer Associated With Enhanced Dustiness”. *Journal of Geophysical Research: Atmospheres* 126 (21). DOI: 10.1029/2021JD034696.

Ryder, C. L., E. J. Highwood, T. M. Lai, H. Sodemann, and J. H. Marsham (2013a). “Impact of atmospheric transport on the evolution of microphysical and optical properties of Saharan dust”. *Geophysical Research Letters* 40.10, pp. 2433–2438. DOI: 10.1002/grl.50482.

Ryder, C. L. et al. (2015). "Advances in understanding mineral dust and boundary layer processes over the Sahara from Fennec aircraft observations". *Atmospheric Chemistry and Physics* 15.14, pp. 8479–8520. DOI: 10.5194/acp-15-8479-2015.

Ryder, C. L. et al. (2019). "Coarse and giant particles are ubiquitous in Saharan dust export regions and are radiatively significant over the Sahara". *Atmospheric Chemistry and Physics* 19.24, pp. 15353–15376. DOI: 10.5194/acp-19-15353-2019.

Ryder, C. et al. (2018). "Coarse-mode mineral dust size distributions, composition and optical properties from AER-D aircraft measurements over the tropical eastern Atlantic". *Atmospheric Chemistry and Physics* 18.23, pp. 17225–17257. DOI: 10.5194/acp-18-17225-2018.

Ryder, C. L. et al. (2013b). "Optical properties of Saharan dust aerosol and contribution from the coarse mode as measured during the Fennec 2011 aircraft campaign". *Atmospheric Chemistry and Physics* 13, pp. 303–325. DOI: 10.3929/ethz-b-000063955.

Ryder, C. L. et al. (2024). "Aircraft Engine Dust Ingestion at Global Airports". *Nat. Hazards Earth Syst. Sci.* DOI: 10.5194/nhess-24-2263-2024.

Samset, B. H. et al. (2016). "Fast and slow precipitation responses to individual climate forcers: A PDRMIP multimodel study". *Geophysical Research Letters* 43 (6), pp. 2782–2791. DOI: 10.1002/2016GL068064.

Sassen, K., P. J. DeMott, J. M. Prospero, and M. R. Poellot (2003). "Saharan dust storms and indirect aerosol effects on clouds: CRYSTAL-FACE results". *Geophysical Research Letters* 30.12. DOI: 10.1029/2003GL017371.

Sauter, K. and T. S. L'Ecuyer (2017). "Observational evidence for the vertical redistribution and scavenging of Saharan dust by tropical cyclones". *Geophysical Research Letters* 44 (12), pp. 6421–6430. DOI: 10.1002/2017GL074166.

Saxby, J., F. Beckett, K. Cashman, A. Rust, and E. Tennant (2018). "The impact of particle shape on fall velocity: Implications for volcanic ash dispersion modelling". *Journal of Volcanology and Geothermal Research* 362, pp. 32–48. DOI: 10.1016/J.JVOLGEORES.2018.08.006.

Sayyah, A., M. N. Horenstein, and M. K. Mazumder (2014). "Energy yield loss caused by dust deposition on photovoltaic panels". *Solar Energy* 107, pp. 576–604. DOI: 10.1016/j.solener.2014.05.030.

Schepanski, K., B. Heinold, and I. Tegen (2017). "Harmattan, Saharan heat low, and West African monsoon circulation: modulations on the Saharan dust outflow towards the North Atlantic". *Atmos. Chem. Phys* 17, pp. 10223–10243. DOI: 10.5194/acp-17-10223-2017.

Scheuvens, D. and K. Kandler (2014). "On Composition, Morphology, and Size Distribution of Airborne Mineral Dust". In: *Mineral Dust: A Key Player in the Earth System.* Dordrecht: Springer. DOI: 10.1007/978-94-017-8978-3.

Seinfeld, J. H. (1986). *Atmospheric Chemistry and Physics of Air Pollution.* New York: John Wiley, p. 738.

Seinfeld, J. H. and S. N. Pandis (2016). *Atmospheric Chemistry and Physics : From Air Pollution to Climate Change*. New York: John Wiley & Sons, Incorporated.

Shao, Y. et al. (2011). "Dust cycle: An emerging core theme in Earth system science". *Aeolian Research* 2.4, pp. 181–204. DOI: 10.1016/j.aeolia.2011.02.001.

Shao, Y. (2001). "A model for mineral dust emission". *Journal of Geophysical Research: Atmospheres* 106.D17, pp. 20239–20254. DOI: 10.1029/2001JD900171.

Shao, Y. and H. Lu (2000). "A simple expression for wind erosion threshold friction velocity". *Journal of Geophysical Research: Atmospheres* 105.D17, pp. 22437–22443. DOI: 10.1029/2000JD900304.

Slingo, J., P. Bates, and P. Bauer (2022). "Ambitious partnership needed for reliable climate prediction". *Nat. Clim. Chang.* 12, pp. 499–503. DOI: 10.1038/s41558-022-01384-8.

Sokolik, I. N. and O. B. Toon (1999). "Incorporation of mineralogical composition into models of the radiative properties of mineral aerosol from UV to IR wavelengths". *Journal of Geophysical Research: Atmospheres* 104 (D8), pp. 9423–9444. DOI: 10.1029/1998JD200048.

Stefanski, R. and M. V. K. Sivakumar (2009). "Impacts of sand and dust storms on agriculture and potential agricultural applications of a SDSWS". *IOP Conference Series: Earth and Environmental Science* 7, p. 012016. DOI: 10.1088/1755-1307/7/1/012016.

Stevens, B. et al. (2024). "Earth Virtualization Engines (EVE)". *Earth System Science Data* 16.4, pp. 2113–2122. DOI: 10.5194/essd-16-2113-2024.

Sulaiman, S. A., A. K. Singh, M. M. M. Mokhtar, and M. A. Bou-Rabee (2014). "Influence of dirt accumulation on performance of PV panels". In: vol. 50. Elsevier Ltd, pp. 50–56. DOI: 10.1016/j.egypro.2014.06.006.

Takemi, T. (2005). "Explicit simulations of Convective-Scale Transport of Mineral Dust in Severe Convective Weather". *Journal of the Meteorological Society of Japan* 83A, pp. 187–203. DOI: 10.2151/jmsj.83A.187.

Tegen, I. and A. A. Lacis (1996). "Modeling of particle size distribution and its influence on the radiative properties of mineral dust aerosol". *Journal of Geophysical Research: Atmospheres* 101.D14, pp. 19237–19244. DOI: 10.1029/95JD03610.

Thorncroft, C. D. and M. Blackburn (1999). "Maintenance of the African easterly jet". *Quarterly Journal of the Royal Meteorological Society* 125 (555), pp. 763–786. DOI: 10.1002/qj.49712555502.

Toth III, J. R. et al. (2020). "Electrostatic forces alter particle size distributions". *Atmospheric Chemistry and Physics* 20, pp. 3181–3190. DOI: 10.5194/acp-20-3181-2020.

Tsamalis, C., A. Chédin, J. Pelon, and V. Capelle (2013). "The seasonal vertical distribution of the Saharan Air Layer and its modulation by the wind". *Atmospheric Chemistry and Physics* 13.22, pp. 11235–11257. DOI: 10.5194/acp-13-11235-2013.

Ulanowski, Z., J. Bailey, P. W. Lucas, J. H. Hough, and E. Hirst (2007). *Atmospheric Chemistry and Physics Alignment of atmospheric mineral dust due to electric field.*

van der Does, M., P. Knippertz, P. Zschenderlein, R. G. Harrison, and J. .-. W. Stuut (2018). "The mysterious long-range transport of giant mineral dust particles". *Science Advances* 4.12. DOI: 10.1126/sciadv.aau2768.

van der Does, M., L. F. Korte, C. I. Munday, G. J. A. Brummer, and J. B. W. Stuut (2016). "Particle size traces modern Saharan dust transport and deposition across the equatorial North Atlantic". *Atmospheric Chemistry and Physics* 16 (21), pp. 13697–13710. DOI: 10.5194/ACP-16-13697-2016.

Van Weverberg, K., I. A. Boutle, C. J. Morcrette, and R. K. Newsom (2016). "Towards retrieving critical relative humidity from ground-based remote-sensing observations". *Quarterly Journal of the Royal Meteorological Society* 142.700, pp. 2867–2881. DOI: https://doi.org/10.1002/qj.2874.

Varga, G., P. Dagsson-Waldhauserová, F. Gresina, and A. Helgadottir (2021). "Saharan dust and giant quartz particle transport towards Iceland". *Scientific Reports 2021 11:1* 11 (1), pp. 1–12. DOI: 10.1038/s41598-021-91481-z.

Vergara-Temprado, J. et al. (2018). "Strong control of Southern Ocean cloud reflectivity by ice-nucleating particles". *PNAS* 115 (11), pp. 2687–2692. DOI: 10.1073/pnas.1721627115.

Volken, M. and T. Schumann (1993). "A Critical review of below-cloud aerosol scavenging results on Mt. Rigi". *Water Air Soil Pollution* 68, pp. 15–28. DOI: 10.1007/BF00479390.

Walser, A. (2017). *On the Saharan Air Layer Aerosol and its Role as a Reservoir of Cloud Condensation Nuclei.*

Walters, D. et al. (2019). "The Met Office Unified Model Global Atmosphere 7.0/7.1 and JULES Global Land 7.0 configurations". *Geoscientific Model Development* 12 (5), pp. 1909–1963. DOI: 10.5194/GMD-12-1909-2019.

Weinzierl, B. et al. (2009). "Airborne measurements of dust layer properties, particle size distribution and mixing state of Saharan dust during SAMUM 2006". *Tellus B: Chemical and Physical Meteorology* 61.1, pp. 96–117. DOI: 10.1111/j.1600-0889.2008.00392.x.

Weinzierl, B. et al. (2011). "Microphysical and optical properties of dust and tropical biomass burning aerosol layers in the Cape Verde region-an overview of the airborne in situ and lidar measurements during SAMUM-2". *Tellus, Series B: Chemical and Physical Meteorology* 63 (4), pp. 589–618. DOI: 10.1111/j.1600-0889.2011.00566.x .

Weinzierl, B. et al. (2017). "The Saharan aerosol long-range transport and aerosol-cloud-interaction experiment: Overview and selected highlights". *Bulletin of the American Meteorological Society* 98.7, pp. 1427–1451. DOI: 10.1175/BAMS-D-15-00142.1.

White, B. R. (1979). "soil transport by winds on Mars". *Journal of Geophysical Research: Solid Earth* 84.B9, pp. 4643–4651. DOI: 10.1029/JB084iB09p04643.

Wieland, L.-M. et al. (2024). "Constraining AOD-dependence of size-resolved dust radiative effects during Saharan mineral dust transport". *[Manuscript in Preparation].*

Wilson, D. R. and S. P. Ballard (1999). “A microphysically based precipitation scheme for the UK meteorological office unified model”. *Quarterly Journal of the Royal Meteorological Society* 125.557, pp. 1607–1636. DOI: https://doi.org/10.1002/qj.49712555707.

Wilson, D. R., A. C. Bushell, A. M. Kerr-Munslow, J. D. Price, and C. J. Morcrette (2008). “PC2: A prognostic cloud fraction and condensation scheme. I: Scheme description”. *Quarterly Journal of the Royal Meteorological Society* 134.637, pp. 2093–2107. DOI: https://doi.org/10.1002/qj.333.

Winker, D. M. et al. (2009). “Overview of the CALIPSO Mission and CALIOP Data Processing Algorithms”. *Journal of Atmospheric and Oceanic Technology* 26.11, pp. 2310–2323. DOI: 10.1175/2009JTECHA1281.1.

Wong, S., A. E. Dessler, N. M. Mahowald, P. Yang, and Q. Feng (2009). “Maintenance of lower tropospheric temperature inversion in the Saharan air layer by dust and dry anomaly”. *Journal of Climate* 22 (19), pp. 5149–5162. DOI: 10.1175/2009JCLI2847.1.

Wood, N. et al. (2014). “An inherently mass-conserving semi-implicit semi-Lagrangian discretization of the deep-atmosphere global non-hydrostatic equations”. *Quarterly Journal of the Royal Meteorological Society* 140.682, pp. 1505–1520. DOI: https://doi.org/10.1002/qj.2235.

Woodward, S. (2001). “Modelling the atmospheric life cycle and radiative impact of mineral dust in the Hadley Centre climate model”. *Journal of Geophysical Research* 106, pp. 18155–18166. DOI: 10.1029/2000JD900795.

Woodward, S. et al. (2022). “The simulation of mineral dust in the United Kingdom Earth System Model UKESM1”. *Atmospheric Chemistry and Physics* 22 (22), pp. 14503–14528. DOI: 10.5194/acp-22-14503-2022.

Xie, X. et al. (2018). “Radiative feedbacks of dust in snow over eastern Asia in CAM4-BAM”. *Atmospheric Chemistry and Physics* 18 (17), pp. 12683–12698. DOI: 10.5194/acp-18-12683-2018.

Xu, C., Y. Ma, K. Yang, and C. You (2018). “Tibetan Plateau Impacts on Global Dust Transport in the Upper Troposphere”. *Journal of Climate* 31. DOI: 10.1175/JCLI-D-17.

Yang, W., A. Marshak, A. B. Kostinski, and T. Várnai (2013). “Shape-induced gravitational sorting of Saharan dust during transatlantic voyage: Evidence from CALIOP lidar depolarization measurements”. *Geophysical Research Letters* 40 (12), pp. 3281–3286. DOI: 10.1002/grl.50603.

Yu, H. et al. (2015). “The fertilizing role of African dust in the Amazon rainforest: A first multiyear assessment based on data from Cloud-Aerosol Lidar and Infrared Pathfinder Satellite Observations”. *Geophysical Research Letters* 42 (6), pp. 1984–1991. DOI: 10.1002/2015GL063040.

Zhang, L., S. Gong, J. Padro, and L. Barrie (2001). “A size-segregated particle dry deposition scheme for an atmospheric aerosol module”. *Atmospheric Environment* 35.3, pp. 549–560. DOI: 10.1016/S1352-2310(00)00326-5.

Zhao, A., C. L. Ryder, and L. J. Wilcox (2022). "How well do the CMIP6 models simulate dust aerosols?" *Atmospheric Chemistry and Physics* 22 (3), pp. 2095–2119. DOI: 10.5194/acp-22-2095-2022.

Zhuang, J., D. J. Jacob, and S. D. Eastham (2018). "The importance of vertical resolution in the free troposphere for modeling intercontinental plumes". *Atmospheric Chemistry and Physics* 18.8, pp. 6039–6055. DOI: 10.5194/acp-18-6039-2018.

Zia-Khan, S. et al. (2015). "Effect of dust deposition on stomatal conductance and leaf temperature of cotton in Northwest China". *Water (Switzerland)* 7 (1), pp. 116–131. DOI: 10.3390/w7010116.